

**Structure, Dynamics and Activity  
of Water in Restricted  
Environments**

*A thesis submitted for the award of the degree of*

**Doctor of Philosophy (Science)**

*in*

**Chemistry (Experimental)**

*by*

**Animesh Patra**

**December, 2015**

Department of Chemistry

**University of Calcutta**

Kolkata, India

*Dedicated to My Parents and Supervisor...*

## Abstract:

This thesis is focused on the study of dynamics, hydrogen bonded structure and activity of water molecules present in restricted environments (e.g. reverse micelle, micelle, biopolymer interface and hydrophobic environment). The dynamics of water molecules present in those systems are measured in the time scale ranging from nanosecond to sub-picosecond using two complementary techniques, viz. time resolved fluorescence spectroscopy (TRFS) and terahertz time domain spectroscopy (TTDS). The steady state hydrogen bonding states of water are obtained from Fourier transform infrared spectroscopy (FTIR). We have investigated the properties of water inside reverse micelles by varying the size of the confinement, interfacial morphology and charge type of the interfaces. The results indicate that confinement does strongly modify the dynamics and hydrogen bonding status of water inside the reverse micelles depending upon the length-scale of confinement. Interfacial morphology has almost negligible effect, however, a regular trend is observed with the charge type of interface on the properties of encapsulated water in the reverse micelle. We have carried out dynamics and activity studies of water in presence of a biopolymer (hydroxypropyl cellulose) which shows noticeable change in the dynamics and activity as the water-polymer solution undergoes composition-induced phase transitions. FTIR and THz dielectric relaxation studies on water present in the binary mixture of a nonpolar solvent 1, 2 di-methoxy ethane (DME) with water reveal that the hydration behavior of this mixture is non-monotonous in nature and it varies with the composition of the mixture. We observe hydrophobicity and nature of the interface to play distinct role on the structure and dynamics of water. In order to understand the effect of restriction on water activity we study the enzymatic kinetics of a model enzyme  $\alpha$ -chymotrypsin (CHT) on two different substrates in presence of cationic micelles of varying hydrophobic chain lengths. Our study confirms the presence of highly structured water molecules at the micellar interface, the extent of which being surfactant dependent, and it plays a key role in determining the super- or sub-activity of the micelles concerned.

## List of publications related to thesis work

1. Animesh Patra, Pramod Kumar Verma, and Rajib Kumar Mitra: *Slow Relaxation Dynamics of Water in Hydroxypropyl Cellulose-Water Mixture Traces its Phase Transition Pathway: A Spectroscopic Investigation*. The Journal of Physical Chemistry B, 2012; 116, 1508-1516.
2. Animesh Patra, Trung Quan Luong, Rajib Kumar Mitra, and Martina Havenith: *Solvent Dynamics in A Reverse Micellar Water-Pool: A Spectroscopic Investigation of DDAB-Cyclohexane-Water Systems*. Physical Chemistry Chemical Physics, 2013, 115, 930-939.
3. Animesh Patra, Trung Quan Luong, Rajib Kumar Mitra, and Martina Havenith: *Influence of Charge on the Structure and Dynamics of Water Encapsulated in Reverse Micelles*. Physical Chemistry Chemical Physics, 2014, 16, 12875-12883.
4. Animesh Patra, Debasish Das Mahanta, Nirnay Samanta, Biswaroop Mukherjee and Rajib Kumar Mitra: *Non-Monotonic Dynamics of Water in its Binary Mixture with 1,2-Dimethoxy Ethane: A Combined THz and FTIR Study (to be submitted)*
5. Animesh Patra, Nirnay Samanta and Rajib Kumar Mitra: *Role of Water in the Superactivity of  $\alpha$ -Chymotrypsin in Aqueous Cationic Micelle Environments. (to be submitted)*

## List of publications apart from thesis work

1. Arindam Das, Animesh Patra, and Rajib Kumar Mitra: *Do the Physical Properties of Water in Mixed Reverse Micelles Follow a Synergistic Effect: A Spectroscopic Investigation*. The Journal of Physical Chemistry B, 2013, 117, 3593–3602.
2. Debanjan Polley, Animesh Patra, and Rajib Kumar Mitra: *Dielectric relaxation of the extended hydration sheathe of DNA in the THz frequency region*. Chemical Physics Letters, 2013, 586, 143-147.
3. Animesh Patra, Soumitra Hazra, Gopinatha Suresh Kumar, and Rajib Kumar Mitra: *Entropy Contribution towards Micelle Driven De-intercalation of Drug-DNA Complex*. The Journal of Physical Chemistry B, 2014, 118, 901–908.

4. Animesh Patra, Soumitra Hazra, Nirnay Samanta, Gopinatha Suresh Kumar and Rajib Kumar Mitra: *Micelle Induced Dissociation of DNA-Ligand Complex: The Effect of Ligand Binding Specificity* International Journal of Biological Macromolecules, 2016, 82, 418-424.
5. Arindam Das, Animesh Parta and Rajib Kumar Mitra: *Modulation of Anionic Reverse Micellar Interface with Non-ionic Surfactants can Regulate Enzyme Activity within the Micellar Water pool.* (communicated)
6. Dipak Kumar Das, Animesh Patra and Rajib Kumar Mitra: Preferential Solvation of Lysozyme in dimethyl sulfoxide/Water Binary Mixture Probed by Terahertz Spectroscopy (communicated) (Equally contributed as first author)
7. Debanjan Polley, Animesh Patra, Rajib Kumar Mitra and Anjan Barman: *Modulating conductivity of Au/CNT composites in THz frequency range: A THz resistor.* 39th International Conference on Infrared, Millimeter, and Terahertz waves (IRMMW-THz), 2014.

# Acknowledgements

*It is a pleasant opportunity to express my thanks to all those who contributed in many ways to made this thesis possible and made it an unforgettable experience for me.*

*At the outset, I would like to express my deepest gratitude to my supervisor, Dr. Rajib Kumar Mitra for his continuous supports, effortless helps, valuable discussions and humble guidance. I have immensely benefited from his in-depth experimental knowledge, valuable inputs and continuous encouragement. He always managed time for me from his busy schedule and stood by me during the ups and downs in my research. He constantly motivated me to think and execute my plans independently. He has an excellent sense of humor and it was always a pleasure to talk to him.*

*I am thankful to Prof. Martina Havenith from Ruhr University, Bochum, Germany, Dr. Gopinatha Suresh Kumar, Senior Principal Scientist and Mr. Soumitra Hazra from Indian Institute of Chemical Biology, Kolkata, Dr. Biswaroop Mukherjee, Scientist-D, from S. N. Bose National Centre for Basic Sciences, Kolkata, Dr. Pramod Kumar Verma, Korea University, South Korea for their fruitful collaborations.*

*For graciously inviting me to those wonderful dinners, I thank Madam (Dr. Sukanya Chakraborti)*

*I would like to thank all my lab mates: Arindam Das, Debanjan Polley, Nirnay Samanta, Debasish Das Mahanta (Deba), Dr. Dipak Kumar Das, Kumar Neeraj and Amit Barh for providing a wonderful and friendly environment inside the lab.*

*I am indebted to my physical chemistry teacher Dr. Aajay Kumar Sannigrahi from Saldaha College for believing in me and his affection. I am thankful to my teachers from the Sambalpur University Prof. Bijay Kumar Mishra, Prof. Pramila Kumari Mishra, Dr. Pradipta Kumar Behera, Dr. Satya Narayan Sahu, Dr. Braja Narayan Patra for their continuous encouragement in research.*

*I would like to thank my friends Asish, Jibardhan, Somenath, Dibhya, Pratima, Raghava, Pabitra, Aditya, Nirmal, Renuka, Shrikant, Rali, Jhilli, Shibani, Kishore, Subhamoy, Subhadip, Sanjib for giving me those sweet memories of university days.*

*I would like to give my gratitude to some of friends from the childhood: Partha Sarathi Mahanti (Jhantu), Atanu Patra (Rintu), Malay Patra, Soumitra Banerjee, Soumen Sinhababu, Bisha Laha, Somenath Panda, Tarak Nath Nag and friends from SNBNCBS Subhasish, Sayani, Ishita, Arghya, Biplab, JB, Kapilda, Sushmitadi, Supriya, Soubhanik, Chiranjit (Prads), Gourab, Suman (Bhuban), Abhishek (Kobi), Arnab (Maubaddi), Mithun, Sushovan, Prasenjit, Kaushik, Ayan, Aslam, Subrata, Sumanta who helped me in every possible ways and made my life more enjoyable with their presence.*

*I must address my special thanks to my special friends as well as brothers in the SNBNCBS - Dr. Surajit Rakshit, Dr. Nirmal Goswami, Dr. Debabrata Sinha (Debuda), Dr. Kinsuk Giri and Abhijit. Their support and the most enjoyable company made me able to easily cross the hurdles during my Ph.D. life.*

*The person who constantly shared and understood all my personal and professional problems is Sonali. Thanks to her for being there to talk sense into me whenever anything was getting me down. My best acknowledgements to Semanti Di for her kindness, love and support. Sonali, Semanti Di, Nirnay and Nitish da always created a very cheerful atmosphere with delicious food and superb sense of humor which kept me going through this long journey.*

*Last but not the least, I would like to pay high regards to my parents, my chotomama (Tulshidas Layek), boromama (Bhaskar Chandra Layek) Tapan Dandapath (Tapanda), Chotopishi (Kalyani Dandapath), Muruli Patra (Murulidadu) for their sacrifices, sincere encouragement, support and inspiration throughout my life that have made me more courageous, dedicated and patient. I owe everything to them and they are the reasons for what I am today. I feel myself very fortunate to have Paltu as my brother Ayan, Samudra as nephew and Mohona, Rimpa, Rakhi, Mun as niece.*

*Finally, I thank the S. N. Bose National Centre for Basic Sciences for giving me an opportunity to work and fellowship.*

---

*Animesh Patra*

## Contents:

Abstract:.....	II
List of publications related to thesis work .....	III
List of publications apart from thesis work .....	III
Acknowledgements.....	V
Chapter 1: Introduction .....	1
References: .....	7
Chapter 2: Experimental Techniques and Systems.....	16
2.1. Steady State and Dynamical Tool .....	16
2.1.1. Solvation Dynamics .....	16
2.1.2. Fluorescence Anisotropy .....	21
2.1.3. Arrhenius theory of activation energy: .....	27
2.1.4. Dielectric Relaxation: .....	28
2.2. Systems: .....	31
2.2.a. Micelle: .....	31
2.2.b. Reverse Micelle: .....	32
2.2.c. Water-Polymer Mixture: .....	32
2.2.d $\alpha$ -Chymotrypsin (CHT): .....	33
2.2.e. Protease Substrates:.....	34
2.2.f. Molecular Probes:.....	35
References: .....	36
Chapter 3: Instruments and Sample preparation .....	39
3.1 Instrumental Setup: .....	39
3.1.1. Steady State Absorption and Emission Technique:.....	39
3.1.2. Circular Dichroism (CD) Spectroscopy:.....	41
3.1.3. Time-Correlated Single Photon Counting (TCSPC) Technique:.....	42
3.1.4. Fourier Transform Infrared (FTIR) Measurement:.....	43
3.1.5. Terahertz Time Domain Measurement: .....	44
3.2. Sample Preparation: .....	47
3.2.1. Preparation of Micellar Solution:.....	47
3.2.2. Preparation of Reverse Micellar Solution:.....	48
3.2.3. Measurement of BzCl hydrolysis rate: .....	48
3.2.4. HPC-Water Mixture:.....	48

3.2.5. DME-Water Mixture:.....	48
3.2.6. Enzyme Solution:.....	48
References .....	49
Chapter 4: Dynamics and Activity of Water in Presence of Biopolymer.....	50
4.1. Introduction: .....	50
4.2. Results and Discussion: (The slow relaxation dynamics of water in hydroxypropyl cellulose-water mixture traces its phase transition pathway: A spectroscopic investigation) .....	52
4.3. Conclusions:.....	67
References: .....	67
Chapter 5: Structure and Dynamics of Water in Confined Environments.....	71
5.1. Introduction: .....	71
5.2. Results and Discussions: .....	74
5.2.1. Solvent Dynamics in Reverse Micellar Water-Pool: A Spectroscopic Investigation of DDAB/Cyclohexane/Water Systems.....	74
5.2.2 Influence of Charge on the Structure and Dynamics of Water Encapsulated in Reverse Micelles .....	86
5.3. Conclusions .....	97
References: .....	99
Chapter 6: Structure and Dynamics of Water in Hydrophobic Environment.....	105
6.1. Introduction: .....	105
6.2. Results and Discussions: (Non-Monotonic Dynamics of Water in its Binary Mixture with 1,2-Dimethoxy Ethane: A Combined THz and FTIR Study) .....	106
6.3. Conclusions:.....	112
References: .....	113
Chapter-7: Activity of Water in Bio-Mimicking Environments.....	116
7.1. Introduction: .....	116
7.2. Result and Discussion: (Role of Water in the Superactivity of $\alpha$ -Chymotrypsin in Aqueous Cationic Micellar Environments).....	119
7.3. Conclusions:.....	125
References: .....	125
Chapter 8: Summary and Future Perspective.....	128

# Chapter 1: Introduction

Water plays crucial role in many physical and biological processes. Sometimes it is called as the lubricant of life because most of the biomolecules e.g. protein, DNA, RNA etc. become biologically inactive in absence of water.<sup>1-4</sup> While water molecules present in biological interfaces are structurally altered, they in turn dictate the native structure of many biomolecules. In many processes, water does not exist in its bulk form, rather it experiences confined environments on a nanometer (nm) length scale, and such type of water is termed as nanoscopic/restricted water, and are often encountered in biology and chemistry, specially for systems involving an interface. Water present at restricted environments offers distinct differences in physical and chemical properties relative to its bulk counterpart.<sup>5-13</sup> Intermolecular hydrogen bonding helps water to exist as big polymer-like network rather than as an isolated individual, the network being dynamic in nature owing to constant hydrogen bond breaking and making occurring in ps and sub-ps time scale. Orientational relaxation of water molecules needs rearrangement of hydrogen bonds. The dynamics changes when water interacts with an interface, an ion or a large molecule.<sup>9, 14-18</sup> Water molecules in the vicinity of a surface is highly structured and retarded in their dynamics, for example, the solvent relaxation dynamics of bulk-water shows a time scale of a few ps<sup>1, 3, 13, 19-22</sup> whereas water present in AOT reverse micelle (RM) shows considerably slow time component of ~100-1000 ps.<sup>23-29</sup> In spite of numerous studies carried out in this direction, there still remains several unaddressed questions relating to the water present in such systems. Some of them are: how does an interface influence the dynamics of water? Whether interfacial morphology plays any role in water structure and dynamics? Does the chemical nature/charge of the interface (cationic, anionic, and neutral) have any influence on the physical/chemical properties of water? How an interface modifies the activity of water molecules towards catalysis reactions? Effect of hydrophobic or less polar interface on the intermolecular hydrogen bond structure and dynamics of water. To throw light on these issues, it is necessary to carry out measurements those have comparable time resolution, with exact choice of the probe (that can provide with information of the interface), proper choice of the systems having the appropriate sizes and geometries.

Several experimental techniques are available to study the dynamics of bulk water and confined water.<sup>5, 7, 13, 14, 18, 30-32</sup> Nuclear Magnetic Resonance (NMR) is a popular method to

study the dynamics of water in many heterogeneous environments.<sup>33-35</sup> NMR experiments in particular measure spin-lattice ( $T_1$ ) and spin-spin ( $T_2$ ) relaxation among the many magnetic relaxation modes.<sup>36</sup> Transverse or spin-spin relaxation indicates only the internal rotation,<sup>37</sup> whereas, spin-lattice relaxation is attributed to the rate at which nuclear spin system comes to equilibrium with other degrees of freedom in the system e.g.  $^{17}\text{O}$  spin-lattice relaxation extracts direct information on the rotational motion of water.<sup>34</sup> The dynamics of confined water in reverse micelles was investigated by measuring the  $^1\text{H}$  and  $^{17}\text{O}$  spin-relaxation of water using NMR;<sup>38, 39</sup> this work revealed that the rotational motion of water slows down as a result of confinement. Inelastic neutron scattering experiments have been widely used in order to measure the microscopic structure and dynamics of both solids and liquids.<sup>40</sup> In a quasielastic neutron scattering (QENS) experiment the measured quantity is the self-dynamic factor  $S_s(Q, \omega)$  which gives the information of self-diffusion coefficient of water molecules. QENS experiments can report a time resolution of ns to few ps<sup>40, 41</sup> and has efficiently demonstrated the presence of super cooled type water near a globular protein interface.<sup>42</sup> Mid infrared pump-probe spectroscopy can measure the dynamics of the OH-stretch vibration of water directly.<sup>43-45</sup> Vibrational pump-probe spectroscopy exploits the fact that vibrationally excited molecules have a somewhat different absorption spectrum than molecules in the vibrational ground state. An intense laser pulse is used to remove a fraction of molecules from the ground state to a vibrational excited state.<sup>9, 16, 43, 46</sup> One of the major advantages of this technique is the time resolution which enables to extract information in the resolution of  $\sim 100$  fs, also it can efficiently distinguish the water present at soft-matter interface and the water molecules far away from it.<sup>10</sup>

Retarded dynamics of water in restricted environment is observed in a variety of systems such as in biological membranes, polymer gels, clays, and organized assemblies.<sup>1, 14</sup> Self-organized assemblies are the molecular aggregates those are held together by weak forces. This is a noticeable fact that the dynamics of water molecules in many organized assemblies show the features closely similar to the dynamics of water in biological systems, and in advantage these bio-mimicking systems are less complex than the real biological systems. For the past few decades RM have been recognized as an ideal platform to study the properties of confined/restricted water.<sup>4, 7, 8, 18, 27, 47, 48</sup> Inside an RM water molecules stay in a pocket/pool inside an organic solvent where water and organic solvent are separated by surfactant molecules. The diameter of the water pool can be experimentally varied from 0.3 to 20 nm by adjusting the water/surfactant ratio ( $w_0$ ).<sup>8, 49</sup> It has been inferred that the

hydrogen bonded water structure gets perturbed upon confinement resulting in the abundance of a noticeable fraction of water molecules with distorted hydrogen bonding relative to its bulk counter-part.<sup>23, 50</sup> Water present inside RM can be decomposed into layers and one of the most commonly used models to describe water inside RM is the Core-Shell model.<sup>8, 43, 51, 52</sup> In this model the water molecules inside RM are divided into two types; firstly the water molecule present in the core of the RM, which is supposed to behave like bulk water and secondly the shell water, which are bound to the head groups.<sup>51</sup> MD simulation result shows that the core and shell water are not static in nature and there exist a slow inter conversion between them.<sup>53</sup> In order to analyse the static and dynamic properties of water present inside RM the 'core water' is modelled as the bulk water whereas the water present at  $w_0=2$ , where all the water molecules are essentially interacting with the surfactant head groups is modelled as 'shell water'. The vibrational relaxation time of shell water ( $\sim 5.2$  ps) is significantly slower compared to that of core water (1.7 ps)<sup>8</sup> and it is interesting that the shell water shows a strong dependency on the nature of the polar interface of RM.

The interaction between hydrophobes and water is of essential chemical interest, and is highly relevant for biochemistry and biology.<sup>1, 2, 13, 54-63</sup> Hydrophobic molecules tend to aggregate in aqueous solution in order to make minimum contact with water molecules as also observed during the folding of a protein. The process 'hydrophobic hydration' is the phenomenon which relates how a nonpolar molecule is solvated by water molecules. Dissolution of hydrophobic solute into water results in enormous change in the heat capacity of the solution. Frank and Evans<sup>64</sup> had explained this observation by means of the change in entropy associated with the transfer of water from the hydration shell to the bulk as a result of the hydrophobic effect. According to this model water molecules around hydrophobic molecules form rigid and ice-like structure and this model is known as the Iceberg Model. Since the Iceberg Model is based on the thermodynamic parameters, the molecular picture it assumes is quite indirect. On the contrary Sharp et al.<sup>65</sup> observed that hydrophobic solutes tend to favourably relocate water molecules that over-coordinate a second water molecule, providing a justification for why hydrophobic solutes lower the amount of network defects.<sup>65, 66</sup> However, such hydrophobic hydration largely depends on the size of the hydrophobic molecule.<sup>67</sup> For small hydrophobic molecules (diameter  $<1$  nm) water molecules can easily arrange a cavity to adopt a hydrogen bonded network around the hydrophobic molecules. On the other hand in larger hydrophobes (diameter  $>1$  nm) water molecule are unable to maintain hydrogen bonded network with the extended surface of the solute.<sup>54, 67, 68</sup> Vibrational sum frequency generation (VSFG) study shows a higher SFG intensity of water at hydrophobic

interfaces compared to water at air/water interfaces. Such increase in the SFG intensity indicates the formation of enhanced ordered hydrogen bonded water near the hydrophobic interfaces.<sup>69, 70</sup> On the contrary neutron diffraction studies have shown that the structure of water present at concentrated short chain alcohol solution does not differ much compared to that of pure water indicating the formation of water clusters.<sup>71, 72</sup> Formation of ordered hydrogen bonded water network indeed slows down the orientational relaxation process which has been supported by many experimental results.<sup>54</sup> However, a recent MD simulation study by Lagge et al. have ruled out the possibility of Iceberg formation as a reason of slowdown of the water orientational dynamics near hydrophobic surface.<sup>66</sup> The authors evidenced that no water molecules are immobilized by hydrophobic solutes and their moderate rotational slowdown compared to that in bulk water is mainly due to a slower hydrogen-bond exchange dynamics. The slowdown is quantitatively described by a solute excluded volume effect at the transition state for the key to the hydrogen-bond exchange in the reorientation mechanism.<sup>73, 74</sup>

Water molecule present in confinement or restricted environment shows unusual behaviour in their activity also.<sup>75-83</sup> The activity of reactants highly depends on the polarity of the medium and the dynamics of reactants. For example water present at poly-ethyleneglycol or hydrophobic solutes (e.g. 1, 4-di-oxane, methyl t-butyl ether etc.) mixture shows retarded rate of benzoyl chloride hydrolysis.<sup>46, 84, 85</sup> Hydrolysis reaction of benzoyl halide encapsulated inside RM can be tuned by changing the level of hydration of RM.<sup>86, 87</sup> Micellar enzymology is one of the popular methods to study activity of water in restricted medium. This field has attracted the attention of many researcher for its application in industrial biocatalytic process. Water molecules at micellar interface are slower in dynamics compared to bulk<sup>88-90</sup> and water bound micellar interface shows unusual rate of enzyme hydrolysis reaction.<sup>91, 92</sup> Rate of enzyme hydrolysis shows a bell shaped curve as a function of  $w_0$  of RM i.e. it shows maximum activity at a certain  $w_0$ ; such observation has been explained by specific hydrogen bonding states of water.<sup>93</sup> It has also been reported that interaction of cationic micellar interface with enzyme enhances the rate of hydrolysis reaction by many folds.<sup>94-97</sup> Such enhancement in activity has been termed as ‘superactivity’. It has been inferred that cationic interface enhances the hydrogen bond donor capacity of water through hydrogen bonding which in turn leads to the formation of superactive water.<sup>92, 98</sup>

Fourier transform infrared (FTIR) spectroscopy is a very sensitive technique to study the hydrogen bonding in water.<sup>14, 44, 99-102</sup> Water produces characteristic symmetric and asymmetric O-H stretching bands in the frequency range of 3000-3700  $\text{cm}^{-1}$ . Further bands of

water are found in the MIR region around  $2100\text{ cm}^{-1}$  (coupled bending and librational motions),  $1650\text{ cm}^{-1}$  (bending).<sup>103</sup> Such a broad stretching spectrum in the mid infrared (MIR) region arises due to the presence of different types of hydrogen bonding states of water and deconvolution of such spectrum provides with a quantitative picture. MIR spectrum of water in different confined environments shows the presence of at least three distinct types of hydrogen bonding environments, namely, isolated water (IW, water molecule which are not hydrogen bonded to any neighbouring molecule), distorted structured water (DW, unable to develop fully hydrogen bonded structure) and hydrogen-bonded water molecules (HW, tetrahedrally hydrogen bonded water).<sup>26, 85, 100, 103, 104</sup> Deconvolution of MIR stretching spectra<sup>103, 105</sup> extracts quantitative picture of hydrogen bonding states of water in confinement.<sup>39, 100, 105, 106</sup> In the far infrared region (FIR,  $60\text{-}700\text{ cm}^{-1}$ ) water shows many acoustic (at  $30\text{-}200\text{ cm}^{-1}$ )<sup>107</sup> and optical bands ( $280\text{-}700\text{ cm}^{-1}$ )<sup>108</sup> which are due to the hydrogen bond vibration, e.g. (i) transverse acoustic (TA,  $60\text{-}75\text{ cm}^{-1}$ ) mode arises due to hydrogen bond bending, (ii) longitudinal acoustic ( $164\text{-}181\text{ cm}^{-1}$ ) mode arises due to hydrogen bond stretching. The optical mode arises due to the librational motion of water: (i)  $\sim 300\text{ cm}^{-1}$  first librational band, (ii)  $\sim 450\text{ cm}^{-1}$  assigned as libration around the  $C_2$  (two-fold symmetry axis) of water, (iii)  $\sim 550\text{ cm}^{-1}$  for in-plane rocking libration and (iv)  $\sim 700\text{ cm}^{-1}$  out-of-plane libration. FIR spectrum of liquid water generally shows only two distinct broad bands which are hydrogen bond stretching band ( $\sim 200\text{ cm}^{-1}$ ) and the libration band ( $\sim 650\text{ cm}^{-1}$ ).<sup>109, 110</sup> The reason for this spectral broadening may be due to the formation of undefined different local structures through hydrogen bond breaking and making in water.<sup>85, 107, 109, 111</sup> The hydrogen bond stretching peak in the FIR region is highly sensitive towards small fluctuations in hydrogen bond strength. The librational band of water under confinement strongly differs from the pure water spectrum.<sup>112</sup> Quan et al. have shown that librational dynamics of small water clusters trapped inside a porous material is highly dependent on the pore size of the material.<sup>111</sup> Librational peak position of water inside RM gets blue shifted with increasing hydration providing with direct evidence of establishment of strong hydrogen bonding at higher hydration level.<sup>110</sup> Combining MIR and FIR spectra a comprehensive picture of hydrogen bond strength and structure of water could be generated in the investigated systems.

Fluorescence spectroscopy is a versatile technique to understand the polarity and microenvironment around a probe molecule.<sup>48, 113, 114</sup> Time resolved fluorescence spectroscopy (TRFS) has been used for years to investigate hydration dynamics in biomolecules, supramolecular assemblies like protein,<sup>2, 115, 116</sup> DNA,<sup>117-119</sup> micelle,<sup>120-124</sup>

reverse micelle,<sup>28, 86, 105, 124-126</sup> cyclodextrin<sup>127, 128</sup> etc. Solvation dynamics study by TRFS of bulk water yields two time scales:  $\sim 126$  fs and  $\sim 880$  fs.<sup>22</sup> However, solvation relaxation is orders of magnitude slower for water at the vicinity of interface. It is interesting to note that there coexist two types of water in these restricted systems, firstly the water molecules having faster dynamics ( $\sim$  few ps) and the other one is slower in dynamics with a timescale of hundreds of ps to several ns.<sup>28, 84, 120, 121, 125, 129-131</sup> The origin of this bimodal distribution of water can be understood in terms of the 'bound' water molecules bound to the polar interface offering a dynamics significantly slower than that of pure water and 'free-type' water molecules those are not hydrogen bonded with the interface but stay in the hydration layer.<sup>132, 133</sup> Since the hydration layer is actively dynamic in nature the inter conversion (hydrogen bond breaking and making) kinetics between these two species determines the amplitude and also the time scale of the hydration layer relaxation. In most of these systems, an Arrhenius type barrier crossing model describes the temperature induced inter-conversion between these two types of water molecules.<sup>1, 2, 89, 125, 134</sup>

TRFS sensitivity is mostly limited to the first two solvation shells and thus is unable to provide information on the extended solvation shell. THz spectroscopy ( $1 \text{ THz} = 10^{12} \text{ Hz} = 1 \text{ ps}^{-1}$ ) has emerged as an efficient tool to provide information about the next 3-4 solvation layers which are mainly concerned with the libration and collective hydrogen bond stretching vibration bands.<sup>107, 135-137</sup> THz absorption coefficient [ $\alpha(\nu)$ ] of hydrated water is found to be higher by  $\sim 10 \text{ cm}^{-1}$  compared to that of pure water ( $\sim 150 \text{ cm}^{-1}$  at 1 THz).<sup>136, 138, 139</sup> For a bulk liquid the collective vibration involving multiple molecules contributes a significant amount in the total dipole correlation function, however, these modes strongly depend on the size of confinement. Mittleman et al. have studied water present inside AOT RM<sup>140-142</sup> and they observed the vibrational density of states of water molecules to be highly dependent on the radius of the water pool and the integrated absorption strength in larger micelles is actually smaller than that of the bulk liquid. This suggests that the THz collective modes of bulk liquid are absent in confined liquids. Dielectric relaxation of water in this region (0.2-3.0 THz) produces three different time constants  $\sim 8$  ps<sup>142-145</sup> (arises due to the cooperative rearrangement of the hydrogen-bonded network)  $\sim 200$  fs (rotational modes of the individual polar water molecules) and  $\sim 90$  fs (owing to the hydrogen-bond bending).<sup>146</sup> This  $\sim 8$  ps time scale is sensitive towards the extent of hydrogen bonded network. THz dielectric relaxation studies indicate a distinct change in hydrogen bonded network when water is introduced to an interface.<sup>142, 143, 147</sup> Dielectric relaxation study of water molecules around amino acids of

varying hydrophobicity showed a more ordered water structure near hydrophobic groups than those around hydrophilic ones,<sup>148</sup> however, the degree of the ordering is not as extreme as the iceberg model of Frank and Evans.<sup>64</sup>

Investigations have been carried out on the structure, dynamics and activity of water present in biopolymer (e.g. hydroxylpropyl cellulose) and different bio-mimicking surfaces (e.g. RMs, micelle) with varying size, charge and geometry of the interface. Hydroxypropyl cellulose (HPC) is a water soluble polymer which shows a structural transition from isotropic to cholesteric liquid crystal when the composition of HPC-water mixture is varied, the consequent changes in the water dynamics and activity during this process seems intriguing. Our investigation shows that there occurs a sharp change in the dynamics of water at the region of phase transition indicating that water dynamics can act as a marker for different physical processes.<sup>149</sup> Our studies with RM systems carry two-fold motivations, firstly, what is the effect of different interfacial geometry (e.g. DDAB/Cy/water RM shows cylindrical to spherical shape transition at  $w_0 = [\text{water}]/[\text{Surfactant}] > 8$ ) on the structure and dynamics of water.<sup>150</sup> Secondly, influence of different charge type (cationic, anionic and neutral) of the interface on the properties of entrapped water inside RM.<sup>151</sup> Our study shows that differently shaped geometrical interface like cylindrical and spherical have negligible effect on the structure and dynamics of water inside RM, whereas, charge type of the interface shows distinct influence. Ionic interfaces offer more perturbing influence on the hydrogen-bonded structure and dynamics of water inside RM over non-ionic interfaces. Our study reveals that the presence of cationic micellar interface produces an enhanced activity of  $\alpha$ -chymotrypsin compared to that in buffer whereas anionic and non-ionic micellar interfaces offer a lower activity. We have also observed that water soluble small organic molecule (e.g. dimethoxyethane) have strong influence over the hydrogen bonded network of water depending on the composition of the mixture. FTIR studies show that water present in such systems evolves from small clusters to hydrogen bonded network while, THz dielectric relaxation dynamics shows a non-linear behaviour in their dynamics over the entire composition range.

## References:

1. Pal, S. K., and Zewail, A. H. (2004) Dynamics of water in biological recognition, *Chemical Reviews* 104, 2099-2123.
2. Pal, S. K., Peon, J., Bagchi, B., and Zewail, A. H. (2002) Biological Water: Femtosecond Dynamics of Macromolecular Hydration, *The Journal of Physical Chemistry B* 106, 12376-12395.
3. Nandi, N., Bhattacharyya, K., and Bagchi, B. (2000) Dielectric relaxation and solvation dynamics of water in complex chemical and biological systems, *Chemical Reviews* 100, 2013-2045.

4. Bhattacharyya, K., and Bagchi, B. (2000) Slow Dynamics of Constrained Water in Complex Geometries, *The Journal of Physical Chemistry A* 104, 10603-10613.
5. Levinger, N. E., and Swafford, L. A. (2009) Ultrafast Dynamics in Reverse Micelles, *Annual Review of Physical Chemistry* 60, 385-406.
6. Levinger, N. E. (2002) Water in confinement *Science* 298, 1722-1723.
7. Fayer, M. D., and Levinger, N. E. (2010) Analysis of Water in Confined Geometries and at Interfaces, *Annual Review of Analytical Chemistry* 3, 89-107.
8. Moilanen, D. E., Levinger, N. E., Spry, D. B., and Fayer, M. D. (2007) Confinement or the Nature of the Interface? Dynamics of Nanoscopic Water, *Journal of the American Chemical Society* 129, 14311-14318.
9. Dokter, A. M., Woutersen, S., and Bakker, H. J. (2006) Inhomogeneous dynamics in confined water nanodroplets *Proceedings of the National Academy of Sciences USA* 103, 15355-15358.
10. Fenn, E. E., Wong, D. B., and Fayer, M. D. (2009) Water dynamics at neutral and ionic interfaces, *Proceedings of the National Academy of Sciences USA* 106, 15243-15248.
11. Bhattacharyya, K. (2003) Solvation Dynamics and Proton Transfer in Supramolecular Assemblies, *Accounts of Chemical Research* 36, 95-101.
12. Fayer, M. D. (2011) Water in a Crowd, *Physiology* 26, 381-392.
13. Bagchi, B. (2005) Water Dynamics in the Hydration Layer around Proteins and Micelles, *Chemical Reviews* 105, 3197-3219.
14. Fayer, M. D. (2012) Dynamics of Water Interacting with Interfaces, Molecules, and Ions, *Accounts of Chemical Research* 45, 3-14.
15. Bakker, H. J., Kropman, M. F., Omta, A. W., and Woutersen, S. (2004) Hydrogen-Bond Dynamics of Water in Ionic Solutions, *Physica Scripta* 69, C14.
16. Dokter, A. M., Woutersen, S., and Bakker, H. J. (2005) Anomalous Slowing Down of the Vibrational Relaxation of Liquid Water upon Nanoscale Confinement, *Physical Review Letters* 94, 178301.
17. Omta, A. W., Kropman, M. F., Woutersen, S., and Bakker, H. J. (2003) Negligible Effect of Ions on the Hydrogen-Bond Structure in Liquid Water, *Science* 301, 347-349.
18. Nandi, N., Bhattacharyya, K., and Bagchi, B. (2000) Dielectric Relaxation and Solvation Dynamics of Water in Complex Chemical and Biological Systems, *Chemical Reviews* 100, 2013-2046.
19. Moilanen, D. E., Fenn, E. E., Lin, Y.-S., Skinner, J. L., Bagchi, B., and Fayer, M. D. (2008) Water inertial reorientation: Hydrogen bond strength and the angular potential, *Proceedings of the National Academy of Sciences* 105, 5295-5300.
20. Asbury, J. B., Steinel, T., Stromberg, C., Corcelli, S. A., Lawrence, C. P., Skinner, J. L., and Fayer, M. D. (2004) Water Dynamics: Vibrational Echo Correlation Spectroscopy and Comparison to Molecular Dynamics Simulations, *The Journal of Physical Chemistry A* 108, 1107-1119.
21. Fecko, C. J., Loparo, J. J., Roberts, S. T., and Tokmakoff, A. (2005) Local hydrogen bonding dynamics and collective reorganization in water: Ultrafast infrared spectroscopy of HOD/D<sub>2</sub>O, *The Journal of Chemical Physics* 122, 054506.
22. Jimenez, R., Fleming, G. R., Kumar, P. V., and Maroncelli, M. (1994) Femtosecond solvation dynamics of water, *Nature* 369, 471-473.
23. Brubach, J.-B., Mermet, A., Filabozzi, A., Gerschel, A., Lairez, D., Krafft, M. P., and Roy, P. (2001) Dependence of Water Dynamics upon Confinement Size, *The Journal of Physical Chemistry B* 105, 430-435.
24. Zhong, Q., Steinhurst, D. A., Carpenter, E. E., and Owrutsky, J. C. (2002) Fourier Transform Infrared Spectroscopy of Azide Ion in Reverse Micelles, *Langmuir* 18, 7401-7408.
25. Zhou, N., Li, Q., Wu, J., Chen, J., Weng, S., and Xu, G. (2001) Spectroscopic Characterization of Solubilized Water in Reversed Micelles and Microemulsions: Sodium Bis(2-ethylhexyl) Sulfosuccinate and Sodium Bis(2-ethylhexyl) Phosphate in n-Heptane, *Langmuir* 17, 4505-4509.
26. Temsamani, M. B., Maeck, M., Hassani, I. E., and Hurwitz, H. D. (1998) Fourier Transform Infrared Investigation of Water States in Aerosol-OT Reverse Micelles as a Function of Counterionic Nature, *The Journal of Physical Chemistry B* 102, 3335-3340.

27. Bakulin, A. A., Cringus, D., Pieniazek, P. A., Skinner, J. L., Jansen, T. L. C., and Pshenichnikov, M. S. (2013) Dynamics of Water Confined in Reversed Micelles: Multidimensional Vibrational Spectroscopy Study, *The Journal of Physical Chemistry B* 117, 15545-15558.
28. Sarkar, N., Das, K., Datta, A., Das, S., and Bhattacharyya, K. (1996) Solvation Dynamics of Coumarin 480 in Reverse Micelles. Slow Relaxation of Water Molecules, *The Journal of Physical Chemistry* 100, 10523-10527.
29. Datta, A., Mandal, D., Pal, S. K., and Bhattacharyya, K. (1997) Intramolecular Charge Transfer Processes in Confined Systems. Nile Red in Reverse Micelles†, *The Journal of Physical Chemistry B* 101, 10221-10225.
30. Piletic, I. R., Moilanen, D. E., Levinger, N. E., and Fayer, M. D. (2006) What Nonlinear-IR Experiments Can Tell You about Water that the IR Spectrum Cannot, *Journal of the American Chemical Society* 128, 10366-10367.
31. Tan, H.-S., Piletic, I. R., and Fayer, M. D. (2005) Orientational dynamics of water confined on a nanometer length scale in reverse micelles, *The Journal of Chemical Physics* 122, 174501.
32. Levinger, N. E. (2000) Ultrafast dynamics in reverse micelles, microemulsions, and vesicles, *Current Opinion in Colloid & Interface Science* 5, 118-124.
33. Bryant, R. G. (1996) THE DYNAMICS OF WATER-PROTEIN INTERACTIONS, *Annual Review of Biophysics and Biomolecular Structure* 25, 29-53.
34. Yoshida, K., Kitajo, A., and Yamaguchi, T. (2006) 17O NMR relaxation study of dynamics of water molecules in aqueous mixtures of methanol, ethanol, and 1-propanol over a temperature range of 283–403 K, *Journal of Molecular Liquids* 125, 158-163.
35. Moreno, M., Castiglione, F., Mele, A., Pasqui, C., and Raos, G. (2008) Interaction of Water with the Model Ionic Liquid [bmim][BF4]: Molecular Dynamics Simulations and Comparison with NMR Data, *The Journal of Physical Chemistry B* 112, 7826-7836.
36. Baumgartner, S., Lahajnar, G., Sepe, A., and Kristl, J. (2002) Investigation of the state and dynamics of water in hydrogels of cellulose ethers by 1H NMR spectroscopy, *AAPS PharmSciTech* 3, 86-93.
37. Kříž, J., and Dybal, J. (2011) Hydration modes of an amphiphilic molecule 2: NMR, FTIR and theoretical study of the interactions in the system water–1,2-dimethoxyethane, *Chemical Physics* 382, 104-112.
38. Carlstroem, G., and Halle, B. (1988) Water dynamics in microemulsion droplets. A nuclear spin relaxation study, *Langmuir* 4, 1346-1352.
39. Li, Q., Li, T., and Wu, J. (2000) Comparative Study on the Structure of Reverse Micelles. 2. FT-IR, 1H NMR, and Electrical Conductance of H<sub>2</sub>O/AOT/NaDEHP/n-Heptane Systems, *The Journal of Physical Chemistry B* 104, 9011-9016.
40. Di Cola, D., Deriu, A., Sampoli, M., and Torcini, A. (1996) Proton dynamics in supercooled water by molecular dynamics simulations and quasielastic neutron scattering, *The Journal of Chemical Physics* 104, 4223-4232.
41. Russo, D., Baglioni, P., Peroni, E., and Teixeira, J. (2003) Hydration water dynamics of a completely hydrophobic oligopeptide, *Chemical Physics* 292, 235-245.
42. Tarek, M., Neumann, D. A., and Tobias, D. J. (2003) Characterization of sub-nanosecond dynamics of the molten globule state of  $\alpha$ -lactalbumin using quasielastic neutron scattering and molecular dynamics simulations, *Chemical Physics* 292, 435-443.
43. Dokter, A. M., Woutersen, S., and Bakker, H. J. (2007) Ultrafast dynamics of water in cationic micelles, *The Journal of Chemical Physics* 126, 124507.
44. Bakulin, A. A., Liang, C., la Cour Jansen, T., Wiersma, D. A., Bakker, H. J., and Pshenichnikov, M. S. (2009) Hydrophobic Solvation: A 2D IR Spectroscopic Inquest, *Accounts of Chemical Research* 42, 1229-1238.
45. Mohammed, O. F., Pines, D., Dreyer, J., Pines, E., and Nibbering, E. T. J. (2005) Sequential Proton Transfer Through Water Bridges in Acid-Base Reactions, *Science* 310, 83-86.
46. Rakshit, S., Saha, R., Chakraborty, A., and Pal, S. K. (2013) Effect of Hydrophobic Interaction on Structure, Dynamics, and Reactivity of Water, *Langmuir* 29, 1808-1817.

47. Costard, R., Levinger, N. E., Nibbering, E. T. J., and Elsaesser, T. (2012) Ultrafast Vibrational Dynamics of Water Confined in Phospholipid Reverse Micelles, *The Journal of Physical Chemistry B* 116, 5752-5759.
48. Bhattacharyya, K. (2003) Solvation Dynamics and Proton Transfer in Supramolecular Assemblies, *Accounts of Chemical Research* 36, 95-101.
49. Rosenfeld, D. E., and Schmuttenmaer, C. A. (2006) Dynamics of Water Confined Within Reverse Micelles, *The Journal of Physical Chemistry B* 110, 14304-14312
50. Moilanen, D. E., Emily E. Fenn, E. E., Wong, D., and Fayer, M. D. (2009) Water dynamics in large and small reverse micelles: From two ensembles to collective behavior *The Journal of Chemical Physics* 131, 014704
51. Piletic, I. R., Moilanen, D. E., Spry, D. B., Levinger, N. E., and Fayer, M. D. (2006) Testing the Core/Shell Model of Nanoconfined Water in Reverse Micelles Using Linear and Nonlinear IR Spectroscopy, *The Journal of Physical Chemistry A* 110, 4985-4999.
52. Biswas, R., Furtado, J., and Bagchi, B. (2013) Layerwise decomposition of water dynamics in reverse micelles: A simulation study of two-dimensional infrared spectrum, *The Journal of Chemical Physics* 139, 144906.
53. Faeder, J., and Ladanyi, B. M. (2000) Molecular Dynamics Simulations of the Interior of Aqueous Reverse Micelles, *The Journal of Physical Chemistry B* 104, 1033-1046.
54. Tielrooij, K.-J., Hunger, J., Buchner, R., Bonn, M., and Bakker, H. J. (2010) Influence of Concentration and Temperature on the Dynamics of Water in the Hydrophobic Hydration Shell of Tetramethylurea, *Journal of the American Chemical Society* 132, 15671-15678.
55. Southall, N. T., Dill, K. A., and Haymet, A. D. J. (2002) A View of the Hydrophobic Effect, *The Journal of Physical Chemistry B* 106, 521-533.
56. Hummer, G., Garde, S., García, A. E., Pohorille, A., and Pratt, L. R. (1996) An information theory model of hydrophobic interactions, *Proceedings of the National Academy of Sciences USA* 93, 8951-8955.
57. Hofinger, S., and Zerbetto, F. (2005) Simple models for hydrophobic hydration, *Chemical Society Reviews* 34, 1012-1020.
58. Cheng, Y.-K., and Rossky, P. J. (1998) Surface topography dependence of biomolecular hydrophobic hydration, *Nature* 392, 696-699.
59. Rajamani, S., Truskett, T. M., and Garde, S. (2005) Hydrophobic hydration from small to large lengthscales: Understanding and manipulating the crossover, *Proceedings of the National Academy of Sciences of the United States of America* 102, 9475-9480.
60. Garde, S., Hummer, G., García, A. E., Paulaitis, M. E., and Pratt, L. R. (1996) Origin of Entropy Convergence in Hydrophobic Hydration and Protein Folding, *Physical Review Letters* 77, 4966-4968.
61. Widom, B., Bhimalapuram, P., and Koga, K. (2003) The hydrophobic effect, *Physical Chemistry Chemical Physics* 5, 3085-3093.
62. Wiggins, P. M. (1997) Hydrophobic hydration, hydrophobic forces and protein folding, *Physica A: Statistical Mechanics and its Applications* 238, 113-128.
63. Blokzijl, W., and Engberts, J. B. F. N. (1993) Hydrophobe Effekte – Ansichten und Tatsachen, *Angewandte Chemie* 105, 1610-1648.
64. Frank, H. S., and Evans, M. W. (1945) Free Volume and Entropy in Condensed Systems III. Entropy in Binary Liquid Mixtures; Partial Molal Entropy in Dilute Solutions; Structure and Thermodynamics in Aqueous Electrolytes, *The Journal of Chemical Physics* 13, 507-532.
65. Gallagher, K. R., and Sharp, K. A. (2003) A New Angle on Heat Capacity Changes in Hydrophobic Solvation, *Journal of the American Chemical Society* 125, 9853-9860.
66. Laage, D., Stirnemann, G., and Hynes, J. T. (2009) Why Water Reorientation Slows without Iceberg Formation around Hydrophobic Solutes, *The Journal of Physical Chemistry B* 113, 2428-2435.
67. Chandler, D. (2002) Hydrophobicity: Two faces of water, *Nature* 417, 491-491.
68. Strazdaite, S., Versluis, J., and Bakker, H. J. (2015) Water orientation at hydrophobic interfaces, *The Journal of Chemical Physics* 143, 084708.

69. Davis, J. G., Gierszal, K. P., Wang, P., and Ben-Amotz, D. (2012) Water structural transformation at molecular hydrophobic interfaces, *Nature* *491*, 582-585.
70. Strazdaite, S., Versluis, J., Backus, E. H. G., and Bakker, H. J. (2014) Enhanced ordering of water at hydrophobic surfaces, *The Journal of Chemical Physics* *140*, 054711.
71. Dixit, S., Crain, J., Poon, W. C. K., Finney, J. L., and Soper, A. K. (2002) Molecular segregation observed in a concentrated alcohol-water solution, *Nature* *416*, 829-832.
72. Soper, A. K., and Finney, J. L. (1993) Hydration of methanol in aqueous solution, *Physical Review Letters* *71*, 4346-4349.
73. Rezus, Y. L. A., and Bakker, H. J. (2007) Observation of Immobilized Water Molecules around Hydrophobic Groups, *Physical Review Letters* *99*, 148301.
74. Laage, D., and Hynes, J. T. (2006) A Molecular Jump Mechanism of Water Reorientation, *Science* *311*, 832-835.
75. Fendler, J. H. (1976) Interactions and reactions in reversed micellar systems, *Accounts of Chemical Research* *9*, 153-161.
76. Thomas, J. K. (1977) Effect of structure and charge on radiation-induced reactions in micellar systems, *Accounts of Chemical Research* *10*, 133-138.
77. Cohen, B., Huppert, D., Solntsev, K. M., Tsfadia, Y., Nachliel, E., and Gutman, M. (2002) Excited State Proton Transfer in Reverse Micelles, *Journal of the American Chemical Society* *124*, 7539-7547.
78. Couderc, S., and Toullec, J. (2001) Catalysis of Phosphate Triester Hydrolysis by Micelles of Hexadecyltrimethylammonium anti-Pyruvaldehyde 1-Oximate, *Langmuir* *17*, 3819-3828.
79. Correa, N. M., Durantini, E. N., and Silber, J. J. (2000) Influence of Anionic and Cationic Reverse Micelles on Nucleophilic Aromatic Substitution Reaction between 1-Fluoro-2,4-dinitrobenzene and Piperidine, *The Journal of Organic Chemistry* *65*, 6427-6433.
80. Pileni, M.-P. (1993) Water in oil colloidal droplets used as microreactors, *Advances in Colloid and Interface Science* *46*, 139-163.
81. Blagoeva, I. B., Gray, P., and Ruasse, M.-F. (1996) Pseudophase Model for Reactivity in Reverse Micelles. The Case of the Water-Promoted Reaction between Two Lipophilic Reagents, Bromine and 1-Octene, in AOT Microemulsions, *The Journal of Physical Chemistry* *100*, 12638-12643.
82. Khan, M. N., Arifin, Z., Yusoff, M. R., and Ismail, E. (1999) Effects of Nonionic, Cationic, and Mixed Nonionic-Cationic Surfactants on the Acid-Base Behavior of Phenyl Salicylate, *Journal of Colloid and Interface Science* *220*, 474-476.
83. E. Cordes, C. G. (1973) *Reaction kinetics in presence of micelle forming surfactants*, Vol. 2, Wiley Interscience, New York.
84. Verma, P. K., Mitra, R. K., and Pal, S. K. (2009) A Molecular Picture of Diffusion Controlled Reaction: Role of Microviscosity and Hydration on Hydrolysis of Benzoyl Chloride at a Polymer Hydration Region, *Langmuir* *25*, 11336-11343.
85. Luong, T. Q., Verma, P. K., Mitra, R. K., and Havenith, M. (2011) Onset of Hydrogen Bonded Collective Network of Water in 1,4-Dioxane, *The Journal of Physical Chemistry A* *115*, 14462-14469.
86. Verma, P. K., Makhal, A., Mitra, R. K., and Pal, S. K. (2009) Role of Solvation Dynamics in the Kinetics of Solvolysis Reactions in Microreactors, *Physical Chemistry Chemical Physics* *11*, 8467-8476.
87. García-Río, L., Hervella, P., and Rodríguez-Dafonte, P. (2006) Solvolysis of Benzoyl Halides in Water/NH<sub>4</sub>DEHP/Isooctane Microemulsions, *Langmuir* *22*, 7499-7506.
88. Balasubramaian, S., Pal, S., and Bagchi, B. (2002) Hydrogen-Bond Dynamics near a Micellar Surface: Origin of the Universal Slow Relaxation at Complex Aqueous Interfaces, *Physics Review Letter* *89*, 115505.
89. Mitra, R. K., Sinha, S. S., and Pal, S. K. (2007) Temperature Dependent Hydration at Micellar Surface: Activation Energy Barrier Crossing Model Revisited, *The Journal of Physical Chemistry B* *111*, 7577-7581.
90. Pal, S., Balasubramaian, S., and Bagchi, B. (2003) Identity, Energy, and Environment of Interfacial Water Molecules in a Micellar Solution, *The Journal of Physical Chemistry B* *107*, 5194-5202.

91. Bales, B. L., and Zana, R. (2002) Characterization of Micelles of Quaternary Ammonium Surfactants as Reaction Media I: Dodecyltrimethylammonium Bromide and Chloride, *The Journal of Physical Chemistry B* 106, 1926-1939.
92. Moyano, F., Falcone, R. D., Mejuto, J. C., Silber, J. J., and Correa, N. M. (2010) Cationic Reverse Micelles Create Water with Super Hydrogen-Bond-Donor Capacity for Enzymatic Catalysis: Hydrolysis of 2-Naphthyl Acetate by  $\alpha$ -Chymotrypsin, *Chemistry - A European Journal* 16, 8887-8893.
93. Biasutti, M. A., Abuin, E. B., Silber, J. J., Correa, N. M., and Lissi, E. A. (2008) Kinetics of reactions catalyzed by enzymes in solutions of surfactants, *Advances in Colloid Interface Science* 136, 1-24.
94. Spreti, N., Alfani, F., Cantarella, M., D'Amico, F., Germani, R., and Savelli, G. (1999)  $\alpha$ -Chymotrypsin superactivity in aqueous solutions of cationic surfactants, *Journal of Molecular Catalysis B: Enzymatic* 6, 99-110.
95. Viparelli, P., Alfani, F., Gallifuoco, A., and Cantarella, M. (2004) Effect of quaternary ammonium salts on the hydrolysis of N-glutaryl-L-phenylalanine catalysed by  $\alpha$ -chymotrypsin, *Journal of Molecular Catalysis B: Enzymatic* 28, 101-110.
96. Abuin, E., Lissi, E., and Duarte, R. (2004) Distinct effect of a cationic surfactant on the transient and steady state phases of 2-naphthyl acetate hydrolysis catalyzed by  $\alpha$ -chymotrypsin, *Journal of Molecular Catalysis B: Enzymatic* 31, 83-85.
97. Spreti, N., Mancini, M. V., Germani, R., Di Profio, P., and Savelli, G. (2008) Substrate effect on  $\alpha$ -chymotrypsin activity in aqueous solutions of "big-head" ammonium salts, *Journal of Molecular Catalysis B: Enzymatic* 50, 1-6.
98. Blach, D., Correa, N. M., Silber, J. J., and Falcone, R. D. (2011) Interfacial water with special electron donor properties: Effect of water-surfactant interaction in confined reversed micellar environments and its influence on the coordination chemistry of a copper complex, *Journal of Colloid Interface Science* 355, 124-130.
99. Cammarata, L., Kazarian, S. G., Salter, P. A., and Welton, T. (2001) Molecular states of water in room temperature ionic liquids, *Physical Chemistry Chemical Physics* 3, 5192-5200.
100. Jain, T. K., Varshney, M., and Maitra, A. (1989) Structural studies of Aerosol OT reverse micellar aggregates by FT-IR spectroscopy, *The Journal of Physical Chemistry* 93, 7409-7416.
101. Scatena, L. F., Brown, M. G., and Richmond, G. L. (2001) Water at Hydrophobic Surfaces: Weak Hydrogen Bonding and Strong Orientation Effects, *Science* 292, 908-912.
102. Maréchal, Y. (1994) HORIZONS IN HYDROGEN BOND RESEARCH 1993 Proceedings of the Xth Workshop \ldHorizons in Hydrogen Bond Research\rd, IR spectroscopy of an exceptional H-bonded liquid: water, *Journal of Molecular Structure* 322, 105-111.
103. Brubach, J.-B., Mermet, A., Filabozzi, A., Gerschel, A., and Roy, P. (2005) Signatures of the hydrogen bonding in the infrared bands of water, *The Journal of Chemical Physics* 122, 184509.
104. Onori, G., and Santucci, A. (1993) IR investigations of water structure in Aerosol OT reverse micellar aggregate, *The Journal of Physical Chemistry* 97, 5430-5434.
105. Das, A., Patra, A., and Mitra, R. K. (2013) Do the Physical Properties of Water in Mixed Reverse Micelles Follow a Synergistic Effect: A Spectroscopic Investigation, *The Journal of Physical Chemistry B* 117, 3593-3602.
106. Valero, M., Sanchez, F., Gomez-Herrera, C., and Lopez-Cornejo, P. (2008) Study of water solubilized in AOT/n-decane/water microemulsions, *Chemical Physics* 345, 65-72.
107. Heyden, M., Sun, J., Funkner, S., Mathias, G., Forbert, H., Havenith, M., and Marx, D. (2010) Dissecting the THz spectrum of liquid water from first principles via correlations in time and space *Proceedings of the National Academy of Sciences USA* 107, 12068-12073.
108. Walrafen, G. E. (1990) Raman spectrum of water: transverse and longitudinal acoustic modes below .apprxeq.300 cm<sup>-1</sup> and optic modes above .apprxeq.300 cm<sup>-1</sup>, *The Journal of Physical Chemistry* 94, 2237-2239.
109. Keutsch, F. N., Fellers, R. S., Brown, M. G., Viant, M. R., Petersen, P. B., and Saykally, R. J. (2001) Hydrogen Bond Breaking Dynamics of the Water Trimer in the Translational and Librational Band Region of Liquid Water, *Journal of the American Chemical Society* 123, 5938-5941.

110. Venables, D. S., Huang, K., and Schmuttenmaer, C. A. (2001) Effect of Reverse Micelle Size on the Librational Band of Confined Water and Methanol, *The Journal of Physical Chemistry B* 105, 9132-9138.
111. Perez-Hernandez, N., Luong, T. Q., Perez, C., Martin, J. D., and Havenith, M. (2010) Pore size dependent dynamics of confined water probed by FIR spectroscopy, *Physical Chemistry Chemical Physics* 12, 6928-6932.
112. Le Caer, S., Pin, S., Esnouf, S., Raffy, Q., Renault, J. P., Brubach, J. B., Creff, G., and Roy, P. (2011) A trapped water network in nanoporous material: the role of interfaces, *Physical Chemistry Chemical Physics* 13, 17658-17666.
113. Bhattacharyya, K. (2008) Nature of biological water: a femtosecond study, *Chemical Communications*, 2848-2857.
114. Bhattacharyya, K. (2001) Study of Organized Media Using Time-Resolved Fluorescence Spectroscopy, *Journal of Fluorescence* 11, 167-176.
115. Pal, S. K., Peon, J., and Zewail, A. H. (2002) Biological water at the protein surface: Dynamical solvation probed directly with femtosecond resolution, *Proceedings of the National Academy of Sciences* 99, 1763-1768.
116. Pal, S. K., Mandal, D., Sukul, D., Sen, S., and Bhattacharyya, K. (2001) Solvation Dynamics of DCM in Human Serum Albumin, *The Journal of Physical Chemistry B* 105, 1438-1441.
117. Pal, S. K., Zhao, L., and Zewail, A. H. (2003) Water at DNA surfaces: Ultrafast dynamics in minor groove recognition, *Proceedings of the National Academy of Sciences* 100, 8113-8118.
118. Verma, S. D., Pal, N., Singh, M. K., and Sen, S. (2015) Sequence-Dependent Solvation Dynamics of Minor-Groove Bound Ligand Inside Duplex-DNA, *The Journal of Physical Chemistry B* 119, 11019-11029.
119. Pal, N., Shweta, H., Singh, M. K., Verma, S. D., and Sen, S. (2015) Power-Law Solvation Dynamics in G-Quadruplex DNA: Role of Hydration Dynamics on Ligand Solvation inside DNA, *The Journal of Physical Chemistry Letters* 6, 1754-1760.
120. Sarkar, N., Datta, A., Das, S., and Bhattacharyya, K. (1996) Solvation Dynamics of Coumarin 480 in Micelles, *The Journal of Physical Chemistry* 100, 15483-15486.
121. Mitra, R., Sinha, S., and Pal, S. (2008) Interactions of Nile Blue with Micelles, Reverse Micelles and a Genomic DNA, *Journal of Fluorescence* 18, 423-432.
122. Patra, A., Hazra, S., Suresh Kumar, G., and Mitra, R. K. (2014) Entropy Contribution toward Micelle-Driven Deintercalation of Drug-DNA Complex, *The Journal of Physical Chemistry B* 118, 901-908.
123. Mandal, D., Sen, S., Bhattacharyya, K., and Tahara, T. (2002) Femtosecond study of solvation dynamics of DCM in micelles, *Chemical Physics Letters* 359, 77-82.
124. Banerjee, D., and Pal, S. K. (2008) Solvation dynamics of LDS 750 in micelles, reverse micelles and proteins, *Chemical Physics Letters* 451, 237-242.
125. Verma, P. K., Saha, R., Mitra, R. K., and Pal, S. K. (2010) Slow water dynamics at the surface of macromolecular assemblies of different morphologies, *Soft Matter* 6, 5971-5979.
126. Mitra, R. K., Sinha, S. S., Verma, P. K., and Pal, S. K. (2008) Modulation of Dynamics and Reactivity of Water in Reverse Micelles of Mixed Surfactants *The Journal of Physical Chemistry B* 112, 12946-12953.
127. Vajda, S., Jimenez, R., Rosenthal, S. J., Fidler, V., Fleming, G. R., and Castner, E. W. (1995) Femtosecond to nanosecond solvation dynamics in pure water and inside the [ $\gamma$ ]-cyclodextrin cavity, *Journal of the Chemical Society, Faraday Transactions* 91, 867-873.
128. Sen, S., Sukul, D., Dutta, P., and Bhattacharyya, K. (2001) Slow Solvation Dynamics of Dimethylformamide in a Nanocavity. 4-Aminophthalimide in  $\beta$ -Cyclodextrin, *The Journal of Physical Chemistry A* 105, 10635-10639.
129. Narayanan, S. S., Sinha, S. S., Sarkar, R., and Pal, S. K. (2008) Picosecond to nanosecond reorganization of water in AOT/lecithin mixed reverse micelles of different morphology, *Chemical Physics Letters* 452, 99-104.

130. Sarkar, R., Ghosh, M., Shaw, A. K., and Pal, S. K. (2005) Ultrafast surface solvation dynamics and functionality of an enzyme  $\alpha$ -chymotrypsin upon interfacial binding to a cationic micelle, *Journal of Photochemistry and Photobiology B: Biology* 79, 67-78.
131. Samanta, N., Das Mahanta, D., and Mitra, R. K. (2014) Does Urea Alter the Collective Water Structure: A Dielectric Relaxation Study in THz Region, *Chemistry – An Asian Journal* 9, 3457-3463.
132. Jimenez, R., Fleming, G. R., Kumar, P. V., and Maroncelli, M. (1994) Femtosecond Solvation Dynamics of Water, *Nature* 369, 471-473.
133. Cho, M., Fleming, G. R., Saito, S., Ohmine, I., and Stratt, R. M. (1994) Instantaneous normal mode analysis of liquid water, *The Journal of Chemical Physics* 100, 6672-6683.
134. Mitra, R. K., Sinha, S. S., and Pal, S. K. (2008) Temperature-Dependent Solvation Dynamics of Water in Sodium Bis(2-ethylhexyl)sulfosuccinate/Isooctane Reverse Micelles, *Langmuir* 24, 49-56.
135. Ebbinghaus, S., Kim, S. J., Heyden, M., Yu, X., Heugen, U., Gruebele, M., Leitner, D. M., and Havenith, M. (2007) An extended dynamical hydration shell around proteins, *Proceedings of the National Academy of Sciences USA* 104, 20749-20752.
136. Born, B., Weingärtner, H., Bründermann, E., and Havenith, M. (2009) Solvation Dynamics of Model Peptides Probed by Terahertz Spectroscopy. Observation of the Onset of Collective Network Motions, *Journal of the American Chemical Society* 131, 3752-3755.
137. Meister, K., Ebbinghaus, S., Xu, Y., Duman, J. G., DeVries, A., Gruebele, M., Leitner, D. M., and Havenith, M. (2013) Long-range protein–water dynamics in hyperactive insect antifreeze proteins, *Proceedings of the National Academy of Sciences* 110, 1617-1622.
138. Heugen, U., Schwaab, G., Bründermann, E., Heyden, M., Yu, X., Leitner, D. M., and Havenith, M. (2006) Solute-induced retardation of water dynamics probed directly by terahertz spectroscopy, *Proceedings of the National Academy of Sciences* 103, 12301-12306.
139. Heyden, M., and Havenith, M. (2010) Combining THz spectroscopy and MD simulations to study protein-hydration coupling *Methods* 52, 74-83.
140. Boyd, J. E., Briskman, A., Sayes, C. M., Middleman, D., and Colvin, V. (2002) Terahertz Vibrational Modes of Inverse Micelles, *The Journal of Physical Chemistry B* 106, 6346-6353.
141. Boyd, J. E., Briskman, A., Colvin, V. L., and Middleman, D. M. (2001) Direct Observation of Terahertz Surface Modes in Nanometer-Sized Liquid Water Pools, *Physical Review Letters* 87, 147401.
142. Middleman, D. M., Nuss, M. C., and Colvin, V. L. (1997) Terahertz spectroscopy of water in inverse micelles *Chemical Physics Letters* 275, 332-338.
143. Rønne, C., Thrane, L., Åstrand, P.-O., Wallqvist, A., Mikkelsen, K. V., and Keiding, S. r. R. (1997) Investigation of the temperature dependence of dielectric relaxation in liquid water by THz reflection spectroscopy and molecular dynamics simulation, *The Journal of Chemical Physics* 107, 5319-5331.
144. Rønne, C., Åstrand, P.-O., and Keiding, S. R. (1999) THz Spectroscopy of Liquid H<sub>2</sub>O and D<sub>2</sub>O, *Physical Review Letters* 82, 2888-2891.
145. Yada, H., Nagai, M., and Tanaka, K. (2008) Origin of the fast relaxation component of water and heavy water revealed by terahertz time-domain attenuated total reflection spectroscopy, *Chemical Physics Letters* 464, 166-170.
146. Polley, D., Patra, A., and Mitra, R. K. (2013) Dielectric relaxation of the extended hydration sheathe of DNA in the THz frequency region, *Chemical Physics Letters* 586, 143-147.
147. Tielrooij, K. J., Paparo, D., Piatkowski, L., Bakker, H. J., and Bonn, M. (2009) Dielectric Relaxation Dynamics of Water in Model Membranes Probed by Terahertz Spectroscopy, *Biophysical Journal* 97, 2484-2492.
148. Shiraga, K., Suzuki, T., Kondo, N., and Ogawa, Y. (2014) Hydration and hydrogen bond network of water around hydrophobic surface investigated by terahertz spectroscopy, *The Journal of Chemical Physics* 141, 235103.
149. Patra, A., Verma, P. K., and Mitra, R. K. (2012) Slow Relaxation Dynamics of Water in Hydroxypropyl Cellulose-Water Mixture Traces Its Phase Transition Pathway: A Spectroscopic Investigation, *The Journal of Physical Chemistry B* 116, 1508-1516.

150. Patra, A., Luong, T. Q., Mitra, R. K., and Havenith, M. (2013) Solvent dynamics in a reverse micellar water-pool: a spectroscopic investigation of DDAB–cyclohexane–water systems, *Physical Chemistry Chemical Physics* 15, 930-939.
151. Patra, A., Luong, T. Q., Mitra, R. K., and Havenith, M. (2014) The influence of charge on the structure and dynamics of water encapsulated in reverse micelles, *Physical Chemistry Chemical Physics* 16, 12875-12883.

## Chapter 2: Experimental Techniques and Systems

In order to explore the structure, dynamics and activity of water in restricted environments different steady-state and dynamical tools have been employed. These include solvation dynamics, fluorescence anisotropy, Fourier transform vibration stretching, THz dielectric relaxation, hydrolysis, enzyme kinetics and determination of activation energy using Arrhenius theory. In this chapter, we have included a brief discussion about the above mentioned dynamical tools. Overviews of the various systems and the fluorescent probes used in the studies have also been provided.

### 2.1. Steady State and Dynamical Tool

#### 2.1.1. Solvation Dynamics

**2.1.1.a. Theory:** Solvation dynamics relates to the way of reorganization of polar solvent molecules around a dipole created instantaneously or an electron/proton injected suddenly in a polar liquid. A change in the probe (solute) is made at time  $t = 0$  by an ultra-short excitation pulse which leads to the creation of a dipole. This dipole gives rise to an instantaneous electric field on the solvent molecules. The interaction of permanent dipoles of the solvent with the instantaneously created electric field shifts the free energy minimum of the solvent to a non-zero value of the polarization. Since the electronic excitation is much faster than the nuclear motion of atoms in molecules (according to the Frank-Condon principle), the instantaneously excited probe in the vicinity of the solvent molecules find themselves in a relatively high-energy configuration at  $t=0$ . Consequently, the solvent molecules around the probe begin to move and relax back to reach their new equilibrium positions (Figure 2.1). The nuclear motion involved in the rearrangement or relaxation process can be broadly classified into rotational and translational motions.<sup>1, 2</sup>

Owing to its extensive hydrogen bonding, the rotational motion of water would also include hindered rotation and libration, while translation would include the intermolecular vibration. There are two specific types of high frequency motions: libration and intermolecular vibration, and those are anticipated to play a leading role in the faster part of solvent relaxation. The molecular motions involved are shown schematically in Figure 2.1. In

Figure 2.2.a. we show a typical solvation time correlation function. For clarity, we approximate the motions responsible for the decay in different regions.

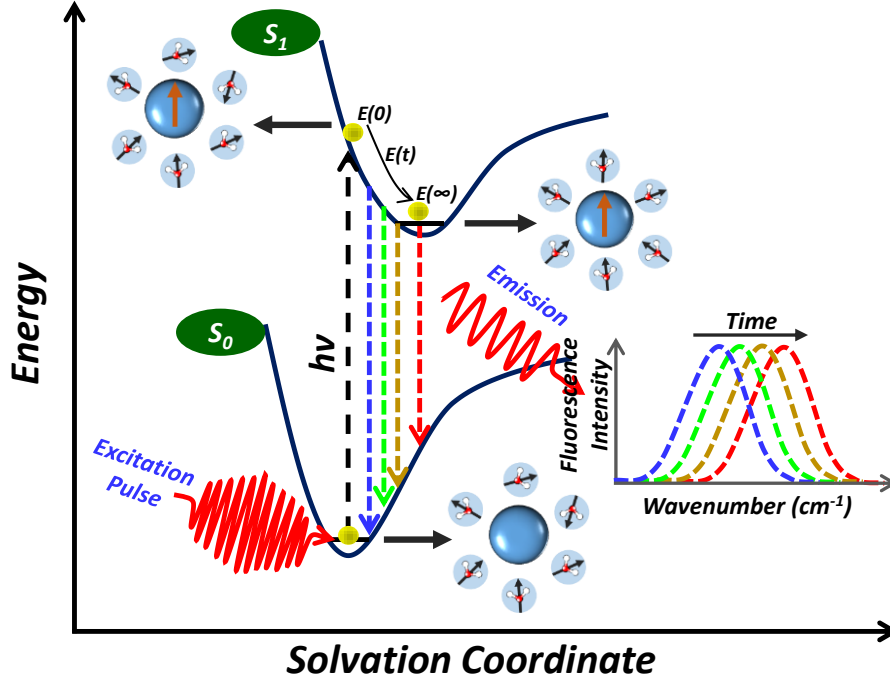


**Figure 2.1:** Schematic representation of the potential energy surfaces involved in solvation relaxation process showing the water orientational motions along the solvation coordinate together with instantaneous excitation. As solvation proceeds the energy of the solute comes down giving rise to a red shift in the fluorescence spectrum.

The solvation energy  $E_{solv}(t)$ , involved in of polar solvation dynamics can be expressed as:<sup>3, 4</sup>

$$E_{solv}(t) = -\frac{1}{2} \int dr E_0(r) \cdot P(r,t) \quad (2.1)$$

where,  $E_0(r)$   $P(r,t)$  are the instantaneously created, position-dependent electric field from the probe and is the position and time-dependent polarization.  $P(r,t)$  can be expressed as:

$$P(r,t) = \int d\Omega \mu(\Omega) \rho(r,\Omega,t) \quad (2.2)$$

where  $\mu(\Omega)$  is the dipole moment vector of a molecule at position  $\mathbf{r}$ , and  $\rho(r,\Omega,t)$  is the position ( $r$ ), orientation ( $\Omega$ ) and time ( $t$ ) dependent density. Consequently, the time dependent solvation energy is obtained by the time dependent polarization which is in turn determined by the time dependence of the density. When the perturbation generated probe on dynamics of bulk water is negligible, then the time dependence of polarization is dictated by the natural dynamics of the liquid. The detailed theoretical development of solvation dynamics can be found in the literature.<sup>5</sup>

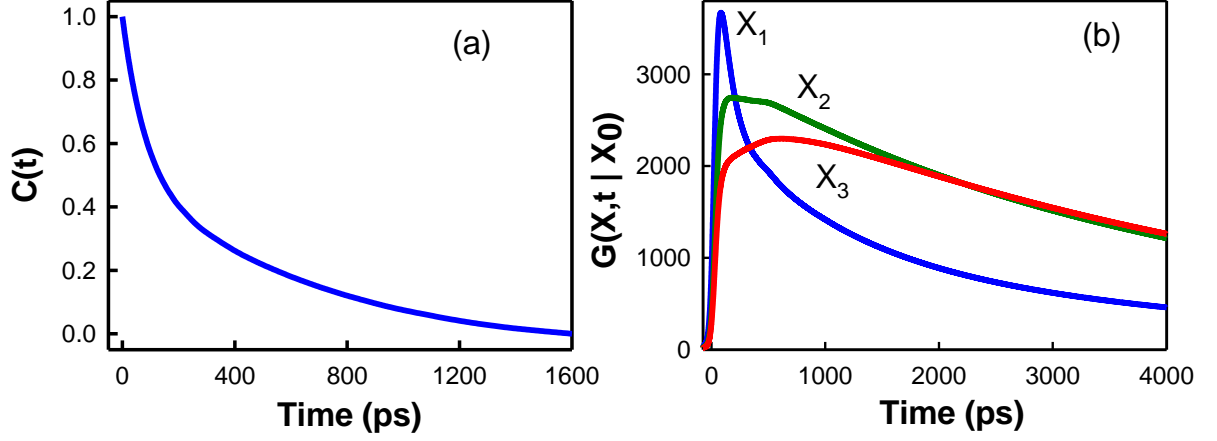


**Figure 2.2:** (a) A typical solvation time correlation function for water in restricted environment. (b) Green's function  $G(X,t|X_0)$  for population relaxation along the solvation coordinate ( $X$ ) is plotted against time in picosecond. In  $G$ ,  $X_0$  is the initial position at  $t = 0$ . This Figure shows the position and time dependence of the population fluorescence intensity. At early times (when the population is at  $X_1$ ) there is ultrafast rise followed by an ultrafast decay. At intermediate times (when the population is at  $X_2$ ) there is a rise followed by a slow decay as shown by the green line. At long times when the population is nearly relaxed (position  $X_3$ , red line) only a rise is observed.

The calculated solvation correlation function is always bi-exponential in nature. Within linear response theory, the solvation correlation function is related to the solvation energy as,

$$C(t) = \frac{\langle E(t) \rangle - \langle E(\infty) \rangle}{\langle E(0) \rangle - \langle E(\infty) \rangle} \quad (2.3)$$

where,  $\langle E(0) \rangle$ ,  $\langle E(t) \rangle$  and  $\langle E(\infty) \rangle$  are energy along the solvation coordinate of the probe at time  $t=0$ ,  $t$  and  $\infty$  respectively.

Figure 2.1 demonstrates a graphical representation of the solvation potential and the motions involved in the relaxation process for the water molecules around the instantaneously created dipole. From the shape of the potential it can be understood that the transient behaviour of the population during solvation should be a decay function on the blue edge of the spectrum and a rise function on the red edge, as depicted in Figure 2.2. These wavelength-dependent features can be explained by a global model of relaxation in which a Gaussian wave packet relaxes on a harmonic surface. The relaxation process is non-exponential and using Green's function one can explain the approaches of the wave packet along the solvation coordinate,  $X$ , to its equilibrium value. For the general non-Markovian case it is given by <sup>6</sup>,

$$G(X, t | X_0) = \frac{1}{\sqrt{2\pi \langle X^2 \rangle [1 - C^2(t)]}} \exp \left[ -\frac{[X - X_0 C(t)]^2}{2 \langle X^2 \rangle [1 - C^2(t)]} \right] \quad (2.4)$$

where  $\langle X^2 \rangle$  is the equilibrium mean square fluctuation of the polarization coordinate in the excited state surface,  $C(t)$  is the solvation correlation function described in equation (2.3) and  $X_0$  is the initial value of the packet on the solvation coordinate. Equation (2.4) describes the motion of the wave packet (polarization density) beginning at  $t = 0$  ( $X_0$ ) as a delta function and according to the solvation correlation function as  $t \rightarrow \infty$ ,  $C(t) \rightarrow 0$  and one recovers the standard Gaussian distribution. Initially, at  $t \rightarrow 0$ , the exponential is large, so the decay is ultrafast, but at long times, the relaxation slows down, ultimately to appear as a rise. In Figure 2.2b, we present the  $G(X, t | X_0)$  which decays at  $X_1$  and  $X_2$ , with different time constants, and a rise at  $X_3$  followed by a decay.

**2.1.1.b. Experimental Methods:** In order to experimentally determine the solvation correlation function of a probe in an environment, a number of fluorescence transients are taken at different wavelengths across the emission spectral range of the probe. All the collected fluorescence transients are fitted by using a nonlinear least square fitting procedure to a function,

$$\left( X(t) = \int_0^t E(t') R(t-t') dt' \right) \quad (2.5)$$

including of convolution of the instrument response function (IRF) ( $E(t)$ ) with a sum of exponentials,

$$\left( R(t) = A + \sum_{i=1}^N B_i \exp(-t/\tau_i) \right) \quad (2.6)$$

where,  $B_i$  is the pre-exponential factors,  $\tau_i$  is the characteristic lifetime of  $i^{\text{th}}$  process and a background ( $A$ ). Relative concentration in a multi-exponential decay is finally expressed as:

$$\alpha_n = \frac{B_n}{\sum_{i=1}^N B_i}. \quad (2.7)$$

The relative contribution of a particular decay component ( $f_n$ ) in the total fluorescence is defined as,

$$f_n = \frac{\tau_n B_n}{\sum_{i=1}^N B_i \tau_i} \times 100. \quad (2.8)$$

The quality of the curve fitting is controlled by reduced chi-square (0.9-1.1) and residual data. The motivation of the fitting is to resolve the decays in an analytical form appropriate for advanced data analysis.

In order to construct time resolved emission spectra (TRES) we follow the technique described in references.<sup>7, 8</sup> As described above, the emission intensity decays are analyzed in terms of the multi-exponential model,

$$I(\lambda, t) = \sum_{i=1}^N \alpha_i(\lambda) \exp(-t/\tau_i(\lambda)) \quad (2.9)$$

where  $\alpha_i(\lambda)$  are the pre-exponential factors, with  $\sum \alpha_i(\lambda) = 1.0$ . In this analysis we compute a new set of intensity decays, which are normalized so that the time-integrated intensity at each wavelength is equal to the steady-state intensity at that wavelength. Considering  $F(\lambda)$  to be the steady-state emission spectrum, we calculate a set of  $H(\lambda)$  values using,

$$H(\lambda) = \frac{F(\lambda)}{\int_0^{\infty} I(\lambda, t) dt} \quad (2.10)$$

which for multi-exponential analysis becomes,

$$H(\lambda) = \frac{F(\lambda)}{\sum_i \alpha_i(\lambda) \tau_i(\lambda)} \quad (2.11)$$

Then, the appropriately normalized intensity decay functions are given by,

$$I'(\lambda, t) = H(\lambda) I(\lambda, t) = \sum_{i=1}^N \alpha'_i(\lambda) \exp(-t/\tau_i(\lambda)) \quad (2.12)$$

where  $\alpha'_i(\lambda) = H(\lambda) \alpha_i(\lambda)$ . The values of  $I'(\lambda, t)$  are used to calculate the intensity at any wavelength and time, and thus the TRES. The values of the emission maxima and spectral width are determined by nonlinear least-square fitting of the spectral shape of the TRES. The spectral shape is assumed to follow a lognormal line shape,

$$I(\bar{\nu}) = I_0 \exp \left\{ - \left[ \ln 2 \left( \frac{\ln(\alpha + 1)}{b} \right)^2 \right] \right\} \quad (2.13)$$

with  $\alpha = \frac{2b(\bar{\nu} - \bar{\nu}_{\max})}{\Delta} - 1$  where  $I_0$  is amplitude,  $\bar{\nu}_{\max}$  is the wavenumber of the emission maximum and spectral width is given by,  $\Gamma = \Delta \left[ \frac{\sinh(b)}{b} \right]$ . The terms  $b$  and  $\Delta$  are asymmetry and width parameters, respectively and equation (2.13) reduces to a Gaussian function for  $b = 0$ . The time-dependent fluorescence Stokes shifts, as estimated from TRES are used to construct the normalized spectral shift correlation function or the solvent correlation function  $C(t)$  and is defined as,

$$C(t) = \frac{\bar{\nu}(t) - \bar{\nu}(\infty)}{\bar{\nu}(0) - \bar{\nu}(\infty)} \quad (2.14)$$

where,  $\bar{\nu}(0)$ ,  $\bar{\nu}(t)$  and  $\bar{\nu}(\infty)$  are the emission maxima (in  $\text{cm}^{-1}$ ) of the TRES at time zero,  $t$  and infinity, respectively. The  $\bar{\nu}(\infty)$  value is considered to be the emission frequency beyond which insignificant or no spectral shift is observed. The  $C(t)$  function represents the temporal response of the solvent relaxation process, as occurs around the probe following its photoexcitation and the associated change in the dipole moment.

In order to understand distribution of probe or any excited state phenomenon occurring during the excitation we have constructed time-resolved area normalized emission spectroscopy (TRANES), which is a well-established technique<sup>9, 10</sup> and is a modified version of TRES. TRANES were constructed by normalizing the area of each spectrum in TRES such that the area of the spectrum at time  $t$  is equal to the area of the spectrum at  $t = 0$ . A useful feature of this method is that presence of an iso-emissive point in the spectra identifies emission from two species, which are kinetically coupled either irreversibly or reversibly or not coupled at all.

**2.1.2. Fluorescence Anisotropy.** Anisotropy is defined as the extent of polarization of the emission from a fluorophore. These measurements are based on the principle of photo-selective excitation of those fluorophore molecules whose absorption transition dipoles are parallel to the electric vector of the polarized excitation light. In an isotropic solution, fluorophores are oriented randomly. However, upon selective excitation, partially oriented population of fluorophores with polarized fluorescence emission results. The relative angle between the absorption and emission transition dipole moments determines the maximum measured anisotropy ( $r_0$ ). The fluorescence anisotropy ( $r$ ) and polarization ( $P$ ) are defined by,

$$r = \frac{I_{\parallel} - I_{\perp}}{I_{\parallel} + 2I_{\perp}} \quad (2.15)$$

$$P = \frac{I_{\parallel} - I_{\perp}}{I_{\parallel} + I_{\perp}} \quad (2.16)$$

where  $I_{\parallel}$  and  $I_{\perp}$  are the fluorescence intensities of vertically and horizontally polarized emission when the fluorophore is excited with vertically polarized light. Polarization and anisotropy are interrelated as,

$$r = \frac{2P}{3 - P} \quad (2.17)$$

$$P = \frac{3r}{2 + r} \quad (2.18)$$

Although polarization and anisotropy provides the same information, anisotropy is preferred since the latter is normalized by the total fluorescence intensity ( $I_T = I_{\parallel} + 2I_{\perp}$ ) and in case of multiple emissive species anisotropy is additive while polarization is not. Several phenomena, including rotational diffusion and energy transfer, can decrease the measured anisotropy to values lower than the maximum theoretical values. Following a pulsed excitation the time resolved fluorescence anisotropy,  $r(t)$  of a sphere is given by,

$$r(t) = r_0 \exp(-t/\tau_{rot}) \quad (2.19)$$

where  $r_0$  is the anisotropy at time  $t = 0$  and  $\tau_{rot}$  is the rotational correlation time of the sphere.

**2.1.2.a. Theory:** For a radiating dipole the intensity of light emitted is proportional to the square of the projection of the electric field of the radiating dipole onto the transmission axis of the polarizer. The intensity of parallel and perpendicular projections are given by,

$$I_{\parallel}(\theta, \psi) = \cos^2 \theta \quad (2.20)$$

$$I_{\perp}(\theta, \psi) = \sin^2 \theta \sin^2 \psi \quad (2.21)$$

where  $\theta$  and  $\psi$  are the orientational angles of a single fluorophore relative to the z and y-axis, respectively (Figure 2.4a). In solution, fluorophores exist in random distribution and anisotropy is calculated by the excitation photoselection. Upon photoexcitation by polarized light, the molecules having absorption transition moments aligned parallel to the electric vector of the polarized light have the highest probability of absorption. For the excitation polarization along the z-axis, all molecules having an angle  $\psi$  with respect to the y-axis will be excited and the population will be symmetrically distributed about the z-axis. For

experimentally accessible molecules, the value of  $\psi$  will be in the range from 0 to  $2\pi$  with equal probability. Thus, the  $\psi$  dependency can be eliminated.

$$\langle \sin^2 \psi \rangle = \frac{\int_0^{2\pi} \sin^2 \psi d\psi}{\int_0^{2\pi} d\psi} = \frac{1}{2} \quad (2.22)$$

$$\text{and } I_{\parallel}(\theta) = \cos^2 \theta \quad (2.23)$$

$$I_{\perp}(\theta) = \frac{1}{2} \sin^2 \theta \quad (2.24)$$

Consider a collection of molecules oriented relative to the z-axis with probability  $f(\theta)$ . Then, measured fluorescence intensities for this collection after photoexcitation are,

$$I_{\parallel} = \int_0^{\pi/2} f(\theta) \cos^2 \theta d\theta = k \langle \cos^2 \theta \rangle \quad (2.25)$$

$$I_{\perp} = \frac{1}{2} \int_0^{\pi/2} f(\theta) \sin^2 \theta d\theta = \frac{k}{2} \langle \sin^2 \theta \rangle \quad (2.26)$$

where  $f(\theta)d\theta$  is the probability that a fluorophore is oriented between  $\theta$  and  $\theta+d\theta$  and is given by,

$$f(\theta)d\theta = \cos^2 \theta \sin \theta d\theta \quad (2.27)$$

$k$  is the instrumental constant. Thus, the anisotropy ( $r$ ) is defined as,

$$r = \frac{3 \langle \cos^2 \theta \rangle - 1}{2} \quad (2.28)$$

For,  $\theta = 54.7^\circ$ ,  $\cos^2 \theta = 1/3$ , the complete loss of anisotropy occurs. Thus, the fluorescence taken at  $\theta = 54.7^\circ$  with respect to the excitation polarization is expected to be free from the effect of anisotropy and is known as the magic angle emission. For collinear absorption and emission dipoles, the value of  $\langle \cos^2 \theta \rangle$  is given by the following equation,

$$\langle \cos^2 \theta \rangle = \frac{\int_0^{\pi/2} \cos^2 \theta f(\theta) d\theta}{\int_0^{\pi/2} f(\theta) d\theta} \quad (2.29)$$

Substituting equation (2.27) in equation (2.29) one can get the value of  $\langle \cos^2 \theta \rangle = 3/5$  and anisotropy value to be 0.4 (from equation (2.28)). This is the maximum value of anisotropy obtained when the absorption and emission dipoles are collinear and when no other depolarization process takes place. However, for most of the fluorophores, the value of anisotropy is less than 0.4 and it is dependent on the excitation wavelength. It is demonstrated that as the displacement of the absorption and emission dipole occurs by an angle  $\gamma$  relative to each other, it causes further loss of anisotropy (reduction by a factor of 2/5) from the value obtained from equation (2.28). Thus, the value of fundamental anisotropy,  $r_0$  is given by,

$$r_0 = \frac{2}{5} \left( \frac{3 \cos^2 \gamma - 1}{2} \right) \quad (2.30)$$

For any fluorophore randomly distributed in solution, with one-photon excitation, the value of  $r_0$  varies from -0.20 to 0.40 for  $\gamma$  values varying from  $90^\circ$  to  $0^\circ$ .

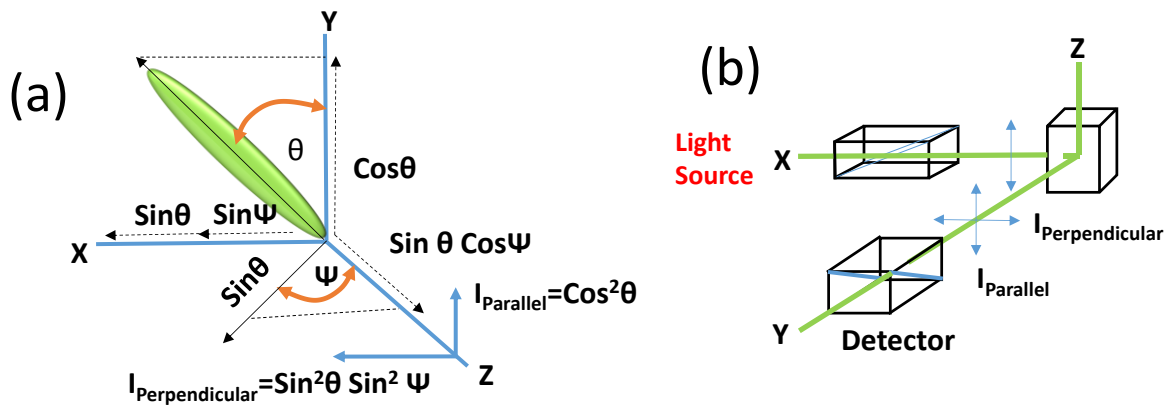


**Figure 2.3:** (a) Emission intensity of a single fluorophore (green ellipsoid) in a coordinate system. (b) Schematic representation of the measurement of fluorescence anisotropy.

**2.1.2.b. Experimental methods:** For time resolved anisotropy ( $r(t)$ ) measurements (Figure 2.3b), emission polarization is adjusted to be parallel and perpendicular to that of the excitation polarization. Spencer and Weber have derived the relevant equations for the time dependence of  $I_{\parallel}(t)$  (equation (2.31)) and  $I_{\perp}(t)$  (equation (2.32)) for single rotational and fluorescence relaxation times,  $\tau_{rot}$  and  $\tau_f$ , respectively,

$$I_{\parallel}(t) = \exp(-t/\tau_f) (1 + 2r_0 \exp(-t/\tau_{rot})) \quad (2.31)$$

$$I_{\perp}(t) = \exp(-t/\tau_f) (1 - r_0 \exp(-t/\tau_{rot})) \quad (2.32)$$

The total fluorescence is given by,

$$F(t) = I_{\parallel}(t) + 2I_{\perp}(t) = 3\exp(-t/\tau_f) = F_0 \exp(-t/\tau_f) \quad (2.33)$$

The time dependent anisotropy,  $r(t)$  is given by,

$$r(t) = \frac{I_{\parallel}(t) - I_{\perp}(t)}{I_{\parallel}(t) + 2I_{\perp}(t)} = r_0 \exp(-t/\tau_{rot}) \quad (2.34)$$

$F(t)$  depends upon  $\tau_f$  while  $r(t)$  depends upon  $\tau_{rot}$ , thus these two lifetimes can be separated. This separation is not possible in steady-state measurements. It should be noted that the degree of polarization ( $P$ ) is not independent of  $\tau_f$  and is therefore not a useful quantity as  $r$ . For reliable measurement of  $r(t)$ , three limiting cases can be considered.

- (a) If  $\tau_f < \tau_{rot}$ , the fluorescence decays before the anisotropy decays, and hence only  $r_0$  can be measured.
- (b) If  $\tau_{rot} < \tau_f$ , in contrast to steady-state measurements,  $\tau_{rot}$  can be measured in principle. The equations (2.31) and (2.32) show that the decay of the parallel and perpendicular components depends only upon  $\tau_{rot}$ . The only experimental drawback of this case is that those photons are emitted after few times period of the  $\tau_{rot}$ , cannot contribute to the determination of  $\tau_{rot}$ .
- (c) If  $\tau_{rot} \approx \tau_f$ , then it becomes the ideal situation since almost all photons are counted within the time (equal to several rotational relaxation times) in which  $r(t)$  shows measurable changes.

For systems with multiple rotational correlation times,  $r(t)$  is given by,

$$r(t) = r_0 \sum_i \beta_i e^{-t/\tau_i} \quad (2.35)$$

where  $\sum_i \beta_i = 1$ . It should be noted that the instrument monitoring the fluorescence, particularly the spectral dispersion element, responds differently to different polarizations of light, thus emerging the need for a correction factor. For example, the use of diffraction gratings can yield intensities of emission, which depends strongly upon the orientation with respect to the plane of the grating. It is inevitably necessary when using such instruments to correct for the anisotropy in response. This instrumental anisotropy is usually termed as G-factor (grating factor) and is defined as the ratio of the transmission efficiency for vertically

polarized light to that for horizontally polarized light ( $G = I_{\parallel} + I_{\perp}$ ). Hence, values of fluorescence anisotropy,  $r(t)$  corrected for instrumental response, would be given by,<sup>11</sup>

$$r(t) = \frac{I_{\parallel}(t) - GI_{\perp}(t)}{I_{\parallel}(t) + 2GI_{\perp}(t)} \quad (2.36)$$

The G-factor at a given wavelength can be determined by exciting the sample with horizontally polarized excitation beam and collecting the two polarized fluorescence decays, one parallel and other perpendicular to the horizontally polarized excitation beam. G-factor can also be determined following long time tail matching technique. If  $\tau_{rot} < \tau_f$ , it is expected that the curves for  $I_{\parallel}(t)$  and  $I_{\perp}(t)$  would become identical. If in any experiment they are not, it can usually be assumed that this is due to a non-unitary G-factor. Hence normalizing the two decay curves on the tail of the decay eliminates the G-factor in the anisotropy measurement.

Since the origin of the slower solvation time constants is diffusive in nature we analyze the anisotropy data with a wobbling-in-cone model.<sup>12-15</sup> According to this model, the rotational anisotropy decay function is defined as,

$$r(t) = r_0[\beta e^{-\frac{t}{\tau_{slow}}} + (1 - \beta)e^{-t/\tau_{fast}}] \quad (2.37)$$

where  $\beta = S^2$ , and S is the generalized order parameter that describes the degree of restriction on the wobbling-in-cone orientational motion. Its magnitude is considered as a measure of the spatial restriction of the probe and can have value from zero (for unrestricted rotation of the probe) to one (for completely restricted motion). The semicone angle  $\theta_w$  is related to the ordered parameter as,

$$S = \frac{1}{2} \cos \theta_w (1 + \cos \theta_w) \quad (2.38)$$

The diffusion coefficient for wobbling motion  $D_w$  can be obtained from the following relation,

$$D_w = \frac{1}{(1 - S^2)\tau_w} \left[ \frac{x^2(1+x)^2}{2(1-x)} \left\{ \ln\left(\frac{1+x}{2}\right) + \frac{1-x}{2} \right\} + \frac{1-x}{24} (6 + 8x - x^2 - 12x^3 - 7x^4) \right] \quad (2.39)$$

where  $x = \cos \theta_w$  and  $\tau_w$  is defined as,  $\frac{1}{\tau_w} = \frac{1}{\tau_{fast}} - \frac{1}{\tau_{slow}}$ .

**2.1.3. Arrhenius theory of activation energy:** The dynamics of solvation at a macromolecular interface can be used to extract information on the energetics of the participating water molecules. Water present at the surface of biomolecules or biomimicking systems can broadly be distinguished as bound type (water hydrogen bonded to the interface) and bulk type water. In the water layer around the surface, the interaction with water involves hydrogen bonding to the polar and charged groups of the interface. When strongly bonded to the biomacromolecules or biomimicking surfaces, the water molecules cannot contribute to solvation dynamics because they can neither rotate nor translate. However, hydrogen bonding is transient and there exists a dynamic equilibrium between the free and the bound water molecules. The potential of interaction can be represented by a double-well structure to symbolize the processes of bond breaking and bond forming. In general, the bonded water molecules become free by translational and rotational motions. The equilibrium between bound and free water can be written as,



Using the dynamic exchange model, an expression for this equilibrium can be derived. In a coupled diffusion-rotation the rate constant  $k_{\pm}$  can be written as,

$$k_{\pm} = 0.5[-B \pm (B^2 - 4D_R k_{bf})^{1/2}] \quad (2.41)$$

where  $B = 2D_R + k_{bf} + k_{fb}$  and  $D_R$  is the rotational diffusion constant,  $k_{bf}$  is the rate constant of the bound to free transition and  $k_{fb}$  is that of the reverse process. Typically, the rate constant of free to bound reaction, is larger than that for the reverse process. It can be shown that, when the rates of interconversion between “bound” and “free” water molecules are smaller as compared to  $2D_R$ , then,

$$\tau_{\text{solw}} \approx k_{bf}^{-1} \quad (2.42)$$

and from the activated complex theory one can have,

$$k_{bf} = (k_B T / h) \exp(-\Delta G^0 / RT) \quad (2.43)$$

If the transition process (2.40) follows a typical Arrhenius type of energy barrier crossing model, one can write,

$$\tau_{\text{slow}}^{-1} \approx k_{bf} = A \exp(-E_{\text{act}} / RT) \quad (2.44)$$

where  $E_{\text{act}}$  is the activation energy for the transition process and  $A$  is the pre-exponential factor. A plot of  $\ln(1/\tau_{\text{slow}})$  against  $1/T$  produces a straight line and from the slope of the line  $E_{\text{act}}$  can be calculated. The temperature dependence of the solvation follows the Arrhenius equation and yields the activation energy needed for the conversion of bound and free forms.

#### 2.1.4. Dielectric Relaxation:

**Dielectric Polarization:** Materials containing permanent or induced dipole moment are called ideal dielectrics. When dielectric materials are placed under external electric field  $\mathbf{E}$  there occurs a charge displacement which in turns creates a macroscopic non-zero dipole moment and this process is known as polarization. This polarization  $\mathbf{P}$  of dielectrics can be expressed as.<sup>16, 17</sup>

$$P = \frac{\langle M \rangle}{V} \quad (2.45)$$

Where,  $\langle M \rangle$  is the ensemble averaged macroscopic dipole moment of the whole sample,  $V$  is the volume. This microscopic polarization is directly proportional to the external electric field.

$$P_i = \varepsilon_0 \chi_{ik} E_k \quad (2.46)$$

$\chi_{ik}$  is the dielectric susceptibility tensor of the material,  $E_k$  is the component of the electric field. For an uniform and isotropic dielectric the equation can be simplified to

$$P_i = \varepsilon_0 \chi E \quad (2.47)$$

According to the macroscopic Maxwell approach, matter is treated as a continuous distribution of charges, and the electric field within the matter ( $\mathbf{E}$ ) is the direct result of electrical displacement (or electrical induction) vector  $\mathbf{D}$ , which is defined as the electric field corrected by polarization.<sup>18</sup>

$$D = \varepsilon_0 E + P \quad (2.48)$$

For a uniform isotropic dielectric medium where  $\mathbf{D}$ ,  $\mathbf{E}$  and  $\mathbf{P}$  have the same direction and a combination of equation 2.47 and 2.48 leads to

$$D = \varepsilon_0 (1 + \chi) E = \varepsilon_0 \varepsilon_s E \quad (2.49)$$

where,  $\varepsilon_l = 1 + \chi$  is the low frequency dielectric constant or static dielectric constant.

Considering equation 2.47 and 2.49 we can have the relation between polarization and electric field

$$P = \varepsilon_0(\varepsilon_s - 1)E \quad (2.50)$$

The total polarization  $\mathbf{P}$  of molecules consists of two parts: (i) the induced polarization  $\mathbf{P}_\alpha$ , caused by charge separation effects, and (ii) the orientational polarization  $\mathbf{P}_\mu$ , caused by the orientation of the permanent dipoles in the applied electric field which converts equation 2.50 into<sup>16, 19</sup>

$$P_\alpha + P_\mu = \varepsilon_0(\varepsilon_s - 1)E \quad (2.51)$$

**Dielectric Polarization in Time-Dependent Electric Fields:** The polarization induced by static electric field is always in equilibrium with the applied electric field. But in case of time dependent applied electric field the molecule needs some time to acquire the certain value of polarization. For a time dependent electric field,  $\mathbf{E}(\mathbf{t})$ , the expressions become

$$P(t) = \varepsilon_0\chi E(t) \quad (2.52)$$

and, 
$$D(t) = \varepsilon_0\varepsilon_s E(t) \quad (2.53)$$

The dynamic case is most easily studied with the help of harmonic time-varying fields. The time dependence of the electric field strength is given by,

$$E^*(t) = E_0 e^{i\omega t} \quad (2.54)$$

Where,  $E_0$  is the amplitude,  $\omega = 2\pi f$  is the angular frequency,  $f$  (Hz) is the frequency. When the motions of the microscopic particles cannot follow the harmonic electric field, the polarization and dielectric displacement will no longer be given by quasi-static relationships, i.e., equations (2.52) and (2.53). In that case, the dielectric displacement can be described also by the harmonic time dependence:

$$D^*(t) = D_0 e^{i(\omega t - \delta(\omega))} \quad (2.55)$$

Here,  $\delta(\omega)$  is the phase difference with respect to the external electric field for a given frequency  $\omega$ . Combining  $E^*$  and  $D^*$  (as presented in the equation (2.54) and (2.55)) in the form of equation (2.49) one can obtain complex frequency dependent dielectric permittivity  $\varepsilon^*(\omega)$ :

$$\varepsilon^*(\omega) = \frac{D_0}{E_0} e^{-i\delta(\omega)} \quad (2.56)$$

Using Euler's relations the frequency dependent dielectric permittivity  $\varepsilon^*(\omega)$  is expressed as

$$\varepsilon^*(\omega) = \varepsilon'(\omega) - i\varepsilon''(\omega) \quad (2.57)$$

where  $\varepsilon'(\omega) = \frac{D_0(\omega)}{E_0(\omega)} \cos[\delta(\omega)]$ ,  $\varepsilon''(\omega) = \frac{D_0(\omega)}{E_0(\omega)} \sin[\delta(\omega)]$  and  $\frac{\varepsilon''(\omega)}{\varepsilon'(\omega)} = \tan[\delta(\omega)]$

**Relaxation Function:** When the applied electric field is suddenly switched on, the polarization of the dielectric reaches its equilibrium value not instantaneously, rather after a characteristic period of time. By analogy, when the field is suddenly removed, the relaxation or decay function of the dielectric polarization  $\varphi(\mathbf{t})$  describes the polarization decay  $\mathbf{P}(\mathbf{t})$  caused by thermal motion<sup>20</sup>

$$\varphi(t) = \frac{P(t)}{P(0)} \quad (2.58)$$

where  $\mathbf{P}(\mathbf{t})$  is a time dependent polarization vector. The expression for the displacement vector  $\mathbf{D}(\mathbf{t})$  becomes:

$$D(t) = \varepsilon_0 \left[ \varepsilon_\infty E(t) + \int_{-\infty}^t \Phi(t') E(t-t') dt' \right] \quad (2.59)$$

$$D(t) = \varepsilon_0 \varepsilon_\infty E(t) + P(t) \quad (2.60)$$

where  $\Phi(t)$  is the dielectric response function,  $\Phi(t) = (\varepsilon_s - \varepsilon_\infty)[1 - \varphi(t)]$ . For a given relaxation process  $\varepsilon_s$  and  $\varepsilon_\infty$  are the low and high frequency limits of the permittivity. The frequency dependent complex permittivity  $\varepsilon^*(\omega)$  is connected to the above relaxation function through Laplace transformation,<sup>17, 20, 21</sup>

$$\frac{\varepsilon^*(\omega) - \varepsilon_\infty}{\varepsilon_s - \varepsilon_\infty} = \hat{L} \left[ \frac{d}{dx} \varphi(t) \right] \quad (2.61)$$

Where  $\hat{L}$  is the operator of the Laplace transformation, which is defined for the arbitrary time dependent function  $f(t)$  as:  $\hat{L}[f(t)] \equiv F(\omega) = \int_0^\infty e^{-pt} f(t) dt$ ,  $p = x + i\omega$  and  $x \rightarrow 0$ . Equation (2.61) indicates that dielectric response of the systems can be measured providing the data are in the form of frequency or time dependent complex dielectric constant. When the relaxation process obeys simple exponential law<sup>16, 21, 22</sup>

$$\varphi(t) = e^{-t/\tau_m} \quad (2.62)$$

where  $\tau_m$  represents characteristic relaxation time, the well-known Debye formula can be obtained by combining equations (2.61) and (2.62):

$$\frac{\varepsilon^*(\omega) - \varepsilon_\infty}{\varepsilon_s - \varepsilon_\infty} = \frac{1}{1 + i\omega\tau_m} \quad (2.63)$$

Which leads to 
$$\varepsilon^*(\omega) = \varepsilon_\infty + \frac{\varepsilon_s - \varepsilon_\infty}{1 + i\omega\tau} \quad (2.64)$$

## 2.2. Systems:

**2.2.a. Micelle:** Micelles can be represented as aggregates of surfactant molecules having hydrophilic heads oriented towards the dissolving solvent (here water) and the hydrophobic tails ordering towards the inside part of the assembly (the micellar core) (Figure 2.4).

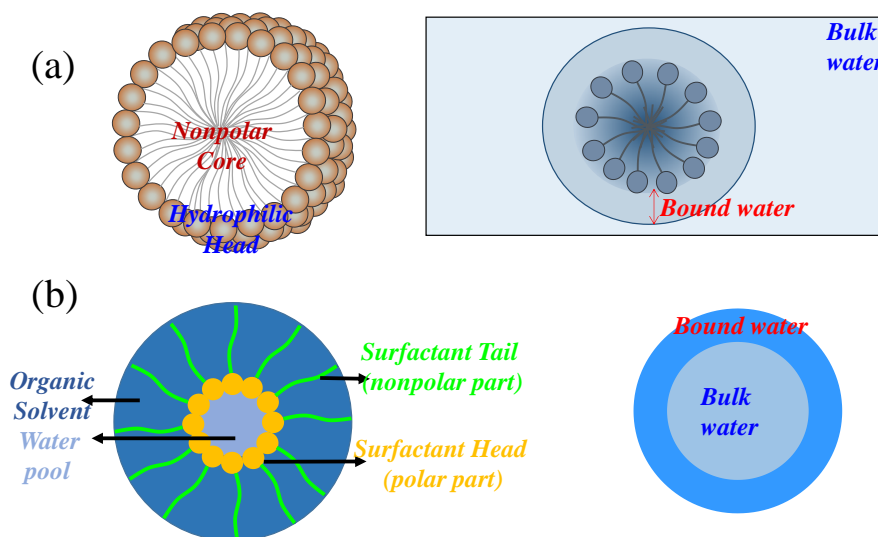


**Figure 2.4.** (a) Schematic presentation of a micelle with its hydrophobic core and hydrophilic surface. (b) Reverse micelle with organic solvent continuum, water pool and surfactants.

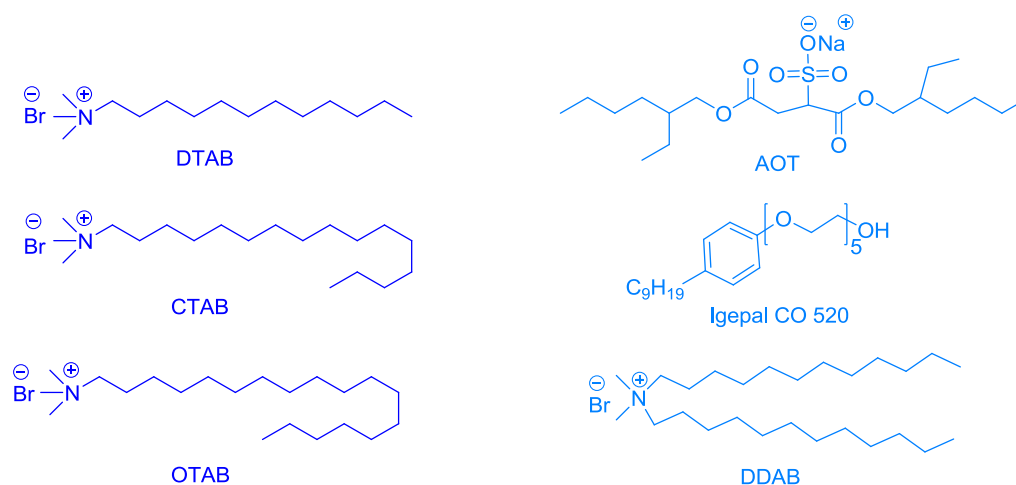


**Figure 2.5.** List of surfactant molecules used for micelle and reverse micelle preparation.

Micelles appear as the dominant form above the so-called ‘critical micelle concentration’, CMC, however, free surfactants are also present in the system as monomers. The aggregation number (the average number of surfactant molecules in a micelle) is dependent on the surfactant type and its concentration.<sup>23</sup> Micelles form strongly hydrogen bonded hydration layer at interface, the thickness of the hydration layer depends on the polar nature of the surfactant head group as well as on the nonpolar chain length of the surfactant. A schematic diagram of micelle with hydration layer in right panel of Figure 2.4.a. Dodecyltrimethylammonium bromide (DTAB), cetyltrimethylammonium bromide (CTAB) and octadecyltrimethylammonium bromide (OTAB) surfactants are used for micelle preparation (molecular structures of these surfactants given in the left panel of Figure 2.5).

**2.2.b. Reverse Micelle:** Reverse micelle (RM) are isotopic mixture of water, surfactant, and organic solvent in which small aqueous droplets coated with a layer of surfactant molecules are dispersed in a nonpolar solvent.<sup>24</sup> In this thesis three surfactants have been used with differently charged head groups, anionic AOT (Sodium 1,4-bis(2-ethylhexoxy)-1,4-dioxobutane-2-sulfonate), nonionic Igepal (Igepal CO-520) and cationic DDAB (didodecyldimethylammonium bromide) (molecular structures of these surfactants given in the left panel of Figure 2.5). Cyclohexane (Cy) has been used as the hydrocarbon phase to prepare RM using all the three surfactants. AOT is soluble in Cy and produces RM systems up to  $w_0 (= [Water]/[Surfactant]) \sim 20$ .<sup>25, 26</sup> Igepal has is also capable to form well defined spherical RM up to  $w_0=20$ .<sup>25</sup> The size of RMs in both the systems increases linearly with  $w_0$  with Igepal forming slightly bigger RMs compared to that of AOT.<sup>27, 28</sup> DDAB in Cy offers a unique class of RM systems; small angle neutron scattering (SANS) studies<sup>29, 30</sup> for the DDAB–Cy–water system have concluded that at low hydration ( $2 \leq w_0 \leq 8$ ), the system consists mainly of aggregated rod-like cylinders having their length in the range of 14–20 nm, and radius varying from 1.5 to 1.6 nm. As hydration is increased ( $w_0 \sim 10$ ) spherical aggregates are formed with diameter in the range of  $\sim 6$  nm. The highest solubilization capacity of DDAB/Cy system has been observed to be  $\sim 13$ .<sup>26</sup>

**2.2.c. Water-Polymer Mixture:** Hydroxy propyl cellulose (HPC) is a water soluble derivative of cellulose with ether linkage (Figure 2.6). This polymeric material has a weight-average molecular mass,  $M_w = 80000$ . With the combination of hydrophobic and hydrophilic groups HPC shows a lower critical solution temperature (LCST) in water  $\sim 40^\circ\text{C}$ .<sup>31</sup> Below this temperature it is soluble in water but above LCST it is no more soluble in water. HPC molecule take on a helical conformation in the crystalline state. At low concentration in water

HPC forms an isotropic liquid crystal phase<sup>32</sup> which grows into an ordered cholesteric liquid crystalline phase at ~ 40 wt% HPC in water.

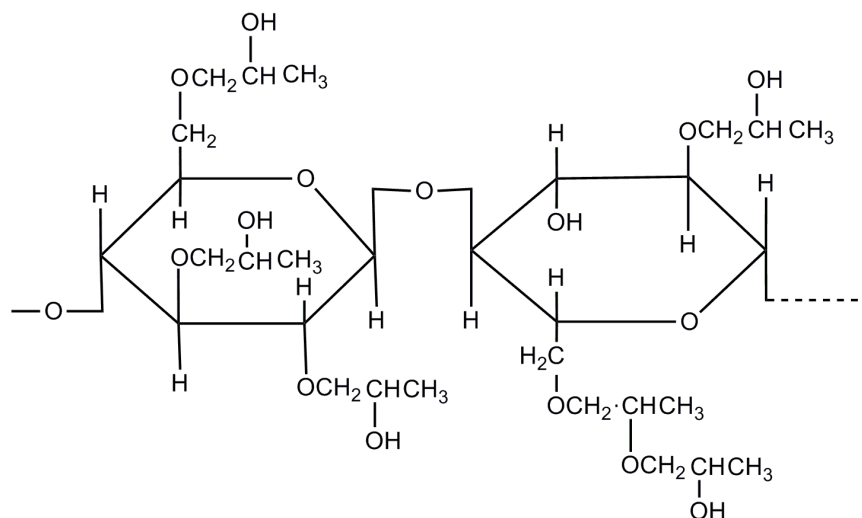


**Figure 2.6.** Molecular structure of HPC monomers with ether linkage.

**2.2.d  $\alpha$ -Chymotrypsin (CHT):**  $\alpha$ -chymotrypsin (Figure 2.5), isolated from bovine pancreas, is a member of the family serine endopeptidase (molecular weight of 25,191 Da) catalysing the hydrolysis of peptides in the small intestine. The three dimensional structure of CHT was solved by David Blow.<sup>33</sup> The molecule is a three-dimensional ellipsoid of dimensions  $51 \times 40 \times 40 \text{ \AA}$  and comprises of 245 amino acid residues. CHT contains several antiparallel  $\beta$ -pleated sheet regions and little  $\alpha$ -helix content. All charged groups are on the surface of the molecule except the catalytic triad of histidine57 (His57), aspartate102 (Asp102) and serine195 (Ser195), which are essential for catalysis. The Ser195 residue is hydrogen bonded to His57 residue, which in turn is hydrogen bonded to  $\beta$ -carboxyl group of Asp102. An oxyanion hole is formed by amide nitrogen of glycine193 and Ser195. It is selective for hydrolysing peptide bonds on the carboxyl side of the aromatic side chains of tyrosine, tryptophan and phenylalanine and of large hydrophobic residues such as methionine. It also catalyses the hydrolysis of ester bonds. CHT enhances the rate of peptide hydrolysis by a factor of  $10^9$ . The reaction has two distinct phases, acylation and deacylation of the enzyme. Upon binding of the substrate, the hydroxyl group of the Ser195 attacks the carbonyl group of peptide bond to generate a tetrahedral intermediate. In this transient structure, the oxygen atom of the substrate now occupies the oxyanion hole. The acyl-enzyme intermediate forms, assisted by the proton donation of His57. The N-terminal portion is then released and replaced by water. The acyl-enzyme intermediate subsequently undergoes hydrolysis and the enzyme is regenerated.

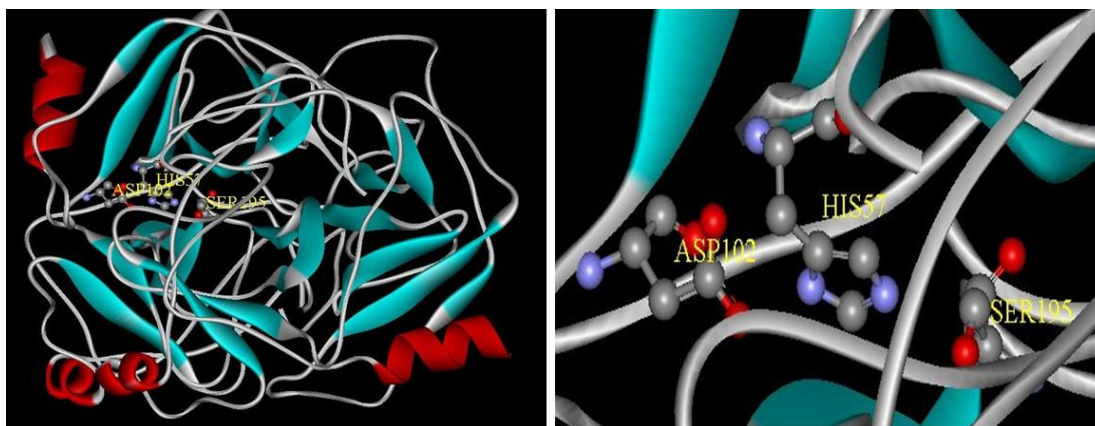


**Figure 2.7:** X-ray crystallographic structure (PDB code: 1YPH) of  $\alpha$ -chymotrypsin depicting the catalytic triad (His57, Asp102 and Ser195).

**2.2.e. Protease Substrates: A. Ala-Ala-Phe-7-amido-4-methylcoumarin:** AMC is a fluorescent aromatic tripeptide substrate (Figure 2.8) suitable for the cleavage by serine protease. Its concentration is determined using the extinction coefficient,  $\epsilon = 16 \text{ mM}^{-1}\text{cm}^{-1}$  at 325 nm. The rate of catalytic activity is determined by monitoring absorbance of cleaved product (7-amido-4-methylcoumarin) having  $\epsilon = 7.6 \text{ mM}^{-1}\text{cm}^{-1}$  at 370 nm in aqueous buffer solution.<sup>34</sup>

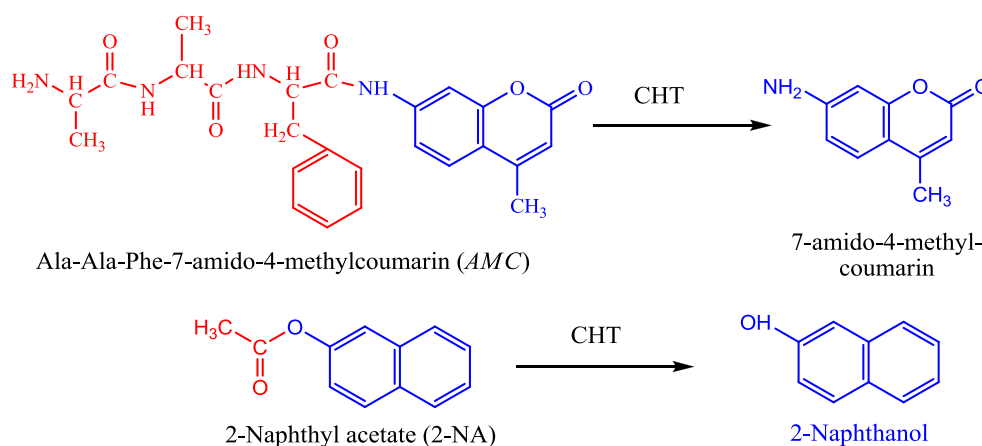


**Figure 2.8.** Molecular structure of substrates and chymotrypsin catalysed hydrolysis product formed from the substrates. (Only spectroscopy monitored products are given, other products are not shown in the figure)

**B. 2-Naphthyl Acetate:** 2-NA has an ester linkage next to the aromatic ring which makes it a suitable protease substrate. 2-NA is almost insoluble water so the concentrated 2-NA stock solution is prepared by dissolving quantitative amount of 2-NA in 10% (v/v) ethanol/water mixture. However, during enzymatic assays the concentration of alcohol in solution was always <4% in order to avoid the effect of alcohol on the enzyme structure. The absorbance of hydrolysed product 2-naphthol is monitored at 330 nm and the concentration of the product

was measured using  $\epsilon=1.53 \times 10^3 \text{ M}^{-1} \text{ cm}^{-1}$ .<sup>35</sup> The molecular structures of 2-Naphthyl acetate and 2-Naphthol are shown in the Figure 2.8.

#### 2.2.f. Molecular Probes:

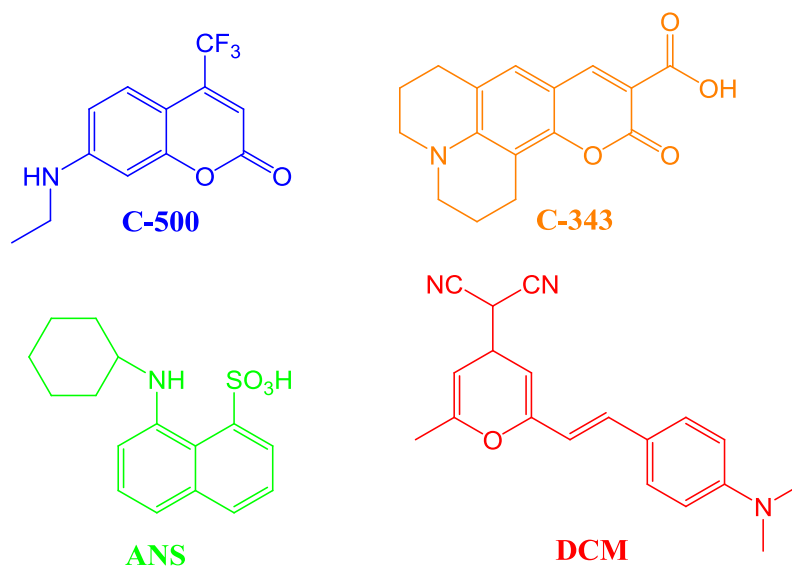


**Figure 2.9:** Molecular structure of C-500, C-343, ANS and, DCM

**A. Coumarin 500 (C500):** The solvation probe C500 (Figure 2.9) is sparingly soluble in water and shows reasonably good solubility in isooctane. In bulk water the absorption peak (400 nm) is significantly red shifted compared to that in isooctane (360 nm). The emission peak of C500 in bulk water (500 nm) also shows a 90 nm red shift compared to that in isooctane (excitation at 350 nm). The significantly large solvchromic effect in the absorption and emission spectra of C500 makes the dye an attractive solvation probe for micro-heterogeneous environments. The photophysics of the probe have previously been studied in details.<sup>36</sup>

**B. Coumarin 343:** C-343 is water soluble dye, however, is insoluble in organic solvent like cyclohexane. Absorption spectrum of C-343 in water produces a peak ~425 whereas in benzene the peak shifts to 442 nm. Upon excitation at 409 nm C-343 produces emission maximum at 490 nm in water and 462 nm in benzene. The photophysics of C-343 in organic solvents had been studied in detail.<sup>37</sup> The molecular structure of C-343 is given in the Figure 2.9.

**C. 1-anilino-8-naphthalenesulfonic acid, ammonium salt (ANS):** ANS is a well-known solvation probe<sup>38</sup> in aqueous solution, the emission quantum yield of ANS is very small (0.004) with emission peak at ~520 nm and a lifetime of ~0.25 ns. The steady-state emission

is quenched dramatically in polar solvents. Because of its bichromophoric structure, ANS is known to undergo charge transfer (CT) from one aromatic moiety to the other ring. In nonpolar solvents, the emission is strong and is mostly from the locally excited state i.e., before charge separation. In polar solvents, the fluorescence decreases and is dominated by the emission from the CT state.

**D. 4-di-(cyanomethylene)-2-methyl-6-(*p*-dimethylaminostyryl)-4H-pyran (DCM):** DCM (Figure 2.9) is insoluble in water, however is soluble polar organic solvent like ethanol and hydrocarbon solvents like n-heptane. DCM possess a considerable high dipole moment in the excited state (26.3 D) compared to its ground state (5.6 D).<sup>39</sup> Femtosecond studies revealed various intramolecular processes in the excited state of DCM e.g. electron transfer process and twisted intramolecular charge-transfer.<sup>40</sup> In n-heptane DCM produce two absorption peaks at ~430 nm and ~470 nm whereas the absorption peak in methanol appears at ~470 nm. The emission peak at ~570 nm is very weak in n-heptane with a quantum yield  $\phi=0.01$ , however, in polar solvent like methanol the quantum yield becomes as high as  $\phi=0.44$  with a peak position at ~625 nm.

## References:

1. Pal, S. K., Peon, J., Bagchi, B., and Zewail, A. H. (2002) Biological Water: Femtosecond Dynamics of Macromolecular Hydration, *The Journal of Physical Chemistry B* 106, 12376-12395.
2. Fleming, G. R., and Cho, M. (1996) Chromophore-Solvent Dynamics, *Annual review of physical chemistry* 47, 109-134.
3. Bagchi, B. (1989) Dynamics of Solvation and Charge Transfer Reactions in Dipolar Liquids, *Annual Review of Physical Chemistry* 40, 115-141.
4. Bagchi, B., and Biswas, R. (2007) Polar and Nonpolar Solvation Dynamics, Ion Diffusion, and Vibrational Relaxation: Role of Biphasic Solvent Response in Chemical Dynamics, In *Advances in Chemical Physics*, pp 207-433, John Wiley & Sons, Inc.
5. Bagchi, B., and Biswas, R. (1999) Polar and nonpolar solvation dynamics, ion diffusion, and vibrational relaxation: role of biphasic solvent response in chemical dynamics, *Advances in Chemical Physics* 109, 207-433.
6. Hynes, J. T. (1986) Outer-sphere electron transfer reactions and frequency-dependent friction, *The Journal of Physical Chemistry* 90, 3701-3706.
7. Horng, M. L., Gardecki, J. A., Papazyan, A., and Maroncelli, M. (1995) Subpicosecond measurements of polar solvation dynamics: coumarin 153 revisited, *The Journal of Physical Chemistry* 99, 17311-17337.
8. Lakowicz, J. R. (1999) *Principles of fluorescence spectroscopy*, Kluwer Academic/Plenum, New York.
9. Periasamy, N., and Koti, A. S. R. (2003) Time resolved fluorescence spectroscopy: TRES and TRANES, *Proceedings of Indian Academy of Sciences* 69A, 41-48.
10. Koti, A. S. R., Krishna, M. M. G., and Periasamy, N. (2001) Time-resolved area-normalized emission spectroscopy (TRANES): A novel method for confirming emission from two excited states, *The Journal of Physical Chemistry A* 105, 1767-1771.
11. Lakowicz, J. R. (2006) *Principles of Fluorescence Spectroscopy*, 2nd ed., Kluwer Academic/Plenum, New York.

12. Lipari, G., and Szabo, A. (1980) Effect of librational motion on fluorescence depolarization and nuclear magnetic resonance relaxation in macromolecules and membranes, *Biophysical Journal* 30, 489.
13. Wang, C. C., and Pecora, R. (1980) Time-correlation functions for restricted rotational diffusion, *The Journal of Chemical Physics* 72, 5333-5340.
14. Tan, H.-S., Piletic, I. R., and Fayer, M. D. (2005) Orientational dynamics of water confined on a nanometer length scale in reverse micelles, *The Journal of Chemical Physics* 122, 174501.
15. Mitra, R. K., Sinha, S. S., and Pal, S. K. (2008) Temperature-Dependent Solvation Dynamics of Water in Sodium Bis(2-ethylhexyl)sulfosuccinate/Isooctane Reverse Micelles, *Langmuir* 24, 49-56.
16. Yuri Feldman, P. B. I., Alexander Puzenko, Valerică Raicu (2015) *Elementary Theory of the Interaction of Electromagnetic Fields with Dielectric Materials*, Oxford University Press, Oxford.
17. Fröhlich, H. (1958) *Theory of dielectrics: dielectric constant and dielectric loss*, Clarendon Press.
18. Böttcher, C. J. F., van Belle, O. C., Bordewijk, P., and Rip, A. (1978) *Theory of electric polarization*, Vol. 2, Elsevier Science Ltd.
19. Davies, M., Hill, N., Vaughan, W., and Price, A. (1969) Dielectric properties and molecular behaviour.
20. Bötcher, C., and Bordewijk, P. (1978) *Theory of Electric Polarization*, vol. II, Dielectrics in Time-Dependent Fields, Elsevier Science.
21. Feldman, Y., Puzenko, A., and Ryabov, Y. (2006) Dielectric Relaxation Phenomena in Complex Materials, *Advances in chemical physics* 133, 1.
22. Debye, P. J. W. (1929) *Polar molecules*, Chemical Catalog Company, Incorporated.
23. Biasutti, M. A., Abuin, E. B., Silber, J. J., Correa, N. M., and Lissi, E. A. (2008) Kinetics of reactions catalyzed by enzymes in solutions of surfactants, *Advances in Colloid Interface Science* 136, 1-24.
24. Moulik, S. P., and Paul, B. K. (1998) Structure, dynamics and transport properties of microemulsions, *Advances in Colloid and Interface Science* 78, 99-195.
25. Das, A., Patra, A., and Mitra, R. K. (2013) Do the Physical Properties of Water in Mixed Reverse Micelles Follow a Synergistic Effect: A Spectroscopic Investigation, *The Journal of Physical Chemistry B* 117, 3593-3602.
26. Paul, B. K., and Mitra, R. K. (2005) Water solubilization capacity of mixed reverse micelles: Effect of surfactant component, the nature of the oil, and electrolyte concentration, *Journal of Colloid and Interface Science* 288, 261-279.
27. Kinugasa, T., Kondo, A., Nishimura, S., Miyauchi, Y., Nishii, Y., Watanabe, K., and Takeuchi, H. (2002) Estimation for size of reverse micelles formed by AOT and SDEHP based on viscosity measurement, *Colloids and Surfaces, A: Physicochemical and Engineering Aspects* 204, 193-199.
28. Lipgens, S., Schuebel, D., Schlicht, L., Spilgies, J.-H., Ilgenfritz, G., Eastoe, J., and Heenan, R. K. (1998) Percolation in Nonionic Water (w/o)-Microemulsion Systems: A Small Angle Neutron Scattering Study, *Langmuir* 14, 1041-1049.
29. Eastoe, J., and Heenan, R. K. (1994) Water-induced structural changes within the L2 phase of didodecyldimethylammonium bromide–cyclohexane–water systems, *Journal of the Chemical Society, Faraday Transactions* 90, 487-492.
30. Eastoe, J. (1992) Small-angle neutron scattering from dilute didodecyldimethylammonium bromide water-in-oil microemulsions. Evidence for polymer-like aggregates, *Langmuir* 8, 1503-1506.
31. Phillies, G. D. J., and Quinlan, C. A. (1995) Analytic structure of the solutionlike-meltlike transition in polymer dynamics, *Macromolecules* 28, 160-164.
32. Werbowyj, R. S., and Gray, D. G. (1980) Ordered Phase Formation in Concentrated Hydroxypropylcellulose Solutions, *Macromolecules* 13, 69-73.
33. Birktoft, J. J., and Blow, D. M. (1972) The Structure of Crystalline Alpha-Chymotrypsin, V. The Atomic Structure of Tosyl-Alpha-Chymotrypsin at 2 Angstroms Resolution, *Journal of Molecular Biology* 68, 187-240.
34. Biswas, R., and Pal, S. K. (2004) Caging enzyme function:  $\alpha$ -chymotrypsin in reverse micelle, *Chemical Physics Letters* 387, 221-226.
35. Abuin, E., Lissi, E., and Duarte, R. (2003) Kinetics of 2-naphthyl acetate hydrolysis catalyzed by  $\alpha$ -chymotrypsin in aqueous solutions of dodecyltrimethylammonium bromide, *Langmuir* 19, 5374-5377.

36. Nad, S., and Pal, H. (2003) Photophysical Properties of coumarin-500 (C500): unusual behavior in nonpolar solvents, *The Journal of Physical Chemistry A* 107, 501-507.
37. Gutierrez, J. A., Falcone, R. D., Silber, J. J., and Correa, N. M. (2010) Role of the medium on the C343 inter/intramolecular hydrogen bond interactions. an absorption, emission, and <sup>1</sup>HNMR investigation of C343 in benzene/n-heptane mixtures, *The Journal of Physical Chemistry A* 114, 7326-7330.
38. DeToma, R. P., Easter, J. H., and Brand, L. (1976) *Journal of the American Chemical Society* 98, 5001-5007.
39. Pal, S. K., Mandal, D., Sukul, D., and Bhattacharyya, K. (1999) Solvation dynamics of 4-(dicyanomethylene)-2-methyl-6-(p-dimethylaminostyryl)-4H-pyran (DCM) in a microemulsion, *Chemical physics letters* 312, 178-184.
40. Gustavsson, T., Baldacchino, G., Mialocq, J.-C., and Pommeret, S. (1995) A femtosecond fluorescence up-conversion study of the dynamic Stokes shift of the DCM dye molecule in polar and non-polar solvents, *Chemical physics letters* 236, 587-594.

## Chapter 3: Instruments and Sample preparation

In this chapter we will discuss the instrumental setup and sample preparation methods used throughout the study.

### 3.1 Instrumental Setup:

#### 3.1.1. Steady State Absorption and Emission Technique:

Steady-state UV-Vis absorption and emission spectra of the probe molecules were measured with Shimadzu UV-2450 spectrophotometer and Jobin Yvon Fluoromax-3 fluorimeter, respectively. Schematic ray diagrams of these two instruments are shown in Figures 3.1 and 3.2.

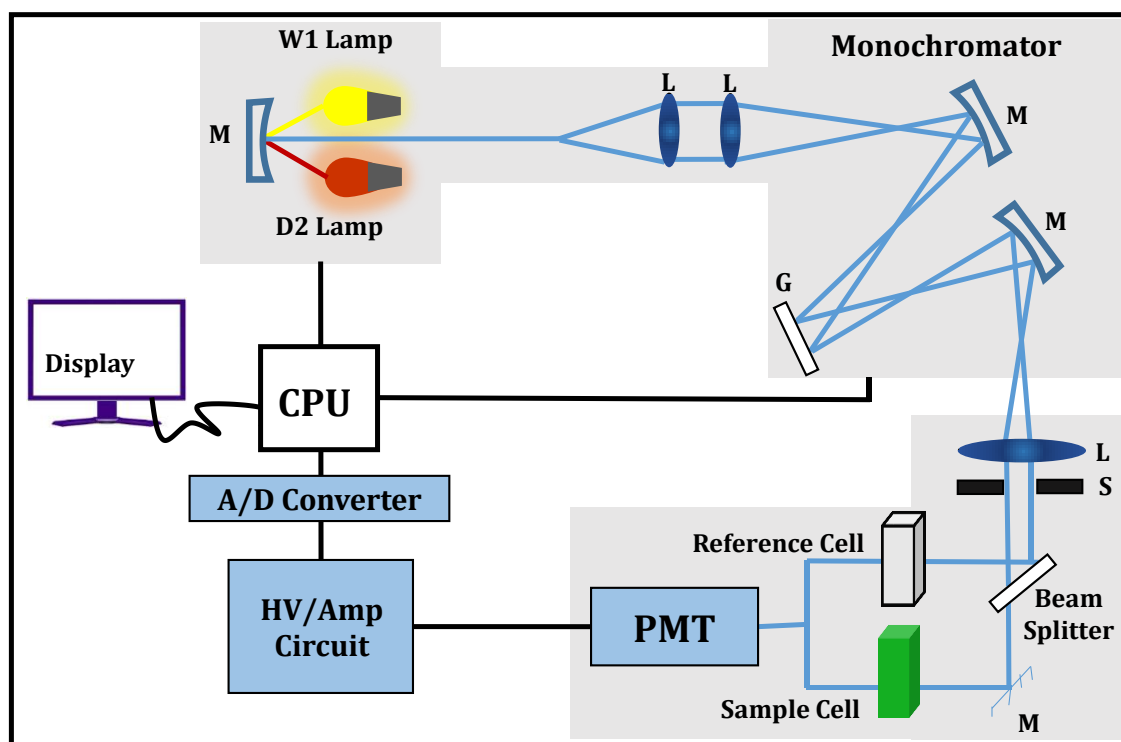


**Figure 3.1.** Schematic ray diagram of an absorption spectrophotometer. Tungsten halogen (W1) and Deuterium lamps (D2) are used as light sources in the visible and UV regions, respectively. M, G, L, S, PMT designate mirror, grating, lens, shutter and photomultiplier tube, respectively. CPU, A/D converter and HV/Amp indicate central processing unit, analog to digital converter and High-voltage/Amplifier circuit, respectively.

Shimadzu UV-2450 gives us the facility to measure absorption spectrum from 190-900 nm with a spectral resolution of 0.1 nm however, experiments are carried out at 1 nm wavelength interval by a cuvette of 1 cm path length. A Deuterium light is used as ultraviolet light source and tungsten light used as visible light source with a lamp interchange wavelength of 282-293 nm. The only monochromator used in this instrument consist high performance blazed

holographic grating and photomultiplier tube (PMT) used as a detector. All the absorption spectra collected prior to baseline correction by reference sample. Working principle of UV-Vis spectroscopy follow Beer's Lambert law according to this law if  $I_0$  is the intensity of light incident on the cell, and  $I$  is that of the emergent light, then absorbance is given by,

$$A = \log_{10}\left(\frac{I_0}{I}\right) = \epsilon cl \quad (3.1)$$

where,  $A$  is proportional to the concentration ( $c$ ) of the optically active substance and optical path length ( $l$ ). If ' $c$ ' is in mole  $l^{-1}$  and ' $l$ ' is in cm, then  $\epsilon$  is called the molar absorptivity or molar extinction coefficient.

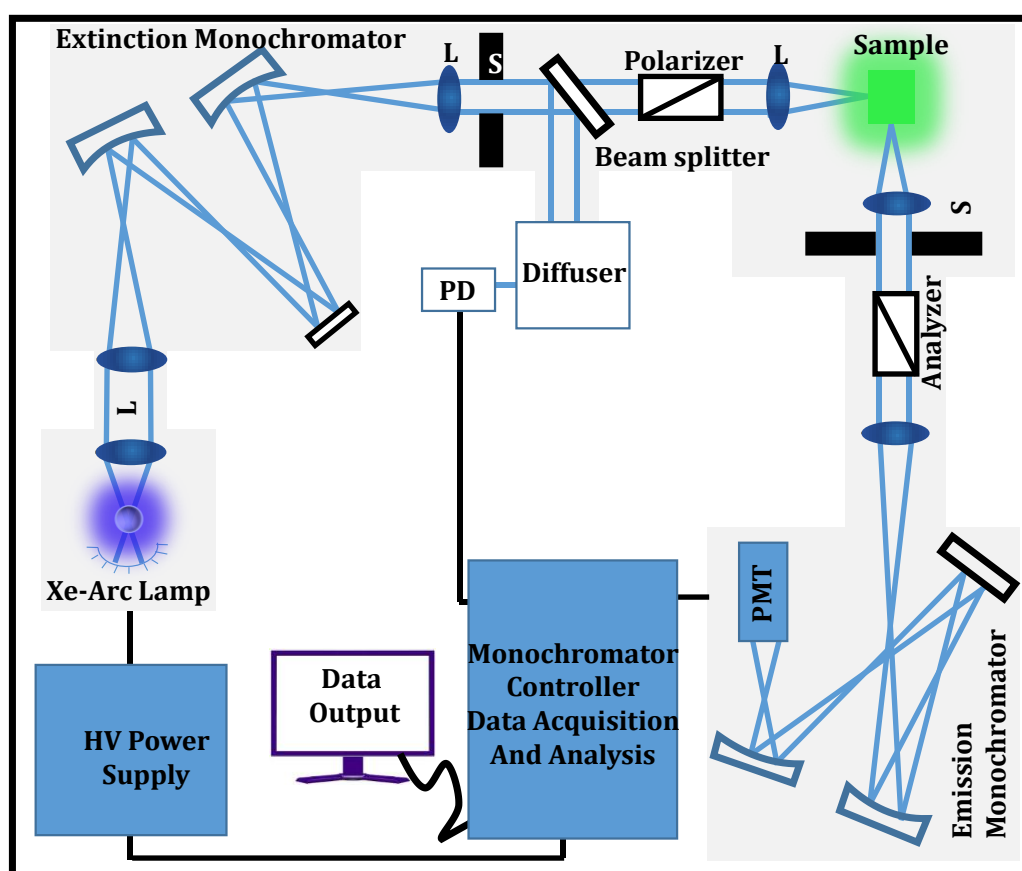


**Figure 3.2.** Schematic ray diagram of an emission spectrofluorimeter.  $M$ ,  $G$ ,  $L$ ,  $S$ ,  $PMT$  and  $PD$  represent mirror, grating, lens, shutter, photomultiplier tube and reference photodiode, respectively.

In Fluoromax-3 an ozone free Xe-Arc lamp has been used as a source of continuous wave light. A Fluoromax-3 consist of two monochromators<sup>1</sup> which are excitation and emission monochromator. The essential part of these monochromators is reflection grating, the gratings of Fluoromax contains 1200 grooves/mm and are blazed at 330 nm (excitation) and 500 nm (emission). These gratings give an excitation wavelength coverage 220-600 nm and

emission wavelength coverage 290-850 nm. All the excitation and emission spectrum are collected in quartz cuvette of 1 cm path length and at 1 nm wavelength interval.

**3.1.2. Circular Dichroism (CD) Spectroscopy:** CD is a form of spectroscopy<sup>2</sup> based on the differential absorption of left and right-handed circularly polarized light. It can be used to determine the structure of macromolecules (including the secondary structure of proteins and the handedness of DNA). All the CD measurements were done in a JASCO J-815 spectropolarimeter with a temperature controller attachment (Peltier) (Figure 3.3). The CD spectra were acquired using a quartz cell of 1 cm path length. For proteins, the typical concentration used for CD measurements were within 10  $\mu\text{M}$ . The secondary structural data of proteins were analysed using CDNN (<http://bioinformatik.biochemtech.uni-halle.de/cdnn>) software.

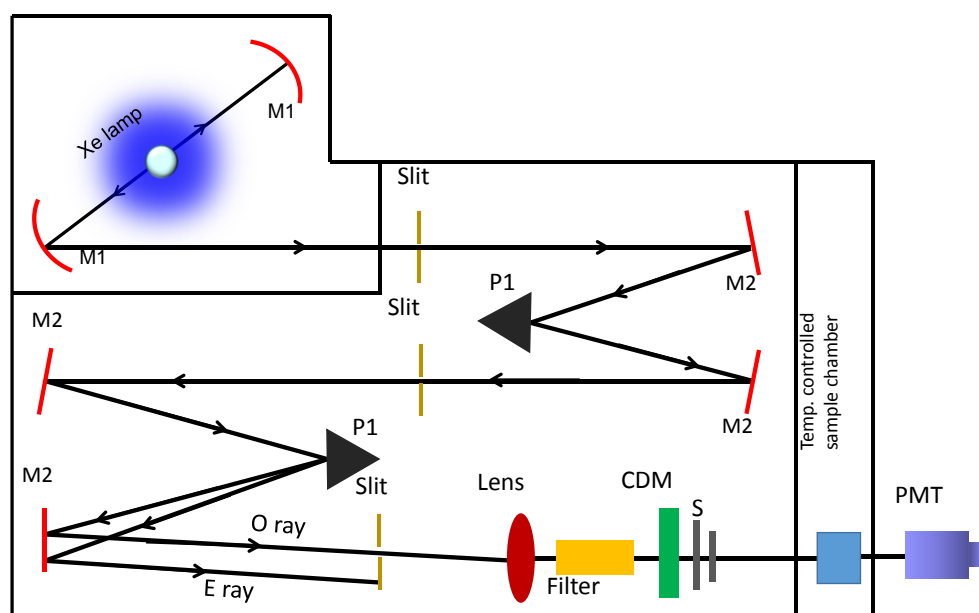


**Figure 3.3.** Schematic ray diagram of a Circular Dichroism (CD) spectropolarimeter. M1, M2, P1, S, PMT, CDM, O-ray and E-ray represent concave mirror, plain mirror, reflecting prism, shutter, photomultiplier tube, CD-modulator, ordinary ray and extraordinary ray, respectively.

The working principle of CD measurement is as follows: when a plane polarized light passes through an optically active substance, not only do the left (L) and right (R) circularly polarized light rays travel at different speeds ( $c_L \neq c_R$ ), but these two rays are absorbed to different extents, i.e.,  $A_L \neq A_R$ . The difference in the absorbance of the left and right circularly polarized light, i.e.,  $\Delta A = A_L - A_R$ , is defined as circular dichroism. CD spectroscopy follows Beer-Lambert law. In an optically active medium, two absorbances,  $A_L$  and  $A_R$  are considered, where  $A_L = \log_{10}(I_0/I_L)$  and  $A_R = \log_{10}(I_0/I_R)$ . At the time of

incidence on the sample, intensity of left and right circularly polarized light are same, i.e.  $I_0 = I_L = I_R$ . Any micrograph passes periodically changing light through the medium, oscillating between left and right circular polarization, and the difference in absorbances are recorded directly<sup>3</sup>.

$$\Delta A = A_L - A_R = \log_{10} \left( \frac{I_0}{I_L} \right) - \log_{10} \left( \frac{I_0}{I_R} \right) = \log_{10} \left( \frac{I_R}{I_L} \right) \quad (3.2)$$

or 
$$\Delta A = (\Delta \epsilon)cl \quad (3.3)$$

As seen from equation 3.2,  $I_0$  does not appear in this final equation, so there is no need for a reference beam. The instruments are, therefore, of single beam type. Most of the CD spectropolarimeters, although measure differential absorption, produce a CD spectrum in terms of ellipticity ( $\theta$ , expressed in millidegrees) as a function of wavelength ( $\lambda$ ), rather than  $\Delta A$  versus  $\lambda$ . The relation between ellipticity and CD is given by,

$$\theta = \frac{2.303 \times 180 \times (A_L - A_R)}{4\pi} \text{ degrees} \quad (3.4)$$

To compare the results from different samples, optical activity is computed on a molar or residue basis. Molar ellipticity,  $[\theta]$  is defined as,

$$[\theta] = \frac{\theta}{cl} \quad (3.5)$$

where, ' $\theta$ ' is in degrees, ' $c$ ' is in  $\text{mol L}^{-1}$  and ' $l$ ' is in cm. The unit of molar ellipticity is  $\text{deg M}^{-1} \text{cm}^{-1}$ .

**3.1.3. Time-Correlated Single Photon Counting (TCSPC) Technique:** All the picosecond-resolved fluorescence<sup>4</sup> transients were recorded using TCSPC technique<sup>1</sup>. The schematic block diagram of a TCSPC system is shown in Figure 3.4. TCSPC setup from Edinburgh instruments, U.K., was used during fluorescence decay acquisitions. The instrument response functions (IRFs) of the laser sources at different excitation wavelengths varied between 60 ps to 80 ps. Fluorescence signal from the samples was detected by a photomultiplier after dispersion through a grating monochromator. For all the transients, the polarizer in the emission side was adjusted to be at  $54.7^\circ$  (magic angle) with respect to the polarization axis of the excitation beam.

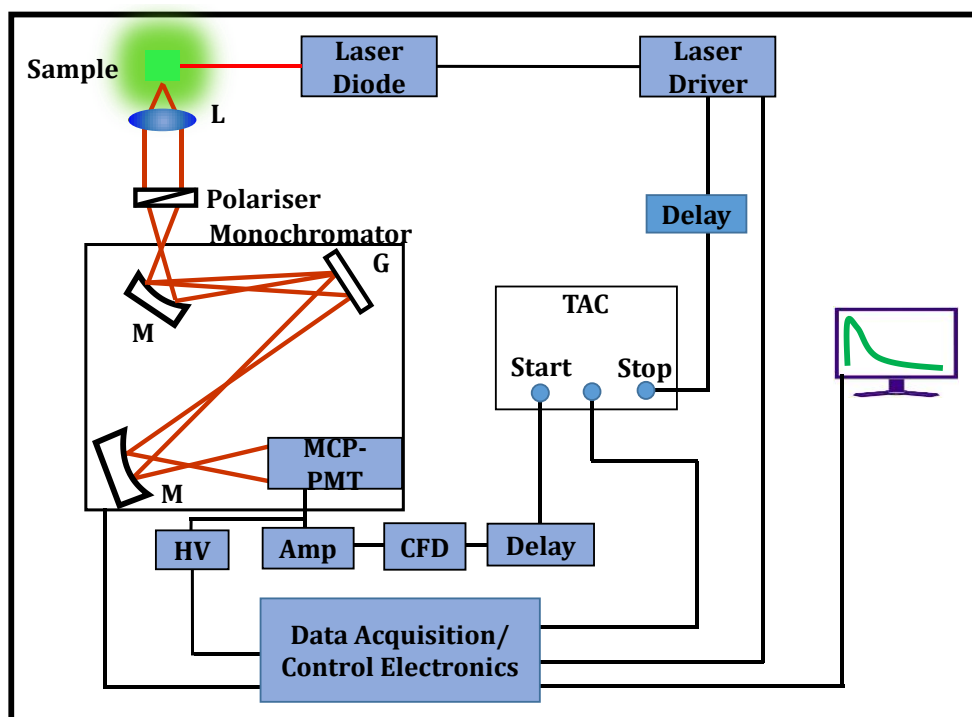


**Figure 3.4.** Schematic ray diagram of a time correlated single photon counting (TCSPC) spectrophotometer. A signal from microchannel plate photomultiplier tube (MCP-PMT) is amplified (Amp) and connected to start channel of time to amplitude converter (TAC) via constant fraction discriminator (CFD) and delay. The stop channel of the TAC is connected to the laser driver via a delay line. L, M, G and HV represent lens, mirror, grating and high voltage source, respectively.

**3.1.4. Fourier Transform Infrared (FTIR) Measurement:** FTIR measurements were performed on a JASCO FTIR-6300 spectrometer (transmission mode). Michelson interferometer<sup>5</sup> is the heart of FTIR spectrometer. It consists of a fixed mirror (M4), a moving mirror (M5) and a beam-splitter (BS1), as illustrated in Figure 3.5. The collimated IR beam from the source is partially transmitted to the moving mirror and partially reflected to the fixed mirror by the beam-splitter. The two IR beams are then reflected back to the beam-splitter by the mirrors. The detector then sees the transmitted beam from the fixed mirror and reflected beam from the moving mirror, simultaneously. The two combined beams interfere constructively or destructively depending on the wavelength of the light (or frequency in wavenumbers) and the optical path difference introduced by the laser moving mirror. The resulting signal is called an interferogram which has the unique property that every data point (a function of the moving mirror position) which makes up the signal has information about every infrared frequency which comes from the source. The measured interferogram signal is then processed through a Fourier transform to obtain the final spectrum. Each spectrum consists of 100 scans ( $1500\text{--}4000\text{ cm}^{-1}$ ) acquired at  $0.5\text{ cm}^{-1}$  resolution.

Far infrared (FIR) measurements in the region of 50 to 650  $\text{cm}^{-1}$  were carried out in Vortex 80v (Bruker Optics) in which a mercury-lamp served as an FIR source and a liquid-helium-cooled silicon bolometer was used as a detector. All the FIR-FTIR measurements were carried out using a liquid cell (model A145, Bruker Optics) with diamond windows with a spacer thickness of  $52.2 \pm 0.3 \mu\text{m}$ .

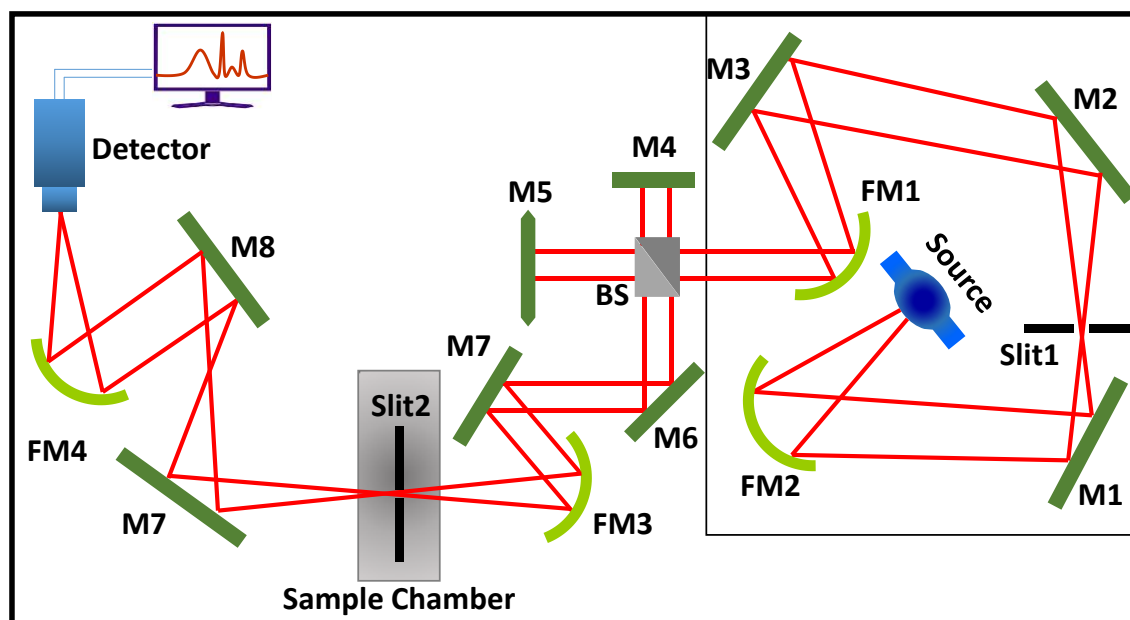


**Figure 3.5.** Schematic of Fourier Transform Infrared (FTIR) spectrometer. It is basically a Michelson interferometer in which one of the two fully-reflecting mirrors is movable, allowing a variable delay (in the travel-time of the light) to be included in one of the beams. M, FM and BS1 represent the mirror, focussing mirror and beam splitter, respectively. M5 is a moving mirror.

### 3.1.5. Terahertz Time Domain Measurement:

The THz time domain measurements were carried out in a commercial spectrometer Tera K8 (Menlo Systems) <sup>6</sup>. A 780 nm mode locked erbium doped linearly polarized p-Ge (p-germenium) <sup>7</sup> fibre laser is used as the low power laser source for the system. Erbium introduces a metastable state ( $\tau \sim 10$  ms) at 1560 nm in the 980 nm energy gap of glass system, which is pumped by a 980 nm diode laser and produces an output of 1560 nm which is then efficiently frequency doubled using a periodically poled lanthanum nitride (PPLN) structure to produce a 120 fs laser output at 780 nm with an average power of 80 mW. A frequency selective device with a high transmission close to 1 in the wavelength range of 400 to 800 nm and close to 0 beyond that frequency window is used outside the laser output port which blocks any unwanted 1560 nm laser that might be present in the output and passes only the 780 nm laser. A neutral density filter with optical density ( $OD = -\log\left(\frac{P_{out}}{P_{in}}\right)$ ) 0.6 is used to control the power of the laser which restricts the output laser to be at the desired level

(20 mW). The linearly polarized (s polarized) 20 mW output laser is then gets reflected through two lenses before passing through a half wave plate whose optic axis is set to  $45^\circ$  with respect to the polarization axis of the laser to make it elliptically polarized.

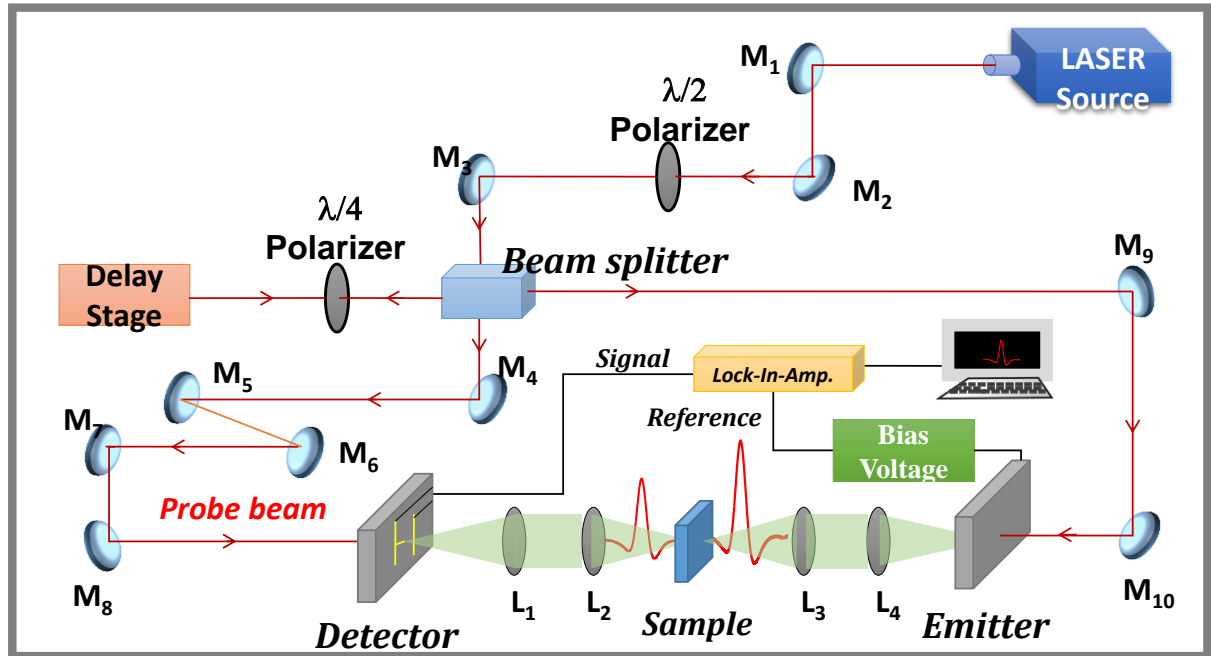


**Figure 3.6.** Schematic ray diagram of Terahertz Time Domain Spectrometer. *M*, *L*, represent silver mirror, convex lens respectively. Photoconductive antenna embedded in Detector/emitter.

This elliptically polarized light is then incident on a polarizing beam splitter which splits the beam into two orthogonal ('s' and 'p') polarization. The 'p' polarized light goes to the THz detector antenna. The 's' polarized beam gets reflected from a mirror attached to the tip of a vibrator mounted on the motorized delay stage and in between passes twice through a quarter wave plate and thereby the final polarization state of the beam becomes 'p' polarized. This 'p' polarized beam then excites the THz emitter antenna guided by two mirrors.

**Photoconductive Antenna (PC):** Identical photo-conductive (PC) antennas (Figure 3.7) were used for THz generation and detection<sup>8</sup>. Low temperature grown Gallium Arsenide (LT-GaAs) is used as this semiconductor substrate as it offers fast carrier recombination time ( $t_c$ ) and high mobility ( $\mu$ ) due to increased defect state. On top of the LT-GaAs substrate a dipole gold (Au) antenna is deposited. The active region of the antenna is of the order of  $\sim 5 \mu\text{m}^2$  and the gap between the dipoles is  $\sim 5 \mu\text{m}$ . An external bias voltage of 20V/30V, 10 kHz is provided to produce an electric field which is of the order of  $\sim 10^6 \text{Vm}^{-1}$  in the antenna for THz generation.

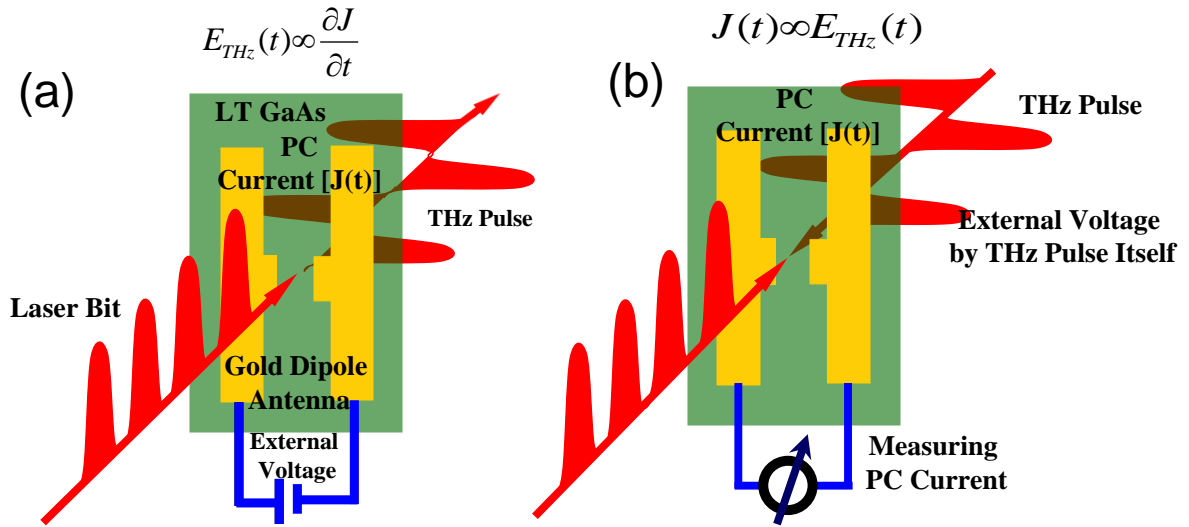


**Figure 3.7.** Schematic ray diagram of generator (a) and detector (b) photoconductive antenna. The green and yellow plates define LT-GaAs and gold dipole, respectively.

**THz Generation:** In the first step the ultrafast laser pulse excites the semiconductor device. The wave length of the excitation photon (780 nm) has to be chosen such that the photon energy ( $h\nu$ ) must be greater than the band gap energy ( $E_{\text{gap}}$ ) of the semiconductor substrate. As a result electron-hole pairs are created in the semiconductor and a thin conductive region down to approximately the absorption depth  $\frac{1}{\alpha}$  is created. The optically generated electron-hole pairs form electrically neutral plasma near the semiconductor surface. The time evolution of the charge density is given by  $N(t)$  with the total carrier density as the sum of that of the electrons and the holes i.e.,  $N(t) = N_e(t) + N_h(t)$ . The free carriers affect the conductivity as:  $\sigma(t) = N(t)e\mu$ . The current density is  $J(t) = \sigma(t)E$ , or  $J(t) = N(t)ev(t)$  with  $v(t)$  being the carrier velocity. The carriers are accelerated in the applied electric field, the time evolution of carrier velocity is determined by the initial acceleration of carriers with effective mass  $m^*$  and by rapid carrier scattering with a characteristic time which is determined by phonon scattering, carrier scattering from the dopants and the photon energy i.e. the energy in the conduction band where the carriers are generated. At longer timescales the excited electron-hole pairs recombine due to the presence of defect states and the transient current decreases. It is the time evolution of the transient current,  $J(t)$ , that generates the THz pulse. In summary, a biased semiconductor has electron-hole plasma created of femtosecond time scales by an optical pulse. The rapid acceleration and separation of the electrons and holes create a current transient. The THz electric field is determined (approximately) by the time derivative of the current which results in a radiated pulse front. In times of hundreds of picoseconds, the semiconductor recovers.

**THz Detection:** The detection of the THz pulses is done by using the phenomenon of ultrafast pulse excitation in a semiconductor causing rapid changes in conductivity. During the generation procedure ultrafast laser pulses generate electron and hole plasma which increases conductivity of the antenna gap. The arrival of the laser pulse is analogous to closing a switch, which allows the antenna gap to conduct in presence of an electric field. During THz detection process no bias voltage is given to the substrate, instead the bias voltage is provided by the THz pulse itself. The short recombination time of the semiconductor causes the gap resistance to change from nearly insulating to conducting (closing the switch) then back to insulating (opening the switch) on a picoseconds time scale. The coplanar strip line is connected to a high-sensitivity current amplifier that detects any current flow through the antenna gap with sub-pico amp resolution. If the resistance of the metal lines is negligible the resistance of the antenna is determined by the antenna gap. The current flow can be calculated from the Ohms law  $I(t) = V(t)/R(t)$ , where the antenna bias voltage is provided by the THz pulse:  $V(t) \sim E_{THz}(t)h$ . Thus, measuring  $V(t)$  with changing the time delay between the pump and the probe laser beam, i.e., changing the time delay between the arriving time of probe laser beam and the THz pulse, one can map the THz field as a function of time.

The whole set up is covered with a glass-top and the inside environment is purged with ultrapure nitrogen gas (99.99% pure  $N_2$  gas) to get rid of the unwanted water vapour absorption lines in the obtained THz spectra. The spectral range essentially extends from 0.1-3.5 THz with highest signal to noise (S/N) ratio of 60 dB at 0.6 THz which then reduces to 30 dB at 3.5 THz.

**3.2. Sample Preparation:** In this section we will discuss the detail of different sample preparation to study water in restricted environments. The details of the chemicals used has been discussed in chapter-2.

**3.2.1. Preparation of Micellar Solution:** The stock solution of aqueous micellar solutions were prepared by dissolving surfactants in water. Micellar solutions of the probe were prepared by adding known concentrated aqueous or a little amount of concentrated aqueous ethanolic probe solution to micellar solution. Desired concentration of micelle was ensured by the addition of quantitative amount of stock solution in water with simultaneous stirring of the mixture for an hour.

**3.2.2. Preparation of Reverse Micellar Solution:** In order to prepare reverse micellar solutions<sup>9</sup> with specific degree of hydration ( $w_0 = [\text{H}_2\text{O}]/[\text{Surfactant}]$ ) calculated volume of water was added to a known volume of 0.1 M surfactant (AOT, DDAB and Igepal) solution in cyclohexane. In case of dissolving a probe inside the water of RM a little amount of aqueous solution of the probe was added during the preparation of specific RM. In order to ensure that each reverse micelle contains not more than one probe molecule, the overall probe concentration was kept less than that of the micellar concentration. All the FTIR, steady state fluorescence and absorption spectra were collected after baseline correction by  $w_0=0$  of that RM.

**3.2.3. Measurement of BzCl hydrolysis rate:** BzCl has an absorption peak at  $\sim 282$  nm; during the hydrolysis reaction<sup>10</sup> we have monitored the rate of change in absorption at 285 nm with respect to time (with 1 second time resolution).

**3.2.4. HPC-Water Mixture:** Hydroxypropyl cellulose (HPC)-water mixture<sup>10</sup> was prepared by vigorous mixing in vortex for 2-3 days inside a 1 cm spectroscopy cell. After that quantitative amount of probe was added into the mixture and again kept on vortexing for the next 3 days until we got homogeneous mixture. 10% to 20% wt percentage HPC-water mixtures produced homogeneous solutions within a day but for 25% and 30% HPC-water mixtures it took almost a week to get a homogeneous mixture.

**3.2.5. DME-Water Mixture:** 1-2 di-methoxy ethane (DME) water mixture were prepared by quantitative mixing of DME and water. HOD solution was prepared by 4%  $\text{D}_2\text{O}$ - $\text{H}_2\text{O}$  (v/v) mixture. During FTIR measurement DME-water samples were prepared by using 4%  $\text{D}_2\text{O}$ - $\text{H}_2\text{O}$  (v/v) mixture instead of water. All the DME-water FTIR data presented in the thesis are differential absorption spectra where absorption spectra of pure DME are deducted from DME-water spectra.

**3.2.6. Enzyme Solution:** For the enzyme kinetics measurements aqueous stock solutions of CHT were prepared in phosphate buffer (10 mM) at pH 7.0 using double distilled water. Concentration of the enzyme samples in aqueous solution was determined using the extinction coefficient ( $\epsilon = 51 \text{ mM}^{-1}\text{cm}^{-1}$ ) value at 280 nm. During enzymatic assays in micellar medium quantitative amount of enzyme solution was added to the micellar solution and kept for an hour before the substrate addition. Enzyme hydrolysis reactions were carried out at a time resolution of 1 second. All the CD spectra collected for CHT was prior to a baseline correction of the medium.

## References

1. J. R. Lakowicz. *Principles of fluorescence spectroscopy*; Springer Science & Business Media 2013.
2. B. Nordén. *Circular dichroism and linear dichroism*; Oxford University Press 1997; Vol. 1.
3. N. Berova and K. Nakanishi. *Circular dichroism: Principles and applications*; Wiley-VCH 2000.
4. D. V. O'connor and D. Philips. *Time correlated single photon counting*; Academic Press: London, 1984.
5. V. Saptari. *Fourier transform spectroscopy instrumentation engineering*; SPIE Optical Engineering Press 2004.
6. D. Polley, A. Patra and R. K. Mitra, "Dielectric relaxation of the extended hydration sheathe of DNA in the THz frequency region". *Chemical Physics Letters* 2013 586, 143-147.
7. A. Bergner, U. Heugen, E. Bründermann, G. Schwaab, M. Havenith, D. R. Chamberlin and E. E. Haller, "New p-Ge THz laser spectrometer for the study of solutions: THz absorption spectroscopy of water". *Review of Scientific Instruments* 2005, 76, 063110.
8. S. L. Dexheimer. *Terahertz spectroscopy: principles and applications*; CRC press 2007.
9. A. Patra, T. Q. Luong, R. K. Mitra and M. Havenith, "Solvent dynamics in a reverse micellar water-pool: a spectroscopic investigation of DDAB–cyclohexane–water systems". *Physical Chemistry Chemical Physics* 2013, 15, 930-939.
10. A. Patra, P. K. Verma and R. K. Mitra, "Slow relaxation dynamics of water in hydroxypropyl cellulose-water mixture traces its phase transition pathway: a spectroscopic investigation". *The Journal of Physical Chemistry B* 2012, 116, 1508-1516.

# Chapter 4: Dynamics and Activity of Water in Presence of Biopolymer

## 4.1. Introduction:

Water in restricted environment has always been a fascinating area of research as it furnishes properties of water markedly different from those of bulk water, specially in biologically relevant environments.<sup>1, 2</sup> In this regard biopolymer-water mixtures<sup>3-11</sup> are of potential interest since these systems provide with a potential environment that mimics real biological systems. Hydroxypropyl cellulose<sup>12</sup> (HPC) is a well-studied biopolymer which shows excellent bio-degradability and biocompatibility, electro-neutrality and high water solubility.<sup>8, 11, 13-25</sup> It is a recommended food additive and finds usage in foods as an emulsifier and encapsulator. In this respect the study of hydration structure and dynamics in HPC-water mixture is strongly demanding in view of its fruitful applications. HPC molecule is known to adopt a helical conformation in the crystalline state,<sup>26, 27</sup> however, its conformation in aqueous solution and liquid crystalline phase is rather complex. At low HPC concentration an isotropic phase dominates<sup>13</sup> and it forms an ordered liquid crystalline phase with cholesteric structure at about 40 wt% polymer in water. The structural transition is not a sharp one and an onset of the phase transition sets off at a relatively lower concentration. The polymer is soluble in cold water, and when the aqueous solution is warmed to ~40°C, a phase separation occurs with a sharp increase in turbidity and a decrease in viscosity. Phillips et al.<sup>19</sup> reported a detailed measurement of the low shear viscosity of HPC in aqueous solution and identified a transition in viscosity dependency on HPC concentration and the transition relates a structural modification of HPC with concentration. Fluorescence recovery after photobleaching (FRAP) studies<sup>18, 24</sup> using different dye molecules have identified a decrease in diffusion coefficient and increase in microviscosity with increase in HPC concentration. Immani et al.<sup>22</sup> reported on the effect of structure and temperature on the rheo-optic behavior of HPC solution in water by measuring flow birefringes and intrinsic viscosity and the observed effects are related to the structural features in the chain backbone. Yakimet et al.<sup>11</sup> reported the effect of water content on the structural recognition and elastic properties of HPC films using FTIR, differential scanning calorimetry (DSC) and X-ray diffraction techniques. They reported the elasticity of the film to be strongly dependent on the water content and even a small increase in the water content led to a relatively large decrease in the

elasticity modulus. Wojciechowski et al.<sup>25</sup> studied the nature of water molecules in HPC hydrogel with liquid crystalline (LC) organization using DSC and dielectric relaxation (DR) techniques. They identified two distinct types of water species to be present in the hydrogel. The first type is a ‘bound type’ water molecules which is constrained in the LC polymer network. The second type is ‘bulk type’ water adsorbed in the pores of LC environment.

The dynamics of water in HPC-water mixture has previously been studied with dielectric relaxation (DR) technique.<sup>8, 9, 21, 25, 28</sup> These studies conclude that the mobility and hence the alignment of molecular chains in the disordered regions of HPC, responsible for dielectric polarization, depend not only on the amount of water present but also on the mode of interaction between water molecules and cellulose chain. Also during thermal treatment the removal of water molecules from the disordered regions results in some changes in the intermolecular interaction between adjacent cellulose chains. The adsorbed water molecules in cellulose could be differentiated into ‘free type’ or loosely bound type and tightly ‘bound’ type, and that different modes of interactions may occur depending on the amount of water in a given solution.<sup>17</sup> At low water content the bound water molecules may associate with the polar OH groups of cellulose chains or form crosslink between chains. When the number of sites available for these tightly bound water molecules is consumed, additional water molecules are bound loosely in such a manner so as these water molecules do not further enhance the dielectric loss mechanism. The activation energy of the relaxation process due to the bound type water, as observed in the MHz region, is observed to decrease with decreasing the moisture content<sup>8</sup>. Recently Sudo et al.<sup>21</sup> have studied the primary relaxation process due to the motion of “free water” restricted by HPC molecules as observed in the GHz region at different HPC concentrations and temperatures. The relaxation process is observed to slow down with increasing HPC concentration with a clear transition at 23 wt% HPC content wherein, according to the authors, lies the onset of the isotropic to a collesteric structural phase transition of the mixture. Such a phase transition involves the release of a fraction of hydrogen bonded water molecules in the form of “free water”. The activation energy has also been observed to increase beyond 23 wt% HPC to reach a value similar to that of the hydrogen bonded energy in bulk water. It is important to note here that at the onset of the cholesteric phase, a fraction of water molecules still remains restricted in the structured HPC network, and it is rather interesting to understand how this restriction modifies the dynamics of water. Our present investigation is thus motivated to underline the slow dynamics of these

water molecules in HPC-water mixture and its manifestation as the biopolymer solution changes its phase.

We have used picoseconds-resolved fluorescence spectroscopic technique to underline the dynamics of water at six different HPC concentrations of 10, 15, 20, 25, 30 and 40 wt% in water at four different temperatures of 273, 283, 293 and 303 K. This study complements our previous investigations on the mode of slow solvation dynamics produced by confined water in micro-heterogeneous assemblies and the corresponding energetics of the cross over between ‘bound’ and ‘free’ type of water molecules present in such systems.<sup>29-34</sup> The choice of the composition and temperature range is based on the isotropic solution limit as obtained from previously reported phase diagrams.<sup>16</sup> The focus of our study to identify the possible modification of slow solvent relaxation dynamics associated with a change in the microscopic phase morphology at ~20% HPC also influences the choice of the compositions. Coumarin-500 (C-500) is used as the fluoroprobe, which has potential to provide information selectively from micro-heterogeneous interfaces.<sup>30</sup> Steady state emission and excitation measurements provide information on the micro-polarity of the immediate environment of the fluorophore. The geometrical restriction on the probe is determined with the help of ps-resolved rotational anisotropy study. Finally the activity of water in these solutions is determined by measuring the kinetics of solvolysis reaction of benzoyl chloride. Our studies clearly demonstrate that water dynamics traces the phase transition pathway of HPC-water mixture and activity of the restricted water molecules in the solution gets modulated accordingly.

## **4.2. Results and Discussion: (The slow relaxation dynamics of water in hydroxypropyl cellulose-water mixture traces its phase transition pathway: A spectroscopic investigation)**

Figure 4.1.a & 4.1.b depicts the emission and excitation spectra of C-500 in HPC-water mixture at different representative HPC concentrations (10, 20, 30 and 40%) measured at 293 K. As evidenced from Figure 4.1.a, the emission spectrum shows a progressive blue shift with increasing HPC concentration. C-500 in water produces an emission peak ( $\lambda_{em}^{max}$ ) at 506 nm and for 40% HPC, the emission peak is blue shifted to 495 nm. We plot the relative shift of  $\lambda_{em}^{max}$  (with respect to that of water) against HPC concentration (Figure 4.1.a, inset), and it is found that the relative shift in  $\lambda_{em}^{max}$  changes rapidly at and beyond 20% HPC concentration. The decreased polarity as experienced by the probe molecule of the system

with increasing HPC concentration is reflected in the blue shift of  $\lambda_{em}^{max}$ , a phenomenon comparable to that found in AOT reverse micellar (RM) systems with decreasing water content.<sup>30</sup> In order to get a deeper insight we measure the excitation spectra of the same systems (Figure 4.1.b). It is found that in water C-500 produces an excitation peak at 390 nm (data not shown), which is consistent with earlier reports for the identical system.<sup>35</sup> With increasing HPC concentration the excitation peak suffers a progressive red shift coupled with an increasing FWHM of the observed spectrum.

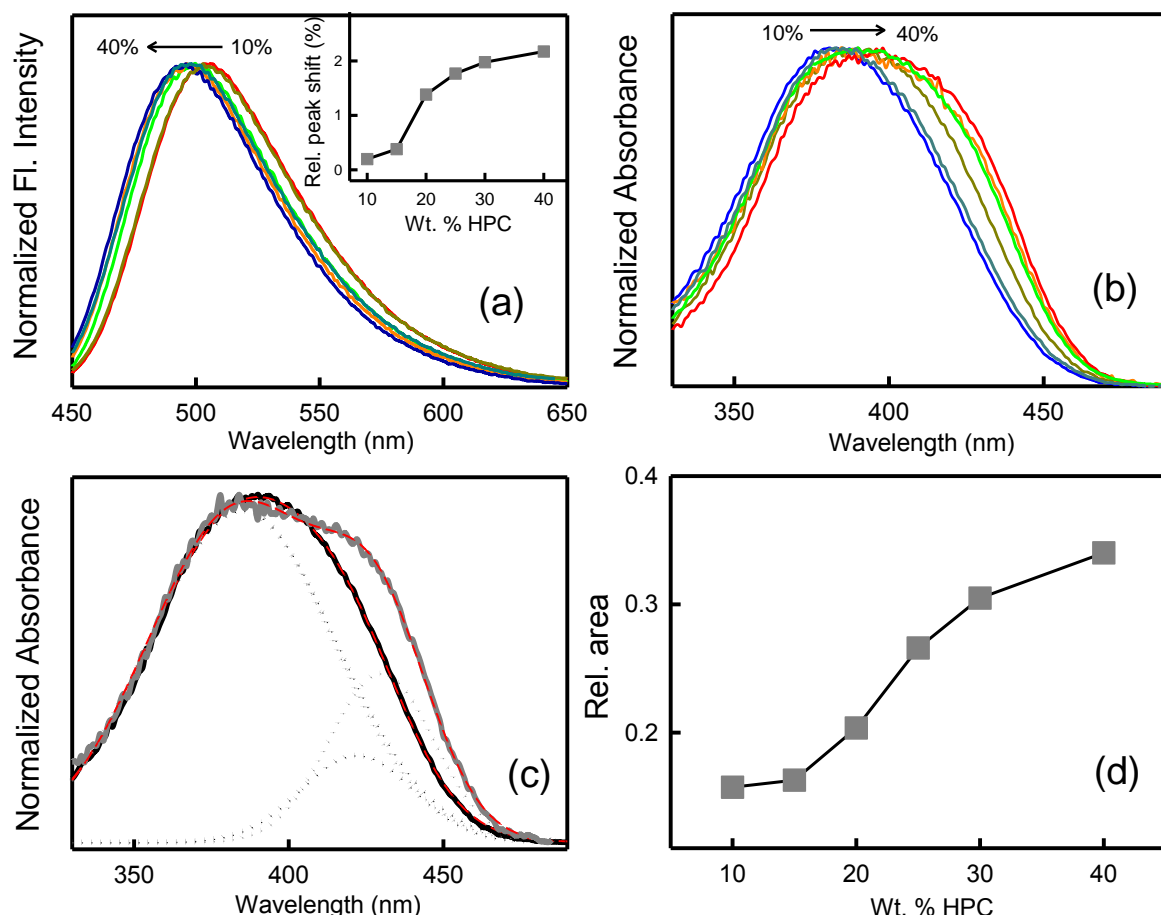


**Figure 4.1.** (a) Emission spectra of C-500 at 293 K in HPC-water mixture with HPC weight percentage of 10, 15, 20, 25, 30 and 40%. The relative peak shift with respect to that in water against HPC concentration is shown in the inset. (b) Excitation spectra of C-500 at 293K in HPC-water mixture with HPC weight percentage of 10, 15, 20, 25, 30 and 40%. (c) Deconvoluted spectra of 10% (black) and 40% (grey) HPC-water mixtures. The red solid lines are the overall fittings. (d) The relative area of the second curve with respect to that of the first one is plotted against HPC concentration.

This broadening could be envisaged as a possible distribution of the probe molecules in different micro-environments in the mixture with a notion that a fraction of the probe is exposed to the bulk type water whereas the rest probes a restricted environment, which has been reported to absorb at a higher wavelength.<sup>30, 36</sup> We therefore deconvolute the observed excitation spectra into two separate spectra with one peak fixed at 390 nm. Representative

deconvoluted figures for 10% and 40% HPC-water solution are presented in the Figure 4.1.c. As evidenced from the Figure 4.2.a, for 10% HPC the second peak appears at 422 nm and for 15, 20, 25, 30 and 40% HPC, the peak suffers progressive red shift to appear at 425, 427, 427, 428 and 429 nm, respectively.

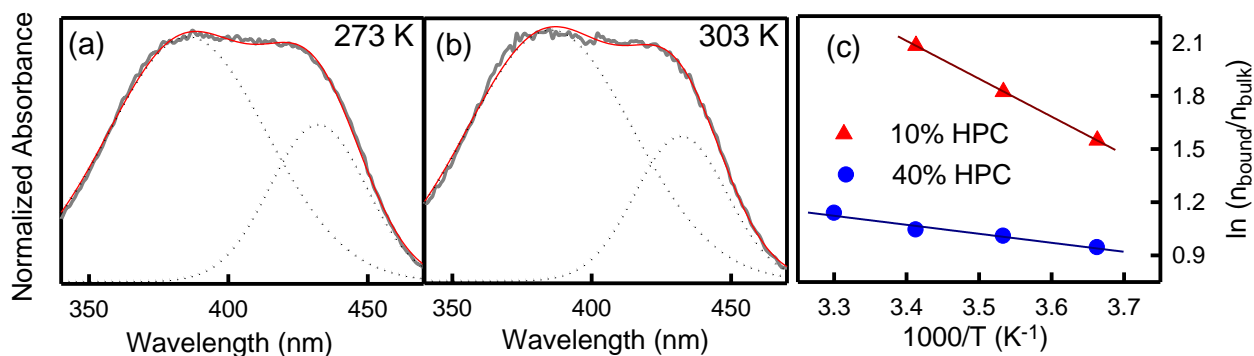


**Figure 4.2.** (a) Deconvoluted excitation spectra C-500 in 40% HPC solution at 273 and (b) 303 K. The red solid line is the overall fit, while the dotted lines are the deconvoluted fits. (c) Plot of  $\ln(n_{\text{bound}}/n_{\text{bulk}})$  against  $1/T$  for 10% and 40% HPC solutions. The solid lines are the linear fits.

It could be intuited that while the first peak arises due to the distribution of C-500 in the bulk aqueous environment (centred at 390 nm), the second one is due preferably to the C-500 residing in the hydrophobic environment of HPC. The area under each curve could well correspond to the number of water molecules belonging to that particular ‘species’. We, therefore, plot the relative ratio of the area under the two curves against HPC concentration (Figure 4.1.d). A progressive increase in the area of the second curve comprehends the increased fraction of C-500 residing in the interfacial region of HPC-water system at lower hydration. The observed red shift in the excitation spectra can be explained in terms of the relative increase in the hydrophobicity of the system with increasing content of HPC which reduces the dipole-dipole interaction of the solvent-fluorophore, thereby stabilizing it. The curve shows a change in slope beyond 20% HPC which in turn corresponds to the onset of phase transition of the polymer as it turns hydrophobic at and beyond this concentration.<sup>21</sup>

We now switch to the time-resolved study. Figure 4.3.a (inset) shows representative fluorescence transients of the probe C-500 in 30% HPC-water mixture at three selected wavelengths of 440, 490 and 500 nm studied at 293 K. The 440 nm decay transient can tri-exponentially be fitted with the time constants of 0.11 ns (57%), 1.02 ns (25%) and 4.44 ns (18%), whereas, for the 600 nm transient, a distinct rise component of 0.45 ns is obtained along with a decay component of 4.9 ns. Similar wavelength dependent transient fittings are also been obtained in solutions with other mixtures. Such wavelength dependency clearly

indicates solvation of the fluoroprobe. In order to estimate the solvation relaxation rate, we construct time resolved emission spectra (TRES) for different HPC-water mixtures using the fitting parameters of the transients and following the procedure described elsewhere.<sup>29</sup> A representative TRES of 30% HPC-water mixture at 293 K has been shown in Figure 4.3.a. It is observed that the spectrum suffers progressive red shift with time. We first need to ensure that the observed time-resolved shift in the emission spectra is not concerned with any internal photophysics associated with the probe itself and it remains as a single species throughout.

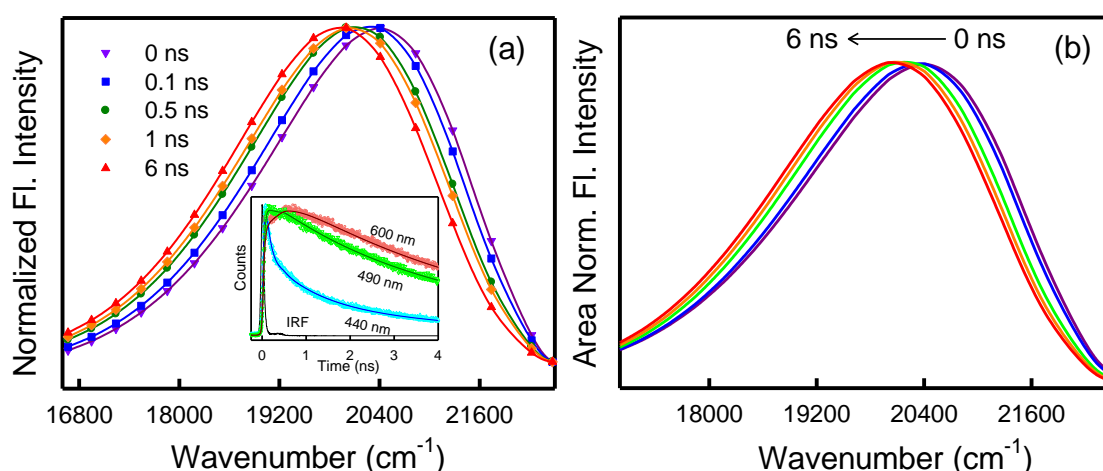


**Figure 4.3:** (a) Time resolved emission spectra (TRES) of C-500 in 30% HPC-water mixture at 293 K decay transient of C-500 in 30% HPC-water mixture at 293 K measured at three wavelengths, the solid lines are the multi-exponential fits of the curves. (b) A representative time resolved area normalized emission spectra (TRANES) for 30% HPC solution at 293 K. The arrow indicates increase in time.

We therefore construct the time-resolved area normalized emission spectra (TRANES)<sup>37</sup> for all the samples and a representative TRANES for 30% HPC at 293 K is depicted in Figure 4.3.b. Existence of an iso-emissive point in a TRANES profile specifies that the observed emission from the probe is due to two different ‘species’ of the probe, irrespective of their origin. As evidenced from the Figure 4.3.b, no iso-emissive point is apparent for any of these systems and this therefore affirms that the observed dynamics is due solely to a single probe species, and any modulation is caused only due to the heterogeneity in the location of the probe.

Solvent correlation function,  $C(t)$  are constructed for all the systems by using equation 2.14. All these curves are fitted bi-exponentially (Figure 4.4.a) using the equation  $C(t) = a_1 \exp(-t/\tau_1) + a_2 \exp(-t/\tau_2)$  where  $\tau_1$  and  $\tau_2$  are the two associated timescales and  $a_i$ ’s are their corresponding weightages.

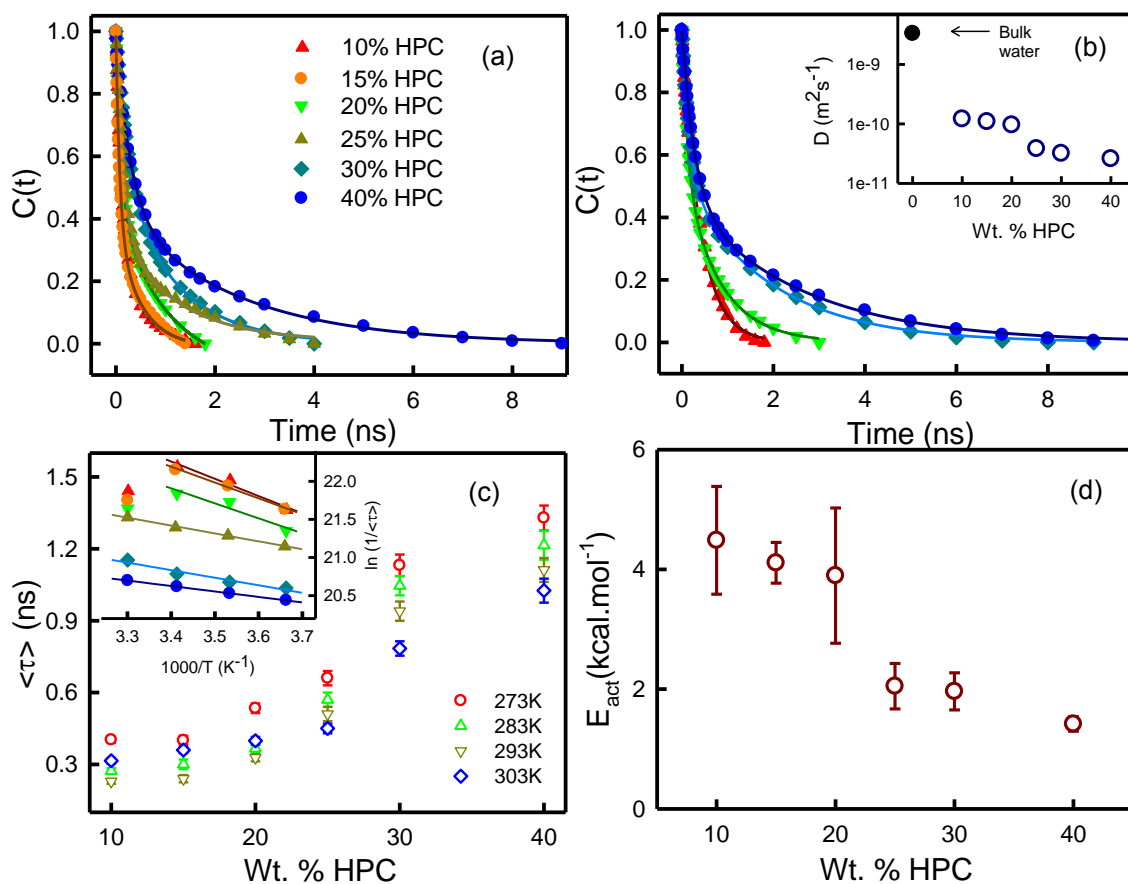


**Figure 4.4.** (a) Solvent correlation function,  $C(t)$  of C-500 in water-HPC mixtures (with HPC Wt. % of 10, 15, 20, 25, 30 and 40%) at 293 K. The solid lines are bi-exponential fittings of the data points. (b)  $C(t)$  plots for 10, 20, 30 and 40% HPC solutions at 273 K. Diffusion coefficients ( $D$ ) of water in water (black circle) and HPC-water mixture as a function of HPC concentration at 293 K are shown in the inset. (c) Average solvent relaxation time constants ( $\langle \tau \rangle$ ) of C-500 in HPC-water mixtures at different temperatures are shown as a function of HPC concentration. Arrhenius plots for different HPC concentrations are shown in the inset. The symbols represent the same as in Figure 4.3.a. The solid lines are the linear fits. (d) The measured activation energy values ( $E_{act}$ ) at different HPC concentrations.

All the corresponding fitting parameters are presented in table 4.1. It is evident from the table that one of the solvation time constants is of the order of a few hundreds of picoseconds (ps), while the other one extends from hundreds of ps to a few nanosecond (ns). The two timescales essentially corresponds to the different modes of coupled translational and rotational motion of the two different type of water molecules present at the HPC-water interface.

The observed timescales are comparable with those obtained in case of polyethylene glycol-water mixture,<sup>32</sup> AOT RM systems<sup>30</sup> and AOT lamellar systems<sup>34</sup> using the same probe molecule. It is worth mentioning here that C-500 in water produces a ultrafast solvation timescales of 300 and 700 fs.<sup>35</sup> Our instrumental resolution (80 ps IRF) limits us to miss a considerable part of the fluorescence signal. To make an estimate of the loss in the

fluorescence signal we determine the time zero frequency of the fluorescence spectrum maximum,  $\nu_{em}^p(0)$

**Table 4.1.** Solvent Relaxation parameters for C-500 in HPC-water mixture at different HPC concentration and temperature

Temperature	$a_1$	$\tau_1$ (ns)	$a_2$	$\tau_2$ (ns)	$\langle \tau \rangle$ (ns)
<b>10% HPC-WATER SOLUTION</b>					
273K	0.11	0.10	0.89	0.44	0.40
283K	0.71	0.16	0.29	0.55	0.27
293K	0.65	0.11	0.35	0.45	0.23
303K	0.43	0.07	0.57	0.5	0.32
<b>15% HPC-WATER SOLUTION</b>					
273K	0.45	0.10	0.55	0.65	0.40
283K	0.52	0.09	0.48	0.52	0.30
293K	0.62	0.08	0.38	0.50	0.24
303K	0.77	0.10	0.23	1.22	0.36
<b>20% HPC-WATER SOLUTION</b>					
273K	0.46	0.14	0.54	0.87	0.53
283K	0.46	0.08	0.54	0.61	0.37
293K	0.47	0.08	0.48	0.57	0.33
303K	0.27	0.07	0.73	0.52	0.40
<b>25% HPC-WATER SOLUTION</b>					
273K	0.65	0.19	0.35	1.52	0.66
283K	0.67	0.19	0.32	1.36	0.57
293K	0.65	0.14	0.35	1.2	0.51
303K	0.68	0.14	0.32	1.1	0.45
<b>30% HPC-WATER SOLUTION</b>					
273K	0.51	0.20	0.49	2.10	1.13
283K	0.48	0.23	0.52	1.80	1.05
293K	0.50	0.18	0.50	1.70	0.94
303K	0.56	0.30	0.44	1.40	0.78
<b>40% HPC-WATER SOLUTION</b>					
273K	0.54	0.28	0.46	2.56	1.33
283K	0.50	0.24	0.50	2.19	1.22
293K	0.54	0.27	0.46	2.10	1.11
303K	0.57	0.23	0.43	2.08	1.03

from the following equation<sup>38</sup>

$$v_{em}^p(0) = v_{abs}^p - [v_{abs}^{np} - v_{em}^{np}] \quad (4.1)$$

where  $v_{abs}^p$ ,  $v_{abs}^{np}$  and  $v_{em}^p$  are the absorption peak of the fluorophore in polar solvent, absorption peak in nonpolar solvent and emission peak in nonpolar solvent, respectively. Considering cyclohexane to be the nonpolar solvent in which C-500 produces absorption and emission peaks at 360 and 410 nm, respectively and water to be the polar solvent, we estimate at the best ~30% recovery of the total fluorescence signal. Our instrumental resolution is far beyond to probe the fast time-scale associated with the ultrafast water relaxation process, however, the essence of this study is focused on the slow dynamics of water and therefore, the observed loss of the ultrafast fluorescence signal does not significantly affect the conclusion drawn.

As observed from Table 4.1, the average solvation time constant  $\langle\tau\rangle$  ( $= a_1\tau_1+a_2\tau_2$ ) increases gradually with increasing HPC concentration in the mixture. A similar retardation of the relaxation process of the dielectric with an increase of the polymer fraction has previously been reported in HPC-water<sup>21</sup> and ethyleneglycol-dioxane<sup>39</sup> mixtures. Our study, however, probes the coupled rotational-translational motion of water molecules in HPC structural network, which is slower than that probed by the DR study, and the observed retardation clearly points out towards a progressive restriction of the translational motion of water with the onset of cholesteric phase at higher HPC concentrations. In order to get a better outlook towards the hindered motion of water at high HPC concentrations, we measure the time-resolved rotational anisotropy of C-500. Representative illustrations of the anisotropy decays at 293 K for 5, 10, 15, 20, 25 and 30% HPC mixtures are depicted in Figure 4.5. As can be observed from the figures, the anisotropy decay gets slower as HPC concentration increases. The rotational anisotropy for 5% to 25% HPC could be fitted bi-exponentially. For 5% HPC, the rotational time constants ( $\tau_r$ ) are 0.12 and 1.3 ns respectively with an average time constant  $\langle\tau_r\rangle$  ( $=a_1\tau_{r1}+a_2\tau_{r2}$ ) of 0.46 ns. It is to be noted here that C-500 in water exhibits a very fast rotational anisotropy with a time constant of ~50 ps at this temperature.<sup>35</sup> For the present bi-exponential decay pattern, the faster time constant is comparable to that of C-500 in bulk water while the other one defines the relatively slow rotational time constant arising out of the restricted motion of water imposed by the HPC molecular network. At 10% HPC, the decay transient gets slower with time constants of 0.13 and 1.4 ns ( $\langle\tau_r\rangle=0.65$  ns). For 15, 20 and 25% HPC solutions the time constants are 0.29 and

3.2 ns; 0.85 and 5.2 ns; and 0.9 and 7.4 ns, respectively. We plot the  $\langle\tau_r\rangle$  values against HPC concentration (Figure 4.6.a) and it is observed that in the HPC concentration range of 15-20%  $\langle\tau_r\rangle$  increases sharply correlating the solvent relaxation dynamics study (Figure 4.4., Table 4.1.).

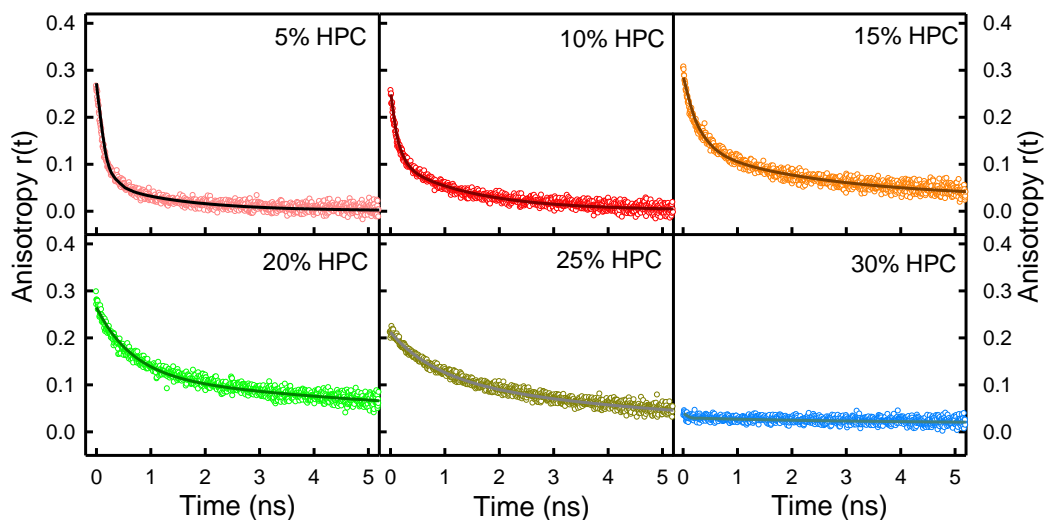


**Figure 4.5.** Time resolved rotational anisotropy decays of C-500 in different HPC-water mixtures at 293 K. The solid lines indicate bi-exponential fittings.

The  $\langle\tau_r\rangle$  values obtained in this study are in the same order of magnitude as reported for the same probe in PEG-water mixture<sup>32</sup> and RM with low water content.<sup>30</sup> The estimated rotational time constants ( $\tau_r$ ) allow us to calculate the microviscosity ( $\eta$ ) experienced by the probe using the Debye-Stokes-Einstein equation

$$\tau_r = \frac{\eta V}{k_B T} \quad (4.2)$$

where  $k_B$  is the Boltzmann constant and  $V$  is the volume of the fluorophore.

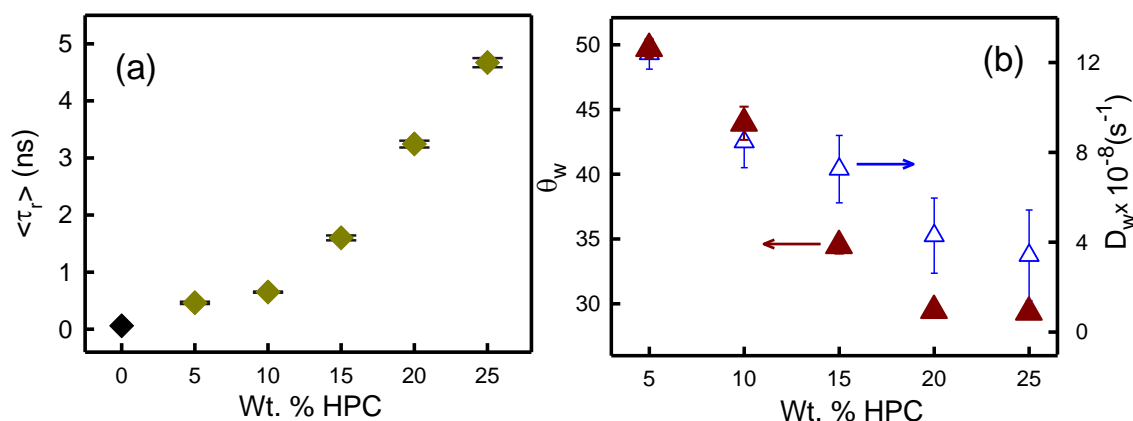


**Figure 4.6.** (a) Average rotational time constant  $\langle\tau_r\rangle$  as a function of HPC concentration at 293 K. (b) The Wobbling-cone angle ( $\theta_w$ , hollow symbols) and diffusion coefficient ( $D_w$ , filled symbols) as a function of HPC concentration at 293 K are shown in the inset.

Considering the radius of C-500 molecule to be  $3.6 \text{ \AA}^{40}$  and taking  $\tau_r$  to be the slow component arising out of the rotation of the probe in 'bound water', we estimate a microviscosity value of  $\sim 3 \text{ cp}$  for 10% HPC solution. This value is significantly larger than that of bulk water, and higher than the microviscosity experienced by the same probe in salt solution,<sup>35</sup> however comparable to that obtained in RM systems<sup>30</sup> and in PEG-water system<sup>32</sup> at 293 K. For higher HPC concentrations the microscopic viscosity increases further. This strongly suggests an HPC-water microenvironment, which is much modified compared to that of bulk water as experienced by the probe. For 30 and 40% HPC solutions, the anisotropy decay gets even slower and the transients could only be fitted considering the presence of an offset, which indicates that the rotation could not be completed within the experimental time window. The observed flat rotational decay transient of the probe in high concentration HPC solution could be explained by considering the rotational motion of the probe in the solution. The rotational anisotropy probes the rotation of the probe (followed by an ultrafast photo-excitation) in the solvent environment. Several modes of rotations are involved and could be realized in the wobbling-in-cone analysis, which concludes that the slow rotational time constant of a probe includes the lateral diffusion of the probe ( $\tau_L$ ) and the overall tumbling motion of the local environment ( $\tau_M$ ), which in turn is connected to the hydrodynamic volume and viscosity of the local environment. In the concentrated HPC solution, both these parameters are high to make  $\tau_{\text{slow}}$  high, and thus not measurable within the experimental time window. This makes the offset in the high HPC concentration region. As has been reported earlier, at low hydration level, the polymer chain behaves as a geometrical constraint for rotational motion of water molecules and their movement is strongly hindered by the polymer chain.<sup>10</sup> This explains the observed slow rotational dynamics and clearly identifies the onset of the appearance of a crystalline phase in which the rotation of the probe essentially freezes, as has also been observed in AOT aqueous lamellar systems using the same probe molecule.<sup>34</sup> We analyze the biexponential anisotropy decay using a wobbling-in-cone model<sup>30, 41, 42</sup> (Figure 4.6.b) and found that the semi-cone angle of the wobbling motion decreases from  $49.3^\circ$  for 5% HPC to  $33.7^\circ$  for 25% HPC whereas the diffusion coefficient for the wobbling motion decreases by an order of magnitude ( $12.6 \times 10^{-8} \text{ s}^{-1}$  to  $8.8 \times 10^{-9} \text{ s}^{-1}$ ) on increasing the HPC concentration from 5% to 25% at 293 K. The observed decrease in the semi-cone angle and diffusion coefficient strongly confirms the

restriction imposed on the wobbling motion of water molecules with increasing HPC concentration.

The slow solvation relaxation time constant ( $\tau_2$ ) corresponds to the diffusional motion of the probe in the water-HPC network and this allows us to estimate the diffusion coefficient (D) of the aqueous environment at the interface. The magnitude of D is directly related to the rms distance  $\langle z \rangle^{1/2}$  traveled by the probe in time t by the relation,  $\langle z^2 \rangle = 2Dt$ . The rms distance can be approximated to as thickness of the bound water layer and for hydrophobic polymers, this has been reported to be equal to 3.3Å.<sup>43</sup> Assuming that only the slower solvation time constant ( $\tau_2$ ) is associated with the diffusional motion of the probe we calculate D and plot it against HPC concentration (Figure 4.4.b, inset). The diffusion coefficient is estimated to be  $12.1 \times 10^{-11} \text{ m}^2\text{s}^{-1}$  for 10% HPC, while it reduces to  $2.6 \times 10^{-11} \text{ m}^2\text{s}^{-1}$  for 40% HPC mixture. The observed D values are in good agreement with those reported for other polymer-water systems and are also reported to decrease with increasing polymer concentration.<sup>43, 44</sup> A previous MD simulation study<sup>43</sup> shows that translational diffusion coefficient for water molecules near the ether oxygen group of PEG is  $\sim 2 \times 10^{-11} \text{ m}^2\text{s}^{-1}$ , which corresponds well to the obtained D values in the present study at high HPC concentrations, while that in the bulk is  $\sim 3.3 \times 10^{-9} \text{ m}^2\text{s}^{-1}$ . The present results thus reflect formation of enhanced structure beyond 20% HPC in which the translational freedom of water near the polymer surface gets significantly reduced, which is well illustrated by a low value of D. As evidenced from the figure, the decrease in D suffers a transition beyond 20% HPC concentration, a result that corresponds to those obtained from solvation dynamics and rotational anisotropy measurements, and signifies the onset of a microscopic phase transition. It could be mentioned here that the slow relaxation process is principally associated with the coupled rotational-translational motion of the solvent molecules, a retardation of both the motions with increasing HPC concentrations is manifested with the phase change.

We now investigate the energetic of the relaxation process involved and in order to estimate the same we perform the time-resolved study at four different temperatures namely 273, 283, 293 and 303 K. Measurements at higher temperatures has not been carried out in order to avoid macroscopic phase separation. All the obtained C(t) curves are fitted bi-exponentially and the results are summarized in table 4.1 and Figure 4.4.c. A few representative C(t) curves at for 10, 20, 30 and 40% HPC at 273K are also shown in the inset

of Figure 4.4.b. As observed from Figure 4.4.c and Table 4.1, the average solvation time constant,  $\langle\tau\rangle$  decreases gradually with increasing temperature with three exceptions at 313 K with 10, 15 and 20% HPC. This observed phenomenon of temperature induced decrease in the relaxation time constant is consistent with earlier report of HPC-water,<sup>21</sup> PEG-water mixtures<sup>32</sup> and AOT lamellar systems.<sup>34</sup> While the study on HPC<sup>21</sup> is more centred on the dynamics of free water, the PEG-water,<sup>30</sup> AOT lamellar<sup>34</sup> and the present studies are essentially involved with the slow solvation dynamics, and both the processes show the same trend. The accelerated solvation dynamics could be attributed to the temperature induced conversion of ‘bound’ to ‘free’ or ‘bulk’ type water molecules present in the system.<sup>45, 46</sup> Such temperature dependency is also observed in rotational anisotropy studies wherein anisotropy decays get faster when temperature is increased (figures not shown). For example, in 10% HPC the fitted rotational time constants are 0.23 and 3.2 ns at 273 K, whereas at 303 K these change to 0.09 and 1.0 ns, respectively. A similar decrease is also noted in case of other solutions.

As corresponds to the other restricted systems studied earlier,<sup>30, 32, 34</sup> we assume the present system to obey an Arrhenius type of model for the solvation process and fit the time resolved C(t) data in the following equation,

$$\frac{1}{\langle\tau\rangle} \approx k = Ae^{-\frac{E_{act}}{RT}} \quad (4.3)$$

where  $E_{act}$  is the Arrhenius activation energy for the process and A is a pre-exponential factor. We plot  $\ln(1/\langle\tau\rangle)$  against  $1/T$  for all the four systems (Figure 4.4.c, inset). Good linear fits are obtained for 30 and 40% HPC systems, while for 10, 15 and 20% HPC a deviation from linearity is observed at 303 K. The reason for this deviation is not properly understandable; however, increased hydrophobicity of the systems at higher temperature might well be responsible for the observed deviation. From the slopes of the curves, we calculate the  $E_{act}$  values of  $4.5\pm 0.9$ ,  $4.1\pm 0.3$ ,  $3.9\pm 1.1$ ,  $2.05\pm 0.4$ ,  $2.0\pm 0.3$  and  $1.4\pm 0.1$  kcal mol<sup>-1</sup> for 10, 15, 20, 25, 30 and 40% HPC systems, respectively. The  $E_{act}$  values obtained for 10, 15 and 20% systems are in excellent agreement with those obtained for identical systems using DR studies.<sup>21</sup> These values are also in good agreement with those obtained for micro-heterogeneous systems like RM,<sup>30</sup> water-PEG mixture,<sup>32</sup> AOT aqueous lamellar system<sup>34</sup> etc.

using the same probe molecule. The free energy change associated with the relaxation process ( $\Delta G^*$ ) could be estimated using an Eyring model:

$$\frac{1}{\langle \tau \rangle} \approx k = \frac{h}{k_B T} e^{-\frac{\Delta G^\ddagger}{RT}} \quad (4.4)$$

and we obtain  $\Delta G^\ddagger$  values of 3.9, 3.5, 3.2, 1.5, 1.4 and 0.8 kcal mol<sup>-1</sup> respectively. An interesting feature is observed when  $E_{\text{act}}$  is plotted against HPC concentration (Figure 4.4.d) that  $E_{\text{act}}$  changes only marginally at low HPC concentration region (10 to 20% HPC), which is in good agreement to what has been obtained by Sudo et al.<sup>21</sup> using DR technique, and at high HPC ( $\geq 25\%$ ) concentration it decreases considerably, a phenomenon strikingly opposite to what has been obtained in the DR studies.<sup>21</sup> This apparently opposing phenomenon is enrooted in the two different relaxation processes probed by Sudo et al. and us. While the former one probes the fast relaxation process of the “free” water molecules our study is mainly aimed towards the slow moving “bound” type water molecules only, and quite intuitively the present decrease in  $E_{\text{act}}$  resembles an identical observation in AOT RM systems when the water content is decreased.<sup>30</sup> In order to investigate the reason behind the decrease in  $E_{\text{act}}$  with increasing HPC content, let us first discuss on the structure of water in HPC as the concentration of HPC changes. The main chain of HPC molecule behaves as a semi-rigid segment in aqueous solution and the side chains behave in a more flexible way.<sup>21, 47</sup> The side chain has an O-H group which can form hydrogen bond with neighboring HPC as well as water molecules. HPC with its high degree of hydroxypropyl substitution has only a few available hydrophilic sites to create a strong interaction with water molecules. At low concentration HPC acts as a hydrophilic polymer forming an isotropic solution and as the concentration increases it exhibits a hydrophobic behavior forming a cholesteric LC network structure, which also changes its interaction with water accordingly. The hydrogen bonding between HPC and water prevails at low concentration wherein water can form small clusters and the solvation process is slower compared to bulk water due to the heteromolecular hydrogen bonded water structure. These water molecules essentially act as “bound water” and contribute to the slow relaxation process (table 4.1). The activation energy values obtained is thus very similar to that obtained in case of other restricted environments like micelles, RM, vesicles, lamellar systems etc. and smaller than that of pure water. With increasing concentration HPC molecules starts forming intermolecular hydrogen bonded

cholesteric structure causing the viscosity of the system to increase significantly and the polymer solution turns hydrophobic in nature. This ruptures a fraction of HPC-water hydrogen bonds and results in a number of water molecules restricted in the structured HPC network. This preferentially reduces the fraction of bulk water molecules present in the solution and slows down the solvation dynamics. On the other hand, it also sets some water molecules ‘free’ and the relaxation time probed by Sudo et al.<sup>21</sup> in the high frequency region is exhibited by these ‘free water’ molecules and due to the less abundance of hetero-molecular water-HPC type hydrogen bonding in this phase, the  $E_{act}$  reaches a value similar to that of pure water and saturates at HPC concentration above 40%. In our present study, owing to the specific excitation of C-500 we preferentially probe the transition of water molecules at the HPC-water interface. At low HPC ( $\leq 20\%$ ) content it views the bound to bulk water transition which has an activation energy of 4-5 kcal mol<sup>-1</sup> and corresponds significantly with the obtained values. On the other hand, at high HPC concentrations ( $\geq 25\%$ ), it envisages the “interfacially bound” to “interfacially free” water transition, which typically has an energy difference of 1.3-2 kcal mol<sup>-1</sup>.<sup>45</sup> The observed  $E_{act}$  values at high HPC concentrations are thus in excellent agreement with this transition. It could also be noted here that with increasing temperature the aqueous solution of HPC turns hydrophobic. This in turn increases the possibility of the formation of intermolecular hydrogen bond network between HPC molecules and this perhaps slows down the solvation time constants for 10, 15 and 20% HPC solutions at 303 K (table 4.1).

In order to understand whether the “bound” to “bulk” type water transition shares the major contribution in the accelerated solvation dynamics at elevated temperatures, we measure the excitation spectra of HPC-water mixtures at different temperatures. As per our discussion earlier, the deconvoluted spectra provide information on the relative amount of water of the two different ‘species’ existing in the system. The temperature induced population ratio thus could lead us to an estimation of the energy barrier between the two ‘species’ of water. Let us first consider an equilibrium between ‘bound’ and ‘bulk’ type of water molecules present in the system,



and the corresponding population be denoted as  $n_{bound}$  and  $n_{bulk}$ . We now consider a simple Boltzmann type of distribution for both types of water species,

$$n_{bound} = n_0 e^{-\frac{E_{bound}}{RT}} \quad (4.6)$$

and

$$n_{bulk} = n_0 e^{-\frac{E_{bulk}}{RT}}$$

this leads us to the ratio,

$$\frac{n_{bound}}{n_{bulk}} = e^{-\frac{\Delta E}{RT}} \quad (4.7)$$

where,  $\Delta E$  stands for the energy difference between  $E_{bound}$  and  $E_{bulk}$ , which in principle be approximated to be equivalent to the activation energy  $E_{act}$  estimated from the solvation studies. To make an estimate of  $\Delta E$ , we deconvolute temperature dependent excitation curves of two samples, namely 10% and 40% HPC. A representative depiction of deconvolution for 40% HPC solution at 273 and 303 K are presented in Figure 4.2.a. We approximate that the excitation peak of C-500 in ‘bulk-water’ does not suffer appreciable change in this temperature range, and fix the bulk water peak at 390 nm while deconvoluting all the spectra. We plot  $\ln(n_{bound}/n_{bulk})$  against  $1/T$  for the two systems (Figure 4.2.b) and from the slopes, we calculate the  $\Delta E$  values to be 4.2 and 1.0 kcal mol<sup>-1</sup> for 10% and 40% HPC solution, respectively. These values are in striking correspondence with the obtained  $E_{act}$  values estimated from solvation studies. This strongly supports our notion that the observed change in  $E_{act}$  is principally governed by the inter-conversion of the two types of water species present in the system.

Finally, we explore the effect of the restriction imposed by the structure of HPC on the activity of water. We measure the reaction kinetics of benzoyl chloride (BzCl) in water-HPC mixtures at different HPC concentrations and the results are depicted in Figure 4.7.

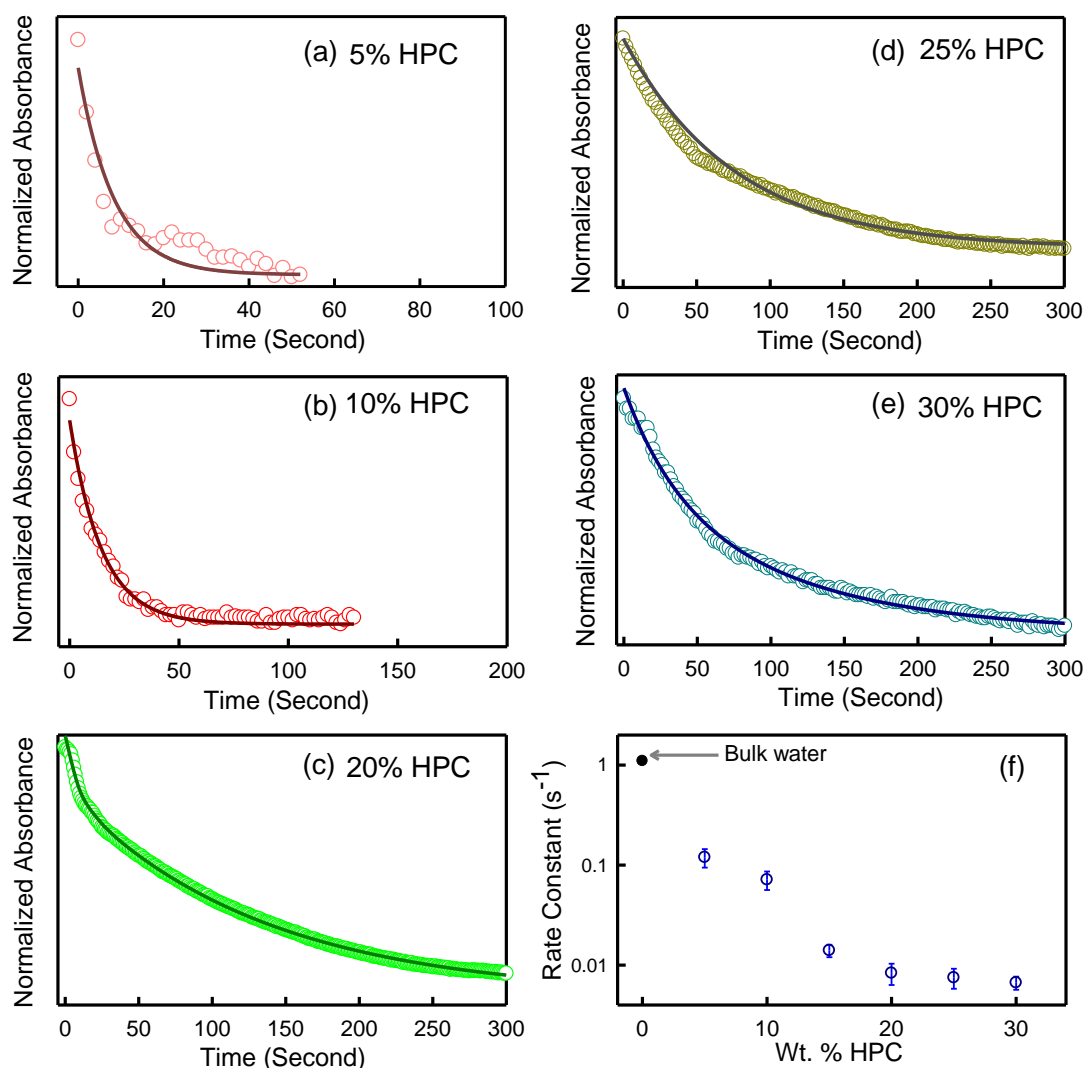


**Figure 4.7.** (a-e) Kinetics of BzCl hydrolysis in HPC-water mixtures at different HPC concentrations. The solid lines are the exponential fits of the data. (f) Rate constant of the hydrolysis reaction of benzoyl chloride at different HPC concentrations. The value for bulk water is shown with a black circle.

Solvolysis of BzCl is essentially a solvent mediated reaction in which water acts as a nucleophile and the rate of the reaction is primarily governed by the stability of the intermediate acylium carbocation, which in turn is dependent on the polarity of the environment.<sup>48</sup>

As evidenced from the figure, the rate of reaction slows down with increasing HPC concentration; for 5% HPC the rate is  $0.12 \text{ s}^{-1}$ , while for 10% it is  $0.07 \text{ s}^{-1}$ , however, with 20% and higher HPC concentrations, it decreases rapidly to a value of  $\sim 6 \times 10^{-3} \text{ s}^{-1}$ . Note that due to the very high absorption of cellulose in this region, we could not measure the kinetics for 40% HPC solution. It is worth noting here that the rate constant in water is  $1.1 \text{ s}^{-1}$ , and it gets reduced by 3-5 orders of magnitude in RMs and polymer solutions depending upon the extent of confinement imposed.<sup>32, 33, 49</sup> The observed rate is thus slower than that of bulk

water, indicating poor nucleophilicity and/or reduced polarity of the environment. Solvation dynamics and anisotropy studies have clearly identified restriction of the translational motion of water owing to heteromolecular hydrogen bonding, which correlates the observed kinetics data. It is interesting to note that the observed reaction rate at low HPC concentrations is an order of magnitude slower than that in water, however, at and beyond 20% HPC it gets another order of magnitude slower. Steady state emission results have clearly indicated a progressive blue shift of the emission maximum of C-500 with HPC concentration (Figure 4.1a), which in turn indicates a reduced polarity of the microenvironment, a situation unfavorable for the product formation. The further decrease of the reaction rate at 20% HPC concentration could be anticipated with the onset of the hydrophobicity of the polymer as well as the cholesteric structure formation in HPC coupled with the imposed restriction on water molecules within such structures as evidenced from solvation dynamics and anisotropy studies.

### 4.3. Conclusions:

The present time-resolved spectroscopic study reveals that the dynamics of water relaxation undergoes a characteristic transition beyond 20% HPC concentration, wherein a microscopic phase transition between isotropic to cholesteric phase sets in. This phenomenon is also supported by steady state emission and excitation studies, and a deconvolution of the excitation spectra clearly indicates transition between two 'species' of water. The calculated activation energy for water relaxation ( $E_{act}$ ) resembles those of other confined systems at low HPC concentrations, however, at higher HPC concentrations, it decreases significantly. This could be explained by the change in the nature of hydrogen bond structure in the water-HPC mixture at higher HPC concentration. The restriction imposed by the structure of HPC on the rotation of the fluorophore is also evident from time-resolved rotational anisotropy measurements. Finally the alteration in structure and dynamics of water molecules in the mixture is observed to affect the reactivity of water in the mixture.

### References:

1. Ball, P. (2008) Water as an Active Constituent in Cell Biology, *Chemical Reviews* 108, 74-108.
2. Pal, S. K., and Zewail, A. H. (2004) Dynamics of water in biological recognition, *Chemical Reviews* 104, 2099-2123.
3. Alvarez-Lorenzo, C., Gómez-Amoza, J. L., Martínez-Pacheco, R., Souto, C., and Concheiro, A. (2000) Interactions between hydroxypropylcelluloses and vapour/liquid water, *European Journal of Pharmaceutics and Biopharmaceutics* 50, 307-318.

4. Chang, Y. P., Karim, A. A., and Seow, C. C. (2006) Interactive plasticizing-antiplasticizing effects of water and glycerol on the tensile properties of tapioca starch films, *Food Hydrocolloids* 20, 1-8.
5. Yakimets, I., Wellner, N., Smith, A. C., Wilson, R. H., Farhat, I., and Mitchell, J. (2005) Mechanical properties with respect to water content of gelatin films in glassy state, *Polymer* 46, 12577-12585.
6. Giraudier, S., Hellio, D., Djabourov, M., and Larreta-Garde, V. (2004 ) Influence of Weak and Covalent Bonds on Formation and Hydrolysis of Gelatin Networks *Biomacromolecules* 5, 1662-1666.
7. Petersson, M., Lorén, N., and Stading, M. (2005) Characterization of Phase Separation in Film Forming Biopolymer Mixtures, *Biomacromolecules* 6, 932-941.
8. Shinouda, H. G., and Moteleb, M. M. A. (2005) Dielectric spectroscopy and relaxation phenomena of moistened and dry polysaccharides, *Journal of Applied Polymer Science* 98, 571-582.
9. Einfeldt, J., Meißner, D., and Kwasniewski, A. (2004) Molecular interpretation of the main relaxations found ID dielectric spectra of cellulose - experimental arguments, *Cellulose* 11, 137-150.
10. Ryabov, Y. E., Feldman, Y., Shinyashiki, N., and Yagihara, S. (2002) The symmetric broadening of the water relaxation peak in polymer-water mixtures and its relationship to the hydrophilic and hydrophobic properties of polymers, *The Journal of Chemical Physics* 116, 8610-8615.
11. Yakimets, I., Paes, S. S., Wellner, N., Smith, A. C., Wilson, R. H., and Mitchell, J. R. (2007) Effect of Water Content on the Structural Reorganization and Elastic Properties of Biopolymer Films: A Comparative Study, *Biomacromolecules* 8, 1710-1722.
12. (1971) *Hydroxypropylcellulose: chemical and physical properties*, Hercules Inc., Wilmington, DE.
13. Werbowyj, R. S., and Gray, D. G. (1980) Ordered Phase Formation in Concentrated Hydroxypropylcellulose Solutions, *Macromolecules* 13, 69-73.
14. Aspler, J. S., and Gray, D. G. (1981 ) Mixing of water with(hydroxypropyl)cellulose liquid crystalline mesophases, *Macromolecules* 14, 1546-1549.
15. Yamazaki, I., Winnik, F. M., Winnik, M. A., and Tazuke, S. (1987) Excimer formation in pyrene-labeled hydroxypropyl cellulose in water: picosecond fluorescence studies, *The Journal of Physical Chemistry* 91, 4213-4216.
16. Fortin, S., and Charlet, G. (1989) Phase diagram of aqueous solutions of (hydroxypropyl)cellulose, *Macromolecules* 22, 2286-2292.
17. Streletsky, K. A., and Phillies, G. D. J. (1998) Relaxational mode structure for optical probe diffusion in high molecular weight hydroxypropylcellulose, *Journal of Polymer Science Part B: Polymer Physics* 36, 3087-3100.
18. Mustafa, M. B., Tipton, D. L., Barkley, M. D., Russo, P. S., and Blum, F. D. (1993) Dye diffusion in isotropic and liquid-crystalline aqueous (hydroxypropyl)cellulose, *Macromolecules* 26, 370-378.
19. Phillies, G. D. J., and Quinlan, C. A. (1995) Analytic structure of the solutionlike-meltlike transition in polymer dynamics, *Macromolecules* 28, 160-164.
20. Phillies, G. D. J., O'Connell, R., Whitford, P., and Streletsky, K. A. (2003) Mode structure of diffusive transport in hydroxypropylcellulose:water, *The Journal of Chemical Physics* 119, 9903-9913.
21. Sudo, S. (2011) Dielectric Properties of the Free Water in Hydroxypropyl Cellulose, *The Journal of Physical Chemistry B* 115, 2-6.
22. Immaneni, A., Kuba, A. L., and McHugh, A. J. (1997) Effects of Temperature and Solvent on the Rheo-optical Behavior of Hydroxypropylcellulose Solutions, *Macromolecules* 30, 4613-4618.
23. Beheshti, N., Bu, H., Zhu, K., Kjøniksen, A.-L., Knudsen, K. D., Pamies, R., Cifre, J. G. H., García de la Torre, J., and Nyström, B. (2006) Characterization of Interactions in Aqueous Solutions of Hydroxyethylcellulose and Its Hydrophobically Modified Analogue in the Presence of a Cyclodextrin Derivative, *The Journal of Physical Chemistry B* 110, 6601-6608.
24. Bu, Z., and Russo, P. S. (1994) Diffusion of Dextran in Aqueous (Hydroxypropyl)cellulose, *Macromolecules* 27, 1187-1194.
25. Wojciechowski, P., Joachimiak, A., and Halamus, T. (2006) Nature of water molecules in hydrogels based on a liquid crystalline cellulose derivative, *Polymers for Advanced Technologies* 14, 826-831.
26. Wirick, M. G., and Waldman, M. H. (1970) Some solution properties of fractionated water-soluble hydroxypropylcellulose, *J. Applied Polym. Sci.* 14, 579-597.

27. Samuels, R. J. (1969) Solid-state characterization of the structure and deformation behavior of water-soluble hydroxypropylcellulose (pages 1197-1258), *Journal of Polymer Science Part B: Polymer Physics* 7, 1197-1258.
28. Sugimoto, H., Miki, T., Kanayama, K., and Norimoto, M. (2008) Dielectric relaxation of water adsorbed on cellulose *J. Non-Cryst. Solids* 354, 3220-3224.
29. Mitra, R. K., Sinha, S. S., and Pal, S. K. (2007) Temperature Dependent Hydration at Micellar Surface: Activation Energy Barrier Crossing Model Revisited, *The Journal of Physical Chemistry B* 111, 7577-7581.
30. Mitra, R. K., Sinha, S. S., and Pal, S. K. (2008) Temperature-Dependent Solvation Dynamics of Water in Sodium Bis(2-ethylhexyl)sulfosuccinate/Isooctane Reverse Micelles, *Langmuir* 24, 49-56.
31. Mitra, R. K., Sinha, S. S., Verma, P. K., and Pal, S. K. (2008) Modulation of Dynamics and Reactivity of Water in Reverse Micelles of Mixed Surfactants *The Journal of Physical Chemistry B* 112, 12946-12953.
32. Verma, P. K., Mitra, R. K., and Pal, S. K. (2009) A Molecular Picture of Diffusion Controlled Reaction: Role of Microviscosity and Hydration on Hydrolysis of Benzoyl Chloride at a Polymer Hydration Region, *Langmuir* 25, 11336-11343.
33. Verma, P. K., Makhil, A., Mitra, R. K., and Pal, S. K. (2009) Role of Solvation Dynamics in the Kinetics of Solvolysis Reactions in Microreactors, *Physical Chemistry Chemical Physics* 11, 8467-8476.
34. Verma, P. K., Saha, R., Mitra, R. K., and Pal, S. K. (2010) Slow water dynamics at the surface of macromolecular assemblies of different morphologies, *Soft Matter* 6, 5971-5979.
35. Banerjee, D., Verma, P. K., and Pal, S. K. (2009) A Temperature Dependent Femtosecond-Resolved Hydration Dynamics of Water in Aqueous Guanidinium Hydrochloride Solution, *Photochemical Photobiological Science*. 8, 1441-1447.
36. Majumder, P., Sarkar, R., Shaw, A. K., Chakraborty, A., and Pal, S. K. (2005) Ultrafast dynamics in a nanocage of enzymes: Solvation and fluorescence resonance energy transfer in reverse micelles, *Journal of Colloid and Interface Science* 290, 462-474.
37. Koti, A. S. R., Krishna, M. M. G., and Periasamy, N. (2001) Time-resolved area-normalized emission spectroscopy (TRANES): A novel method for confirming emission from two excited states, *The Journal of Physical Chemistry A* 105, 1767-1771.
38. Fee, R. S., and Maroncelli, M. (1994) Estimating the time-zero spectrum in time-resolved emission measurements of solvation dynamics, *Chemical Physics* 183, 235-247.
39. Sudo, S., Oshiki, N., Shinyashiki, N., and Yagihara, S. (2007) Dielectric Properties of Ethyleneglycol-1,4-Dioxane Mixtures Using TDR Method, *The Journal of Physical Chemistry A* 111, 2993-2998.
40. Nad, S., and Pal, H. (2003) Photophysical Properties of Coumarin-500 (C500): Unusual Behavior in Nonpolar Solvents, *The Journal of Physical Chemistry A* 107, 501-507.
41. Lipari, G., and Szabo, A. (1982) Model-free approach to the interpretation of nuclear magnetic resonance relaxation in macromolecules. 1. Theory and range of validity, *Journal of the American Chemical Society* 104, 4546-4559.
42. Lipari, G., and Szabo, A. (1980) Effect of librational motion on fluorescence depolarization and nuclear magnetic resonance relaxation in macromolecules and membranes, *Biophysical Journal* 30, 489.
43. Tasaki, K. (1996) Poly(oxyethylene)-Water Interactions: A Molecular Dynamics Study, *Journal of the American Chemical Society* 118 8459-8469.
44. Faraone, A., Magazù, S., Maisano, G., Migliardo, P., Tettamanti, E., and Villari, V. (1999) The puzzle of poly(ethylene oxide) aggregation in water: Experimental findings, *The Journal of Chemical Physics* 110, 1801-1806.
45. Pal, S., Balasubramanian, S., and Bagchi, B. (2003) Identity, Energy, and Environment of Interfacial Water Molecules in a Micellar Solution, *The Journal of Physical Chemistry B* 107, 5194-5202.

46. Balasubramaian, S., Pal, S., and Bagchi, B. (2002) Hydrogen-Bond Dynamics near a Micellar Surface: Origin of the Universal Slow Relaxation at Complex Aqueous Interfaces, *Physics Review Letter* 89, 115505.
47. Evmenenko, G., Yu, C.-J., Kewalramani, S., and Dutta, P. (2004) Structural Characterization of Thin Hydroxypropylcellulose Films. X-ray Reflectivity Studies, *Langmuir* 20, 1698-1703.
48. Bentley, T. W., Carter, G. E., and Harris, H. C. (1984) S N 2 character of hydrolysis of benzoyl chloride, *Journal of the Chemical Society, Chemical Communications*, 387-389.
49. Garcia-Rio, L., Leis, J. R., and Iglesias, E. (1995) Influence of Water Structure on Solvolysis in Water-in-Oil Microemulsions, *The Journal of Physical Chemistry* 99, 12318-12326.

# Chapter 5: Structure and Dynamics of Water in Confined Environments

**5.1. Introduction:** Water involved in most of the biological processes does not exist in its bulk form, rather it finds itself in restricted environments with the nm range length scale in which the confined water molecules strongly interact with the interface, ions and molecular groups. Reverse micelles (RMs) serve as one of the most potential platforms to study the properties of water under nano-confinement. RMs are isotopic mixture of water, surfactant, and organic solvent in which small aqueous droplets coated with a layer of surfactant molecules are dispersed in a nonpolar solvent.<sup>1</sup> Water encapsulated in reverse micellar (RM) water-pool often show significant differences in their physical and chemical properties relative to its bulk properties. This has attracted major attention in the scientific community as RM systems often serve as a potential platform to mimic membranes. Such modifications are attributed to the heterogeneous bonding of the encapsulated water molecules with the RM interface. Water in the vicinity of the surface are supposed to be highly structured and retarded in their dynamics.<sup>2-8</sup> NMR studies of confining proteins within the nanoscale interior of AOT RM report significant reduced motion of the protein hydration water<sup>9, 10</sup>. Studies have also shown that the interaction of surfactant head group and water does play a pivotal role, however, the influence of charge of the interface, role of surface topology and surfactant film curvature on the hydration structure and dynamics has been neglected so far.

Structure<sup>11-15</sup> and dynamics<sup>2, 5, 16-21</sup> of confined water in RM systems have been studied in detail using various experimental techniques as well as MD simulation.<sup>2, 4, 8, 22-33</sup> It has been inferred that the hydrogen bonded water structure gets perturbed upon confinement resulting in a larger fraction of water molecules with distorted hydrogen bonding relative to its bulk counterpart. Also it has been shown that dynamics of water molecules get retarded due to its interaction with the surfactant head groups. Time resolved IR<sup>5, 7, 18, 34</sup> and fluorescence<sup>2, 35-37</sup> spectroscopic studies have revealed that there exists at least two types of water species inside the RM water pool, namely ‘bound’ (water molecules bound to the surfactant head group with a dynamics significantly slower than that of bulk water) and ‘bulk-type’ (water molecules having regular tetrahedral hydrogen bonded network). The ‘bound’ water molecules exhibit a coupled rotational-translational solvation dynamics which is order of magnitude slower than the ultrafast relaxation dynamics observed in bulk water.<sup>20</sup>

<sup>38-40</sup> It is debatable whether a third contribution of water, which is not bound but retarded in hydration dynamics, had to be taken into consideration. The exchange equilibrium between these two types of water molecules is believed to depend upon the nature of the RMs, however, it needs a generalized approach to understand how the chemical, mechanical and electrical properties of the interface govern the nature of the confined water molecules.<sup>41</sup> In most of these systems, an Arrhenius type of barrier crossing model defines the temperature induced cross over between the two types of water molecules.<sup>40, 42</sup> Most of these earlier studies have been carried out using anionic surfactant AOT as it can form spherical RM droplets of tunable water pool size over a wide range.<sup>43</sup> Recent efforts from the Fayer group<sup>4, 41, 44</sup> in order to underline such questions have revealed that the vibrational stretching dynamics of water molecules (ps to sub-ps order) is indeed dependent on the nanoscopic dimension of the water pool. It appears therefore interesting to investigate whether the same conjecture holds true for the slower relaxation dynamics in such systems. In addition it is also interesting to investigate how a change in the morphology of RM interface affects the water dynamics inside the RM water-pool.

Depending upon the nature of the head group, surfactants are classified into four types: cationic, anionic, zwitterionic and nonionic. In order to study the effect of interfacial charge on the structure and dynamics of water in confinement we have used three surfactants with differently charged head groups, anionic AOT, nonionic Igepal (Igepal CO-520) and cationic DDAB. Cyclohexane (Cy) has been used as the hydrocarbon phase. AOT is soluble in Cy and produces RM systems up to  $w_0$  ( $w_0 = [Water]/[Surfactant]$ )  $\sim 20$ .<sup>45, 46</sup> Igepal has head group terminated by an alcohol hydroxyl group and is also capable to form well defined spherical RM up to  $w_0=20$ .<sup>45</sup> The size of RMs in both the systems increases linearly with  $w_0$  with Igepal forming slightly bigger RMs compared to that of AOT.<sup>47, 48</sup> Due to the double tailed wedge shape AOT stands as a perfect candidate for the formation of RMs in almost all hydrocarbons.<sup>43</sup> There have been a few studies to establish the influence of the interface charge type (cationic and anionic) on the activity of water inside RMs following solvolysis and/or enzyme catalysis reactions; these studies concluded greater nucleophilicity of water inside anionic RM while higher hydrogen bond donor capability inside cationic RM.<sup>49-52</sup> It has also been reported<sup>5</sup> that the relaxation dynamics of confined water is faster in nonionic (Igepal) RM than the ionic (AOT) one.<sup>53</sup> It is also interesting to note that the penetration of the hydrocarbon into the surfactant monolayer does affect its chemical and mechanical properties.<sup>54</sup> Thus, in order to discard this effect, it is important to use a single

hydrocarbon oil to prepare all the RM systems. The choice of DDAB/alkane/water as a model system is quite deliberate, since this system offers a rather unusual phase behavior along the  $w_0$  in the ternary phase diagram.<sup>55</sup> The maximum water solubilization capacity,  $w_0$  of this system is usually smaller than the conventional surfactant systems<sup>56</sup> due to the low hydrophilicity of quaternary ammonium head group of DDAB.<sup>57</sup> At low hydration the system essentially consists of cylindrical rod-like aggregated structures. As the water content is gradually increased, the microstructure changes into discrete droplet type,<sup>55, 58-68</sup> which strongly corresponds to a substantial modification of the elastic property of the DDAB monolayer curving around water in alkane continuum during the course of microscopic phase transition. Small angle neutron scattering (SANS) studies for DDAB/Cy/water system<sup>55</sup> have demonstrated that at low hydration ( $2 < w_0 < 8$ ), the system consists mainly of aggregated rod-like cylinders with length ( $l$ ) varying from 14-20 nm, and radius ( $r$ ) varying from 1.5 to 1.6 nm. At increased hydration ( $w_0 \geq 10$ ) spherical aggregates are formed having a diameter of  $\sim 6$  nm. Such a transition has successfully been explained on the basis of a distorted-open-connected cylinders (DOC) model.<sup>58</sup> The cylindrical rod to sphere transition essentially corresponds to a restricted degree of freedom in the translational motion, which might enforce a modification in the relaxation dynamics. Also, in contrast to conventional RM systems, DDAB RM systems exhibit both 'volume induced' and 'temperature induced' reverse percolation of conductance<sup>69-71</sup> which manifests a transition from connected to discrete structures with increasing  $w_0$  as well as increasing temperature.

In order to determine the restriction on motion upon confinement, the slow relaxation dynamics of water molecules in RMs has been measured using ps-resolved fluorescence spectroscopic technique using different fluorophores, namely C-500, C-343 and ANS (molecular structure and details are given in chapter-2). The choice of the fluorophores lies on the specific location of the probes in the RMs so that the relaxation dynamics of water at different region of the RMs could be extracted. To underline the dependence of physical properties of water on the nature of interface we have carried out mid-IR (MIR) and far-IR (FIR) FTIR spectroscopic investigation. MIR and FIR data provide information on the hydrogen bonding ability and the hydrogen bonded connectivity network of water inside these RMs. For FTIR measurements we have used several hydration levels, namely  $w_0 = 2, 5, 7.5, 10$  and  $12.5$ . As a complementary information on the estimation of the dynamics of the collective motion of water molecules we carry out dielectric relaxation study using THz time domain spectroscopy in the 0.2-2.0 THz frequency range using double Debye relaxation as a

fitting model. Our study is aimed to underline any possible correlation of the water structure and dynamics in RM systems with the geometry and charge type of the interface.

## 5.2. Results and Discussions:

### 5.2.1. Solvent Dynamics in Reverse Micellar Water-Pool: A Spectroscopic Investigation of DDAB/Cyclohexane/Water Systems

**MIR-FTIR:** Figure 5.1.a shows a representative difference absorbance spectra (in the 3000-3700  $\text{cm}^{-1}$  region) of DDAB/Cy/water system at  $w_0=2.0$  and 10 at two limiting temperatures (293 and 323 K). It is worth mentioning here that Cy has negligible absorbance in this studied frequency range (data not shown). The difference absorbance spectra are the differences between the measured absorbance of the samples with that of the stock solution at  $w_0=1$ . For the sample at highest water content ( $w_0=12.5$ ), the added volume of water is only 2% compared to the total volume of the stock solution, indicating that the reduced volume fraction of the stock solution in all investigated RM systems is negligible. Therefore, the difference spectra can be attributed to the water molecules present in the RM systems. The MIR spectrum of water at 293 K could be deconvoluted into three Gaussian curves with peaks at  $\sim 3590$  ( $\nu_3$ ), 3460 ( $\nu_2$ ) and 3330  $\text{cm}^{-1}$  ( $\nu_1$ ). These bands correspond to isolated, distorted structured and hydrogen-bonded water molecules, respectively.<sup>72</sup> With increasing temperature from 293 to 323 K, the peak positions at  $\sim 3590$  and 3330  $\text{cm}^{-1}$  change marginally, whereas that at 3460  $\text{cm}^{-1}$  undergoes a considerable blue shift.<sup>72-74</sup>

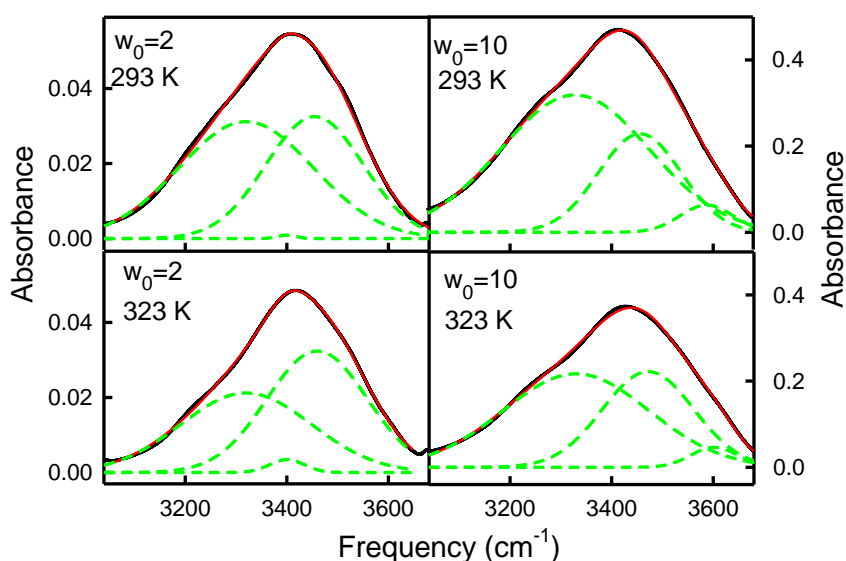


**Figure 5.1.** MIR-FTIR spectra of DDAB/Cy/water reverse micellar systems with  $w_0=2$  and  $w_0=10$  at 293 and 323 K (black solid lines). Each spectrum is deconvoluted into three curves (green broken lines), the red curves represent overall fitting.

We deconvolute the spectra of water obtained at different temperatures.<sup>72</sup> The relative contributions of each band at 293 and 323 K are depicted as blue and red colored hollow symbols, respectively in Figure 5.2.a. The population of ‘isolated water molecules’ ( $v_3$ ) is expected to be low (<10%) and does not change appreciably with temperature. When we increase the temperature from 293 to 323K, the intensity of the  $v_2$  band increases gradually (from 30% to 34%), whereas that of the  $v_1$  band decreases from 65% to 62%. This change could be attributed to a decrease in the number of strongly hydrogen bonded water molecules as with thermal energy a fraction of hydrogen bonded water network gets disrupted. For the deconvolution, we have fixed the three peak positions to those of bulk water. Better fitting results could be obtained when the peak positions were varied; however, when fixing the peak positions, we obtain information on the relative change in population of each sub-bands compared to those of pure water. In case of  $w_0=2$  system no peak can be found in the  $\sim 3595$   $\text{cm}^{-1}$  region, instead a weak peak at  $\sim 3400$   $\text{cm}^{-1}$  can be observed (Figure 5.1.a). For the other samples, the curves can be fitted using the peak positions of bulk water and a representative illustration for  $w_0=10$  system is shown in Figure 5.1.a. The relative integrated area of each band relative to the total area is plotted as a function of  $w_0$  for four different temperatures (Figure 5.2.a).

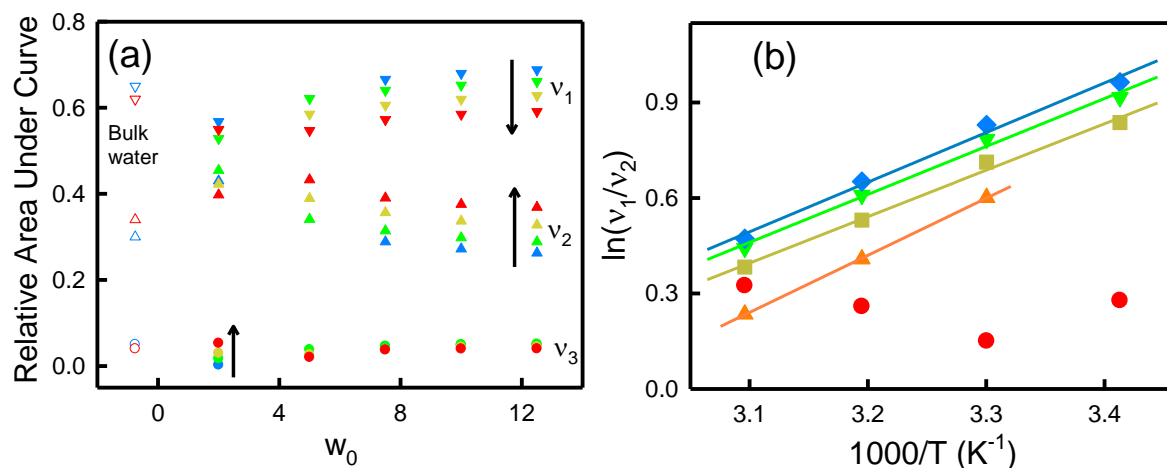


**Figure 5.2.** (a) Relative area under each deconvoluted curve is shown as a function of  $w_0$  and temperature (blue: 20°C, green: 30°C, yellow: 40°C, red: 50°C). The arrows indicate increasing temperature.  $v_1$  and  $v_2$  represents the curves with peak frequency at  $\sim 3300$  and  $3460$   $\text{cm}^{-1}$ , respectively.  $v_3$  stands for the  $\sim 3400$   $\text{cm}^{-1}$  curve for  $w_0=2$  system and  $\sim 3590$   $\text{cm}^{-1}$  curve for the remaining systems. The corresponding values for pure water at 293 (blue) and 323 K (red) are shown in hollow symbols for comparison. (b) Plot of  $\ln(v_1/v_2)$  against  $1/T$  for  $w_0=2$  (circle), 5 (up triangle), 7.5 (square), 10 (down triangle) and 12.5 (diamond). The solid lines are linear fits.

This relative contribution is essentially proportional to the relative abundance of that particular ‘species’ of water molecules. It has been observed that the water molecules

contributing to  $\nu_3$  have a very low population ( $\leq 10\%$ ), while that for  $\nu_1$  are the most abundant. Such a population difference is also evident in bulk water, however, their relative population is different. At small  $w_0$  values ( $w_0 \leq 5$ ), the intensity of the  $\nu_1$  band is decreased compared to that in bulk water, whereas, it is found to be increased for the  $\nu_2$  band.  $\nu_1$  increases while  $\nu_2$  decreases with hydration and at  $w_0 \geq 7.5$ , the population distribution resembles that of bulk water. The difference in the abundance of different water species in RM as compared to bulk water indicates the inhomogeneity in bonding of water molecules with the RM interface.<sup>11-15, 75</sup> At low hydration, water molecules in contact with the surface are dominating. This can be correlated with the observed higher abundance of distorted H-bond network. We observe a higher population of  $\nu_2$  species with increasing hydration when stronger hydrogen bonds between water molecules start building and the  $\nu_1$  population reaches that of pure water. As observed from the Figure 5.2.a, the relative abundance of three types of water molecules in the systems remain practically unaltered at and beyond  $w_0 = 7.5$ . It could be argued that further addition of water does not modify the interface-water interaction significantly and the structural evolution of water as evidenced in lower hydration limit levels off. Such invariance has also been observed in the time resolved fluorescence studies (see later).

With increasing temperature, the intensity of  $\nu_2$  band increases gradually at the expense of the  $\nu_1$  band for all the  $w_0$  systems, while that of  $\nu_3$  remains almost constant with temperature. It can thus be concluded that the effective decrease in the population of water molecules contributing to  $\nu_1$  is compensated by the increase in those contributing to  $\nu_2$ . Such a temperature induced variation in the relative population corresponds to an activation barrier crossing model.

**FIR-FTIR:** In order to investigate the collective dynamics of water molecules encapsulated in the RM systems, we have carried out far-infrared (FIR) FTIR measurements of all the systems at different temperatures. Some representative results are shown in Figure 5.3. In pure water, two characteristic peaks can be found in this frequency range, one in the  $\sim 200$   $\text{cm}^{-1}$  region and the other in the  $\sim 600$   $\text{cm}^{-1}$  region, the former peak is assigned to the intermolecular collective vibration mode of water molecules while the later one results from the librational motion of water molecules in a hydrogen bonded connected network.<sup>76-78</sup> With increasing temperature the peaks undergo progressive red shift which is attributed to the weakening of hydrogen bonding.<sup>76</sup> It is interesting to note that in all the studied RM systems,

both the two bands are distinctly apparent confirming the presence of intermolecular connective water network even at low  $w_0$  values. This agrees well with the anticipated cylindrical structure of the droplets at low hydration. However, both bands are significantly red shifted compared to that of bulk water, especially at low  $w_0$ .

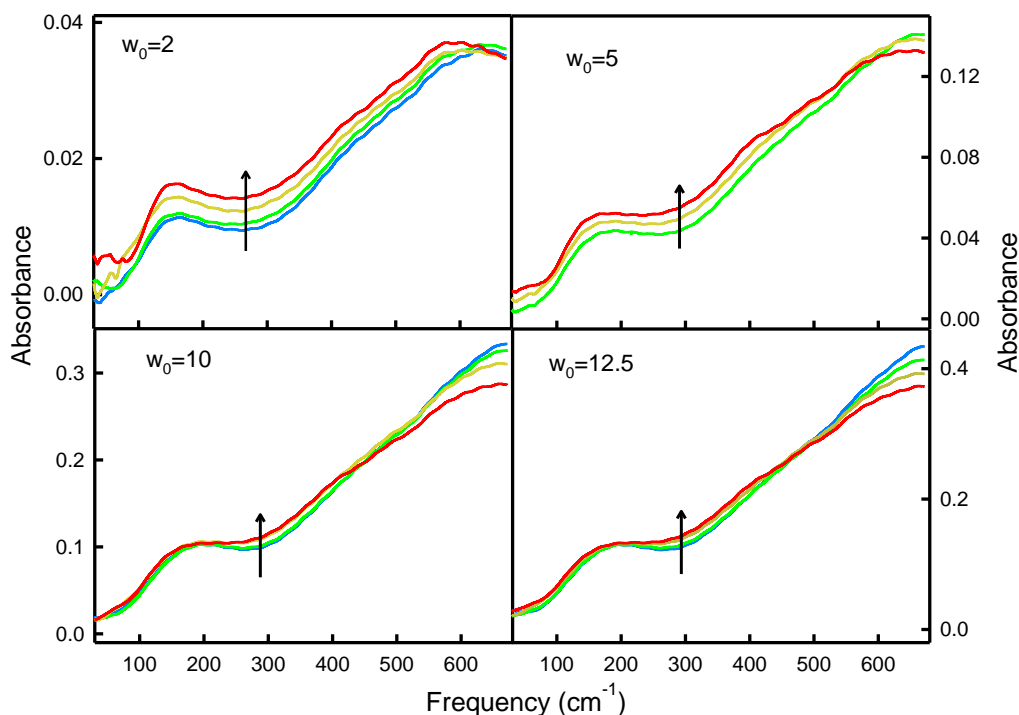


**Figure 5.3.** FIR-FTIR spectra of DDAB/Cy/water reverse micellar systems at different  $w_0$  values at temperatures of 293, 303, 313 and 323 K. The arrows show the trend for increasing temperature.

The red shift originates from the perturbation of the hydrogen bonded network in the RM waterpool caused by the inhomogeneous hydrogen bonding of water molecules with the interface. As a consequence the hydrogen bonds in the ‘bound’ water region get weakened due to significant interfacial interaction and high degree of orientation relative to the surface head group.<sup>79, 80</sup> In pure water the relative intensity of the  $\sim 200\text{ cm}^{-1}$  peak is 2.3 times smaller than that of the librational peak, whereas for the RM systems, this ratio is 3.4 for  $w_0=2$  and 3.1 for  $w_0=10$  at 293 K, indicating a considerable modification of the collective hydrogen bonded network in the RM interior. Both the peak positions show only a marginal shift with hydration as compared to the conventional AOT RM systems in which considerable shift of the librational band was found with increasing hydration.<sup>80</sup> The librational peak suffers a small red shift with temperature, whereas that of the intermolecular stretching remains unaltered.

**Fluorescence Spectroscopy:** Steady-state and time resolved fluorescence measurements have been carried out using coumarin 500 (C-500), which has extensively been used as a fluorophore to study the relaxation dynamics of water in confined systems.<sup>40, 81-84</sup> The absorption spectrum of C-500 in Cy produces a peak at ~360 nm along with a shoulder at ~380 nm (Figure not shown). C-500 is sparingly soluble in water and produces a peak at ~390 nm, however, in the RM systems this peak is red shifted as a result of the contribution of the fraction of C-500 population residing in the interfacial region.

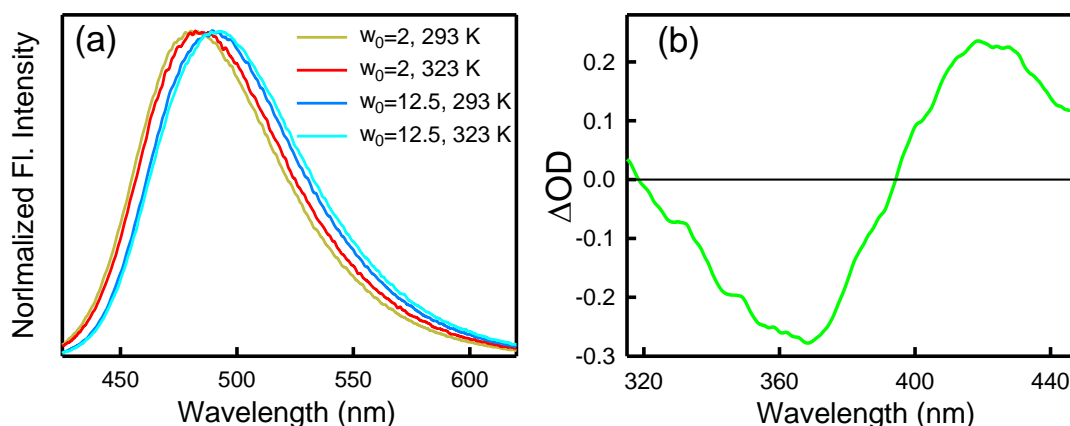


**Figure 5.4.** (a) Steady state fluorescence spectra of C-500 in DDAB/Cy/water reverse micellar systems at different  $w_0$  and temperature. (b) The difference absorption spectrum of C-500.

When we subtract the absorbance of C-500 in water from that of the RM we find a prominent peak at 420 nm (Figure 5.4.b). In the present investigation we excite the probe at 409 nm which selectively excites the probe molecules residing at the DDAB interface only. In all the studied RM systems, C-500 (excited at 409 nm) exhibits a single emission peak which undergoes a ~10 nm red shift when  $w_0$  is increased from 2 to 12.5 (Table 5.1.1, Figure 5.4.a). It can be observed that at and beyond  $w_0=7.5$ , there occurs only marginal change in the peak maximum, a phenomenon in accordance with MIR-FTIR studies. A marginal red shift (2-3 nm) is observed when temperature is increased. The DDAB RM systems yield 5-6 nm blue shifted emission maximum of C-500 compared to AOT RM,<sup>40</sup> which identifies a less polar environment in the former system as experienced by the fluorophore.

In order to understand the dynamics of the encapsulated water in these RM systems, we carry out time-resolved fluorescence (TRF) studies. Figure 5.5.a shows a representative decay transient of C-500 in  $w_0=10$  system at 293 K.

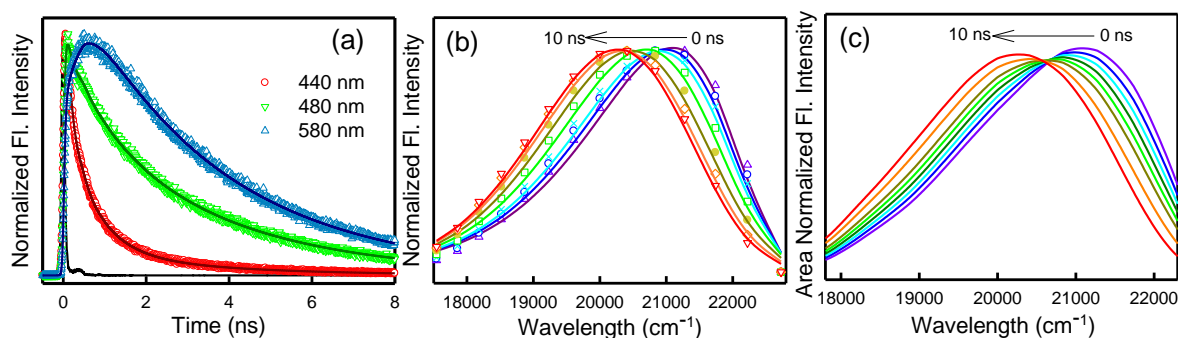


**Figure 5.5.** (a) Wavelength dependent decay transients of C-500 present in DDAB/Cy/water reverse micellar systems with  $w_0=10$  at 293 K. The solid lines represent multi-exponential fittings. (b) Time resolved emission spectra (TRES) of C-500 present in DDAB/Cy/water reverse micellar systems with  $w_0=10$  at 293 K. (c) The corresponding Time-resolved area normalized emission spectra (TRANES).

**Table 5.1.1.** Fitting parameters of bi-exponential fitting of solvent correlation function  $C(t)$  for C-500 in DDAB/Cy/water RM systems at different  $w_0$  and temperatures.  $\lambda_{max}$  presents the emission maximum of C-500 in each system. (1. from reference 70.)

Temperature	$\lambda_{max}$ (nm)	$a_1$	$a_2$	$\tau_1$ (ns)	$\tau_2$ (ns)	$\langle\tau\rangle$ (ns)
<b>Water<sup>1</sup></b>						
283 K	~505	-	-	0.00031	0.001	-
293 K	-	-	-	0.00033	0.00071	-
307 K	-	-	-	0.00038	0.00055	-
328 K	~505	-	-	0.0003	-	-
<b><math>w_0=2</math></b>						
293 K	480	0.38	0.62	0.27	1.45	1.00
303 K	483	0.33	0.67	0.21	0.88	0.66
313 K	485	0.25	0.75	0.97	0.23	0.41
323 K	482	0.50	0.50	0.20	0.75	0.48
<b><math>w_0=5</math></b>						
293 K	-	-	-	-	-	-
303 K	487	0.41	0.59	0.20	0.59	0.43
313 K	488	0.49	0.51	0.20	0.52	0.36
323 K	489	0.66	0.34	0.20	0.56	0.32
<b><math>w_0=7.5</math></b>						
293 K	488	0.23	0.77	0.16	0.51	0.43
303 K	489	0.43	0.57	0.20	0.50	0.37
313 K	489	0.56	0.44	0.21	0.47	0.32
323 K	491	0.67	0.33	0.18	0.53	0.29
<b><math>w_0=10</math></b>						
293 K	489	0.19	0.81	0.17	0.44	0.38
303 K	491	0.51	0.49	0.22	0.43	0.32
313 K	492	0.60	0.40	0.18	0.45	0.28
323 K	492	0.79	0.21	0.18	0.51	0.25
<b><math>w_0=12.5</math></b>						
293 K	490	0.18	0.82	0.15	0.42	0.38
303 K	491	0.51	0.49	0.19	0.46	0.32
313 K	492	0.65	0.35	0.19	0.43	0.27
323 K	492	0.86	0.14	0.18	0.55	0.23

The decay transients are wavelength dependent. For example, with  $w_0=10$  at 293 K, the transient at 440 nm can be fitted to three decay components of 165 (50%), 705 (36%) and 3320 (14%) ps, whereas the transient at 580 nm shows a distinct rise component of 370 ps,

along with two decay components of 1600 and 3600 ps. Such a wavelength dependency of decay transients clearly indicates solvation of the probe by water molecules. We construct the time resolved emission spectra (TRES) (a representative TRES for  $w_0=10$  system at 293 K is shown in Figure 5.5.b) and have deduced the solvent correlation functions,  $C(t)$  for all these systems. At a first step, we check that the observed time resolved spectral shift is not associated with any internal photophysics of the probe itself. In order to do so we construct the time-resolved area normalized emission spectra (TRANES)<sup>85</sup> for all these systems. A representative illustration for  $w_0=10$  at 293 K is shown in Figure 5.5.c. No apparent iso-emissive point is recognized in the TRANES profile, which confirms that the probe contains only a single ‘species’. Therefore, the observed time dependent spectral shift can be attributed solely to the inhomogeneity of the microenvironment experienced by the probe. The  $C(t)$  curves can be fitted using the following bi-exponential decay function,  $C(t) = a_1 e^{-t/\tau_1} + a_2 e^{-t/\tau_2}$  where  $\tau_1$  and  $\tau_2$  represent two characteristic time scales assigned to two different relaxation processes of water molecules. Some representative fitted curves at 303 K are shown in Figure 5.6.a. The results of all the fits at different  $w_0$  and temperatures are shown in Table 5.1.1. The relaxation time constants are in the order of a few hundreds ps, which in turn is an order of magnitude slower than those of bulk water.<sup>86</sup>

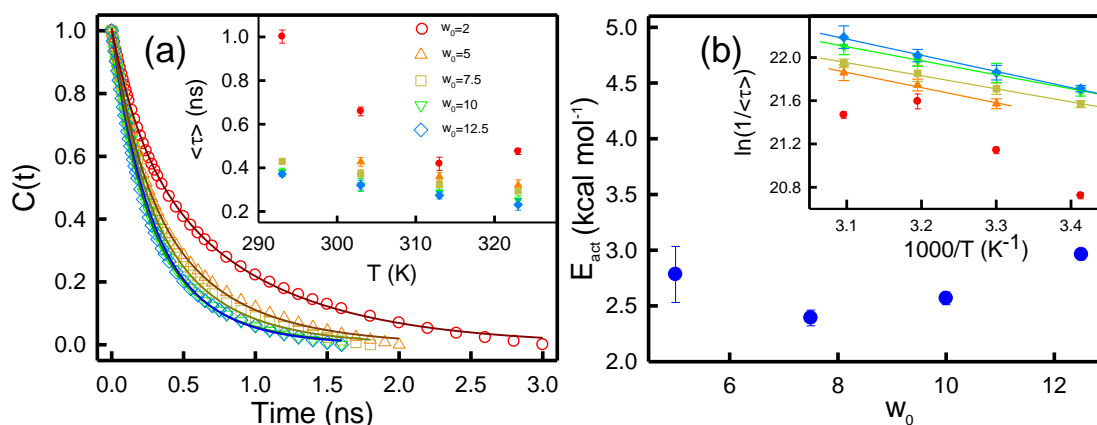


**Figure 5.6.** (a) Solvent correlation function  $C(t)$  curves for C-500 in DDAB/Cy/water reverse micellar systems at different  $w_0$  values at 303 K. The solid lines represent biexponential fit of the curves. The obtained average solvation time constant  $\langle \tau \rangle$  at different  $w_0$  values at four different temperatures are shown in the inset. (b) The Arrhenius plots of  $\ln(1/\langle \tau \rangle)$  against  $1/T$  for all the systems are shown in the inset. The solid lines are linear fitting. The obtained activation energies are plotted against  $w_0$  in the main figure.

Earlier studies have revealed the ultrafast relaxation time constants of C-500 in bulk water to be 0.3 ps and 0.7 ps at 293 K.<sup>87</sup> In order to compare the slow dynamics in RM with the fast dynamics of bulk water, we present the time constants of bulk water (as obtained from reference 70) in Table 5.1.1. Among the observed two slow relaxation timescales in RM

systems,  $\tau_1$  mainly emanates from the hindered rotation of the water molecules at the RM surface, whereas  $\tau_2$  has its major share from the corresponding translational motion. The observed Stokes shift is in the order of  $950 \pm 50 \text{ cm}^{-1}$ . The time resolution of our instrument is  $\sim 80 \text{ ps}$  FWHM. Therefore, we miss a considerable fraction of the ultrafast fluorescence signal at faster time scales. The loss can be estimated by calculating the zero frequency of the fluorescence maximum,  $\nu_{em}^p(0)$  using the formula developed by Fee and Maroncelli,<sup>88</sup>  $\nu_{em}^p(0) = \nu_{abs}^p - [\nu_{abs}^{np} - \nu_{em}^{np}]$  where  $\nu_{abs}^p$ ,  $\nu_{abs}^{np}$  and  $\nu_{em}^{np}$  are the absorption peak of the fluorophore in polar solvent, absorption peak in nonpolar solvent and emission peak in nonpolar solvent, respectively. Considering Cy to be the nonpolar solvent, in which C-500 produces absorption peak at 360 nm and emission peak at 410 nm, and water to be the polar solvent, we estimate  $\sim 53\%$  and  $58\%$  loss for  $w_0=2$  and 10 respectively at 293 K. The ultrafast fluorescence signal that we miss originates from the fast relaxation of bulk-like water molecules present in the system and thus does not significantly affect the conclusion drawn from the obtained slow relaxation data.

As can be observed from the inset of Figure 5.4.b, the average solvation time constant  $\langle \tau \rangle$  ( $= \sum_i a_i \tau_i$ ) decreases first steadily with increasing  $w_0$  and then marginally beyond  $w_0=7.5$ . It has to be considered here that DDAB/Cy RM size decreases with increasing  $w_0$  and temperature. It has been observed for the conventional RM systems that the increase in droplet size (increase in  $w_0$ ) results in an accelerated relaxation dynamics. In this regard the observation in the present measurement is contradicting to the previous observation as transition in the droplet dimension hardly affects the water dynamics. The slower relaxation time constant ( $\tau_2$ ) is related to the diffusional motion of the probe through the DDAB-water interface and this allows to estimate the diffusion coefficient ( $D^w$ ) of the aqueous environment at the interface. The magnitude of  $D^w$  can be correlated to the rms distance  $\langle z^2 \rangle^{1/2}$  travelled by the probe in time  $t$  using  $\langle z^2 \rangle = 2D^w t$ , in which  $t$  can be approximated as  $\tau_2$ . For DBAB/Cy/water ternary systems the measured self-diffusion coefficient of water are in the order of  $D^w = 10^{-10} \text{ m}^2\text{s}^{-1}$  which then decreases to  $D^w = 1.3 \times 10^{-11} \text{ m}^2\text{s}^{-1}$  at higher hydration.<sup>66, 70</sup> Using the above equation we obtain the following values of  $\langle z^2 \rangle^{1/2}$  (which could roughly be approximated as the thickness of the bound water layer at the DDAB interface):  $4 \pm 0.5 \text{ \AA}$  at low hydration and  $1.7 \pm 0.4 \text{ \AA}$  for  $w_0=12.5$ . It needs to be considered here that the use of the mentioned  $D^w$  values instead of those obtained from NMR studies gives only an approximation. However, we can safely conclude that the ‘bound or retarded

water' layer concentration at the DDAB interface decreases with increasing water concentration. This explains the accelerated solvation dynamics with increasing  $w_0$  in spite of the decreasing size.

In order to understand the geometrical restrictions imposed on the fluorophore by the local environment, we measure the time resolved fluorescence anisotropy for all the RM systems at different temperatures. Two representative decay transients at two terminal temperatures are shown in Figure 5.7. All the decay transients are fitted using the following equation  $r(t) = r_0[\beta e^{-t/t_{slow}} + (1 - \beta)e^{-t/t_{fast}}]$ . The fitting parameters are listed in Table 5.1.2. The average time constant  $\langle\tau_r\rangle = \beta\tau_{slow} + (1 - \beta)\tau_{fast}$  has been plotted as a function of  $w_0$  and temperature in Figure 5.8.a. The deduced decay constants are in the order of a few hundreds of ps up to a few ns, respectively. For comparison, the probe exhibits a single rotational time constant of  $\sim 60$  ps in bulk water at room temperature.<sup>87</sup> In the present study the faster component  $\tau_{fast}$  is of the order of 160-240 ps and is therefore correlated with the rotation of the probe in a bulk-like environment of the water pool. The observed 2-4 times retarded value of  $\tau_{fast}$  compared to that of pure water is explained by the existence of secondary hydrogen bonding in these water molecules with the interface.

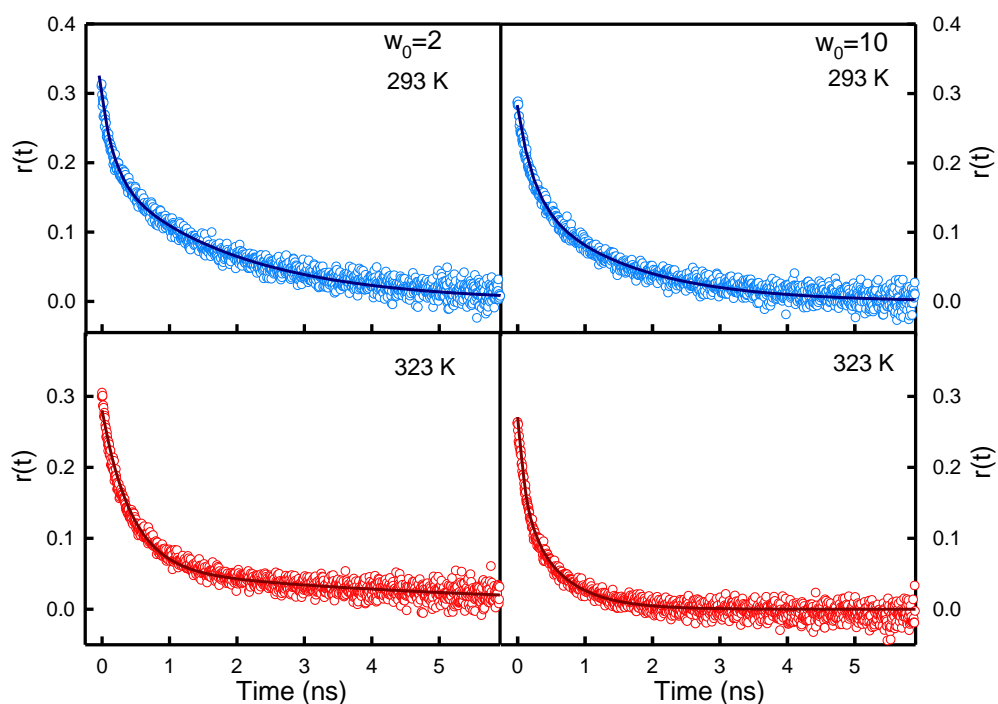


**Figure 5.7.** Representative rotational anisotropy transients for C-500 in DDAB/Cy/water reverse micellar systems with  $w_0$  values of 2 and 10 at 293 and 323 K. The solid lines are bi-exponential fits.

The slower component ( $\tau_{\text{slow}}$ ) is assigned to the rotation of the ‘bound water’ molecules.  $\tau_{\text{fast}}$  and  $\tau_{\text{slow}}$  decrease with increasing temperature (Table 5.1.2), which is explained by the increased rotational mobility of the probe with increasing temperature. In order to obtain a deeper insight into this we analyze the anisotropy data using the wobbling-in-cone analysis<sup>89, 90</sup> (The details of wobbling-in-cone analysis given in chapter 2). The diffusion coefficient for the wobbling motion  $D_{\text{wob}}$  can be obtained using equation 2.39. The calculated  $D_{\text{wob}}$  values for all the system are summarized in Table 5.1.2.  $D_{\text{wob}}$  obtained in the present study are of the same order of magnitude to those obtained in AOT RM systems<sup>40, 91</sup> and are found to increase with temperature (Figure 5.8.b and Table 5.1.2), which is a clear signature of the ease of the probe motion with temperature. The increase is explained by the fact that the probe experiences a less viscous environment at elevated temperature and manifests the breakdown of hydrogen bond network as has earlier been evidenced in FTIR and solvation dynamics studies.

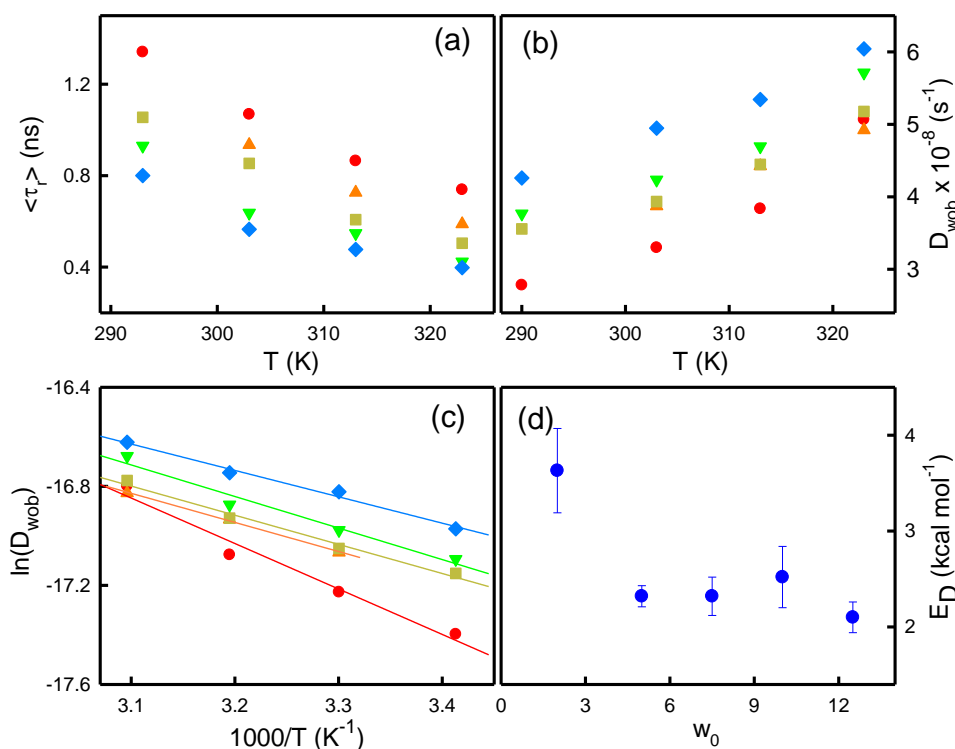


**Figure 5.8.** (a) Average rotational time constant  $\langle \tau_r \rangle$  and (b) Diffusion coefficient ( $D_{\text{wob}}$ ) for different RM systems with  $w_0=2$  (circle), 5 (up triangle), 7.5 (square), 10 (down triangle) and 12.5 (diamond) as measured from wobbling-in-cone analysis at four different temperatures (c) Plot of  $\ln(D_{\text{wob}})$  against  $1/T$ . The solid lines are linear fits. The corresponding activation energies are shown in (d).

As observed from Table 5.1.1,  $\langle \tau \rangle$  decreases with increasing temperature which is a direct consequence of the temperature induced inter-conversion between ‘bound’ and ‘bulk’ type water. Such temperature induced transition could be correlated with an Arrhenius type of

transition in a following manner: it has been established in earlier studies<sup>40, 42, 83, 84, 92, 93</sup> that the transition of water molecules at the RM and other micro-heterogeneous assemblies follows an Arrhenius type barrier crossing model given as:

$$k \approx \frac{1}{\langle \tau \rangle} = A e^{-\frac{E_{act}}{RT}} \quad (5.1)$$

where  $E_{act}$  is the barrier energy associated with the transition of different types of water molecules. Plotting  $\ln(1/\langle \tau \rangle)$  against  $1/T$  (inset of Figure 5.6.b) and using a linear fit, we obtained  $E_{act}$  values of  $2.8 \pm 0.5$ ,  $2.4 \pm 0.1$ ,  $2.6 \pm 0.1$  and  $3.0 \pm 0.1$  kcal mol<sup>-1</sup> for  $w_0=5, 7.5, 10$  and  $12.5$  respectively (Figure 5.6.b). For  $w_0=2$  system, a linear fit up to 313 K yields an activation energy of  $8 \pm 1$  kcal mol<sup>-1</sup>. It is interesting to note that the  $E_{act}$  values obtained for  $w_0 \geq 5$  systems are comparable or smaller than those obtained for AOT RM systems using the same probe<sup>40</sup> and do not change much with hydration.

**Table 5.1.2.** Wobbling-in-cone analysis of anisotropy decay transients for C-500 in DDAB/Cy/ water RM systems at different  $w_0$  and temperatures.

Temperature	$\tau_{fast}$ (ns)	$\tau_{slow}$ (ns)	$\beta$	$\langle \tau_r \rangle$ (ns)	$D_w \times 10^{-8}$ (s <sup>-1</sup> )
<b><math>w_0=2</math></b>					
293 K	0.24	1.96	0.64	1.34	2.78
303 K	0.24	1.69	0.57	1.07	3.30
313 K	0.23	1.45	0.52	0.86	3.84
323 K	0.26	1.71	0.33	0.74	5.07
<b><math>w_0=5</math></b>					
293 K	-	-	-	-	-
303 K	0.21	1.5	0.56	0.93	3.87
313 K	0.20	1.22	0.52	0.73	4.43
323 K	0.19	1.02	0.48	0.59	4.92
<b><math>w_0=7.5</math></b>					
293 K	0.22	1.66	0.58	1.06	3.56
303 K	0.21	1.38	0.55	0.85	3.94
313 K	0.20	1.02	0.50	0.61	4.45
323 K	0.18	0.87	0.47	0.50	5.18
<b><math>w_0=10</math></b>					
293 K	0.21	1.47	0.57	0.93	3.77
303 K	0.20	1.04	0.52	0.64	4.24
313 K	0.19	0.92	0.49	0.55	4.69
323 K	0.16	0.72	0.47	0.42	5.71
<b><math>w_0=12.5</math></b>					
293 K	0.19	1.28	0.56	0.80	4.26
303 K	0.18	0.95	0.50	0.57	4.95
313 K	0.17	0.81	0.48	0.48	5.34
323 K	0.16	0.70	0.44	0.40	6.04

The  $E_{act}$  values as obtained in the present study essentially describe the energy cost associated with the change in coupled rotational-translational solvent (water) relaxation dynamics upon the transition from surface bound to unbound state.<sup>94, 95</sup> Hence, the value of the  $E_{act}$  mostly

depends on the probe location as well as on the interaction of the probe molecule with the interface. The observed  $E_{act}$  values are considerably smaller than those in bulk water ( $\sim 8-9$  kcal mol<sup>-1</sup>).<sup>96</sup> However, they are in a good agreement with that for interfacially bound water (IBW) to interfacially free water (IFW) transition energy which is of the order of 2.4-4 kcal mol<sup>-1</sup>.<sup>94</sup> It is also interesting to note that the values for  $E_{act}$  are not affected much with a change in hydration and hence on surface morphology, suggesting its marginal role on the local environment of the probe for the present system.

The exchange of water molecules at the interface essentially involves the diffusion of water molecules.  $D_{wob}$  values as calculated from the wobbling-in-cone analysis allow to estimate the activation energy of this diffusion process. In order to estimate this, we plot  $\ln(D_{wob})$  against  $1/T$ , and we obtain good linear fits for all the systems (Figure 5.8.c). The activation energy of diffusion ( $E_D$ ) is  $3.6 \pm 0.4$ ,  $2.3 \pm 0.1$ ,  $2.3 \pm 0.2$ ,  $2.5 \pm 0.5$  and  $2.1 \pm 0.2$  kcal mol<sup>-1</sup> for  $w_0$  values of 2, 5, 7.5, 10 and 12.5 respectively (Figure 5.8.d). These values are in excellent agreement with those obtained for the solvent relaxation process. This agreement strongly suggests that the temperature induced acceleration of solvent relaxation is strongly correlated with the diffusion of water molecules.

Further information on the process could be made on the basis of the change in the relative population of water molecules as observed in the temperature dependent MIR spectrum analysis (Figure 5.2.a). We consider an equilibrium between bound and bulk water:

$n_w^{bound} \rightleftharpoons n_w^{bulk}$  where  $n_w^{bound}$  and  $n_w^{bulk}$  represent the number of water molecules in the ‘bound’ and ‘bulk’ states, respectively. The ratio between  $n_w^{bound}$  and  $n_w^{bulk}$  can be described by a Boltzmann type population distribution:<sup>84, 97</sup>

$$n_w^{bound} = n_w e^{-\frac{E_{bound}}{RT}}; \quad n_w^{bulk} = n_w e^{-\frac{E_{bulk}}{RT}}$$

We therefore obtain:  $\frac{n_w^{bound}}{n_w^{bulk}} = e^{-\frac{\Delta E_{tr}}{RT}}$

where  $n_w$  is the total number of water molecules,  $\Delta E_{tr}$  is the energy associated with the ‘bound’ to ‘bulk’ transition and should correspond to the activation energy of the water transition as envisaged in solvent relaxation process ( $E_{act}$ ). The number of water molecules in the ‘bound’ and ‘bulk’ states can be estimated from the relative area (A) under the band at  $\nu_1$  and  $\nu_2$  respectively:

$$\frac{A_{v_1}}{A_{v_2}} = e^{-\frac{\Delta E_{tr}}{RT}} \quad (5.2)$$

When we plot  $\ln(A_{v_1}/A_{v_2})$  against  $1/T$ , we obtain a linear curve for  $w_0 \geq 5$  RM systems (Figure 5.2.b). The fitting provides with  $\Delta E_{tr}$  values of  $3.5 \pm 0.1$ ,  $2.9 \pm 0.2$ ,  $3.0 \pm 0.2$  and  $3.1 \pm 0.2$  kcal mol<sup>-1</sup> for  $w_0$  values of 5, 7.5, 10 and 12.5, respectively. It must be taken into consideration that Equation (5.2) is a rather simplified approach based on the assumptions that the ratio  $n_w^{v_1}/n_w^{v_2}$  directly correspond to the relative area ratio  $A_{v_1}/A_{v_2}$ . However, the similarities between  $E_{act}$  and  $\Delta E_{tr}$  are striking. This agreement supports our analysis and the inherent assumption.

The relaxation dynamics also gradually accelerates with increasing temperature, in spite of the decrease in the droplet dimension. In a previous study<sup>40</sup> Mitra et al. found that in AOT RM, increasing temperature accelerated the relaxation process. It was argued that in AOT RM systems, the droplet size increases with temperature, which consequently increases the fraction of bulk water in the pool, resulting in a faster relaxation dynamics. However, in the present system, the droplet dimension indeed decreases with temperature and thus it can be concluded that the ‘bound’ to ‘bulk’ transition is the sole contribution towards the observed accelerated dynamics. In summary, we find a significant change of the water relaxation dynamics with changes in droplet size and temperature. However, these changes are independent of the topological curvature.

### 5.2.2 Influence of Charge on the Structure and Dynamics of Water Encapsulated in Reverse Micelles

**Fluorescence measurements:** In order to determine the retarded dynamics of the water molecules inside RMs and a possible correlation with the interface, we carry out both steady state and time resolved fluorescence measurements using two probes, namely C-343<sup>35, 36, 98-100</sup> and ANS<sup>101, 102</sup> in three differently charged RMs.

C-343 is water soluble and insoluble in Cy. Upon excitation at 409 nm, C-343 produces emission maximum at 490 nm in water and 465 nm in dioxane. The emission maximum of C-343 exhibits a blue shift in RMs compared to that in pure water, the effect being more prominent in case of Igepal (Table 5.2.1). The observed ~15-18 nm blue shift in Igepal RM is comparable to that obtained in earlier studies using the same probe in various nonionic surfactant RM systems.<sup>36, 103</sup>

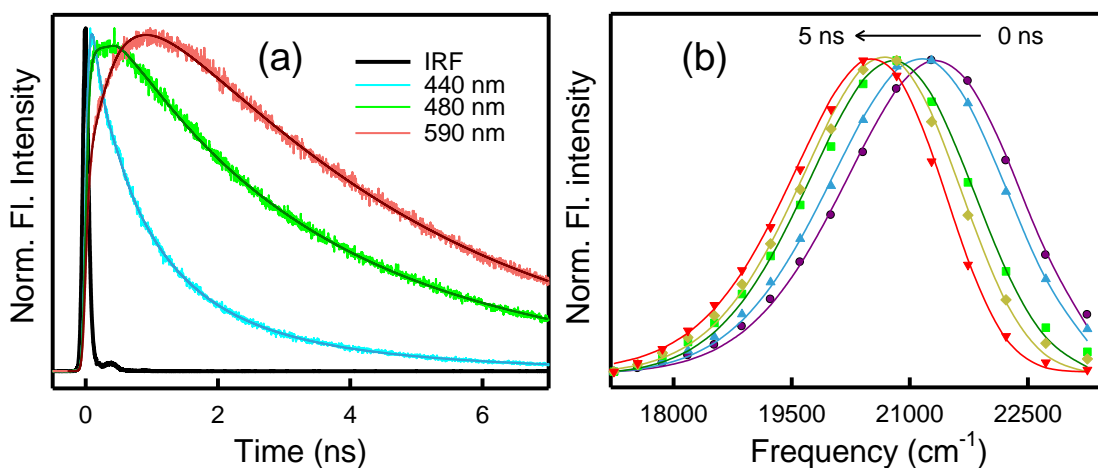


**Figure 5.9.** (a) A representative fluorescence decay transient of C343 in AOT RM at  $w_0=10$ . The solid lines represent multi-exponential fittings. (b) Time resolved emission spectra (TRES) of C-343 in AOT RM at  $w_0=10$ . The arrow indicates increasing time.

The emission maximum is observed to get progressively red shifted with increasing hydration ( $w_0$ ) as envisaged from the increased population of the bulk type water and hence an increased polarity.<sup>40</sup> In DDAB, the peak position does not change much with  $w_0$ .

To study the slow relaxation dynamics of water inside the investigated RM systems we construct TRES and deduce the solvent correlation function  $C(t)$ .<sup>97</sup> A representative fluorescence decay transient of C-343 in AOT RM at  $w_0=10$  is shown in Figure 5.9.a. It is evident that the blue end (440 nm) shows only decay components, whereas the red end (590 nm) could only be fitted after considering a rise component. This clearly indicates the solvation of the probe.<sup>104</sup> The corresponding TRES is presented in Figure 5.9.b. Some representative  $C(t)$  curves are shown in Figure 5.10.a & 5.10.c. The  $C(t)$  curves are fitted using a bi-exponential decay function,  $C(t) = a_1 e^{-t/\tau_1} + a_2 e^{-t/\tau_2}$  where  $\tau_1$  and  $\tau_2$  represent two characteristic time scales assigned to two different relaxation processes of water molecules:  $\tau_1$  (~ hundreds of ps) stems from the hindered rotation of the water molecules at the RM surface, whereas  $\tau_2$  (~ several ns) is attributed to the coupled rotational- translational motions.<sup>95</sup>

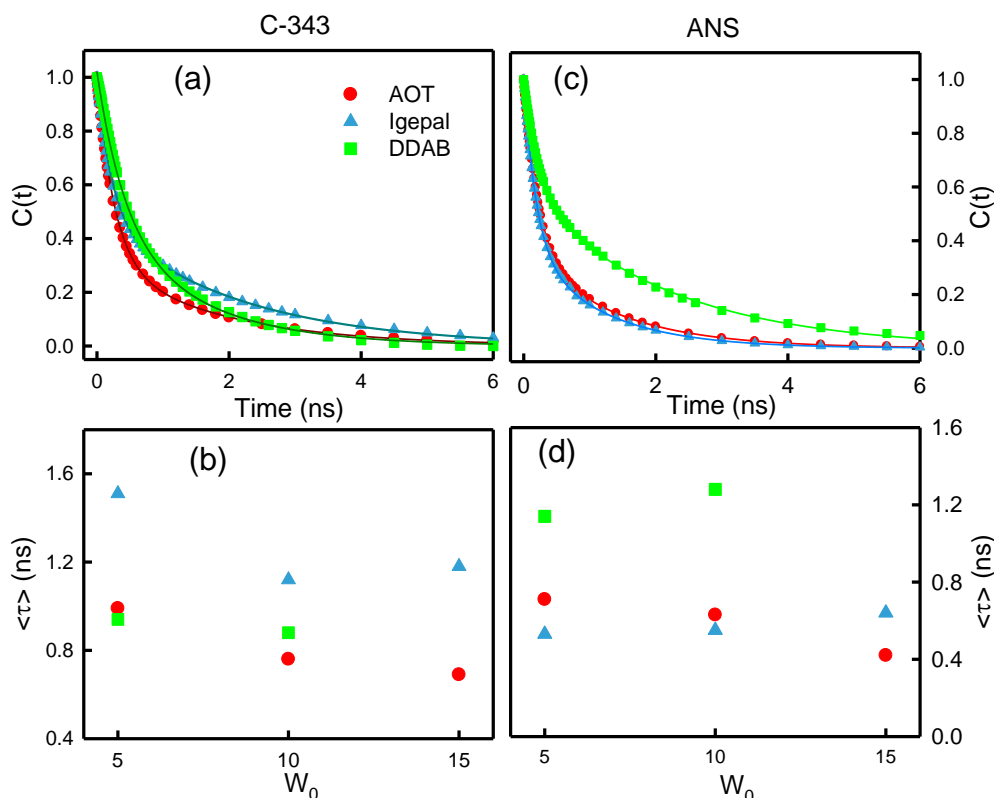


**Figure 5.10.** Left panel (data obtained using C-343 as the fluoroprobe): (a) A representative  $C(t)$  plot for different RM systems with  $w_0=10$ , (b) Average time constant ( $\langle \tau \rangle$ ) for different RM systems at different  $w_0$  values. Right panel (data obtained using ANS as the fluoroprobe): (c) A representative  $C(t)$  plot for different RM systems with  $w_0=10$ , (d) Average time constant ( $\langle \tau \rangle$ ) for different RM systems at different  $w_0$  values.

It could be noted here that the limited time resolution of our instrument (IRF~80 ps) refrains us from extracting the ultrafast response of bulk water which is orders of magnitude faster than  $\tau_1$  and  $\tau_2$ .<sup>86</sup> The loss can be estimated by calculating the zero frequency of the fluorescence maximum,  $\nu_{em}^p(0)$  using the formula developed by Fee and Maroncelli,<sup>88</sup>  $\nu_{em}^p(0) = \nu_{abs}^p - [\nu_{abs}^{np} - \nu_{em}^{np}]$  where,  $\nu_{abs}^p$ ,  $\nu_{abs}^{np}$ ,  $\nu_{em}^{np}$  are the absorption peak of the fluorophore in polar solvent, absorption peak in nonpolar solvent and emission peak in nonpolar solvent, respectively. The absorption maximum of C-343 is 435 nm in dioxane and 425 nm in water and we estimate ~46% loss for  $w_0=10$  of AOT RM. It can be argued that the undetected fluorescence signal originates from the ultrafast (sub-ps) relaxation of bulk-like water molecules present in the system. Since the present investigation is primarily concerned with the dynamics of interfacial water, the missing contribution from bulk water does not significantly affect the conclusion drawn from the detected slow relaxation data. The solvent correlation time constants for all the RM systems are presented in Table 5.2.1.

**Table 5.2.1.** Steady state fluorescence maxima, solvation time correlation and time resolved anisotropy parameters for Coumarin-343 in AOT, DDAB and Igepal RM at different levels of hydration.

$w_0$	$\lambda_{max} (nm)$	$\tau_1$ (ns)	$\tau_2$ (ns)	$\langle \tau \rangle$ (ns)	$\tau_{r1}$ (ns)	$\tau_{r2}$ (ns)	$\langle \tau_r \rangle$ (ns)	$\theta_w$	$D_w \times 10^8$ ( $s^{-1}$ )
<b>AOT</b>									
5	482	0.34 (55%)	1.80 (45%)	1.01	0.25 (42%)	1.85 (58%)	1.17	33.9	3.14
10	485	0.26 (68%)	1.85 (32%)	0.76	0.24 (47%)	1.41 (53%)	0.86	36.3	3.54
15	485	0.20 (62%)	1.52 (37%)	0.69	0.26 (54%)	1.35 (46%)	0.76	39.8	3.71
<b>Igepal</b>									
5	472	0.25 (48%)	2.65 (52%)	1.51	0.4 (45%)	2.34 (55%)	1.46	35.3	2.02
10	477	0.23 (53%)	2.12 (47%)	1.12	0.38 (48%)	2.01 (52%)	1.23	36.8	2.24
15	477	0.26 (51%)	2.14 (49%)	1.18	0.36 (50%)	1.91 (50%)	1.14	37.8	2.48
<b>DDAB</b>									
5	488	0.39 (53%)	1.58 (47%)	0.94	0.29 (43%)	1.9 (57%)	1.21	34.2	2.71
10	490	0.42 (55%)	1.45 (45%)	0.88	0.24 (46%)	1.62 (54%)	0.99	35.8	3.50

For all the RM systems the average time constant ( $\langle \tau \rangle = \sum_i a_i \tau_i$ ) decreases with increasing  $w_0$  (Figure 5.10.b) which is consistent with earlier studies and is attributed to the increased fraction of fast moving bulk water molecules in the system at elevated hydration.<sup>40, 45, 105</sup> Among all the studied systems Igepal offers the slowest relaxation time relative to the other two systems. In order to explore the geometrical restriction imposed on the fluorophore inside the RM systems, we measure the time resolved rotational anisotropy,  $r(t)$ . Earlier simulation studies have concluded that the water rotational anisotropy relaxation in RM systems is complex and can be described using a sum of three exponential functions where each relaxation time scale is associated with different types of water: ‘surface layer’ or ‘intermediate layer’ or ‘central layer’.<sup>31, 106</sup> Since our study is mainly associated with a rather slower dynamics of confined water, which essentially originates from the surface and/or intermediate layer, we fit the decay transients using a double exponential model,  $r(t) = r_0 + \sum_{i=1}^2 a_{r_i} \exp(-\frac{t}{\tau_{r_i}})$  where  $\tau_r$  represents the rotational time constant.

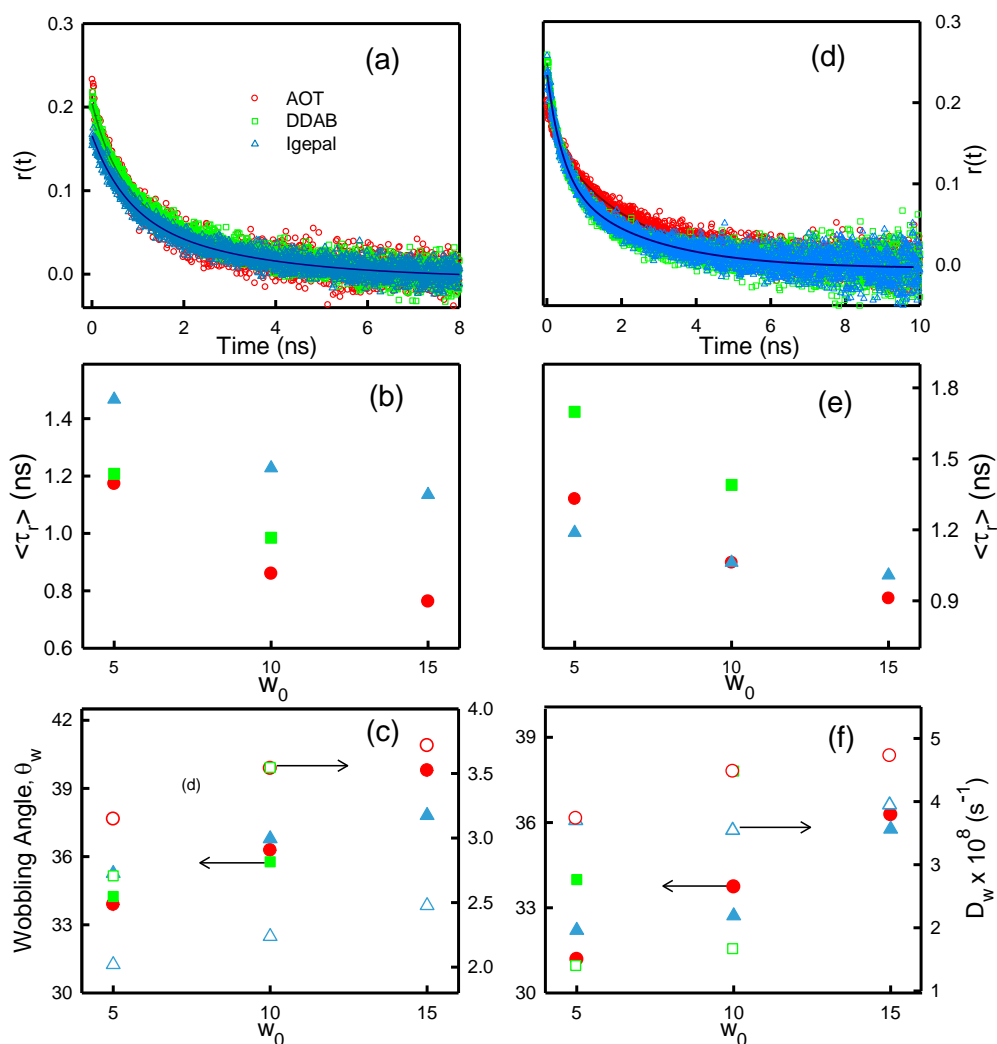


**Figure 5.11.** Left Panel (Data obtained using c-343) Right Panel (Data obtained using ANS) (a) and (d) Anisotropy decay at  $w_0=5$ . (b) and (e) Average rotational anisotropy time constant ( $\langle \tau_r \rangle$ ). (c) and (f) Wobbling angle (solid symbols, arrow pointing in the direction of left side) and diffusion coefficient (open symbols, arrow pointing in the direction of right-side) for different RM systems at different  $w_0$  values.

A representative double exponential fit of the anisotropy transient is shown in Figure 5.11.a. All the fitting parameters are presented in Table 5.2.1. It can be observed that the average rotational time constant ( $\langle \tau_r \rangle = \sum_i a_{r_i} \tau_{r_i}$ ) is the slowest for the Igepal RM systems, while those for AOT and DDAB are comparable (Figure 5.11.b).

**Table 5.2.2.** Steady state fluorescence maxima, solvation time correlation parameters and time resolved anisotropy parameters for ANS in AOT, DDAB and Igepal RM at different levels of hydration.

$w_0$	$\lambda_{\max}$ (nm)	$\tau_1$ (ns)	$\tau_2$ (ns)	$\langle\tau\rangle$ (ns)	$\tau_{r1}$ (ns)	$\tau_{r2}$ (ns)	$\langle\tau_r\rangle$ (ns)	$\theta_w$	$D_w \times 10^8$ ( $s^{-1}$ )
<b>AOT</b>									
5	476	0.23 (64%)	1.54 (36%)	0.71	0.19 (37%)	2.0 (63%)	1.33	31.2	3.74
10	480	0.22 (63%)	1.33 (37%)	0.63	0.18 (42%)	1.7 (58%)	1.06	33.7	4.48
15	480	0.16 (64%)	0.87 (36%)	0.42	0.19 (47%)	1.55 (53%)	0.91	36.3	4.73
<b>Igepal</b>									
5	479	0.18 (61%)	1.36 (39%)	0.64	0.2 (39%)	1.82 (61%)	1.19	32.2	3.70
10	482	0.19 (62%)	1.15 (38%)	0.55	0.21 (40%)	1.63 (60%)	1.06	32.7	3.55
15	484	0.17 (60%)	1.07 (40%)	0.53	0.22 (46%)	1.68 (54%)	1.01	35.8	3.95
<b>DDAB</b>									
5	462	0.20 (46%)	2.18 (54%)	1.29	0.52 (42%)	2.57 (58%)	1.70	34.0	1.40
10	469	0.59 (65%)	2.14 (36%)	1.14	0.51 (50%)	2.27 (50%)	1.39	37.8	1.67

For further discussion, it should be taken into consideration that the location of the probe in a micro-heterogeneous environment is of the utmost importance in fluorescence spectroscopy and the information drawn from fluorescence measurements is essentially governed by the nature of the immediate local environment experienced by the probe. We can compare the solvation dynamics for the three RM systems at a fixed hydration level ( $w_0=10$ ): the  $\langle\tau\rangle$  values for C-343 are 0.76, 1.12 and 0.88 ns in AOT, Igepal and DDAB RM systems, respectively (table 5.2.1). In Igepal RMs, C-343 essentially stays at the interface as evident from the blue shifted fluorescence maximum, whereas in AOT and DDAB the probe resides near the bulk core of the RM. For identical  $w_0$ , Igepal produces larger droplets than AOT,<sup>45</sup> however, offers slower solvation time scale. Restricted rotation of the probe inside RM can be deduced from the anisotropy measurements. Since the origin of the slower solvation time constants is diffusive in nature we analyze the anisotropy data with a wobbling-in-cone model (the details have been discussed in chapter 2).<sup>40, 107-109</sup> The  $\theta_w$  and  $D_w$  values obtained from this analysis are summarized in Table 5.2.1 and shown in Figure 5.11.c. The wobbling angle as well as diffusion coefficient increases with increasing hydration, indicating an overall ease of rotation with increasing  $w_0$  which is correlated with the observed decrease in  $\langle\tau_r\rangle$ . The obtained  $D_w$  values are of the same order of magnitude as those obtained for AOT RM systems in earlier studies and is slower compared to that of bulk water.<sup>40, 92</sup> The trend observed in  $D_w$  can be related to that in  $\langle\tau\rangle$ , with the latter being mostly associated with the

diffusive nature of restricted water.  $D_w$  of Igepal is low compared to the other two systems (Table 5.2.1, Figure 5.11.b), which enforces a slower solvation timescale for the Igepal system. On the other hand, AOT and DDAB systems offer a more polar environment to the probe, which in turn is manifested by the faster  $D_w$  and  $\langle\tau\rangle$  values.

In addition, we employed a second probe, ANS, which is also a water soluble dye and produces emission maximum at 515 nm in water;<sup>110</sup> in RMs it shows considerable blue shift to produce the maxima at 480, 482 and 469 nm in AOT, Igepal and DDAB RM respectively at a hydration level of  $w_0=10$  (Table 5.2.2). DDAB is observed to produce the slowest relaxation dynamics. ANS prefers to stay at the bulk core in AOT RM<sup>102</sup> to minimize the charge interaction and as a result produces a faster dynamics. On the other hand, the favourable charge interaction tends to keep the probe in the vicinity of the oppositely charged DDAB interface, and consequently it experiences a larger fraction of interfacially bound water molecules which eventually results in a delayed solvation response. The  $D_w$  values of DDAB are also small compared to the other two systems (Table 5.2.2, Figure 5.11.d-f). The fluorescence results thus confirm a considerably retarded dynamics of water molecules inside all the three different RM systems owing to their confinement, the information obtained on the extent of retardation is found to be specific of the location of the probe. In order to obtain complementary information on the hydrogen bond dynamics, we perform additional FTIR and THz experiments.

***FIR FTIR measurements:*** In order to investigate on the collective dynamics of water molecules encapsulated in the RM systems, we carry out FIR FTIR measurements of all the studied systems. Some representative results are depicted in Figure 5.12.a-c. The FIR spectra for all these systems are found to be considerably changed compared to that of bulk water. In pure water, two characteristic peaks can be found in this frequency range, one in the  $\sim 200$   $\text{cm}^{-1}$  and the other one in the  $\sim 600$   $\text{cm}^{-1}$  region. The peak at  $\sim 200$   $\text{cm}^{-1}$  is essentially an optimized hydrogen bond stretching band (SB) contributed by one symmetric stretching (at  $\sim 160$   $\text{cm}^{-1}$ ) and several antisymmetric stretching modes ( $\sim 220$  and  $290$   $\text{cm}^{-1}$ ) of hydrogen bonded network at the first solvation shell of water.<sup>78</sup>

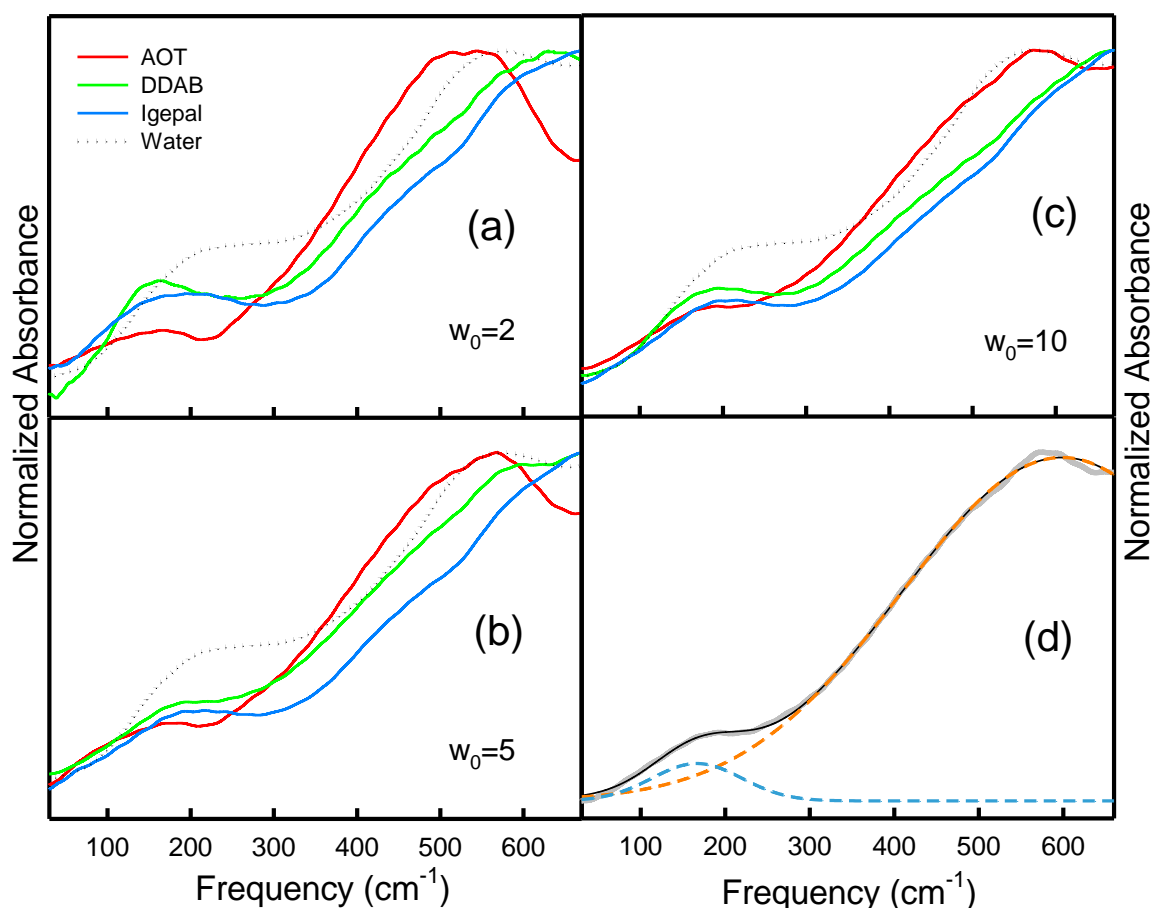


**Figure 5.12.** (a-c) FIR-FTIR spectra of AOT, DDAB and Igepal RM systems at three different  $w_0$  values (2, 5 and 10). The FIR spectrum of pure water in this frequency region is shown as black broken line in an adjusted scale for comparison (d) The deconvoluted FIR spectrum of AOT RM (grey solid line). The black line is the overall fitted curve, the blue and orange broken lines are the two Gaussian decomposition curves designated as SB and LB, respectively.

The band at  $\sim 600\text{ cm}^{-1}$  results from the librational motion of water molecules in a hydrogen bonded connected network, called the “librational band” (LB).<sup>11, 78, 111</sup> Position of LB depends upon the strength of hydrogen bond in network structure of water, whereas SB arises from the longitudinal motion of the hydrogen atom along the hydrogen bond axis (i.e., hydrogen-bond stretching) and therefore characterizes the level of hydrogen bonding between neighbouring water molecules. In order to obtain a quantitative information about the SB in the RM system the FIR absorbance spectra in the  $30\text{--}650\text{ cm}^{-1}$  region is fitted as a sum of two Gaussian functions in which the position of the low energy Gaussian (near  $200\text{ cm}^{-1}$ ) is related to the strength of the SB and consequently on the extent of the collective hydrogen bonded network structure of water.

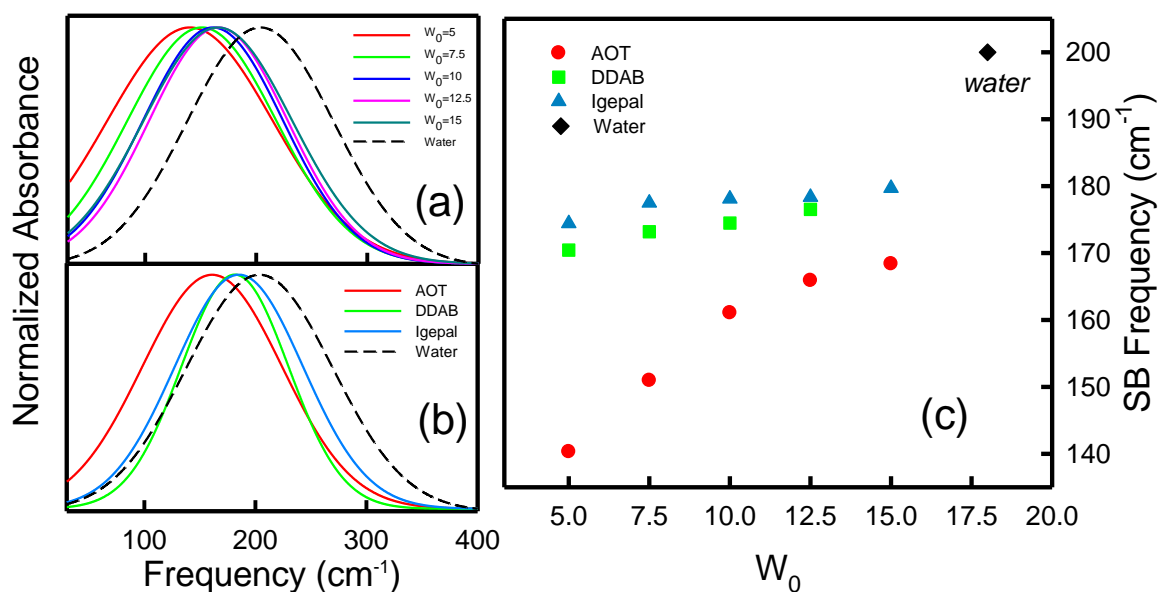


**Figure 5.13.** (a) The deconvoluted stretching band (SB) of water in different RM systems at  $w_0=10$ . The broken line represents the SB for pure water. (b) SB of water in AOT RM at different  $w_0$  values. (c) Peak position of SB for different RM systems and pure water.

A representative graph for deconvoluted AOT RM system is presented in Figure 5.12.d. We plot the deconvoluted Gaussian SB curves for different RM systems at  $w_0=10$  in Figure 5.13.b. It is evident from Figure 5.13.b that in RM the SB shows a clear red shift compared to that of pure water, the effect being more prominent in case of AOT RMs. Such a red shift in the SB band indicates that the stretching modes of network water are strongly affected by confinement. A similar red shift in the librational band of water (at  $\sim 670$  cm $^{-1}$ ) was previously been observed in case of AOT RM.<sup>80</sup> It can be observed from the Figure 5.13.c that SB appears at  $\sim 180$  cm $^{-1}$  for DDAB and Igepal at  $w_0=10$ , while for AOT it is further red shifted to  $\sim 160$  cm $^{-1}$ . The enhanced red shift in AOT clearly suggests a decrease in the collective hydrogen bonding of water inside the RM system as a considerable fraction of water molecules are associated with the interface.

Figure 5.13.a depicts the SB of water in AOT nano-pool with varying hydration ( $w_0$ ). The position of the SB peak as a function of  $w_0$  for all the three surfactant systems has been plotted in Figure 5.13.c. It is observed that at each hydration level, AOT RM offers the largest red shift compared to DDAB and Igepal with DDAB being little more distorted than Igepal. The SB position remains highly red shifted up to  $w_0=5$ , beyond which a progressive blue shift of the peak is observed with increasing hydration.

**THz-TDS measurements:** THz spectroscopy was used to investigate ultrafast collective dynamics of water in RM systems. We performed the THz-TDS measurements on all the RM systems in the frequency range of 0.2-2.0 THz.

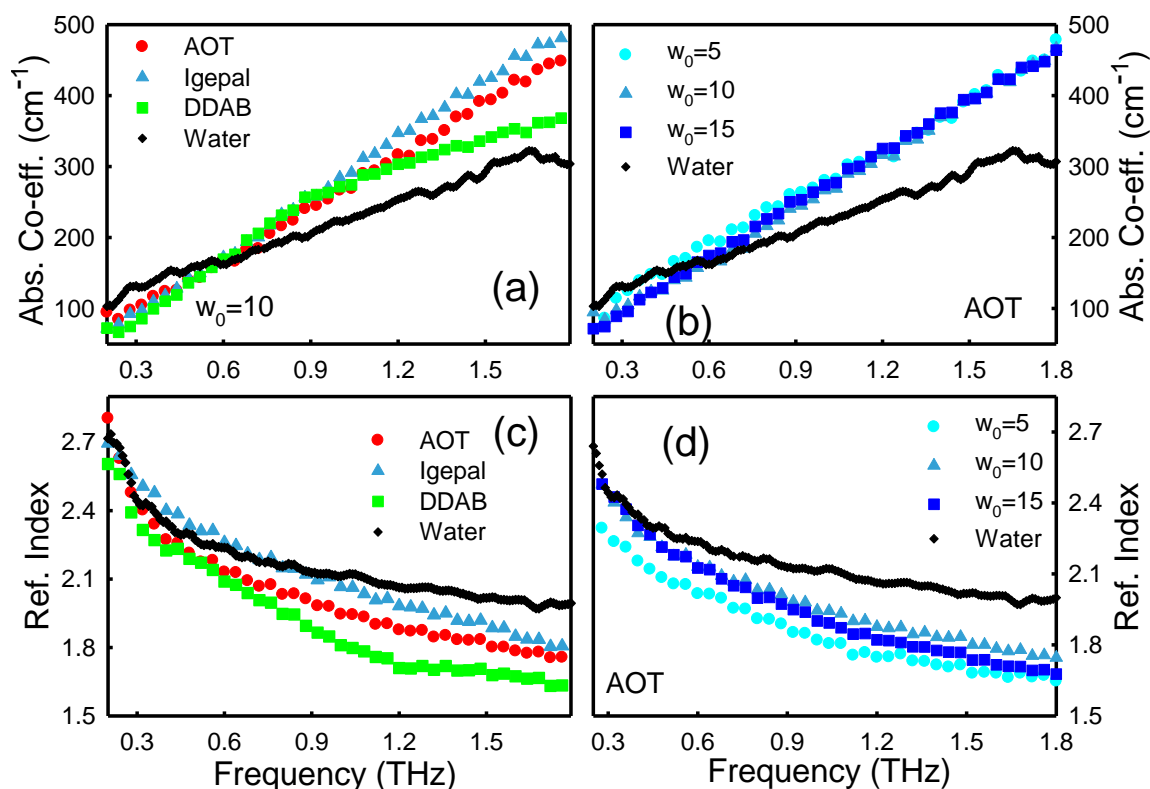


**Figure 5.14.** (a) and (c) show absorption coefficient and refractive index as a function of frequency of water inside AOT, DDAB and Igepal RM at a hydration level of  $w_0=10$ . The same values for water have been given for comparison. (b) and (d) show absorption coefficient and refractive index as a function of frequency of water inside AOT RM for different level of hydration.

Optical parameters of water (absorption coefficient and refractive index) in various RM systems are shown in Figure 5.14. As observed from the Figure 5.14.a the absorption coefficient ( $\alpha$ ) of water in the RM is decreased compared to that of pure water in the low frequency region (0.2 to 0.7 THz), whereas it is increased in the higher frequency region. A similar trend has previously been observed for AOT/heptane RM systems<sup>112</sup> and oil-water interface,<sup>113</sup> and can be explained on the basis of a high-frequency shift of the fast water relaxation and a simultaneous low frequency shift of the hydrogen bond stretching mode compared to that of pure water.<sup>113</sup> This can be interpreted in terms of a significant exposure of water molecules towards more hydrophobic/hydrophilic environment as has previously been observed during protein folding/unfolding process.<sup>114</sup>

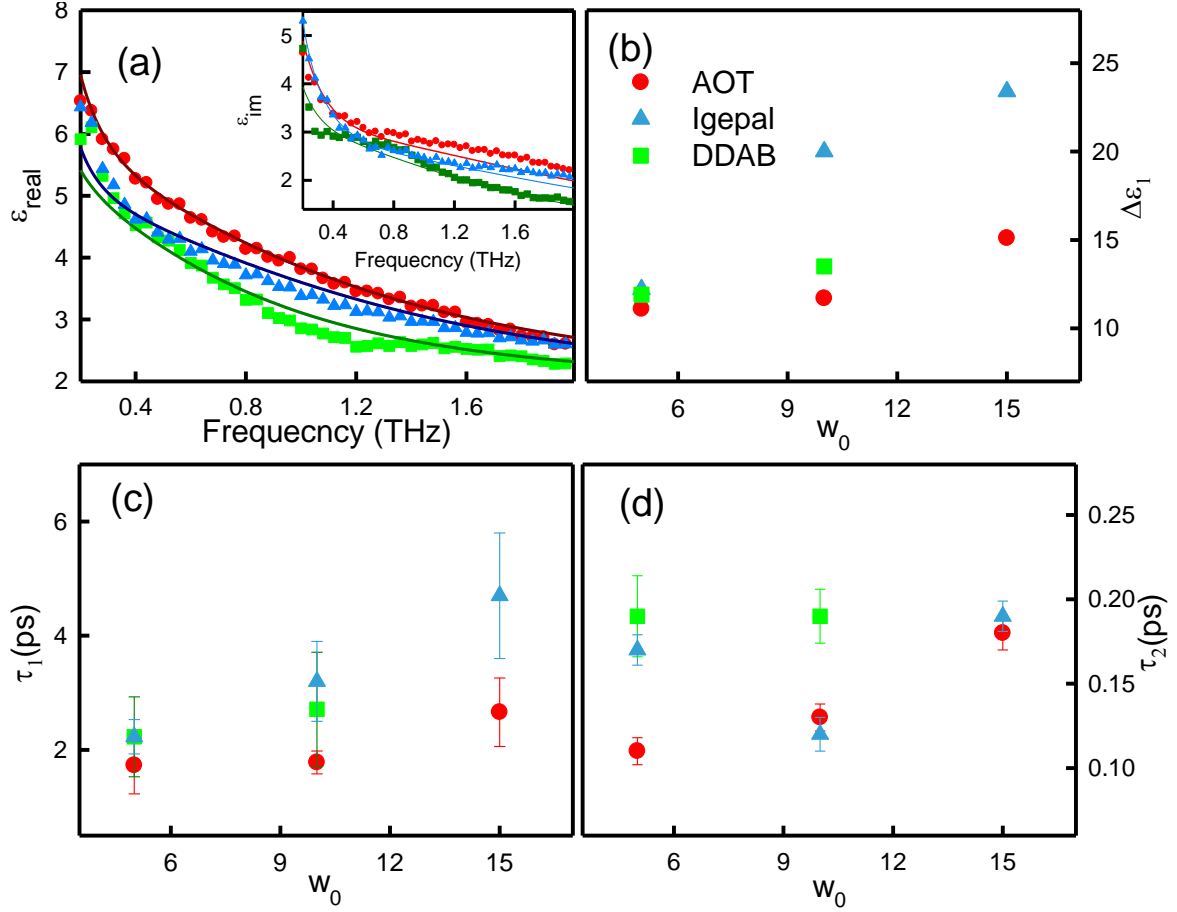


**Figure 5.15.** (a) THz-TDS dielectric relaxation spectra and fitted spectra using Double Debye relaxation model of water inside RM for AOT, DDAB and Igepal RM at  $w_0=10$ . (b) Dielectric strength ( $\Delta\epsilon_1=\epsilon_s-\epsilon_2$ ) as a function of  $w_0$  for different RM systems. (c) and (d) show the relaxation times as a function of  $w_0$  for all the RM systems.

In order to obtain the dynamics of entrapped water, the dielectric response of water has been fitted using a two component Debye model as,

$$\epsilon(\omega) = \epsilon'(\omega) - i\epsilon''(\omega) = \epsilon_\infty + \frac{\Delta\epsilon_1}{1+i\omega\tau_1} + \frac{\Delta\epsilon_2}{1+i\omega\tau_2} \quad (5.3)$$

where  $\tau_i$  is the time constant for the  $i$ -th relaxation mode and  $\Delta\epsilon_i$  is the corresponding relaxation strength,  $\epsilon_\infty$  is the high frequency dielectric constant. The slower time constant  $\tau_1$  is associated with a cooperative reorientation of an ensemble of molecules ( $\sim 8$  ps for pure water) whereas the slower one,  $\tau_2$ , emanates from hydrogen bond formation and dissociation ( $\sim 200$  fs for pure water).<sup>115, 116</sup> Some representative double Debye fits are shown in Figure 5.14a and the corresponding fitting parameters have been plotted as a function of  $w_0$  (Figure 5.15.b-d). It can be observed from the Figure 5.15. that the time constant  $\tau_1$  as well as the corresponding relaxation strength ( $\Delta\epsilon_1=\epsilon_s-\epsilon_2$ , where  $\epsilon_s$  is the static dielectric constant of pure water,  $\Delta\epsilon_1\sim 73$  for pure water) are considerably smaller in RMs compared to those of bulk

water, the effect being more prominent in case of AOT followed by DDAB and Igepal. A similar decrease in  $\tau_1$  and  $\Delta\epsilon_1$  has previously been reported for AOT/heptane RM systems by Mittelman et al.<sup>112</sup> The observed decrease suggests that the confinement strongly perturbs the large-scale collective modes, which are predominantly observed in pure water.<sup>78</sup> Even weak confinement has also been reported<sup>112</sup> to significantly perturb the collective<sup>117</sup> hydrogen bond bending (TA phonon) mode of liquid water which appears at  $\sim 50 \text{ cm}^{-1}$ .<sup>118</sup> The reduction in the dielectric constant stems from a change in the hydration bond dynamics. As observed from Figure 5.15, the extent of change in  $\tau_1$  and  $\Delta\epsilon_1$  are comparable for all the three RM systems at low hydration ( $w_0=5$ ) indicating a highly perturbed structure at low hydration. The perturbation is released at higher hydration, specially to a considerable extent in the Igepal RM. The THz study thus corroborates with the FIR results which concluded the disruption of hydrogen bonded network structure inside RM as manifested in the observed decrease of connectivity network and a consequent faster relaxation dynamics. The distortion is found to be governed by the charge type of the interface with the effect being more severe for AOT followed by DDAB and Igepal.

### 5.3. Conclusions:

The initial objective of the present study has been to investigate the influence of the elastic properties of RM surface on the relaxation dynamics of water, more specifically the coupled rotational-translational relaxation dynamics of the interfacially bound water molecules at the RM water-pool. Unlike many conventional surfactants, DDAB is insoluble in both Cy and water, and thus resides at the RM interface only having negligible monomer abundance.<sup>59, 119</sup> DDAB/alkane/water systems offer an unusual phase behavior in which a connected cylindrical structure prevails at low water concentration and discrete droplet type formulations evolve with increasing hydration.<sup>55, 61, 65-68, 70</sup> Such decrease in the overall RM dimension with increasing hydration is quite contrary to that in conventional systems wherein size generally increases with  $w_0$ . Since the change in phase is directly related to the modification of the elastic properties and curvature of the surfactant monolayer,<sup>54</sup> the present system offers a wide range of surface geometry, both with hydration and with temperature, keeping the constituent composition unaltered. FTIR-MIR measurements reveal that the partial population of water molecules with strongly structured hydrogen bond ( $\nu_1$ ) increases, whereas that of the distorted water molecules ( $\nu_2$ ) decreases with increasing  $w_0$  and reach values comparable to that of bulk water, a scenario resembling conventional globular RM

systems.<sup>11-14, 120</sup> This similarity supports our conclusion that interfacial morphology has only a marginal effect on the hydration structure. FIR-FTIR studies confirm that the collective hydrogen bonded network dynamics in water molecules adopts a bulk like behavior with increasing  $w_0$  and temperature. Existence of a slow (sub-ns) relaxation dynamics as evident from time resolved fluorescence studies is attributed to a ‘confinement effect’<sup>5, 6</sup> similar to what has been observed in conventional RM systems.<sup>40</sup> It is interesting to note that in all these systems the average solvation time constant  $\langle\tau\rangle$  decreases marginally with increasing  $w_0$  (Table 5.2.1), in spite of the transition from interconnected cylinder like structures (large radius of curvature) towards discrete droplet like structure (small radius of curvature) with an additional constrain in the translational degree of freedom. This points us to the fact that it is the load of water rather than the surface geometry that determines the overall water structure and dynamics for a fixed surface stoichiometry.

In order to understand the effect of interfacial charge on the water inside RM we have carried out time-resolved fluorescence, FIR-FTIR and THz-TDS spectroscopic studies of water present inside anionic, cationic and nonionic RMs. The TRFS study unambiguously confirmed a restricted dynamics of the entrapped water molecules irrespective of the nature of the interface. The slow solvation dynamics of water is also correlated with the change in its diffusive motion as evident from the time resolved anisotropy measurements. However, the extent of water structure perturbation seems not very conclusive from the TRFS study owing to the location specific information obtained from the different fluoroprobes. FIR measurement also supports this result by recording a red shift of the hydrogen bond stretching band (SB) when the interface changes from nonionic to cationic to anionic. Dielectric relaxation study in the THz region confirms the fact that the collective dynamics is highly perturbed at low hydration in all the RM systems, and the perturbation is released upon increasing hydration, the release being more prominent in Igepal compared to the two ionic surfactants. All these measurements thus suggest that anionic AOT RM interface has the largest influence on the hydration bond dynamics, followed by DDAB and Igepal. The primary motivation of these works was to understand the effect of interfacial morphology of RM on the structure and dynamics of encapsulated water. Our results conclude that different morphology has negligible influence on the properties of water, however, it follows a systematic trend with the charge of the RM surface having a larger effect than the cationic and nonionic surface.

## References:

1. Moulik, S. P., and Paul, B. K. (1998) Structure, dynamics and transport properties of microemulsions, *Advances in Colloid and Interface Science* 78, 99-195.
2. Levinger, N. E., and Swafford, L. A. (2009) Ultrafast Dynamics in Reverse Micelles, *Annual Review of Physical Chemistry* 60, 385-406.
3. Levinger, N. E. (2002) Water in confinement *Science* 298, 1722-1723.
4. Fayer, M. D., and Levinger, N. E. (2010) Analysis of Water in Confined Geometries and at Interfaces, *Annual Review of Analytical Chemistry* 3, 89-107.
5. Moilanen, D. E., Levinger, N. E., Spry, D. B., and Fayer, M. D. (2007) Confinement or the Nature of the Interface? Dynamics of Nanoscopic Water, *Journal of the American Chemical Society* 129, 14311-14318.
6. Dokter, A. M., Woutersen, S., and Bakker, H. J. (2006) Inhomogeneous dynamics in confined water nanodroplets *Proceedings of the National Academy of Sciences USA* 103, 15355-15358.
7. Fenn, E. E., Wong, D. B., and Fayer, M. D. (2009) Water dynamics at neutral and ionic interfaces, *Proceedings of the National Academy of Sciences USA* 106, 15243-15248.
8. Bhattacharyya, K. (2003) Solvation Dynamics and Proton Transfer in Supramolecular Assemblies, *Accounts of Chemical Research* 36, 95-101.
9. Nucci, N. V., Pometun, M. S., and Wand, A. J. (2011) Site-resolved measurement of water-protein interactions by solution NMR, *Nature Structural & Molecular Biology* 18, 245-249.
10. Nucci, N. V., Pometun, M. S., and Wand, A. J. (2011) Mapping the Hydration Dynamics of Ubiquitin, *Journal of the American Chemical Society* 133, 12326-12329.
11. Brubach, J.-B., Mermet, A., Filabozzi, A., Gerschel, A., Lairez, D., Krafft, M. P., and Roy, P. (2001) Dependence of Water Dynamics upon Confinement Size, *The Journal of Physical Chemistry B* 105, 430-435.
12. Zhong, Q., Steinhurst, D. A., Carpenter, E. E., and Owruksy, J. C. (2002) Fourier Transform Infrared Spectroscopy of Azide Ion in Reverse Micelles, *Langmuir* 18, 7401-7408.
13. Zhou, N., Li, Q., Wu, J., Chen, J., Weng, S., and Xu, G. (2001) Spectroscopic Characterization of Solubilized Water in Reversed Micelles and Microemulsions: Sodium Bis(2-ethylhexyl) Sulfosuccinate and Sodium Bis(2-ethylhexyl) Phosphate in n-Heptane, *Langmuir* 17, 4505-4509.
14. Tamsamani, M. B., Maeck, M., Hassani, I. E., and Hurwitz, H. D. (1998) Fourier Transform Infrared Investigation of Water States in Aerosol-OT Reverse Micelles as a Function of Counterionic Nature, *The Journal of Physical Chemistry B* 102, 3335-3340.
15. Zhou, G.-W., Li, G.-Z., and Chen, W.-J. (2002) Fourier Transform Infrared Investigation on Water States and the Conformations of Aerosol-OT in Reverse Microemulsions *Langmuir* 18, 4566-4571.
16. Tan, H.-S., R., P. I., Riter, R. E., Levinger, N. E., and Fayer, M. D. (2005) Dynamics of water confined on a nanometer length scale in reverse micelles: ultrafast infrared vibrational echo spectroscopy, *Physical Review Letters* 94, 057405.
17. Piletic, I. R., Moilanen, D. E., Levinger, N. E., and Fayer, M. D. (2006) What Nonlinear-IR Experiments Can Tell You about Water that the IR Spectrum Cannot, *Journal of the American Chemical Society* 128, 10366-10367.
18. Cringus, D., Bakulin, A., Lindner, J., Voehringer, P., Pshenichnikov, M. S., and Wiersma, D. A. (2007) Ultrafast Energy Transfer in Water-AOT Reverse Micelles, *The Journal of Physical Chemistry B* 111, 14193-14207.
19. Riter, R. E., Undiks, E. P., and Levinger, N. E. (1998) Impact of Counterion on Water Motion in Aerosol OT Reverse Micelles, *Journal of the American Chemical Society* 120, 6062-6067.
20. Sarkar, N., Das, K., Datta, A., Das, S., and Bhattacharyya, K. (1996) Solvation Dynamics of Coumarin 480 in Reverse Micelles. Slow Relaxation of Water Molecules, *The Journal of Physical Chemistry* 100, 10523-10527.
21. Dutta, P., Sen, P., Mukherjee, S., Halder, A., and Bhattacharyya, K. (2003) Solvation Dynamics in the Water Pool of an Aerosol-OT Microemulsion. Effect of Sodium Salicylate and Sodium Cholate, *The Journal of Physical Chemistry B* 107, 10815-10822.

22. Harpham, M. R., Ladanyi, B. M., and Levinger, N. E. (2005) The Effect of the Counterion on Water Mobility in Reverse Micelles Studied by Molecular Dynamics Simulations, *The Journal of Physical Chemistry B* 109, 16891-16900.
23. Faeder, J., and Ladanyi, B. M. (2000) Molecular Dynamics Simulations of the Interior of Aqueous Reverse Micelles, *The Journal of Physical Chemistry B* 104, 1033-1046.
24. Senapati, S., and Berkowitz, M. L. (2003) Water structure and dynamics in phosphate fluorosurfactant based reverse micelle. A computer simulation study, *The Journal of Chemical Physics* 118, 1937-1944.
25. Bruce, C. D., Senapati, S., Berkowitz, M. L., Perera, L., and Forbes, M. D. E. (2002) Molecular Dynamics Simulations of Sodium Dodecyl Sulfate Micelle in Water: The Behavior of Water, *The Journal of Physical Chemistry B* 106, 10902-10907.
26. Levinger, N. E. (2000) Ultrafast dynamics in reverse micelles, microemulsions, and vesicles, *Current Opinion in Colloid & Interface Science* 5, 118-124.
27. Pieniazek, P. A., Lin, Y. S., Chowdhary, J., Ladanyi, B. M., and Skinner, J. L. (2009) Vibrational spectroscopy and dynamics of water confined inside reverse micelles, *The Journal of Physical Chemistry B* 113, 15017-15028.
28. El Seoud, O. A. (1997) Use of NMR to probe the structure of water at interfaces of organized assemblies, *Journal of Molecular Liquids* 72, 85-103.
29. Rosenfeld, D. E., and Schmuttenmaer, C. A. (2006) Dynamics of Water Confined Within Reverse Micelles, *The Journal of Physical Chemistry B* 110, 14304-14312
30. van der Loop, T. H., Panman, M. R., Lotze, S., Zhang, J., Vad, T., Bakker, H. J., Sager, W. F. C., and Woutersen, S. (2012) Structure and dynamics of water in nonionic reverse micelles: A combined time-resolved infrared and small angle x-ray scattering study, *The Journal of Chemical Physics* 137, 044503.
31. Martinez, A. V., Dominguez, L., Małolepsza, E., Moser, A., Ziegler, Z., and Straub, J. E. (2013 ) Probing the Structure and Dynamics of Confined Water in AOT Reverse Micelles, *The Journal of Physical Chemistry B* 117, 7345-7351.
32. Law, S. J., and Britton, M. M. (2012) Sizing of Reverse Micelles in Microemulsions using NMR Measurements of Diffusion, *Langmuir* 28, 11699-11706.
33. Amararene, A., Gindre, M., Le Huérou, J.-Y., Urbach, W., Valdez, D., and Waks, M. (2000) Adiabatic compressibility of AOT [sodium bis(2-ethylhexyl)sulfosuccinate] reverse micelles: Analysis of a simple model based on micellar size and volumetric measurements, *Phys. Rev. E* 61, 682 - 689.
34. Moilanen, D. E., Emily E. Fenn, E. E., Wong, D., and Fayer, M. D. (2009) Water dynamics in large and small reverse micelles: From two ensembles to collective behavior *The Journal of Chemical Physics* 131, 014704
35. Riter, R. E., Willard, D. M., and Levinger, N. E. (1998) Water Immobilization at Surfactant Interfaces in Reverse Micelles, *The Journal of Physical Chemistry B*. 102, 2705-2714.
36. Pant, D., and Levinger, N. E. (2000) Polar Solvation Dynamics in Nonionic Reverse Micelles and Model Polymer Solutions, *Langmuir* 16, 10123-10130.
37. Corbeil, E. M., and Levinger, N. E. (2003) Dynamics of Polar Solvation in Quaternary Microemulsions, *Langmuir* 19, 7264-7270.
38. Bhattacharyya, K. B., B. (2000) Slow Dynamics of Constrained Water in Complex Geometries *The Journal of Physical Chemistry A* 104, 10603-10613.
39. Dutta, P., Sen, P., Mukherjee, S., Halder, A., and Bhattacharyya, K. (2003) Solvation Dynamics in the Water Pool of an Aerosol-OT Microemulsion. Effect of Sodium Salicylate and Sodium Cholate *The Journal of Physical Chemistry B* 107, 10815-10822.
40. Mitra, R. K., Sinha, S. S., and Pal, S. K. (2008) Temperature-Dependent Solvation Dynamics of Water in Sodium Bis(2-ethylhexyl)sulfosuccinate/Isooctane Reverse Micelles, *Langmuir* 24, 49-56.
41. Fayer, M. D. (2011) Water in a Crowd, *Physiology* 26, 381-392.
42. Mitra, R. K., Sinha, S. S., and Pal, S. K. (2007) *The Journal of Physical Chemistry B* 111, 7577.
43. Nave, S., Eastoe, J., Heenan, R. K., Steytler, D., and Grillo, I. (2000) What Is So Special about Aerosol-OT? 2. Microemulsion Systems, *Langmuir* 16, 8741-8748.
44. Fayer, M. D. (2012) Dynamics of Water Interacting with Interfaces, Molecules, and Ions, *Accounts of Chemical Research* 45, 3-14.

45. Das, A., Patra, A., and Mitra, R. K. (2013) Do the Physical Properties of Water in Mixed Reverse Micelles Follow a Synergistic Effect: A Spectroscopic Investigation, *The Journal of Physical Chemistry B* 117, 3593-3602.
46. Paul, B. K., and Mitra, R. K. (2005) Water solubilization capacity of mixed reverse micelles: Effect of surfactant component, the nature of the oil, and electrolyte concentration, *Journal of Colloid and Interface Science* 288, 261-279.
47. Kinugasa, T., Kondo, A., Nishimura, S., Miyauchi, Y., Nishii, Y., Watanabe, K., and Takeuchi, H. (2002) Estimation for size of reverse micelles formed by AOT and SDEHP based on viscosity measurement, *Colloids and Surfaces, A: Physicochemical and Engineering Aspects* 204, 193-199.
48. Lipgens, S., Schuebel, D., Schlicht, L., Spilgies, J.-H., Ilgenfritz, G., Eastoe, J., and Heenan, R. K. (1998) Percolation in Nonionic Water (w/o)-Microemulsion Systems: A Small Angle Neutron Scattering Study, *Langmuir* 14, 1041-1049.
49. Quintana, S. S., Moyano, F., Falcone, R. D., Silber, J. J., and Correa, N. M. (2009) Characterization of Multifunctional Reverse Micelles' Interfaces Using Hemicyanines as Molecular Probes. II: Effect of the Surfactant, *The Journal of Physical Chemistry B* 113, 6718-6724.
50. Moyano, F., Falcone, R. D., Mejuto, J. C., Silber, J. J., and Correa, N. M. (2010) Cationic Reverse Micelles Create Water with Super Hydrogen-Bond-Donor Capacity for Enzymatic Catalysis: Hydrolysis of 2-Naphthyl Acetate by  $\alpha$ -Chymotrypsin, *Chemistry - A European Journal* 16, 8887-8893.
51. Silva, O. F., Fernández, M. A., Silber, J. J., de Rossi, R. H., and Correa, N. M. (2012) Inhibited Phenol Ionization in Reverse Micelles: Confinement Effect at the Nanometer Scale, *CHEMPHYSCHEM* 13, 124-130.
52. Blach, D., Correa, N. M., Silber, J. J., and Falcone, R. D. (2011) Interfacial water with special electron donor properties: Effect of water-surfactant interaction in confined reversed micellar environments and its influence on the coordination chemistry of a copper complex, *Journal of Colloid Interface Science* 355, 124-130.
53. Sando, G. M., Dahl, K., and Owrutsky, J. C. (2005) Surfactant Charge Effects on the Location, Vibrational Spectra, and Relaxation Dynamics of Cyanoferrates in Reverse Micelles, *The Journal of Physical Chemistry B* 109, 4084-4095.
54. Evans, D. F., and Wennerström, H. (1999) *The Colloidal Domain: Where Physics, Chemistry, Biology, and Technology Meet*, 2nd Edition, 2nd ed., p 560, Wiley-VCH, New York.
55. Eastoe, J., and Heenan, R. K. (1994) Water-induced structural changes within the L2 phase of didodecyldimethylammonium bromide-cyclohexane-water systems, *Journal of the Chemical Society, Faraday Transactions* 90, 487-492.
56. Paul, B. K., and Mitra, R. K. (2005) Water solubilization capacity of mixed reverse micelles: Effect of surfactant component, the nature of the oil and electrolyte concentration, *J. Colloid Interface Sci.* 288, 261.
57. Verbeeck, A., Voortmans, G., Jackers, C., and Schryver, F. C. D. (1989) Characterization and stabilization of inverse micelles, *Langmuir* 5, 766-776.
58. Zemb, T. N., Hyde, S. T., Derian, P. J., Barnes, I. S., and Ninham, B. W. (1987) Microstructure from x-ray scattering: the disordered open connected model of microemulsions, *The Journal of Physical Chemistry* 91, 3814-3820.
59. Evans, D. F., Mitchell, D. J., and Ninham, B. W. (1986) Oil, water, and surfactant: properties and conjectured structure of simple microemulsions, *The Journal of Physical Chemistry* 90, 2817-2825.
60. Barnes, I. S., Hyde, S. T., Ninham, B. W., Derian, P. J., Drifford, M., and Zemb, T. N. (1988) Small-angle x-ray scattering from ternary microemulsions determines microstructure, *The Journal of Physical Chemistry* 92, 2286-2293.
61. Eastoe, J. (1992) Small-angle neutron scattering from dilute didodecyldimethylammonium bromide water-in-oil microemulsions. Evidence for polymer-like aggregates, *Langmuir* 8, 1503-1506.
62. Barois, P., Hyde, S., Ninham, B., and Dowling, T. (1990) Observation of Two Phases within the Cubic Phase Region of a Ternary Surfactant Solution *Langmuir* 6, 1136-1140.

63. Stroem, P., and Anderson, D. M. (1992) The cubic phase region in the system didodecyldimethylammonium bromide-water-styrene, *Langmuir* 8, 691-709.
64. Olla, M., and Monduzzi, M. (2000) DDAB Microemulsions: Influence of an Aromatic Oil on Microstructure, *Langmuir* 16, 6141-6147.
65. Shioi, A., Harada, M., Obika, M., and Adachi, M. (1998) Structure and Properties of Fluids Composed of Polyelectrolyte and Ionic Surfactant in Organic Phase: Poly(acrylic acid) and Didodecyldimethylammonium Bromide, *Langmuir* 14, 4737-4743.
66. Skurtveit, R., and Olsson, U. (1991) A self-diffusion study of the microstructure in didodecyldimethylammonium bromide-dodecane-brine microemulsions, *The Journal of Physical Chemistry* 95, 5353-5358.
67. Skurtveit, R., and Olsson, U. (1992) Microstructure near the oil corner of a ternary microemulsion, *The Journal of Physical Chemistry* 96, 8640-8646.
68. Jonstroemer, M., Olsson, U., and Parker, J., W.O. (1995) A Self-Diffusion Study of Microemulsion Structure Using a Polar Solvent Mixture, *Langmuir* 11, 61-69.
69. Tingey, J. M., Fulton, J. F., Matson, D. W., and Smith, R. D. (1991) Micellar and Bicontinuous Microemulsions Formed In both Near-Critical and Supercritical Propane with Didodecyldimethylammonium Bromide and Water *The Journal of Physical Chemistry* 95, 1445-1448.
70. Knackstedt, M. A., Ninham, B. W., and Monduzzi, M. (1995) Diffusion in Model Disordered Media, *Physical Review Letters* 75, 653-656.
71. Mitra, R. K., and Paul, B. K. (2005) Investigation on percolation in conductance of mixed reverse micelles, *Colloids and Surfaces A: Physicochemical and Engineering Aspects* 252, 243-259.
72. Lock, A. J., and Bakker, H. J. (2002) Temperature dependence of vibrational relaxation in liquid H<sub>2</sub>O, *The Journal of Chemical Physics* 117, 1708-1713.
73. Corcelli, S. A., and Skinner, J. L. (2005) Infrared and Raman Line Shapes of Dilute HOD in Liquid H<sub>2</sub>O and D<sub>2</sub>O from 10 to 90 °C, *The Journal of Physical Chemistry A* 109, 6154-6165.
74. Libnau, F. O., Toft, J., Christy, A. A., and Kvalheim, O. M. (1994) Structure of Liquid Water Determined from Infrared Temperature Profiling and Evolutionary Curve Resolution *Journal of the American Chemical Society* 116, 8311-8316.
75. Onori, G., and Santucci, A. (1993) IR investigations of water structure in Aerosol OT reverse micellar aggregate, *The Journal of Physical Chemistry* 97, 5430-5434.
76. Yagasaki, T., Ono, J., and Saito, S. (2009) Ultrafast energy relaxation and anisotropy decay of the librational motion in liquid water: A molecular dynamics study, *The Journal of Chemical Physics* 131, 164511.
77. Gaiduk, V. I., and Vij, J. K. (2001) The concept of two stochastic processes in liquid water and analytical theory of the complex permittivity in the wavenumber range 0–1000 cm<sup>-1</sup>, *Physical Chemistry Chemical Physics* 3, 5173-5181.
78. Heyden, M., Sun, J., Funkner, S., Mathias, G., Forbert, H., Havenith, M., and Marx, D. (2010) Dissecting the THz spectrum of liquid water from first principles via correlations in time and space *Proceedings of the National Academy of Sciences USA* 107, 12068-12073.
79. Cooksey, C. C., Greer, B. J., and Heilweil, E. J. (2009) Terahertz spectroscopy of l-proline in reverse aqueous micelles Original Research Article, *Chemical Physics Letters* 467, 424-429.
80. Venables, D. S., Huang, K., and Schmuttenmaer, C. A. (2001) Effect of Reverse Micelle Size on the Librational Band of Confined Water and Methanol, *The Journal of Physical Chemistry B* 105, 9132-9138.
81. Majumder, P., Sarkar, R., Shaw, A. K., Chakraborty, A., and Pal, S. K. (2005) Ultrafast dynamics in a nanocage of enzymes: Solvation and fluorescence resonance energy transfer in reverse micelles, *Journal of Colloid and Interface Science* 290, 462-474.
82. Mitra, R. K., Sinha, S. S., Verma, P. K., and Pal, S. K. (2008) Modulation of Dynamics and Reactivity of Water in Reverse Micelles of Mixed Surfactants *The Journal of Physical Chemistry B* 112, 12946-12953.
83. Verma, P. K., Saha, R., Mitra, R. K., and Pal, S. K. (2010) Slow water dynamics at the surface of macromolecular assemblies of different morphologies, *Soft Matter* 6, 5971-5979.

84. Patra, A., Verma, P. K., and Mitra, R. K. (2012) Slow Relaxation Dynamics of Water in Hydroxypropyl Cellulose-Water Mixture Traces Its Phase Transition Pathway: A Spectroscopic Investigation, *The Journal of Physical Chemistry B* 116, 1508-1516.
85. Koti, A. S. R., Krishna, M. M. G., and Periasamy, N. (2001) Time-resolved area-normalized emission spectroscopy (TRANES): A novel method for confirming emission from two excited states, *The Journal of Physical Chemistry A* 105, 1767-1771.
86. Jimenez, R., Fleming, G. R., Kumar, P. V., and Maroncelli, M. (1994) Femtosecond Solvation Dynamics of Water, *Nature* 369, 471-473.
87. Banerjee, D., Verma, P. K., and Pal, S. K. (2009) A Temperature Dependent Femtosecond-Resolved Hydration Dynamics of Water in Aqueous Guanidinium Hydrochloride Solution, *Photochemical Photobiological Science* 8, 1441-1447.
88. Fee, R. S., and Maroncelli, M. (1994) Estimating the time-zero spectrum in time-resolved emission measurements of solvation dynamics, *Chemical Physics* 183, 235-247.
89. Lipari, G., and Szabo, A. (1981) Padé approximants to correlation functions for restricted rotational diffusion, *The Journal of Chemical Physics* 75, 2971-2976.
90. Lipari, G., and Szabo, A. (1982) Model-free approach to the interpretation of nuclear magnetic resonance relaxation in macromolecules. 1. Theory and range of validity, *Journal of the American Chemical Society* 104, 4546-4559.
91. Shaw, A. K., and Pal, S. K. (2007) Fluorescence Relaxation Dynamics of Acridine Orange in Nanosized Micellar Systems and DNA, *The Journal of Physical Chemistry B* 111, 4189-4199.
92. Verma, P. K., Makhil, A., Mitra, R. K., and Pal, S. K. (2009) Role of Solvation Dynamics in the Kinetics of Solvolysis Reactions in Microreactors, *Physical Chemistry Chemical Physics* 11, 8467-8476.
93. Verma, P. K., Mitra, R. K., and Pal, S. K. (2009) A Molecular Picture of Diffusion Controlled Reaction: Role of Microviscosity and Hydration on Hydrolysis of Benzoyl Chloride at a Polymer Hydration Region, *Langmuir* 25, 11336-11343.
94. Pal, S., Balasubramanian, S., and Bagchi, B. (2002) Temperature dependence of water dynamics at an aqueous micellar surface: Atomistic molecular dynamics simulation studies of a complex system, *The Journal of Chemical Physics* 117, 2852-2859.
95. Nandi, N., Bhattacharyya, K., and Bagchi, B. (2000) Dielectric relaxation and solvation dynamics of water in complex chemical and biological systems, *Chemical Reviews* 100, 2013-2045.
96. Mukherjee, S., Sahu, K., Roy, D., Mondal, S. K., and Bhattacharyya, K. (2004) Solvation dynamics of 4-aminophthalimide in dioxane-water mixture, *Chemical Physics Letters* 384, 128-133.
97. Mitra, R. K., Sinha, S. S., and Pal, S. K. (2007) Temperature Dependent Hydration at Micellar Surface: Activation Energy Barrier Crossing Model Revisited, *The Journal of Physical Chemistry B* 111, 7577-7581.
98. Satpati, A. K., Kumbhakar, M., Nath, S., and Pal, H. (2009) Influence of Confined Water on the Photophysics of Dissolved Solutes in Reverse Micelles, *CHEMPHYSICHEM* 10, 2966-2978.
99. Singh, P. K., Kumbhakar, M., Pal, H., and Nath, S. (2008) Effect of electrostatic interaction on the location of molecular probe in polymer - Surfactant supramolecular assembly: A solvent relaxation study, *The Journal of Physical Chemistry B* 112, 7771-7777.
100. Pant, D., Riter, R. E., and Levinger, N. E. (1998) Influence of restricted environment and ionic interactions on water solvation dynamics, *The Journal of Chemical Physics* 109, 9995-10003.
101. Narayanan, S. S., Sinha, S. S., Sarkar, R., and Pal, S. K. (2008) Picosecond to nanosecond reorganization of water in AOT/lecithin mixed reverse micelles of different morphology, *Chemical Physics Letters* 452, 99-104.
102. Narayanan, S. S., Sinha, S. S., Sarkar, R., and Pal, S. K. (2008) Validation and divergence of the activation energy barrier crossing transition at AOT/lecithin reverse micellar interface, *The Journal of Physical Chemistry B* 112, 2859.
103. Willard, D. M., Riter, R. E., and Levinger, N. E. (1998) Dynamics of Polar Solvation in Lecithin/Water/Cyclohexane Reverse Micelles, *Journal of the American Chemical Society* 120, 4151-4160.

104. Maroncelli, M., and Fleming, G. R. (1987) Picosecond solvation dynamics of coumarin 153: the importance of molecular aspects of solvation, *The Journal of Chemical Physics* 86, 6221-6238.
105. Patra, A., Luong, T. Q., Mitra, R. K., and Havenith, M. (2013) Solvent dynamics in a reverse micellar water-pool: a spectroscopic investigation of DDAB–cyclohexane–water systems, *Physical Chemistry Chemical Physics* 15, 930-939.
106. Biswas, R., Chakraborti, T., Bagchi, B., and Ayappa, K. G. (2012) Non-monotonic, distance-dependent relaxation of water in reverse micelles: Propagation of surface induced frustration along hydrogen bond networks, *The Journal of Chemical Physics* 137, 014515
107. Lipari, G., and Szabo, A. (1980) Effect of librational motion on fluorescence depolarization and nuclear magnetic resonance relaxation in macromolecules and membranes, *Biophysical Journal* 30, 489.
108. Wang, C. C., and Pecora, R. (1980) Time-correlation functions for restricted rotational diffusion, *The Journal of Chemical Physics* 72, 5333-5340.
109. Tan, H.-S., Piletic, I. R., and Fayer, M. D. (2005) Orientational dynamics of water confined on a nanometer length scale in reverse micelles, *The Journal of Chemical Physics* 122, 174501.
110. Kitamura, N., Sakata, N., Kim, H.-B., and Habuchi, S. (1999) Energy Gap Dependence of the Nonradiative Decay Rate Constant of 1-Anilino-8-naphthalene Sulfonate in Reverse Micelles, *Analytical Sciences* 15, 413-420.
111. Luong, T. Q., Verma, P. K., Mitra, R. K., and Havenith, M. (2011) Onset of Hydrogen Bonded Collective Network of Water in 1,4-Dioxane, *The Journal of Physical Chemistry A* 115, 14462-14469.
112. Mittleman, D. M., Nuss, M. C., and Colvin, V. L. (1997) Terahertz spectroscopy of water in inverse micelles *Chemical Physics Letters* 275, 332-338.
113. Gorenflo, S., Tauer, U., Hinkov, I., Lambrecht, A., Buchner, R., and Helm, H. (2006 ) Dielectric properties of oil–water complexes using terahertz transmission spectroscopy, *Chemical Physics Letters* 421, 494-498.
114. Heyden, M., and Havenith, M. (2010) Combining THz spectroscopy and MD simulations to study protein-hydration coupling *Methods* 52, 74-83.
115. Kindt, J. T., and Schmittenmaer, C. A. (1996) Far-infrared dielectric properties of polar liquids probed by femtosecond terahertz pulse spectroscopy, *The Journal of Physical Chemistry* 100, 10373-10379.
116. Rønne, C., Åstrand, P. O., and Keiding, S. R. (1999) THz Spectroscopy of Liquid H<sub>2</sub>O and D<sub>2</sub>O, *Physical Review Letters* 82, 2888-2891
117. Cho, M., Fleming, G. R., Saito, S., Ohmine, I., and Stratt, R. M. (1994) Instantaneous normal mode analysis of liquid water, *The Journal of Chemical Physics* 100, 6672-6683.
118. Hasted, J. B., Husain, S. K., Frescura, F. A. M., and Birch, J. R. (1985) Far-infrared absorption in liquid water, *Chemical Physics Letters* 118, 622-625.
119. Warr, G. G., Sen, R., Evans, D. F., and Trend, J. E. (1988) Microemulsion formation and phase behavior of dialkydimethylammonium bromide surfactants, *The Journal of Physical Chemistry* 92, 774-783.
120. Onori, G., and Santucci, A. (1993) IR Investigations of Water Structure in Aerosol OT Reverse Micellar Aggregates, *The Journal of Physical Chemistry* 97, 5430-5434.

# Chapter 6: Structure and Dynamics of Water in Hydrophobic Environment

## 6.1. Introduction:

Water, unlike conventional liquids, possesses several fascinating properties owing to its unique intermolecular hydrogen bond network<sup>1</sup> and this makes this apparently innocent molecule to play ‘the key’ role in many biological and chemical processes.<sup>2, 3</sup> While the various dynamical modes of water in its pure state has been well understood,<sup>4</sup> its behaviour in the vicinity of an amphiphilic (i.e. partly hydrophilic and partly hydrophobic) molecule or macromolecular fragment has still been a popular subject of scientific interest.<sup>5</sup> A proper apprehension of such model ‘hydrophobic hydration’<sup>6</sup> is of prime importance in order to understand its behaviour in the real biological milieu. The polymer poly(oxyethylene) (POE) is a perfect candidate to model such systems owing to its varied conformational properties,<sup>7</sup> amphiphilic character and high solubility in water.<sup>8</sup> The interaction pattern of water with POE changes with the composition of the mixture,<sup>9</sup> and this phenomenon provides with a unique opportunity to study water dynamics in varied hydrophobic environments without essentially altering the chemical nature of the system. In the present investigation we have studied the hydrogen bonded structure by Fourier transform infrared (FTIR) spectroscopy and cooperative dynamics by THz time domain spectroscopy (TTDS) of water in its mixture with 1,2-dimethoxyethane (DME) at varied compositions.

DME is the simplest member of the POE family and the choice of this solvent is justified from its unlimited solubility in water which allows probing the whole range of concentration in which water evolves from being a solute to a solvent. Moreover, DME ( $\text{CH}_3\text{-O-CH}_2\text{-CH}_2\text{-O-CH}_3$ ) is structurally related to two hydrophobic and water insoluble polymers: poly-(oxymethylene), with one  $-\text{CH}_2$  group less in the monomer unit, and poly-(oxytrimethylene), with one  $-\text{CH}_2$  group more.<sup>10</sup> DME-water mixture has been a subject of various experimental investigations including NMR relaxation,<sup>11</sup> FTIR,<sup>12</sup> Raman spectroscopy,<sup>13-15</sup> volumetric and thermodynamic measurements<sup>16</sup> as well as several theoretical and simulation studies.<sup>17-22</sup> It has been revealed that many macroscopic thermodynamic parameters of this binary mixture, e.g., viscosity,<sup>23</sup> partial molar volume<sup>16</sup> including some microscopic parameters like diffusion coefficient<sup>22</sup> pass through an inflation point in the composition profile, which clearly identifies the micro-heterogeneous

environment of the mixtures. While most of these aforementioned studies have been carried out addressing the conformational changes of DME, less attention has been paid on the associated changes in the structure and dynamics of water itself. In the present investigation we have tried to explore the structure and dynamics of water in its mixture with DME covering the whole concentration range, with special attention paid to the very low water content region in which water is expected to be present mostly in its isolated form; such an environment experimentally reproduces the notion of ‘hydrophobic hydration’.

The structure of water in this binary mixture has been obtained using FTIR spectroscopy in the mid-IR region while its collective dynamics is explored using TTDS technique in the frequency window of 0.3-1.6 THz. TTDS has recently been evolved as a potential tool that label free estimates the collective hydration dynamics which extends beyond the first few hydration layers of an interface and essentially leaves its imprint in this elusive frequency region only.<sup>24, 25</sup> This technique thus offers a unique advantage to examine the fate of the H-bonded network dynamics of water in otherwise less polar environments including biological interfaces.<sup>26-29</sup> Various frequency-dependent optical parameters of the solution (viz. absorption coefficient,  $\alpha(\nu)$ , complex refractive index,  $\tilde{n}(\nu)$ , complex dielectric constants,  $\tilde{\epsilon}(\nu)$ ) etc. can be extracted from a single measurement<sup>30</sup> and the dynamics of water can be obtained following a Debye relaxation model.<sup>31</sup> In the present investigation the composition of the mixture is varied carefully and since one of our major emphases is on the low water content region, several compositions have been considered in the concentration range of  $X_w=0$  to 0.1 (where  $X_w$  is the mole fraction of water in the mixture).  $X_w$  is then increased in regular interval, and again several data points are considered in the water rich region ( $X_w=0.8$  to 1.0). It has been observed that the collective dynamics of water show a non-monotonous behaviour as a function of the mixture composition.

## **6.2. Results and Discussions: (Non-Monotonic Dynamics of Water in its Binary Mixture with 1, 2-Dimethoxy Ethane: A Combined THz and FTIR Study)**

**MIR study:** The O-D vibrational stretch of HOD (4% D<sub>2</sub>O in pure water) in the 2400 –2700 cm<sup>-1</sup> frequency window is an ideal tool to study solute hydration and is highly sensitive to its local intra-molecular H-bond.<sup>32</sup> It is important to note that the difference absorbance data reported in the present study (Figure 6.1.) involve explicitly the signature of water and the composition dependent MIR features correspond to the changes in the structure of water only.

Figure 6.1.a represents the O-D stretching of HOD in pure water and in water-DME mixtures at different  $X_w$ . Pure water produces an absorption peak at  $2505\text{ cm}^{-1}$  (designated as  $\nu_w$ )<sup>33</sup> and this peak suffers progressive blue shift coupled with asymmetric deformation of the absorption profile with increasing DME content, especially in the low water content region.<sup>9</sup>

14, 27, 34

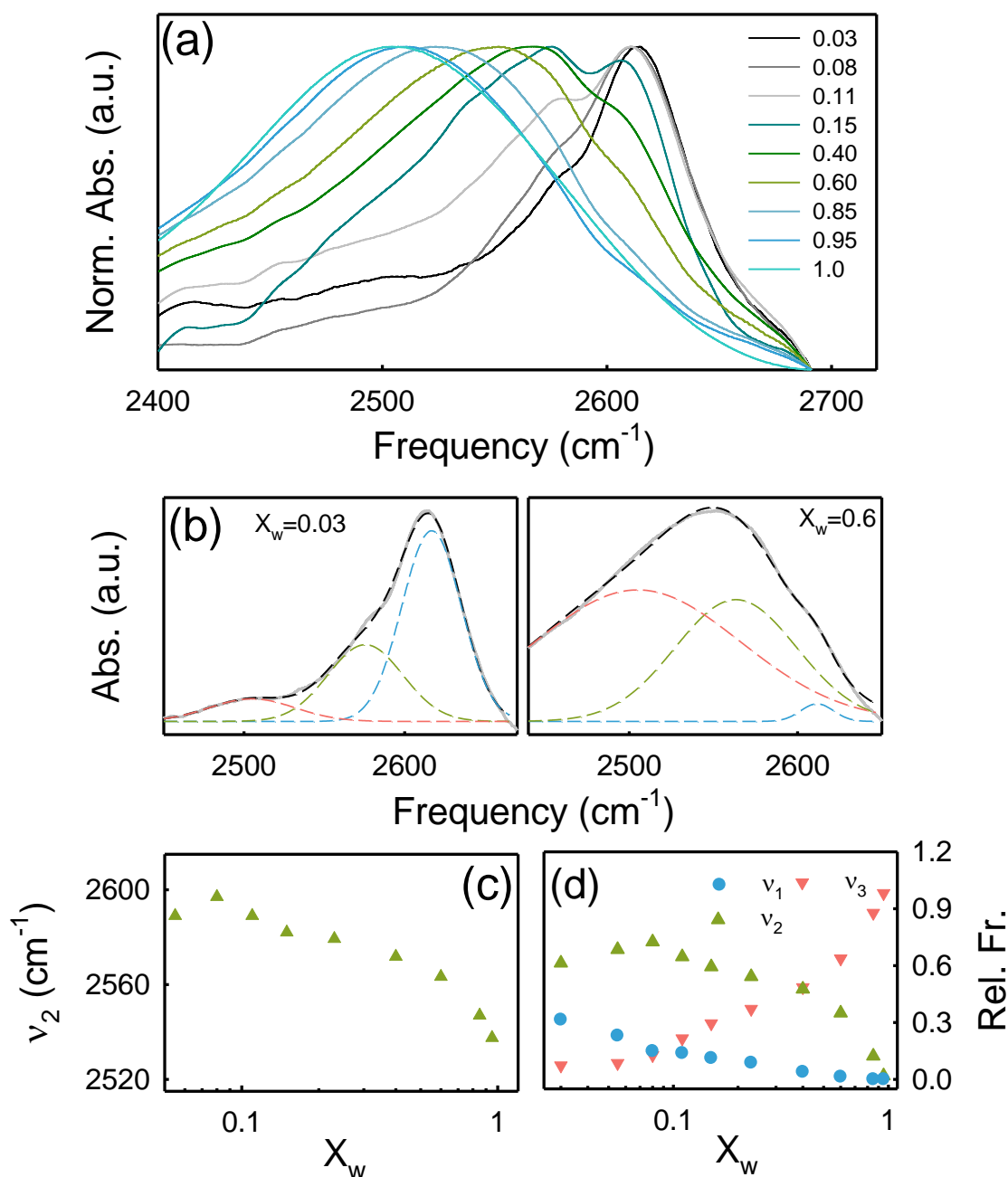


**Figure 6.1.** (a) FTIR absorption spectra of the OD stretch of HOD in water for water/DME mixtures at different mole fractions of water ( $X_w$ ) ranging from 0.03 to 1.0. The arrow indicates increasing water content. (b) Deconvoluted O-D stretching spectrum of HOD in water-DME mixture at  $X_w=0.03$  and 0.6. The orange broken line is centred at  $2505\text{ cm}^{-1}$  and corresponds to bulk water. The black broken line represents the overall fitting. (c) Peak frequency  $\nu_2$  as a function of  $X_w$ . (d) Relative population of different types of water present at different water/DME mixing ratios.

The observed blue shift can be explained in terms of the reduction of the electric field along the O-D stretch<sup>35</sup> as well as weakening of the H-bond strength,<sup>9, 11</sup> the effect being more prominent in the low water content region where enhanced DME-water H-bond formation prevails. In order to obtain a quantitative insight about the H-bonding state we deconvolute the absorption spectra of DME-water mixtures into different Gaussian sub-bands and for a comparative understanding we keep one sub-band peak fixed at 2505 cm<sup>-1</sup>.<sup>14, 27</sup> Two such representative spectra for X<sub>w</sub>=0.03 and 0.6 are presented in Figure 6.1.b. For all the systems with X<sub>w</sub> ≥ 0.8, the observed spectra can be fitted with two such Gaussian sub-bands; apart from the bulk water (2505 cm<sup>-1</sup>) band, a new blue shifted band appears (designated as ν<sub>2</sub>) furnishing the evidence of water-DME H-bond formation which in turn weakens the water-water H-bonds. The frequency ν<sub>2</sub> gradually increases with decreasing X<sub>w</sub> (Figure 6.1.c) which signifies greater number of DME-water H-bond formation with increasing DME content. At low water content (X<sub>w</sub> ≤ 0.6), the total spectra could only be fitted considering a new band (designated as ν<sub>1</sub>) appearing around ~2610 cm<sup>-1</sup> region. This band is associated with the vibrational stretch of isolated or uncoordinated water molecules that share H-bonding with DME oxygen atoms only or water molecules that do not share any H-bond with any neighbouring molecule.<sup>36, 37</sup> The DME-water mixed system thus corresponds to three types of water molecules associated with three different Gaussian peaks, ν<sub>w</sub>, ν<sub>2</sub> and ν<sub>1</sub>. The relative abundance of these three types of water could approximately be estimated by calculating the relative area under each individual curve towards the total spectra. The relative population profile is provided in Figure 6.1.d. At high water content, the population is effectively governed by the bulk water (ν<sub>w</sub>) with a steady grow of the ν<sub>2</sub> population. On the other hand, the contribution of ν<sub>w</sub> is notably small in the low water content region, the population been mostly governed by ν<sub>2</sub> and ν<sub>1</sub>.

At low DME concentrations (0.8 ≤ X<sub>w</sub> ≤ 1) DME molecules fit themselves into a slightly distorted network structure of liquid water. Brillouin light scattering and sound velocity experiments have revealed that the average maximum hydration number per ether oxygen of DME is ~ 1.8,<sup>38</sup> which corresponds to X<sub>w</sub> ~ 0.8. It can be concluded that in this region all the DME molecules are fully hydrated and can fit themselves in a slightly deformed H-bonded water cage. On further increase in the DME content the bulk water contribution decreases considerably only to be compensated with a concomitant increase in the ν<sub>1</sub> water content, ν<sub>2</sub> population being increased modestly. It could be noted that with

increasing DME concentration the number of water molecules available to hydrate DME molecules decreases, as a result the fully H-bonded water network structure melts down to form  $v_2$  and  $v_1$  water molecules.<sup>11</sup> At  $X_w < 0.1$  the  $v_1$  water contributes significantly with negligible abundance of bulk water. However, a notable abundance of  $v_2$  type of water even in this small water content indicates the presence of discrete water clusters<sup>9, 14</sup> at higher DME concentrations.

**THz TDS study:** The various optical parameters of water-DME mixtures obtained from TTDS measurements in the frequency range of 0.3 to 1.6 THz are summarized in Figure 6.2. The frequency dependent absorption coefficient,  $\alpha(\nu)$ , of water and DME-water mixtures are presented in Figure 6.2.a.  $\alpha(\nu)$  increases gradually with increasing  $X_w$ , the observed increase is rather intuitive considering the replacement of low absorbing DME molecules with high THz absorbing water.<sup>39</sup>

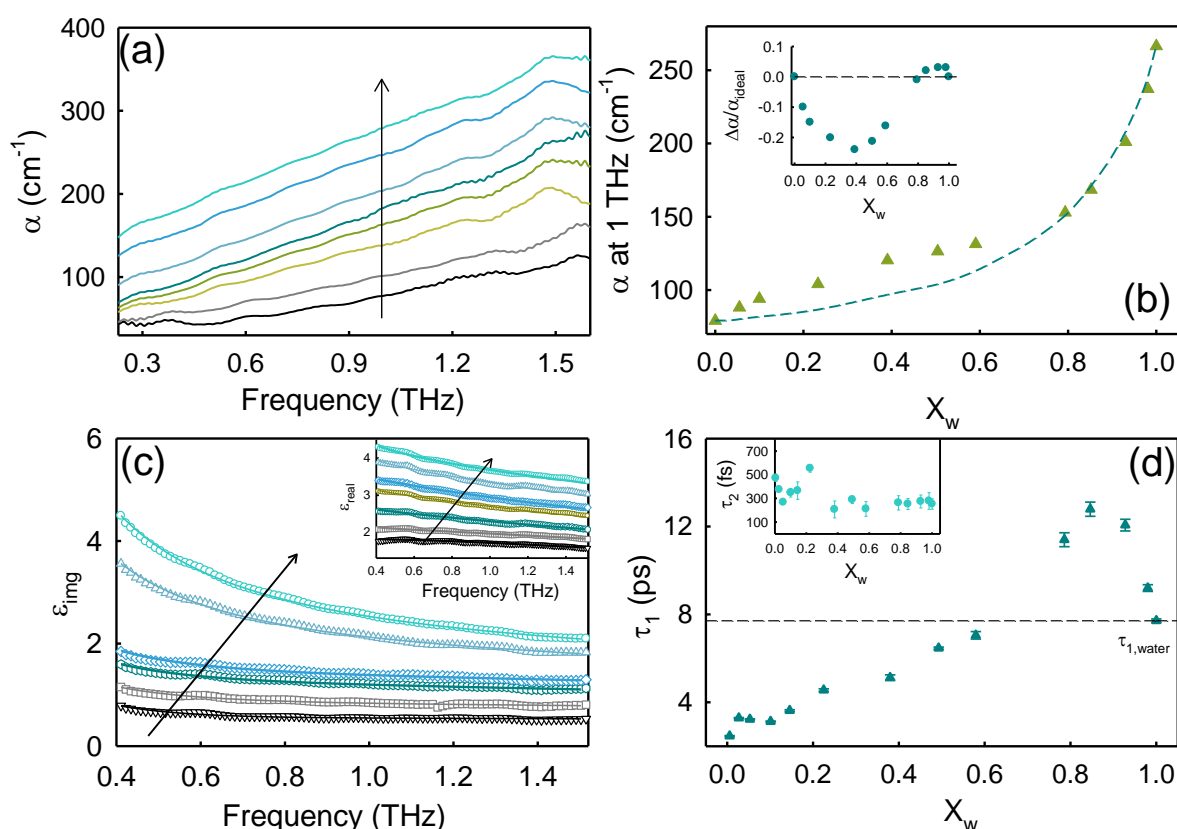


**Figure 6.2.** (a) Frequency dependent absorption coefficient of water-DME mixture. The arrow indicates increasing water content. (b) Absorption coefficient ( $\alpha$ ) measured at 1 THz as a function of  $X_w$ . The broken line represents calculated  $\alpha_{\text{ideal}}$  of the mixture assuming an ideal mixing. The inset shows the extent of deviation from the calculated values as a function of  $X_w$ . (c) Real ( $\epsilon_{\text{real}}$ ) and imaginary ( $\epsilon_{\text{img}}$ ) dielectric constant of water-DME mixtures at different mole fractions of water in the THz region. The solid lines represent the triple Debye relaxation fittings. The arrows indicate increasing water mole fraction in the mixture. (d) Debye relaxation time scales ( $\tau_1$  and  $\tau_2$ ) as a function of  $X_w$ . The broken line is a measure of cooperative hydrogen bond relaxation time of pure water.

In order to obtain a quantitative outlook, we plot the absorption coefficient measured at 1 THz for different mixed systems and is plotted as a function of  $X_w$  (Figure 6.2.b). For an ideal mixture the absorption coefficient ( $\alpha_{ideal}$ ) can be calculated using the following relation<sup>27, 40</sup>

$$\alpha_{ideal} = \frac{\rho_{real}}{\rho_{ideal}} \sum_i \phi_i \alpha_i(\nu) \quad (6.1)$$

where  $\phi_i$  is the volume fraction of the  $i$ -th species,  $\rho_{real}$  is the measured density of the mixture and  $\rho_{ideal} = \sum_i X_i \rho_i$ . We include the  $\alpha_{ideal}$  values in the same plot for comparison, and it is observed that the measured values suffer significant deviation from the calculated ones, specially in the low water content region. In the inset of Figure 6.2.b we plot the relative deviation of  $\alpha$  ( $\Delta\alpha = \alpha_{ideal} - \alpha_{real}$ ) as a function of  $X_w$ , and the non-ideal behaviour of the mixture seems evident from it. Such non-idealistic behaviour in the low water concentration region has previously been reported for dioxane-water<sup>27</sup> and water-acetonitrile<sup>40</sup> mixtures. On the other hand, the high water content region appears to behave more or less ideally with only marginal deviation from the ideal values (Figure 6.2.b, inset). The deviation of this ideal behaviour at low  $X_w$  also reciprocates the MIR results which show clear evidence of the existence of isolated or uncoordinated water. It would be interesting to investigate whether this observed non-ideal to near-ideal makeover would also be reflected in the corresponding hydration dynamics.

The frequency dependent real and imaginary permittivity profiles of water-DME mixtures at different compositions are presented in Figure 6.2.c. Both  $\epsilon_{real}$  and  $\epsilon_{img}$  show gradual increase with increasing  $X_w$ . The complex dielectric profiles have been fitted using the triple Debye relaxation model<sup>31, 41, 42</sup> as describe below to extract the hydration dynamics:

$$\tilde{\epsilon}(\nu) = \epsilon_{\infty} + \sum_{j=1}^3 \frac{\epsilon_j - \epsilon_{j+1}}{1 + i2\pi\nu\tau_j} \quad (6.2)$$

where,  $\tau_j$  is the relaxation time for the  $j$ -th relaxation mode,  $\epsilon_1$  is the static dielectric constant,  $\epsilon_j$  are the dielectric constants for different relaxation processes,  $\epsilon_{\infty}$  is the extrapolated dielectric constant at a very high frequency, and  $m$  describes the number of relaxation modes. We have fixed the value of the static dielectric constant ( $\epsilon_s$ ) from the literature.<sup>43</sup> The fitted parameters are presented in Table 6.1. Dielectric relaxation of pure water in THz region produces three relaxation time constants of  $\sim 8$  ps,  $\sim 200$  fs and  $\sim 90$  fs. The  $\sim 8$  ps timescale of

water explicitly associates with the spontaneous restructuring of the H-bond network,<sup>44, 45</sup> whereas the  $\sim 200$  fs timescale emanates from either quick jumps of under-coordinated water or a small angular rotation preceding a large angle jump.<sup>46, 47</sup> The  $\sim 80$  fs timescale has its origin rooted to the  $60\text{ cm}^{-1}$  vibrational band due to the H-bond bending and the related transverse acoustic phonons which propagate in a direction normal to the H-bonds in between two neighbouring water molecules.<sup>48, 49</sup> Let us discuss the observed timescales in details. We plot  $\tau_1$  and  $\tau_2$  as a function of  $X_w$  in Figure 6.2.d. The  $\tau_1$  profile has two very distinct features. At  $X_w \leq 0.6$ , the  $\tau_1$  values lie well below  $\tau_{1,\text{water}}$  and increases linearly with increasing  $X_w$ . As discussed earlier this mode is specifically assigned to the cooperative relaxation of H-bond network and a distinctly smaller timescale compared to that of pure water unambiguously identifies the rupture of the tetrahedral H-bonding network as had also been observed in reverse micellar water pool.<sup>50</sup>

**Table 6.1.** Triple Debye relaxation fitting parameters with error bars for water-DME mixtures at different compositions. We have fixed the value of  $\tau_3$ .

$X_w$	$\epsilon_\infty$	$\epsilon_s$	$\epsilon_1$	$\epsilon_2$	$\tau_1$ (ps)	$\tau_2$ (fs)	$\tau_3$ (fs)
0.03	1.11	8.29	1.59	1.94	3.28 $\pm$ 0.02	374.5 $\pm$ 15.7	88.00
0.05	1.14	8.55	1.80	2.04	3.22 $\pm$ 0.02	267.7 $\pm$ 18.6	81.00
0.10	1.20	9.40	1.98	2.14	3.12 $\pm$ 0.02	347.8 $\pm$ 36.5	74.00
0.15	1.36	10.19	1.93	2.15	3.62 $\pm$ 0.04	365.7 $\pm$ 73.7	94.36
0.22	1.10	11.58	1.20	1.90	4.55 $\pm$ 0.06	402.7 $\pm$ 62.5	96.45
0.38	1.23	14.14	2.44	2.23	5.12 $\pm$ 0.13	206.8 $\pm$ 71.0	71.00
0.49	1.30	18.22	2.56	2.38	6.46 $\pm$ 0.05	289.0 $\pm$ 31.8	78.84
0.58	1.34	20.72	2.65	2.38	7.05 $\pm$ 0.17	210.7 $\pm$ 61.9	76.32
0.79	1.52	36.80	3.27	2.88	11.40 $\pm$ 0.32	262.4 $\pm$ 60.6	84.00
0.85	1.54	47.46	3.60	3.10	12.78 $\pm$ 0.32	252.9 $\pm$ 46.8	78.07
0.93	1.64	62.55	3.80	3.25	12.06 $\pm$ 0.27	273.7 $\pm$ 54.9	77.30
0.98	1.82	75.09	4.04	3.53	9.20 $\pm$ 0.15	278.3 $\pm$ 70.0	78.40
1.00	1.98	79.05	4.37	3.76	8.13 $\pm$ 0.077	227.6 $\pm$ 43.6	71.89

At such low water content the dynamics is found to be 3-4 fold faster which indicates the lack of any cooperative H-bonded network and supports the notion of the formation of un- or under-coordinated water or the formation of some dangling OH bonds as a result of the bond ruptures. With increase in  $X_w$ , more water molecules participate in the H-bond network which eventually forms larger water clusters and increases  $\tau_1$ .<sup>27</sup> The region  $X_w > 0.6$ , on the other hand, evidences an intriguing retardation of the dynamics compared to  $\tau_{1,water}$ , and at  $X_w = 0.85$ , it becomes as slow as  $\sim 12$  ps. The retardation in  $\tau_1$  could be correlated with DME hydration by solvent water molecules wherein DME-water interaction slows down the cooperative rearrangement of water network as has previously been observed for sucrose hydration.<sup>41</sup>

The changes in  $\tau_2$  (Figure 6.2.d, inset) are, however, not much remarkable. In the moderate to high water concentration region ( $X_w \geq 0.3$ ) the obtained  $\tau_2$  values are more or less comparable to that of  $\tau_{2,water}$  and the changes are within the error limit. However, in the low  $X_w$  region the observed values of  $\tau_2$  are somewhat slower than that of  $\tau_{2,water}$ , a behaviour contrary to what has been observed for  $\tau_1$ . This apparent dissimilarity can be rationalized from the different origins of these two timescales. As mentioned earlier, while a cooperative rearrangement is responsible for  $\tau_1$ ,  $\tau_2$  essentially originate from a small angular rotation of water molecules followed by a jump. At low water content, the water molecules are mostly bonded to one or more DME molecules, which perhaps hinders the small rotation and jump dynamics and thus slows down  $\tau_2$ . At a higher  $X_w$ , when the formation of water cluster predominates, the jump motion gradually gets eased and  $\tau_2$  approaches  $\tau_{2,water}$ .

The FTIR study shows strong modification of intramolecular hydrogen bonded structure of water and TTDS studies establish non-monotonous dynamics as water switches from being solute to a solvent in the mixture. Such transition can be explained by apprehending a structural transition from small water cluster to fully grown H-bonded structure.

### 6.3. Conclusions:

The structure and dynamics of water in its binary mixture with a less polar liquid DME are investigated by FTIR and THz spectroscopy study. MIR-FTIR measurements reveal the existence of essentially under-coordinated water molecules in DME continuum with dangling O-H bonds at low water concentrations. Such systems successfully imitate the hydrophobic

environment in the interior of carbon nanotubes. With increasing  $X_w$  bulk like water evolves with the establishment of H-bonded network. The collective H-bond relaxation dynamics, as determined from THz Debye relaxation, is found to be accelerated in the low  $X_w$  region while at  $X_w \sim 0.8$  region it is intriguingly slower than that of pure water. The accelerated dynamics at higher concentration of DME ( $X_w < 0.6$ ) can be explained by complete breakdown of the tetrahedral H-bond structure and formation of small water clusters, leading to acceleration of the relaxation dynamics. However at  $X_w \sim 0.8$  where all the DME molecules are essentially completely hydrated and form an extended hydrogen bonded network leading to slower collective relaxation dynamics. We assume hydrogen bonding nature between solute and solvent are function of composition which is central key to such non-monotonous behaviour of water-DME binary mixture.

## References:

1. Roberts, S. T., Ramasesha, K., and Tokmakoff, A. (2009) Structural Rearrangements in Water Viewed Through Two-Dimensional Infrared Spectroscopy, *Accounts of Chemical Research* 42, 1239-1249.
2. Ball, P. (2008) Water as an Active Constituent in Cell Biology, *Chemical Reviews* 108, 74-108.
3. Halle, B. (2004) *Philos. Trans. R. soc. London B* 359, 1207-1224.
4. Bakker, H. J., and Skinner, J. L. (2010) Vibrational Spectroscopy as a Probe of Structure and Dynamics in Liquid Water, *Chemical Reviews* 110, 1498-1517.
5. Fayer, M. D. (2011) Water in a Crowd, *Physiology* 26, 381-392.
6. Yaminsky, V. V., and Voglerb, E. A. (2001) Hydrophobic hydration, *Current Opinion in Colloid & Interface Science* 6, 342-349.
7. Begum, R., and Matsuura, H. (1997) Conformational properties of short poly(oxyethylene) chains in water studied by IR spectroscopy, *Journal of the Chemical Society, Faraday Transactions* 93, 3839-3848.
8. Molyneux, P. (1983) *Water-Soluble Synthetic Polymers Properties and Behavior*, Vol. 1, CRC Press, Boca Raton, FL.
9. Fenn, E. E., Moilanen, D. E., Levinger, N. E., and Fayer, M. D. (2009) Water Dynamics and Interactions in Water–Polyether Binary Mixtures, *Journal of the American Chemical Society* 131, 5530-5539.
10. Wada, R., Fujimoto, K., and Kato, M. (2014) Why Is Poly(oxyethylene) Soluble in Water? Evidence from the Thermodynamic Profile of the Conformational Equilibria of 1,2-Dimethoxyethane and Dimethoxymethane Revealed by Raman Spectroscopy, *The Journal of Physical Chemistry B* 118, 12223-12231.
11. Kříž, J., and Dybal, J. (2011) Hydration modes of an amphiphilic molecule 2: NMR, FTIR and theoretical study of the interactions in the system water–1,2-dimethoxyethane, *Chemical Physics* 382, 104-112.
12. Matsuura, H., and Sagawa, T. (1995) Anomalous conformational behavior of short poly(oxyethylene) chains in water: An FT-IR spectroscopic study, *Journal of Molecular Liquids* 65-66, 313-316.
13. Goutev, N., Nickolov, Z. S., and Matsuura, H. (1998) Hydration structure of 1,2-dimethoxyethane (C1E1C1): O-H Raman band studies, *Journal of Molecular Liquids* 76, 117-126.
14. Nickolov, Z. S., Goutev, N., and Matsuura, H. (2001) Hydrogen Bonding in Concentrated Aqueous Solutions of 1,2-Dimethoxyethane: Formation of Water Clusters, *The Journal of Physical Chemistry A* 105, 10884 - 10889.

15. Goutev, N., Ohno, K., and Matsuura, H. (2000) Raman Spectroscopic Study on the Conformation of 1,2-Dimethoxyethane in the Liquid Phase and in Aqueous Solutions, *The Journal of Physical Chemistry A* 104, 9226-9232.
16. Douheret, G., Reis, J. C. R., Davis, M. I., Fjellanger, I. J., and Høiland, H. (2004) Aggregative processes in aqueous solutions of mono- to tetra-ethylene glycol dimethyl ether at 298.15 K, *Physical Chemistry Chemical Physics* 6, 784-792.
17. Bedrov, D., Borodin, O., and Smith, G. D. (1998) Molecular Dynamics Simulations of 1,2-Dimethoxyethane/Water Solutions. 1. Conformational and Structural Properties, *The Journal of Physical Chemistry B* 102, 5683-5690.
18. Bedrov, D., and Smith, G. D. (1999) Molecular Dynamics Simulations of 1,2-Dimethoxyethane in Aqueous Solution: Influence of the Water Potential, *The Journal of Physical Chemistry B* 103, 3791-3796.
19. Bedrov, D., Pekny, M., and Smith, G. D. (1998) Quantum-Chemistry-Based Force Field for 1,2-Dimethoxyethane and Poly(ethylene oxide) in Aqueous Solution, *The Journal of Physical Chemistry B* 102, 996 - 1001.
20. Smith, G. D., Bedrov, D., and Borodin, O. (2000) Molecular Dynamics Simulation Study of Hydrogen Bonding in Aqueous Poly(Ethylene Oxide) Solutions, *Physical Review Letters* 85, 5583.
21. Hezaveh, S., Samanta, S., Milano, G., and Roccatano, D. (2011) Structure and dynamics of 1,2-dimethoxyethane and 1,2-dimethoxypropane in aqueous and non-aqueous solutions: A molecular dynamics study, *The Journal of Chemical Physics* 135, 164501.
22. Bedrov, D., Borodin, O., and Smith, G. D. (1998) Molecular Dynamics Simulation of 1,2-Dimethoxyethane/Water Solutions. 2. Dynamical Properties, *The Journal of Physical Chemistry B* 102, 9565-9570.
23. Saleh, M. A., Akhtar, S., and Ahmed, M. S. (2008) Density, viscosity and thermodynamics for viscous flow of water + 1,2-dimethoxyethane, *Physics and Chemistry of Liquids* 46, 140-153.
24. Schmuttenmaer, C. A. (2004) Exploring Dynamics in the Far-Infrared with Terahertz Spectroscopy, *Chemical Reviews* 104, 1759-1780.
25. Heyden, M., Sun, J., Funkner, S., Mathias, G., Forbert, H., Havenith, M., and Marx, D. (2010) Dissecting the THz spectrum of liquid water from first principles via correlations in time and space *Proceedings of the National Academy of Sciences USA* 107, 12068-12073.
26. Tielrooij, K. J., Paparo, D., Piatkowski, L., Bakker, H. J., and Bonn, M. (2009) Dielectric Relaxation Dynamics of Water in Model Membranes Probed by Terahertz Spectroscopy, *Biophysical Journal* 97, 2484-2492.
27. Luong, T. Q., Verma, P. K., Mitra, R. K., and Havenith, M. (2011) Onset of Hydrogen Bonded Collective Network of Water in 1,4-Dioxane, *The Journal of Physical Chemistry A* 115, 14462-14469.
28. Heyden, M., and Havenith, M. (2010) Combining THz spectroscopy and MD simulations to study protein-hydration coupling *Methods* 52, 74-83.
29. He, Y., Ku, P. I., Knab, J. R., Chen, J. Y., and Markelz, A. G. (2008) Protein Dynamical Transition Does Not Require Protein Structure, *Physical Review Letters* 101, 178103.
30. Beard, M. C., Turner, G. M., and Schmuttenmaer, C. A. (2002) Terahertz Spectroscopy, *The Journal of Physical Chemistry B* 106, 7146-7159.
31. Polley, D., Patra, A., and Mitra, R. K. (2013 ) Dielectric relaxation of the extended hydration sheathe of DNA in the THz frequency region, *Chemical Physics Letters* 586, 143-147.
32. Śmiechowski, M., and Stangret, J. (2010) Vibrational spectroscopy of semiheavy water (HDO) as a probe of solute hydration, *Pure and Applied Chemistry* 82, 1869-1887.
33. Stangret, J., and Gampe, T. (1999) Hydration Sphere of Tetrabutylammonium Cation. FTIR Studies of HDO Spectra, *The Journal of Physical Chemistry B* 103, 3778-3783.
34. Cringus, D., Yeremenko, S., Pshenichnikov, M. S., and Wiersma, D. A. (2004) Hydrogen Bonding and Vibrational Energy Relaxation in Water-Acetonitrile Mixtures, *The Journal of Physical Chemistry B* 108, 10376-10387.
35. Smith, J. D., Saykally, R. J., and Geissler, P. L. (2007) The Effects of Dissolved Halide Anions on Hydrogen Bonding in Liquid Water, *Journal of the American Chemical Society* 129, 13847-13856.

36. Graener, H., and Seifert, G. (1993) Vibrational and orientational relaxation of monomeric water molecules in liquids, *The Journal of Chemical Physics* 98, 36-45.
37. Scatena, L. F., Brown, M. G., and Richmond, G. L. (2001) Water at Hydrophobic Surfaces: Weak Hydrogen Bonding and Strong Orientation Effects, *Science* 292, 908-912.
38. Matsuura, H., and Fukuhara, K. (1986) Hydration of the Oxyethylene Chain. Hypersonic Velocities in Aqueous Solutions of  $\alpha$ -Methyl- $\omega$ -methoxyoligo(oxyethylene)s and  $\alpha$ -Methyl- $\omega$ -hydroxyoligo(oxyethylene)s as Studied by Brillouin Scattering, *Bulletin of the Chemical Society of Japan* 59, 763-768.
39. Heugen, U., Schwaab, G., Bründermann, E., Heyden, M., Yu, X., Leitner, D. M., and Havenith, M. (2006) Solute-induced retardation of water dynamics probed directly by terahertz spectroscopy, *Proceedings of the National Academy of Sciences USA* 103, 12301-12306.
40. Venables, D. S., and Schmuttenmaer, C. A. (2000) Spectroscopy and dynamics of mixtures of water with acetone, acetonitrile, and methanol, *The Journal of Chemical Physics* 113, 11222-11236.
41. Samanta, N., Das Mahanta, D., and Mitra, R. K. (2014) Does Urea Alter the Collective Water Structure: A Dielectric Relaxation Study in THz Region, *Chemistry – An Asian Journal* 9, 3457-3463.
42. Samanta, N., Das Mahanta, D., and Mitra, R. K. (2014) Collective hydration dynamics of guanidinium chloride solutions and its possible role in protein denaturation: a terahertz spectroscopic study, *Physical Chemistry Chemical Physics* 16, 23308--23315.
43. Marcheselli, L., Marchetti, A., Tagliazucchi, M., Tassi, L., and Tosi, G. (1993) The Relative Permittivity of 1,2-Dimethoxyethane/Water Solvent Mixtures From -10 to 80°C, *Australian Journal of Chemistry* 46, 633-639.
44. van der Post, S. T., Tielrooij, K.-J., Hunger, J., Backus, E. H. G., and Bakker, H. J. (2013) Femtosecond study of the effects of ions and hydrophobes on the dynamics of water, *Faraday Discuss.* 160, 171-189.
45. Fukasawa, T., Sato, T., Watanabe, J., Hama, Y., Kunz, W., and Buchner, R. (2005) Relation between Dielectric and Low-Frequency Raman Spectra of Hydrogen-Bond Liquids, *Physical Review Letters* 95, 197802.
46. Laage, D., and Hynes, J. T. (2006) A Molecular Jump Mechanism of Water Reorientation *Science* 311, 832-835.
47. Fecko, C. J., Eaves, J. D., and Tokmakoff, A. (2002) Isotropic and anisotropic Raman scattering from molecular liquids measured by spatially masked optical Kerr effect spectroscopy, *The Journal of Chemical Physics* 117, 1139-1154.
48. Walrafen, G. E., Chu, Y. C., and Piermarini, G. J. (1996) Low-Frequency Raman Scattering from Water at High Pressures and High Temperatures, *The Journal of Physical Chemistry* 100 10363-10372.
49. Vij, J. K., Simpson, D. R. J., and Panarina, O. E. (2004) Far infrared spectroscopy of water at different temperatures: GHz to THz dielectric spectroscopy of water *Journal of Molecular Liquids* 112, 125-135.
50. Patra, A., Luong, T. Q., Mitra, R. K., and Havenith, M. (2014) Influence of Charge on the Structure and Dynamics of Water Encapsulated in Reverse Micelles, *Physical Chemistry Chemical Physics* 16, 12875-12883.

# Chapter-7: Activity of Water in Bio-Mimicking Environments

## 7.1. Introduction:

Enzymes are the class of protein molecules that implement important role to preserve functionality and ability of biological systems through their catalytic activity.<sup>1-3</sup> In-vitro studies of enzyme activity are usually carried out in water, however, inside a living cell enzyme activity mostly takes place on the surface of biological membranes or in many heterogeneous environments. Water plays a key role in various biological activities<sup>3-5</sup> and the physical properties of water get altered in these heterogeneous medium as it interacts with many types of interfaces.<sup>6-9</sup> Water can influence enzyme activity in the following way: stability of enzyme requires a strong hydration layer around it,<sup>10</sup> in hydrolytic reactions water takes part as a reactant and availability of water changes the enzyme specificity,<sup>11</sup> for example, a minimum of amount of water is required in order to achieve the maximum enzyme activity in hydrophobic solvents.<sup>12</sup>

Micellar enzymology has become a popular mode to replicate the enzyme kinetics study in heterogeneous media or to mimic the in vivo conditions.<sup>13-17</sup> Most of the enzymatic assays have so far been carried out in reverse micellar medium where the enzyme molecules are encapsulated inside the water pool of reverse micelles (RM).<sup>13, 14, 17</sup> It has been observed that enzymes retains their activity while present at the core of the RMs and bell-shaped activity curve has been observed with respect to the hydration ( $w_0$ ) of RM.<sup>17-19</sup> Presence of surfactant may either lead to activation<sup>20, 21</sup> or deactivation<sup>15, 22</sup> of enzymes. The phenomenon of enzymes showing higher efficiency in presence of organized assemblies compared to that in pure water is often termed as ‘superactivity’; the phenomenon can be explained in terms of several factors arising out of the heterogeneous environment created by organized assemblies. Higher efficiency of enzymes in RM systems has occasionally been explained by the presence of specific hydrogen bonding states of water,<sup>23</sup> however, the role water in enzyme activity at micellar medium has not yet been well addressed.

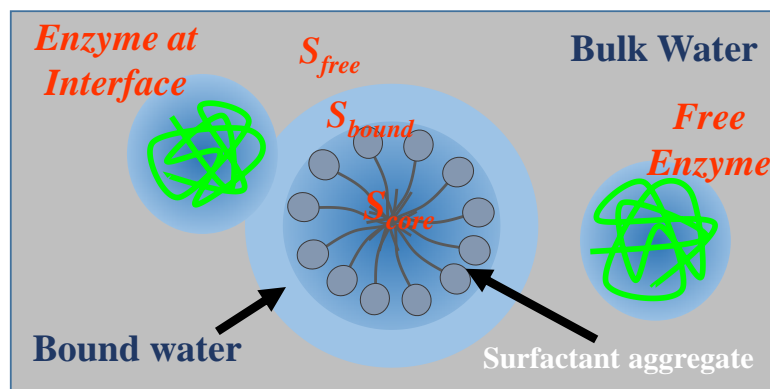
Superactivity in micellar environment has been observed both in pre- and post-micellar concentration,<sup>24, 25</sup> enzyme assays of  $\alpha$ -chymotrypsin (CHT) show an increase in the enzyme turn over number in micellar environment.<sup>26</sup> Such enhanced activity can be explained

assuming higher efficiency of the enzyme towards the micellized substrate compared to the free substrate in bulk water.<sup>15, 21, 26</sup> It has been concluded that longer the hydrophobic tail of the surfactant lesser is the efficiency of the enzyme.<sup>24</sup> This phenomenon has been explained based on the fact that surfactant monomers with longer chain length are more likely to form micelle rather than interacting with enzymes.<sup>24</sup> Due to non-specific interaction between surfactant and enzyme there may exist hydrophobic microenvironment next to the active site, which may enhance the catalytic activity by increasing nucleophilicity of the concerned amino acid residue.<sup>26</sup> However, the extent of superactivity of an enzyme strongly depends upon the length of the substrate also.<sup>26</sup>

Properties of micelle strongly depends on the nature of the surfactants, counter ion<sup>27</sup> and solvent continuum. The free energy of micellization decreases with increasing hydrocarbon chain length,<sup>28</sup> indicating higher chain length surfactants to have greater tendency towards micelle formation. As the hydrocarbon chain length increases so does the aggregation number, and size of the micelle.<sup>29</sup> The critical micelle concentration (c.m.c) and fractional charge of the ionic micelles gets lower and thickness of the stern layer decreases with increasing length of the hydrophobic chain.<sup>30</sup> Water present at micellar environment can be broadly classify into two classes, bound water (water molecules present at interfacial hydration layer) and bulk water (present at enough distance from the interface to experience any influence of the interface).<sup>31-34</sup> The alignment of water molecules at micellar interface strongly depends on the charge type of the surfactant molecules. Such water mimics the structure of intercellular water and hydrated water of many biomolecules and have longer hydrogen bond lifetime compared to water molecules hydrogen bonded with water only.<sup>32</sup>

$\alpha$ -chymotrypsin (CHT) is a well-studied serine protease enzyme with an established mechanism of action in aqueous media.<sup>15</sup> One of the major advantages of it is the wide selectivity range towards substrate and offers extended binding site for peptide substrates.<sup>26</sup> Depending upon their kinetic parameters CHT substrates can be divided into two types 'poor' and 'good'.<sup>35</sup> The total kinetic behaviour has been understood by considering the different types of substrate and enzyme present in the system. The aqueous micellar solution can be divided into three regions bulk water, interfacial water (hydration layer) and hydrophobic core.<sup>31, 36, 37</sup> The substrate molecules can partition into all three pseudo phases, the enzyme can only be considered as surfactant bound or free. The substrate molecule located at hydrophobic core of the micelle cannot participate in hydrolysis reaction. Therefore the overall reaction rate can be described by the other substrates located in different

environments.<sup>36</sup> Since the free enzyme has the access of free substrate only, the reaction can occur between bound enzyme with free and bound substrates and between free enzyme and free substrates.



**Scheme 1:** A schematic representation of enzyme and substrate partition in different phases of aqueous micellar medium.

Superactivity in micellar medium has been rigorously studied for years using different surfactants and substrates. However, in most of the cases the observed phenomenon has been explained by partitioning of the substrate in different pseudo phases and activation of enzymes. But a comprehensive study addressing the effect of different surfactant molecules on the enzyme conformational structure and the role of water in aqueous micellar enzymology have not yet been addressed. In this study we have chosen three different cationic micelles of varying chain lengths (DTAB, CTAB and OTAB with chain lengths of 12, 16 and 18, respectively) and two different substrates 2-NA and AMC with different organic residues are used to study the enzyme activity of CHT in micellar environments. In order to study the influence of micellar interface on the hydrogen bonded structure and dynamics of water we have performed Fourier transform infrared spectroscopy (FTIR) of  $-O-D$  stretching of HOD in micellar medium and time resolved fluorescence spectroscopy (TRFS) using DCM as a probe. DCM shows ultrafast solvation in polar solvent medium, photo physical study of DCM has revealed that it possesses a considerably high excited state dipole moment compared to its ground state.<sup>38</sup> DCM is insoluble in water, so in micellar environments it is expected to stay mostly inside the micellar aggregates, however, solvation dynamics results indicate a considerable exposure of DCM towards the hydration layer of micelle.<sup>39</sup> Previous steady state and time resolved studies of DCM in micellar environment have identified the location of DCM at the micellar interface rather than in the dry core.<sup>38, 39</sup> This makes DCM a good choice to extract information on the hydration dynamics at the

micellar interface. Circular Dichroism (CD) spectroscopy has been carried out to understand the effect ionic surfactant on the secondary and tertiary structures of the enzyme. Enzyme activity studies of CHT for both the substrates are carried out in pre- and post- micellar concentrations in all the three different micellar medium. The observed superactivity in micellar environments has been explained on the basis of the involvement of different types of water, activation of protein structure and partition of substrate in different pseudo phases.

## 7.2. Result and Discussion: (Role of Water in the Superactivity of $\alpha$ -Chymotrypsin in Aqueous Cationic Micellar Environments)

**FTIR Study:** Water gives rise to broad stretching spectrum in the MIR region, such a broad spectrum arises due to inhomogeneous hydrogen bonding states of water. Instead of pure water the use of HOD molecule as a probe has been shown to be advantageous, as the O–D band is decoupled from the O–H band and appears in a region ( $2300\text{--}2800\text{ cm}^{-1}$ ) which is comparatively free from other strong absorptions.<sup>40, 41</sup> Figure 7.1.a shows IR absorption spectra of HOD in aqueous micellar environment which are found to be narrower compared to bulk water spectrum, indicating an alternation of hydrogen bonding structure of water in micellar environment compared to its pure form. We observe an elevated intensity in the red end of the spectrum which indicates the formation of stronger hydrogen bond in the system as has previously been reported from multi-curve resolution Raman spectroscopy study.<sup>42</sup>

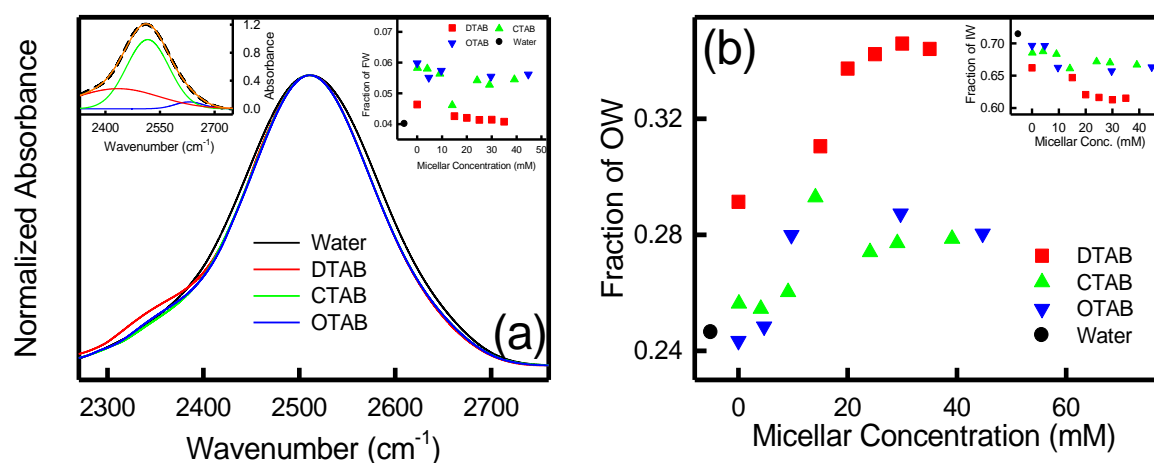


**Figure 7.1:** (a) MIR  $-O-D$  stretching spectra of HOD in pure water and in micellar environments, the inset is a representative of the three component deconvolution of  $-O-D$  stretching spectrum of HOD in DTAB micellar solution. The other inset shows the relative abundance of free water (FW) in different micellar environments. (b) Fraction of ordered water (OW) and intermediate water (IW, inset) in micellar environments, black symbol represent its value in water.

The  $-O-D$  stretching peak of HOD in pure water appears at  $\sim 2515\text{ cm}^{-1}$ . In order to have a quantitative picture on the hydrogen bonding state of water we have deconvoluted the

micellar spectrum into three peaks having centers at  $2630\pm 5$ ,  $2515\pm 5$  and  $2440\pm 5$   $\text{cm}^{-1}$ . The contribution at the blue end ( $2630$   $\text{cm}^{-1}$ ) arises due to the free water (FW) molecules, which are not in hydrogen bonded with other water molecules, i.e. water molecules present at the interface but not hydrogen bonded to the interface or other water molecules and the dangling water residing between hydrocarbon chains of surfactants of micelle.<sup>42</sup> The intermediate peak ( $2515$   $\text{cm}^{-1}$ ) arises due to the water molecules which are unable to form strong tetrahedral network, this is the most abundant type of water and are termed as intermediate water (IW). The red end peak ( $2440$   $\text{cm}^{-1}$ ) is due to the more ordered hydrogen bonded water molecules and are assigned as ordered water (OW), the origin of OW can be understood on the basis of the alignment of water molecules under the electrostatic field created by the cationic interface, and formation of extended hydration layer at ionic micellar interface having hydrogen atoms facing towards bulk water.<sup>43</sup> Deconvolution results have been presented in Figure 7.1.a and b, which demonstrates that the abundance of OW is significantly higher for DTAB micelle compared to higher chain length CTAB and OTAB micelles. The increased OW is at the expense of a decreased abundance of IW compared to that in pure water, which identifies a considerable ordering of water at the micellar interface, the effect being surfactant specific. The abundance of FW is rather small, however, their abundance is higher in the longer chain length CTAB and OTAB, while in DTAB its abundance is comparable to that in water.

**Steady State Fluorescence and Solvent Relaxation Study:** Figure 7.2.a represents steady state fluorescence spectra of DCM in different micellar environments, a blue shift in the emission maximum is observed with increasing surfactant chain length indicating that DTAB interface is more polar in nature compared to CTAB and OTAB micelles. The decay transients are found to be wavelength dependent (Figure 7.2b (inset)). The red end decay consists of a distinct rise followed by a decay, whereas, for the blue only a decay is observed. Such wavelength dependency of emission decay transients<sup>44-46</sup> clearly indicates solvation of the probe. We have constructed the time resolved emission spectra (TRES) and from the TRES, we construct the corresponding solvent correlation function,  $C(t)$  using equation 2.14. Some representative  $C(t)$  for the studied micellar systems are shown in Figure 7.2.d. In order to check whether the observed time resolved spectral shift is associated with any internal photo-physics of the probe itself we construct the time-resolved area normalized emission spectra (TRANES);<sup>47</sup> a representative plot is shown in Figure 7.2.c. No iso-emissive point appears in the TRANES profile. Absence of iso-emissive point indicates the absence of multiple species of the probe and affirms the fact that the probe remains as a single ‘species’ only. Therefore, the observed time dependent spectral shift can be attributed solely to the

inhomogeneity of the microenvironment experienced by the probe.  $C(t)$  vs. time curve is fitted bi-exponentially and the solvation parameters are summarized in the Table 7.1. The bi-exponential distribution is observed due to the different relaxation mode of water at micellar interface. While the faster time scale (hundreds of ps) arises due to the relaxation of water molecules presence at the extended Stern layer at the micellar interface, the slower component (thousands of ps) is associated with the relaxation of water molecules strongly bound to the micellar interface.

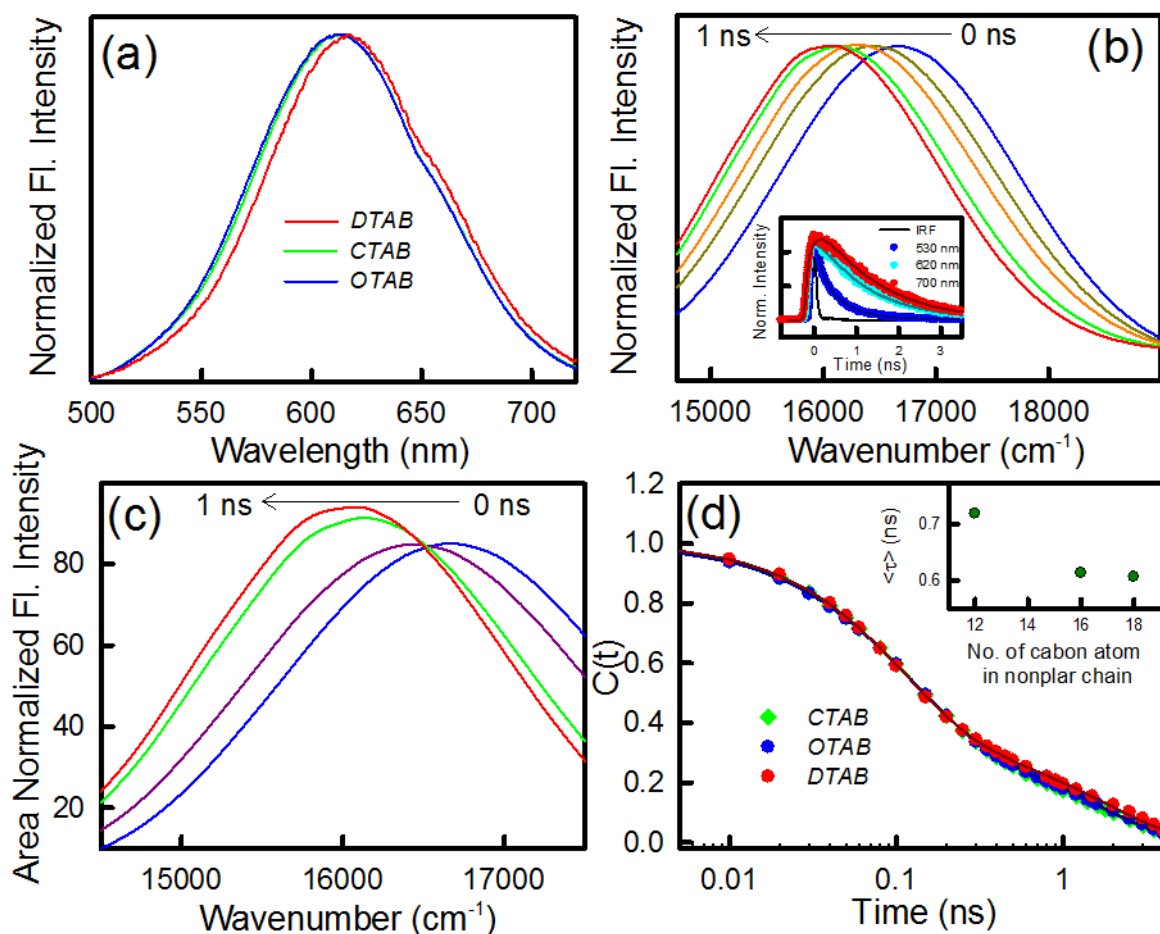


**Figure 7.2.** (a) Steady state fluorescence emission spectra of DCM micellar environment (b) TRES of DCM in 20 mM aqueous DTAB solution (c) TRAFES of DCM 20 mM aqueous DTAB solution (d) Bi-exponential fitting solvation correlation function of DCM in different micellar solution. The inset shows the average solvation time as a function of carbon chain length of the surfactants.

It can be noted that both the components are slower in comparison to the  $\sim 1$  ps relaxation time scale of bulk water which unambiguously recognizes a considerable fraction of slow water molecules present in the micellar interface. We plot the average solvation time constant [ $\langle \tau \rangle = \sum_{i=1}^2 a_i \tau_i$ ] as a function of the carbon chain length (Figure 7.2.d) and it is observed that solvation gets faster with increasing hydrophobic chain length of the micelle. The thickness of the stern layer of cationic micelle gets thinner for surfactants with longer

hydrophobic chain. FTIR results have confirmed a strong hydrogen bonded ordered water network at DTAB micellar interface compared to CTAB and OTAB, so the major fraction of the probe molecule DCM senses slower solvation dynamics.

**Table 7.1.** Solvation Parameters calculated from bi-exponential fitting of solvation correlation of DCM in micellar solution.

Systems ( $\lambda_{max}^{em}$ )	C.M.C ( $N_{agg}$ ) <sup>29</sup>	$a_1$	$\tau_1$ (ns)	$a_2$	$\tau_2$ (ns)	$\langle\tau\rangle$ (ns)
DTAB (617 nm)	15.4 mM (58)	0.65	0.11	0.35	1.85	0.72
CTAB (613 nm)	0.91 mM (98)	0.66	0.12	0.34	1.57	0.61
OTAB (611 nm)	0.39 mM (180)	0.66	0.12	0.34	1.55	0.61

**Circular Dichroism (CD) Spectra:** The far-UV and near-UV CD spectra provide with information on the secondary and tertiary structures of  $\alpha$ -CHT,<sup>48</sup> respectively. The Far-UV CD spectrum of  $\alpha$ -CHT in buffer has been shown in Figure 7.3.a (Inset) in the region 190-250 nm.

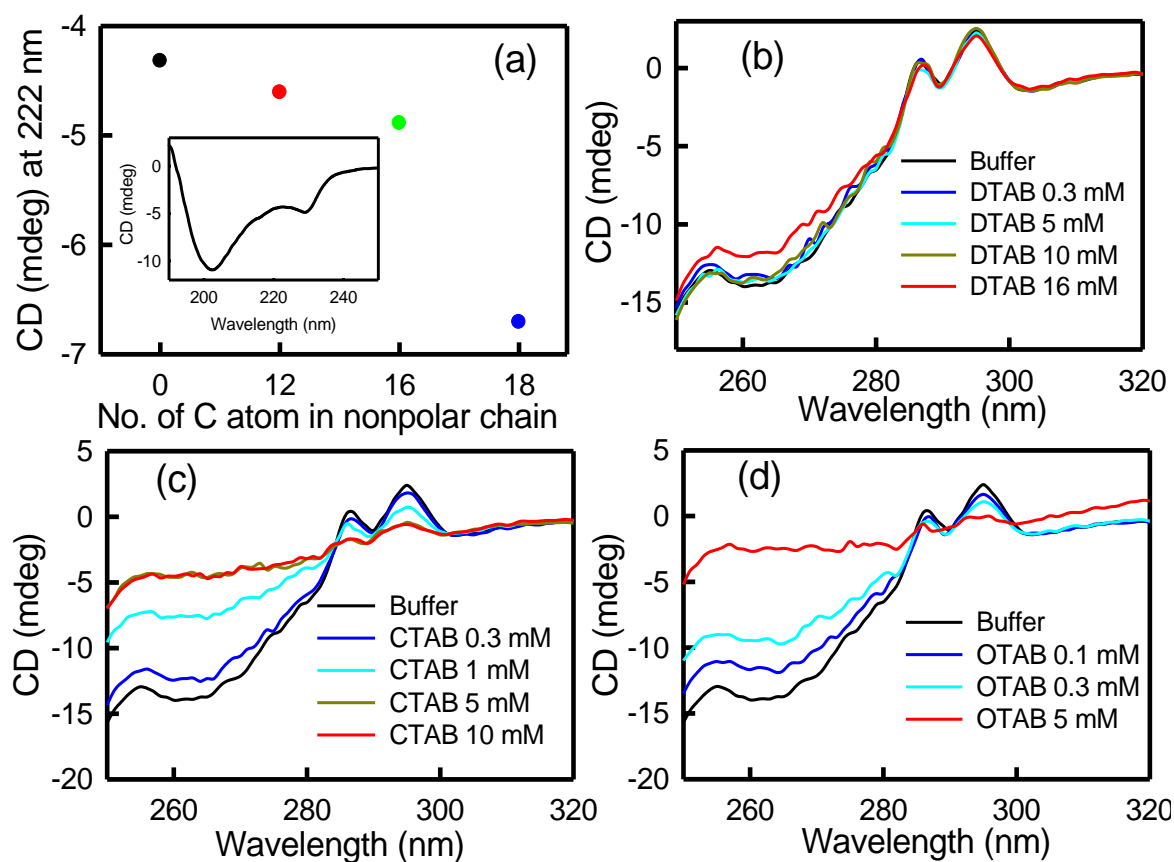


**Figure 7.3.** (a) Far UV CD signal of  $\alpha$ -CHT at 222 nm in presence of DTAB, CTAB and OTAB at their respective CMCs. Inset: Full spectra of  $\alpha$ -CHT in buffer (pH 7) at 20 C. (b), (c) and (d) Near-UV CD spectra of  $\alpha$ -CHT in presence of buffer, DTAB, CTAB and OTAB at different concentrations.

The protein shows two characteristic negative peaks at 202 nm and 232.<sup>49, 50</sup> By deconvolution of the spectrum we obtain that  $\alpha$ -CHT is constituted of ~15%  $\alpha$ -Helix, ~33% antiparallel  $\beta$ -sheet, ~8% parallel  $\beta$ -sheet, ~16%  $\beta$ -turn and ~27% random coil.<sup>50</sup> In presence of surfactants (DTAB, CTAB and OTAB) the CD signals are found to be non-reliable in the  $\lambda < 210$  nm region. We plot the CD signal at 222 nm as a function of surfactant chain length (Figure 7.3a) at their respective CMC, the signal decreases with increase in the chain length of surfactants indicating a concomitant increase in the  $\alpha$ -helix content of CHT. Similar increase in the  $\alpha$ -helix content has previously been observed in presence of CTAB micelles indicating an increased folded state of the protein.<sup>21</sup>

Near-UV CD spectrum (250-320 nm range) of a protein reflects the aromatic amino acid environment and disulphide bonds between two amino acids. Trp shows absorption near 300 nm, Tyr and Phe show absorption near 280 nm and 260 nm respectively.<sup>48</sup> We observe (Figure 7.3.b) a negative peak at 262 nm and two positive maxima at 287 and 296 nm, which corroborates earlier studies.<sup>49</sup> In presence of DTAB the spectra change only marginally in the pre micellar concentration whereas at CMC we observe a slight modification, specially in the 260-280 nm regime. For the other two surfactants (Figure 7.3.c, d) the spectra gradually change with the increase in surfactant concentration and beyond micelle formation a huge change in the spectra is observed. This result indicates that in presence of CTAB and OTAB the protein conformation alters, which perhaps decreases its activity (see later).

**Enzyme Activity:** The activity of CHT was measured in the presence of DTAB, CTAB and OTAB micellar environment by determining the rate of enzyme-catalysed hydrolysis of AMC and 2-NA at room temperature. CHT catalysed hydrolysis of AMC and 2-NA are carried out at both pre- and post- micellar concentration of the surfactants. Figure 7.4.a and b represent relative activity of CHT (ratio between the rates of hydrolysis in micellar environment ( $r$ ) to that in pure water ( $r_0$ )) as a function of surfactant concentration. The nature of CHT activity in micellar medium shows a strong dependency on the nature of surfactant, such type of dependency of enzyme activity on surfactant nature has been observed in many cases e.g. bigger alkyl head group with higher hydrophobicity produces noticeable enhancement of CHT activity.<sup>15, 24, 51</sup>

It has been observed that CHT shows enhanced enzymatic activity for both the substrate molecules exclusively in DTAB environment, however, a decrease in the catalytic activity is observed in CTAB and OTAB. The activity of CHT in DTAB environment shows a bell

shaped curve,<sup>15, 20, 21, 24</sup> the initial increase in the rate arises due to the favourable interaction between the surfactant and enzyme which leads to the activation of the enzyme, as the surfactant concentration increases the unfavourable partition of the substrate in the micellar environment increases, which leads to a decrease in the rate of hydrolysis. However, the observed enhanced activity in DTAB is not very straightforward to only be explained on the basis of the partition of the substrate, there should be other factors, specially the associated hydration at the micellar interface, to be considered.

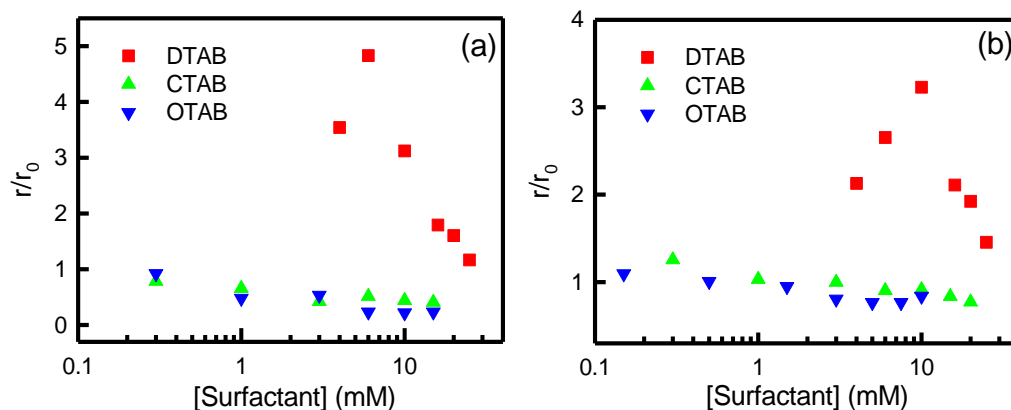


**Figure 7.4.** Surfactant concentration dependent  $r/r_0$  value of enzyme hydrolysis of AMC ( $25 \mu\text{M}$ ) (a) and 2-NA ( $200 \mu\text{M}$ ) (b) at an enzyme concentration  $2 \mu\text{M}$ .

We first consider the structural perturbation of the protein itself in presence of the micelles. CD measurements have revealed that the  $\alpha$ -helical structure of the protein gets considerably enhanced in presence of CTAB and OTAB, the effect being most pronounced in case of OTAB. However, in DTAB, the effect is only marginal; a nominal change is observed in comparison to the protein in water. If the enhanced structure formation in the longer chain surfactants be held responsible for the decreased activity of the enzyme, the absence of any such structure formation in DTAB strongly indicates that the protein structural perturbation is not responsible for the observed enhanced activity in DTAB. One then has to take into consideration other factors, which includes the nature of hydration at the micellar surface. It is interesting to note that the substrates used in the present study are only mildly soluble in water and thus it can be assumed that most of the active substrates are present at the micellar interface. This leads to intuit that hydration at the micellar surface does play a major role in determining the enzyme activity.

### 7.3. Conclusions:

FTIR and TRFS studies have confirmed that there exists a considerable fraction of ordered water at micellar interface, the abundance of such water decreases with increasing length of the surfactant hydrocarbon chain. The stronger hydrogen bonded layer at DTAB interface perhaps prevents the enzyme molecules to interact directly with the cationic interface, which also helps the enzyme molecules to retain its structure in DTAB micellar environment (see figure 7.3). Earlier studies have concluded that water molecules hydrogen bonded to a cationic interface offer higher hydrogen bond donor capacity compared to pure water<sup>52</sup> which creates more active water and in turn they lead to a higher activity.

### References:

1. Daniel, R. M., Dunn, R. V., Finney, J. L., and Smith, J. C. (2003) The role of dynamics in enzyme activity, *Annual review of biophysics and biomolecular structure* 32, 69-92.
2. Matés, J. M., Pérez-Gómez, C., and De Castro, I. N. (1999) Antioxidant enzymes and human diseases, *Clinical biochemistry* 32, 595-603.
3. Pal, S. K., and Zewail, A. H. (2004) Dynamics of water in biological recognition, *Chemical Reviews* 104, 2099-2123.
4. Chaplin, M. (2006) Do we underestimate the importance of water in cell biology?, *Nat Rev Mol Cell Biol* 7, 861-866.
5. Bagchi, B. (2012) From anomalies in neat liquid to structure, dynamics and function in the biological world, *Chemical Physics Letters* 529, 1-9.
6. Patra, A., Luong, T. Q., Mitra, R. K., and Havenith, M. (2014) The influence of charge on the structure and dynamics of water encapsulated in reverse micelles, *Physical Chemistry Chemical Physics* 16, 12875-12883.
7. Moilanen, D. E., Levinger, N. E., Spry, D. B., and Fayer, M. D. (2007) Confinement or the Nature of the Interface? Dynamics of Nanoscopic Water, *Journal of the American Chemical Society* 129, 14311-14318.
8. Fenn, E. E., Wong, D. B., and Fayer, M. D. (2009) Water dynamics at neutral and ionic interfaces, *Proceedings of the National Academy of Sciences USA* 106, 15243-15248.
9. Verma, P. K., Saha, R., Mitra, R. K., and Pal, S. K. (2010) Slow water dynamics at the surface of macromolecular assemblies of different morphologies, *Soft Matter* 6, 5971-5979.
10. Verma, P. K., Rakshit, S., Mitra, R. K., and Pal, S. K. (2011) Role of hydration on the functionality of a proteolytic enzyme  $\alpha$ -chymotrypsin under crowded environment, *Biochimie* 93, 1424-1433.
11. Rubingh, D. N. (1996) The influence of surfactants on enzyme activity, *Current Opinion in Colloid & Interface Science* 1, 598-603.
12. Zaks, A., and Klivanov, A. M. (1988) The effect of water on enzyme action in organic media, *Journal of Biological Chemistry* 263, 8017-8021.
13. Martinek, K., Levashov, A., Khmelnskiy, Y. L., Klyachko, N., and Berezin, I. (1982) Colloidal solution of water in organic solvents: a microheterogeneous medium for enzymatic reactions, *Science* 218, 889-891.
14. Martinek, K., Berezin, I., Khmelnski, Y. L., Klyachko, N., and Levashov, A. (1987) Enzymes entrapped into reversed micelles of surfactants in organic solvents: key trends in applied enzymology (biotechnology), *Biocatalysis* 1, 9-15.
15. Spreti, N., Alfani, F., Cantarella, M., D'Amico, F., Germani, R., and Savelli, G. (1999)  $\alpha$ -Chymotrypsin superactivity in aqueous solutions of cationic surfactants, *Journal of Molecular Catalysis B: Enzymatic* 6, 99-110.

16. Biasutti, M. A., Abuin, E. B., Silber, J. J., Correa, N. M., and Lissi, E. A. (2008) Kinetics of reactions catalyzed by enzymes in solutions of surfactants, *Advances in Colloid and Interface Science* 136, 1-24.
17. Orlich, B., and Schomäcker, R. (2002) Enzyme catalysis in reverse micelles, In *History and Trends in Bioprocessing and Biotransformation*, pp 185-208, Springer.
18. Verma, S. K., and Ghosh, K. K. (2013) Activity, stability and kinetic parameters for  $\alpha$ -chymotrypsin catalysed reactions in AOT/isooctane reverse micelles with nonionic and zwitterionic mixed surfactants, *Journal of Chemical Sciences* 125, 875-882.
19. Piera-Velázquez, S., Marhuenda-Egea, F., and Cadenas, E. (2001) The dependence of a halophilic malate dehydrogenase on  $\omega$  and surfactant concentration in reverse micelles, *Journal of Molecular Catalysis B: Enzymatic* 13, 49-55.
20. Abuin, E., Lissi, E., and Duarte, R. (2005) Kinetics of N-glutaryl-L-phenylalanine p-nitroanilide hydrolysis catalyzed by  $\alpha$ -chymotrypsin in aqueous solutions of dodecyltrimethylammonium bromide, *Journal of colloid and interface science* 283, 539-543.
21. Celej, M. S., D'Andrea, M. G., Campana, P. T., Fidelio, G. D., and Bianconi, M. L. (2004) Superactivity and conformational changes on alpha-chymotrypsin upon interfacial binding to cationic micelles, *Biochemical Journal* 378, 1059-1066.
22. Paolo Viparelli, F. A., Maria Cantarella. (2001) Experimental validation of a model for  $\alpha$ -chymotrypsin activity in aqueous solutions of surfactant aggregates, *Journal of Molecular Catalysis B: Enzymatic* 15, 1-8.
23. Will Chen, C., and Yeh, C.-W. (1998) Kinetic model for enzymatic hydrolysis in reverse micelles, *Biotechnology Letters* 20, 49-52.
24. Abuin, E., Lissi, E., and Calderón, C. (2007) Kinetics of N-glutaryl-L-phenylalanine p-nitroanilide hydrolysis catalyzed by  $\alpha$ -chymotrypsin in aqueous solutions of alkyltrimethylammonium bromides, *Journal of colloid and interface science* 308, 573-576.
25. Sintra, T. E., Ventura, S. P., and Coutinho, J. A. (2014) Superactivity induced by micellar systems as the key for boosting the yield of enzymatic reactions, *Journal of Molecular Catalysis B: Enzymatic* 107, 140-151.
26. Spreti, N., Mancini, M. V., Germani, R., Di Profio, P., and Savelli, G. (2008) Substrate effect on  $\alpha$ -chymotrypsin activity in aqueous solutions of "big-head" ammonium salts, *Journal of Molecular Catalysis B: Enzymatic* 50, 1-6.
27. Jiang, N., Li, P., Wang, Y., Wang, J., Yan, H., and Thomas, R. K. (2005) Aggregation behavior of hexadecyltrimethylammonium surfactants with various counterions in aqueous solution, *Journal of Colloid and Interface Science* 286, 755-760.
28. Berr, S. (1987) Solvent isotope effects on alkyltrimethylammonium bromide micelles as a function of alkyl chain length, *Journal of Physical Chemistry* 91, 4760-4765.
29. Mata, J., Varade, D., and Bahadur, P. (2005) Aggregation behavior of quaternary salt based cationic surfactants, *Thermochimica Acta* 428, 147-155.
30. Berr, S., Jones, R. R. M., and Johnson, J. S. (1992) Effect of counterion on the size and charge of alkyltrimethylammonium halide micelles as a function of chain length and concentration as determined by small-angle neutron scattering, *The Journal of Physical Chemistry* 96, 5611-5614.
31. Patra, A., Hazra, S., Samanta, N., Kumar, G. S., and Mitra, R. K. Micelle induced dissociation of DNA-ligand complexes: the effect of ligand binding specificity, *International Journal of Biological Macromolecules*.
32. Balasubramanian, S., Pal, S., and Bagchi, B. (2002) Hydrogen-Bond Dynamics near a Micellar Surface: Origin of the Universal Slow Relaxation at Complex Aqueous Interfaces, *Physics Review Letter* 89, 115505.
33. Balasubramanian, S., and Bagchi, B. (2002) Slow orientational dynamics of water molecules at a micellar surface, *The Journal of Physical Chemistry B* 106, 3668-3672.
34. Patra, A., Hazra, S., Suresh Kumar, G., and Mitra, R. K. (2014) Entropy Contribution toward Micelle-Driven Deintercalation of Drug–DNA Complex, *The Journal of Physical Chemistry B* 118, 901-908.
35. Schellenberger, V., Braune, K., Hofmann, H. J., and Jakubke, H. D. (1991) The specificity of chymotrypsin, *European Journal of Biochemistry* 199, 623-636.

36. Viparelli, P., Alfani, F., and Cantarella, M. (1999) Models for enzyme superactivity in aqueous solutions of surfactants, *Biochemical Journal* 344, 765-773.
37. Bagchi, B. (2005) Water Dynamics in the Hydration Layer around Proteins and Micelles, *Chemical Reviews* 105, 3197-3219.
38. Mandal, D., Sen, S., Bhattacharyya, K., and Tahara, T. (2002) Femtosecond study of solvation dynamics of DCM in micelles, *Chemical Physics Letters* 359, 77-82.
39. Pal, S. K., Sukul, D., Mandal, D., Sen, S., and Bhattacharyya, K. (2000) Solvation dynamics of DCM in micelles, *Chemical Physics Letters* 327, 91-96.
40. Novaki, L. P., Correa, N. M., Silber, J. J., and El Seoud, O. A. (2000) FTIR and <sup>1</sup>H NMR Studies of the Solubilization of Pure and Aqueous 1,2-Ethanol in the Reverse Aggregates of Aerosol-OT, *Langmuir* 16, 5573-5578.
41. Novaki, L. P., Pires, P. A. R., and El Seoud, O. A. (2000) Fourier transform-IR and <sup>1</sup>H NMR studies on the structure of water solubilized by reverse aggregates of calcium bis(2-ethylhexyl) sulfosuccinate in organic solvents, *Colloid Polymer Science* 178, 143-149.
42. Long, J. A., Rankin, B. M., and Ben-Amotz, D. (2015) Micelle Structure and Hydrophobic Hydration, *Journal of the American Chemical Society* 137, 10809-10815.
43. Gragson, D., McCarty, B., and Richmond, G. (1997) Ordering of interfacial water molecules at the charged air/water interface observed by vibrational sum frequency generation, *Journal of the American Chemical Society* 119, 6144-6152.
44. Nandi, N., Bhattacharyya, K., and Bagchi, B. (2000) Dielectric relaxation and solvation dynamics of water in complex chemical and biological systems, *Chemical Reviews* 100, 2013-2045.
45. Verma, P. K., Mitra, R. K., and Pal, S. K. (2009) A Molecular Picture of Diffusion Controlled Reaction: Role of Microviscosity and Hydration on Hydrolysis of Benzoyl Chloride at a Polymer Hydration Region, *Langmuir* 25, 11336-11343.
46. Patra, A., Verma, P. K., and Mitra, R. K. (2012) Slow Relaxation Dynamics of Water in Hydroxypropyl Cellulose-Water Mixture Traces Its Phase Transition Pathway: A Spectroscopic Investigation, *The Journal of Physical Chemistry B* 116, 1508-1516.
47. Koti, A. S. R., Krishna, M. M. G., and Periasamy, N. (2001) Time-resolved area-normalized emission spectroscopy (TRANES): A novel method for confirming emission from two excited states, *The Journal of Physical Chemistry A* 105, 1767-1771.
48. Kelly, S. M., Jess, T. J., and Price, N. C. (2005) How to study proteins by circular dichroism, *Biochimica et Biophysica Acta (BBA)-Proteins and Proteomics* 1751, 119-139.
49. Rather, G. M., Mukherjee, J., Halling, P. J., and Gupta, M. N. (2012) Activation of Alpha Chymotrypsin by Three Phase Partitioning Is Accompanied by Aggregation, *PLoS ONE* 7, e49241.
50. Hennessey Jr, J. P., and Johnson Jr, W. C. (1981) Information content in the circular dichroism of proteins, *Biochemistry* 20, 1085-1094.
51. Alfani, F., Cantarella, M., Spreti, N., Germani, R., and Savelli, G. (2000)  $\alpha$ -chymotrypsin superactivity in cetyltrialkylammonium bromide-rich media, *Applied biochemistry and biotechnology* 88, 1-15.
52. Moyano, F., Falcone, R. D., Mejuto, J. C., Silber, J. J., and Correa, N. M. (2010) Cationic Reverse Micelles Create Water with Super Hydrogen-Bond-Donor Capacity for Enzymatic Catalysis: Hydrolysis of 2-Naphthyl Acetate by  $\alpha$ -Chymotrypsin, *Chemistry - A European Journal* 16, 8887-8893.

## Chapter 8: Summary and Future Perspective

In this thesis we have investigated the physical properties (structure, dynamics and activity) of water in various environments like in biopolymers, in reverse micelles, in micelles and in hydrophobic environments. The ultrafast dynamics of water was measured using two complementary techniques: (i) time resolved fluorescence spectroscopy (TRFS, with a time resolution of ns to hundreds of ps) using fluorescent probe like C-343, C-500, ANS and DCM (details of these probes are given in chapter-2), and (ii) THz dielectric relaxation (with a time resolution of a few ps to sub-ps). The hydrogen bonded structure of water was obtained by studying the -O-H stretching band (in the mid-IR region), hydrogen bond stretching and libration band (in the far-IR region). In order to acquire knowledge about the activity of water in restricted media we have studied the hydrolysis of benzoyl chloride and hydrolysis of protease substrates by enzyme.

The TRFS study reveals that the slow relaxation dynamics ( $\sim 1$  ns) of confined water in cellulose-water mixture undergoes a characteristic transition beyond 20% hydroxyl propyl cellulose (HPC) concentration, wherein a microscopic phase transition between isotropic to cholesteric phase take places; such transition is also supported by steady state emission and deconvolution of the excitation spectra. The calculated activation energy for transition of bound to bulk type water ( $E_{act}$ ) decreases significantly at higher HPC concentrations, which was explained by the modification in the nature of hydrogen bond structure in the water-HPC mixture at higher HPC concentration. Time-resolved rotational anisotropy measurements indicates the restriction imposed by the structure of HPC-water on the rotational motion of C-500 is a function of composition of system. The alteration in the structure and dynamics of water molecules in the mixture is observed also to affect the reactivity of water in the mixture.

The effect of RM interfacial morphology on the encapsulated water was examined using DDAB/CY RM, which offers a unique phase behavior in which a connected cylindrical structure dominate at lower hydration level and discrete droplet type formulations evolve with increasing hydration. Such a shape transition is directly related to the modification of the elastic properties and curvature of the surfactant monolayer, therefore this system offers with a wide range of surface geometry, both with hydration and with temperature, keeping the constituent composition unaffected. Deconvolution of MIR -O-H stretching measurements of

water revealed that the relative population of water molecules with strongly structured hydrogen bond increases, whereas that of the distorted water molecules decreases with increasing  $w_0$  and reach values comparable to that of bulk water, a situation similar to conventional spherical RM systems. This similarity strongly concludes that interfacial morphology has only a marginal effect on the hydration structure. FIR studies confirm that the collective hydrogen bonded network dynamics in water molecules inside DDAB RM adopts a bulk like behavior with increasing  $w_0$  and temperature. From time resolved fluorescence studies using C-500, a slow (sub-ns) relaxation dynamics has been observed which is recognized to a ‘confinement effect’ similar to that observed in case of conventional RM systems. For DDAB RM systems, with increasing  $w_0$  interconnected cylinder like structures (large radius of curvature) modify towards discrete droplet like structure (small radius of curvature), which induces additional constrain in the translational degree of freedom; in spite of that the average solvation relaxation time constant  $\langle\tau\rangle$  decreases marginally (see Table 5.2.1). The calculated activation energy for bound to bulk transition ( $E_{act}$ ) also shows a negligible effect on this structural transition. All these results point out to the fact that it is the load of water rather than the surface geometry that determines the overall water structure and dynamics for a fixed surface stoichiometry.

TRFS, FIR-FTIR and THz-TDS spectroscopic studies have been carried out in different interfacially charged RMs: AOT (anionic), (DDAB) cationic and Igepal (nonionic) in a fixed hydrocarbon (cyclohexane). The TRFS study clearly established a restricted dynamics of the encapsulated water molecules regardless of the nature of the interface of RM. However, depending on the nature of interface the relative structural perturbation of water appears not very conclusive from the TRFS study due to the location specific information obtained from the different probe molecules (C-343 and ANS). Deconvolution of FIR spectra of water in various RMs shows a red shift of the hydrogen bond stretching band (SB) when the interface changes from nonionic to cationic to anionic. THz dielectric relaxation study supports the fact that the collective vibrational dynamics of water is significantly perturbed at lower hydration in all the RM systems, and the perturbation relaxes with increasing hydration, the release being more prominent in Igepal compared to the other two ionic surfactants (AOT and DDAB). All the above studies thus conclude that anionic (AOT) interface has the largest influence on the hydrogen bond dynamics of confined water, followed by cationic (DDAB) and neutral (Igepal). So the overall studies on AOT, DDAB and Igepal RM conclude that different interfacial morphology may have negligible influence

on the properties of encapsulated water, but, it follows a regular trend with the charge type of the RM interface indicating that charge type of the interface is an important parameter in order to assess the properties of water in that system.

DME belongs to the type of molecules which contain both hydrophobic and hydrophilic segments; FTIR and THz spectroscopy studies of DME-water binary mixture had been employed to investigate the dynamics and hydrogen bonding states of water in this binary mixture. FTIR study shows a strong modification of hydrogen bonding nature of water over the whole composition range. Deconvolution of mid-IR –O-D stretch of HOD in water-DME binary mixture reveals the presence of isolated or under-coordinated water molecules having dangling O-H bonds at low water concentrations ( $X_w$ ), however, with increasing  $X_w$  bulk like water evolves with the formation of H-bonded network. The collective hydrogen bond vibration dynamics of water was determined from THz dielectric relaxation study, which is found to be faster in the low  $X_w$  region while at  $X_w \sim 0.8$  region it is noticeably slower ( $\sim 13$  ps) than that of pure water ( $\sim 8$  ps). The faster dynamics at higher concentration of DME ( $X_w < 0.6$ ) can be explained by the complete breakdown of the tetrahedral H-bond structure and formation of small water clusters leading to faster relaxation dynamics. However at  $X_w \sim 0.8$  the DME molecules are in completely hydrated state and arrange themselves like an extended hydrogen bonded network leading to slower collective relaxation dynamics. The relative change in  $\alpha$  (THz absorption coefficient) also shows strong deviation from the ideal behavior at  $X_w < 0.6$ . FTIR and THz study therefore indicate hydrogen bonding nature between DME and water is a function of composition which is the central key to such non-monotonous dynamical behavior of water-DME binary mixture.

We have studied water hydrogen bonding and dynamics at three different cationic micellar interface (DTAB, CTAB & OTAB) of the same head group but different hydrophobic chain length and used them as a medium to study micellar enzymology. FTIR and TRFS (using DCM as the fluoroprobe) studies confirmed the building up of an ordered water structure at the micellar interface, the abundance of such water decreases with increasing length of the surfactant hydrocarbon chain.  $\alpha$ -chymotrypsin catalyzed hydrolysis of the substrates (2-NA & AMC) shows an enhance activity in DTAB micellar environment, whereas, a moderate deactivation is observed in CTAB and OTAB micellar environment. The enhanced hydrogen bonded layer at DTAB micellar interface possibly prevents the enzyme molecules to interact directly with the cationic interface, which also helps the enzyme molecules to retain its structure in DTAB micellar environment. The water molecules

hydrogen bonded to the cationic interface of DTAB offer higher hydrogen bond donor capacity compared to pure water which in turn they lead to the higher activity.

The motivation of this thesis was to study the restricted water to understand the role of water in various biological processes following the notion that water present in most of the biological environments does not stay in its pure form, rather stays under confinement or interact with various types of interfaces. The presence of water at protein surface plays a pivotal role during its conformational makeover. It also acts as an integral part in the intracellular enzyme activity of biological reactions. Therefore it is important to distinguish the role of different types of interfaces on the properties of water under confinement, also to understand how water molecules arrange themselves in presence of small and large hydrophobic molecules which in turn modifies the physical properties water. Along with this line it is also required to understand the combination of hydrophobicity and charge type of an interface to regulate an enzyme catalysis reaction where water itself acts as a constituent of the reaction. The present thesis presents an approach to systematically address some of the above mentioned concerns and the conclusions drawn herein would facilitate further studies in this very emerging field of research.